Novel mid-IR light sources for emerging applications

By

Paulami Ray

DOCTOR OF PHILOSOPHY

Aston University

December 2022

ABSTRACT

The short-wave mid-infrared, i.e., the wavelength band within 2.5–5 μm has been of keen interest in recent research due to the presence of the molecular fingerprinting region exhibiting strong absorption and resonance of bonds of organic molecules like H_2O, CO_2, CO and CH_4 and a highly efficient water absorption maxima within this spectral range, making this wavelength window exceedingly viable for spectroscopy and material processing applications, that can be extended to medical diagnostics and surgery amongst others. Such high precision applications require the development of novel sources in the mid-IR that can deliver sufficient output power or high pulse energies, along with reasonably broad tunability and good beam quality to cover the region of interest. Additionally, it necessitates the prospect of using ns- and ps-laser sources to treat, and ablate materials with high accuracy, particularly ones containing O-H molecular bonds, usually present as contaminants in glasses, and as natural component of organic materials, and biological tissues.

As tunable sources, optical parametric oscillator (OPO) can generate tailored output wavelengths by the process of nonlinear frequency conversion, with reasonable output powers in CW and pulsed mode operations. Selecting suitable nonlinear materials like MgO:PPLN, that can be quasiphasematched for nonlinear conversion, provides adequate transparency to generate mid-IR wavelengths up to 5 μm. For applications that require delivery of power with high precision and good beam quality, fibre amplifiers are excellent choices. For mid-IR, currently, fluoride-based fibres, like ZBLAN, with rare earth doping have been able to deliver sufficiently high pulse energies for several applications with Er^{3+} dopant capable of offering the highest output powers. From the analysis of energy levels and lifetimes of Erbium doping in ZBLAN, these fibres can also allow

sufficiently broad tunability, covering the water absorption window.

The PhD work presented here investigates the amplification, gain-bandwidth and wavelength tuning of a 2.1 m long, single stage, double-clad, single mode, 7 mol% Erbium-doped ZBLAN fibre amplifier, pumped by a high-power multimode diode near 980 nm, and seeded by nanosecond pulses of 5.2 ns pulse-width, derived from a broadly tunable MgO-PPLN based OPO, operating at a repetition rate of 10 kHz. At the most efficient wavelength of 2790 ± 1 nm, the highest gain of up to 20 dB with 52.7 μJ pulse energy and up to 8 kW peak power, using 0.5 μJ seed pulses, were obtained. Over hundred nanometre continuous wavelength tuning between 2712-2818 nm was achieved at a slightly lower seed pulse energy of 0.27 μJ, and a lower pump power, recording a maximum gain of 26 dB at 2790 ± 1 nm, corresponding to 37.5 μJ peak pulse energy. The investigation also sheds light on practical limitations to power scaling and wavelength tuning, arising from self-phase modulation, self-lasing and fibre degradation due to back reflections.

Keywords: Mid-infrared, Fibre amplifier, Nanosecond pulse, Fluoride fibre, ZBLAN fibre, Erbium-doped fibre.

DEDICATION

To my late father Dr. Shyamal Ray,

who loved and cherished me, and would be happy with anything I do, just because I was his dear little girl;

and my mother for supporting us through it all.

ACKNOWLEDGMENTS

Who would I have been, if not for the philosophy of my father.

How would I have known duty, motivation, courage, and commitment if not from my mother, Aparna.

Where would I have learnt diligence and resilience from, if it was not my brothers Rajkumar and Sourish.

From my supervisors Edik, Natalia, and Sergey I have received timely care, advice, guidance and affection in the form of unlimited chicken wings.

From Niko, I have learnt everything that builds this thesis.

To Srikanth, I offer my deepest gratitude for being a validating mentor I have banked upon.

To Raghavan and Aneesh for the tremendous encouragement, and counsel.

To Morteza, for all those last minute panic support.

To Amit, for being there, nonetheless.

To Semyon, Siarhei and Nikita for being a part of the company I have appreciated so truly, in the last few years

To Marie, Karina, Nasir, Namita, Mahmood, and my PhD cohort at AiPT, and of course my colleagues in our research group, I am indebted to you for supporting through the most isolating times of PhD, COVID-19 lockdown and the new normal. To my other colleagues at AiPT, I offer my gratitude for making this PhD journey a good adventure. And of course to Debjanidi for being the closest image of a guardian, through the course of this PhD.

To Priya, Devesh, Dolon, Debasmita, Sreemoyee, Samprikta, Prachi, Pallabi, Siti, Malini, Piya, Aditi and Soumya for being sometimes the rocks, sometimes the safety nets and almost always a phone call away.

To Nand, Geeta, Preeti, Mou, Debarun and Nowo for being a part of my community, for your kindness and care, especially when I needed it most.

And to Subhanwita and Sunny, for I would not have dared otherwise.

As one lamp lights another,

nor grows less,

So nobleness enkindleth nobleness

James Russell Lowell, "Yussouf"

Contents

List of Figures

List of Tables

Acronyms

ESA Excited State Absorption. 60

MOPA Laser Induced Forward Transfer. 107

MOPA Master Oscillator Power Amplifier. 107

NA Numerical Aperture. 126

OP − GaAs Orientation patterned gallium arsenide. 60

OPO Optical parametric amplification. 60

OPO Optical parametric oscillation. 60

PPLN Periodically poled lithium niobate. 60

QPM Quasi-Phasematching. 60

SC Supercontinuum. 60

SPM Self-Phase Modulation. 126

ZBLAN ZrF_4-BaF_2-LaF_3-AlF_3-NaF. 60

List of Publications

Conference

- Ray, P., Chichkov, N., Cozic, S., Yadav, A., Joulain, F., Hinze, U., Poulain, S., Rafailov, E. (2022). Wavelength tuning of nanosecond pulses in Erbium-doped fluoride fibre amplifier. In C. Jáuregui-Misas & V. R. Supradeepa (Eds.), Fiber Lasers XIX: Technology and Systems. SPIE. https://doi.org/10.1117/12.2609553

Journal

- Chichkov, N. B., Ray, P., Cozic, S., Yadav, A., Joulain, F., Smirnov, S. V., Hinze, U., Poulain, S., Rafailov, E. U. (2022). Amplification of nanosecond pulses in a single-mode erbium-doped fluoride fibre amplifier. In IEEE Photonics Technology Letters (pp. 1–1). Institute of Electrical and Electronics Engineers (IEEE). https://doi.org/10.1109/lpt.2022.3182149

- Ray, P., Yadav, A., Cozic, S., Joulain, F., Berthelot, T., Hinze, U., Poulain, S., Rafailov, E. U., Chichkov, N. B. (2022). Wavelength-Tuning of Nanosecond Pulses in Er-Doped Fluoride Fibre Amplifier. In IEEE Photonics Journal (Vol. 14, Issue 5, pp. 1–5). Institute of Electrical and Electronics Engineers (IEEE). https://doi.org/10.1109/jphot.2022.3206104

Chapter One

Introduction

1.1 The Mid-Infrared

Looking into the electromagnetic spectrum, the mid-wave infrared (MWIR) or mid-infrared (Mid-IR) sits within the extended infrared region, beyond the visible spectrum, and is a supplementary classification within the IR. ISO20473:2007 defines the spectral bands for Optics and Photonics and places the mid-IR in the 3–50 μm range. However, the research community has long considered the mid-IR concomitant with the 2.5–25 μm molecular fingerprinting region [1], a significant area which opens up opportunities for a plethora of commercial applications.

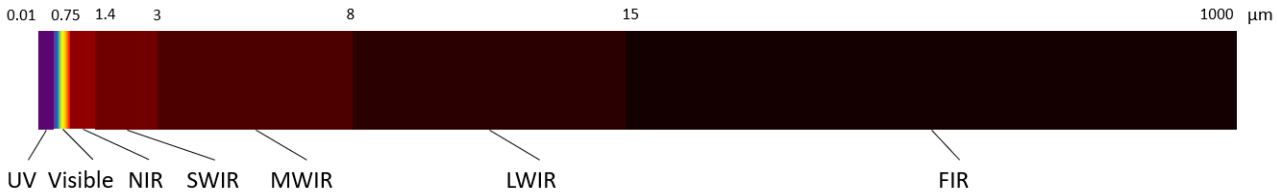

Figure 1.1: Mid-IR Spectrum

The mid-IR region has drawn interest since the 1960s with its potential for exploration into the molecular fingerprinting region Fig.1.2 [2] as it maps into the rotational-vibrational excitation spectra of the functional groups of many biological molecules, making it viable for spectroscopic

sensing, by the measurement of absorptive and transmissive properties of such substances. Mid-IR spectroscopic applications include detection of organic molecules for gas and chemical identification, food authentication, breath analysis, environmental monitoring, detection of colour neutral plastics, monitoring of industrial processes and analysis of fast chemical events. Highly efficient water absorption windows within this region also facilitates mid-IR based technologies in remote sensing applications [3], like LIDAR [4], and free space optical communications [5, 6].

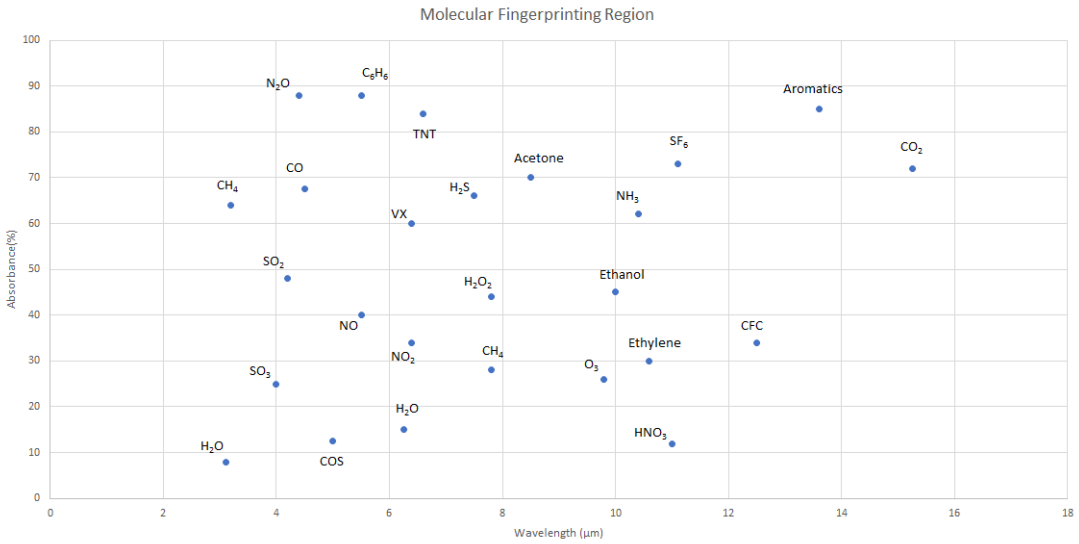

Figure 1.2: Molecular Fingerprinting Region

In medicine, mid-IR technologies become notably more significant. Mid-IR based medical instrumentation helps precise identification of bio-molecules, making them substantially sensitive and safer imaging and sensing diagnostic tools [7, 8]. Access to the molecular fingerprinting region gives the mid-IR wavelengths an inherent advantage over its UV and NIR counterparts in the electromagnetic spectrum. Additionally, presence of the strong water absorption window between 3-5 μm and 8–13 μm [9, 10], allows more absorption of these wavelengths in water compared to surrounding tissues, enabling more heat deposition in a sub-micron level spot size, without additional damage to the adjacent areas. This property also makes mid-IR lasers ideal contenders for tissue ablation applications. While shorter wavelengths like x-ray and UV radiation with smaller beam-spot size and resolution may be commonly applied in medicine, they exhibit ionisation properties

which have reportedly led to carcinogenic effects in tissue. In this context, longer mid-IR wavelengths are non-ionising, hence theoretically less risky alternatives to these established technologies.

NIR vs Mid-IR

Amongst infrared laser applications, the most competitive rival for a mid-IR source are the ones operating in the near-IR wavelength window. The major advantage of IR spectroscopy is that the methods offer non-destructive testing with little to no sample preparation. When evaluating options in IR spectroscopy, both near infrared (NIR) and mid-infrared (mid-IR) sources become competing varieties to choose from. While NIR spectroscopy require a larger energy input, the output spectra are slightly complex due to interaction of the fundamental with combination and overtone bands. On the other hand, mid-IR spectroscopy involves light interaction with the fundamental band thereby producing an unadulterated spectrum, permitting easier component analysis. NIR spectroscopy have at least two distinctive advantages over mid-IR, as it employs reflection measurements in addition to absorption and transmission. Besides, NIR sampling also have been demonstrated to be better for large volumes, inhomogeneous distributions, and trace analysis, than mid-IR which needs smaller, more evenly distributed volume of samples. Due to the severe absorption of the mid-IR spectral range, NIR imaging is the superior option compared to mid-IR, allowing NIR images to have better resolution of the fine internal structures, while making the process non-destructive. The mid-IR imaging modality, on the other hand, needs to be accompanied by additional chemical analysis requiring very small, sample sizes [11].

According to current statistical estimates, global mid-infrared lasers market was estimated to be at $ 747.60 million (£ 611.78 mn) in 2020 and is predicted to be worth $1,467.91 million (£ 1200.49 mn) by 2028, with an annual rate of increase of 8.8%. The market growth is attributed to the rising demand for laser-spectroscopic devices, especially due to their potential in environmental monitoring applications [12].

Currently, the main limitations for mid-IR based technologies are the bulky size and weight of lasers, a lack of available tunable sources, and a dearth of efficient light delivery systems operating

in this wavelength region. Recent developments in semiconductor quantum cascade, inter-band cascade, and distributed feedback laser diodes generating light in the mid-IR, have been deemed as promising sources. Furthermore, for environmental sensing and breath analysis applications, the portability of the instrument can be an added advantage. Optical parametric oscillator (OPO)-based systems can provide broad tunability, however, they involve intricate alignment susceptible to being de-aligned during transportation for remote applications. For applications in medicine, an essential requirement is the appropriate configuration of light delivery for laser tissue interaction, so having bulky lasers often poses a restriction of space and ease of operation. For this purpose, fibre-based systems are remarkable due to their diffraction-limited beam quality, significant conversion efficiency, longer interaction length, and capability to deliver high power pulses at a distance from the pump and seed sources while still providing a relatively compact geometry for easier operation. By combining the qualities of tunable sources with fibre-based systems, it is possible to build compact, broad-band, tunable mid-IR sources with effective systems to deliver light at a distance away from the source.

1.2 Brief Review of Applications of Mid-IR Lasers

To develop efficient mid-IR sources, it is critical to review potential applications briefly and estimate required parameters to optimise for building practical mid-IR sources. The foremost motivation in investing in and investigating such sources is the presence of the strongest water absorption maxima in the IR region and the capacity of these wavelengths to produce resonance in the bonds of organic molecules. These properties make them excellent candidates for any diagnostic, sensing, or heat delivery application in broad areas.

Applications In Medicine

Promising applications for Mid-IR laser sources in medicine have been implemented in both diagnostics and surgery. To identify nitric oxide (NO) detection in exhaled breath for detection of

inflammation in airway as a result of lung diseases, Off-axis integrated-cavity output spectroscopy (OA-ICOS) scheme was demonstrated with a CW mid-IR DFB-QC laser [13]. Studies have reported [14] solid-state lasers generating tunable, parametric light in Mid-IR, with high radiation intensity and low pulse energy at high repetition rate for minimally invasive and precise neuro-, cardio- and ophthalmic surgeries. Solid state Er:YAG, Tm:YAG in combination with Tm fibre laser have been used to perform Lithotripsy for removal of urinary stones [15]. Diode pumped Er:YAG solid state lasers were used for dental composite ablation in the research carried out by Fried et al.[16]. Clinical spectroscopic Mid-IR laser breath analyser have been implemented for fast, non-invasive monitoring of patients health from exhaled air [17]. Skin cancer detection with Raman spectroscopy have been explored at mid-IR wavelengths[18]. Moreover, mid-IR supercontinuum generation between 3-15 μm with chalcogenide glass fibres have been proposed for in-vivo early cancer diagnosis by photoluminescence of colon tissue [19].

Applications In Imaging

Recently, there have been a few noteworthy applications in mid-IR imaging based on the principle of bond selective detection with mid-IR wavelengths. Investigational studies have utilised the mid-IR photo-thermal effect in microscopy to suppress excess water absorption background to produce high quality images with sub-micron resolution[20]. Current research have demonstrated dynamic intracellular imaging using mid-infrared optoacoustic microscopy, where bond specific optical absorption is detected with ultrasound transducers [21]. Third-order Sum Frequency Generation microscopy [22] is another mid-IR driven, bond selective microscopy technique with an OPO source integrated with a laser-scanning imaging system and an inverted microscope frame. There have been few emergent technologies applied to developing mid-IR time-domain optical coherent tomographs [23, 24, 25] which have combined mid-IR sources with Michelson's interferometer for detection. Recently, high speed mid-IR OCTs with standard silicon-based CCD cameras have been also been demonstrated [26].

Applications In Environmental Sensing

In the field of environmental sensing, various Mid-IR systems, including ones with the capabilities of remote operation, have been investigated over the last decade. Explosive detection from over 100 m using mid-IR technology have been reported [27]. Mid-IR techniques like degenerate four-wave mixing (DFWM), polarisation spectroscopy (PS), and laser-induced thermal grating spectroscopy (LITGS) have been applied in sensitive combustion diagnostics [28]. The concept of remote detection of radioactivity by inducing electron avalanche breakdown of air with mid-IR lasers have been reported [29]. Mid-IR laser spectroscopy have been implemented in Huabei Oilfield to detect oil content in sludge to determine further treatment and discharge [30]. With the prospect of so many applications, Mid-IR detection has even been employed for detecting the chemical composition of articles with cultural heritage [31]. These applications warrant the need for sophisticated Mid-IR sources for the further advancement of these technologies, as well as for finding more use-cases in the field.

Applications In Material Processing

There are several Mid-IR laser material processing applications which have been explored, e.g., Cr:CdSe has been proposed as economic mid-IR laser material for biomaterial processing applications. Research [32] describes the construction of tunable Cr:CdSe laser with nanosecond pulse operation operating within 2.25 to 3.08 μm and have been considered for clinical dental ablation. Mid-IR nanosecond pulses have been used to study the process of light-to-mechanical energy conversion by analysing the emission of shock waves and cavitation, which are important processes for laser etching and ablation [33]. Mid-IR lasers have also found a place in industrial applications for their ability to write fine surface structures (laser-induced periodic surface structures or LIPSS or ripples) on substrates with femtosecond and nanosecond pulses [34, 35, 36], a method that is implemented for developing solar cells [37] and waveguides, creating colours without coatings [38, 39] and for inducing nonlinear processes like surface Raman scattering (SRS). These applications provide a compelling justification for research and development of mid-IR sources with parameters catered to

material processing applications.

Applications In Defence

Mid-IR lasers have been considered for military applications[40]. Mid-IR laser sources can be implemented for military countermeasures, as they could help prevent heat-seeking missiles with mid-IR detectors from homing in on aircraft thermal signatures [41]. GaSb Laser diodes have been used for atmospheric propagation research to detect atmospheric effects at optical wavelengths [42, 43]. For defence, aerospace and security applications, micro-structured Photonic band-gap fibres (PBGF) have also been studied [44]. Research on methods to produce simple component configuration, feasible nonlinear wavelength conversion, efficient power scaling, good beam quality, and the possibility to transit between cw and pulse operations with ease can result in proficient mid-IR sources for defence applications.

1.3 Brief introduction to sources in Mid-IR

Depending on the nature of commercial and scientific applications in the mid-IR, various sources have been devised. The most common mid-IR source is a laser which can provide a coherent, tunable, narrow linewidth, virtually diffraction-limited beam, with options of continuous wave and pulsed mode operation. Mid-IR lasers again can belong to different categories including thermal emitters, solid-state, semiconductors, parametric, crystalline, and fibre-based systems. Though not as prevalent, there are also thermal sources which are used for applications working in this wavelength range. Relevant mid-IR sources have been reviewed by [45, 46, 47, 48].

Thermal emitters

Classically, IR sources have a thermal origin, but efficient thermal sources in the mid-IR are not as common. Recently, studies have explored development of thermal mid-IR sources[49, 50, 51] for

practical applications in gas sensing [52, 53, 54] which can subsequently be translated to the fields of spectroscopy, medicine, military, transportation, aerospace, HVAC (heating, ventilation & air conditioning), and industrial or environmental monitoring.Thermal emitters in mid-IR can consist of ceramic elements emitting 2–10 μm and quartz elements emitting 1.5–8 μm. More sophisticated ones include plasmonic sources [55, 56, 57] where periodic 2D metallic microstructures are fabricated on a substrate followed by a selective surface plasmon resonance enhancement in the metals determined by the periodicity of the structure, and photonic crystal-MQW structures [58] which utilises a narrowband response photonic crystal pattern (3D) etched on a p-n diode structure consisting of MQW. An inter-sub-band transition in the MQW resonates with the photonic crystal resonance, emitting mid-IR radiation with high efficiency[59].

Solid State or Crystalline Lasers

Traditional solid-state lasers worked on the principle of vibrionic processes occurring in transition metal ions (chromium, copper, iron, cobalt vanadium etc), which were doped in a host crystal substrate. In such lasers, interaction between the electronic levels and lattice vibrations can cause emission and absorption of both photons and phonons during the laser transitions. The net result of such a vibrational-electronic phenomena is the homogeneous broadening of the laser transition, leading to a significant gain bandwidth. However, the transition metals do not emit in the mid-IR. The close alternatives are rare earth, lanthanide ions like Tm^{3+}, Ho^{3+}, Er^{3+}, Dy^{3+}, Pr^{3+}, etc., and the trivalent actinides, but the transition processes in these ions are not always vibrionic in nature. Even if vibrionic processes exist in rare earth ions, they have much smaller bandwidths. Despite this, phonons play a crucial role for laser transitions in rare earth ions. The bandwidth of transitions in rare earth ions is determined by Stark splitting and inhomogeneous broadening, in addition to the vibrionic interactions. The influence of phonons on the laser transition cause a broadening of the laser bands, making them tunable. Moreover, divalent transition ions like Co, Ni, Cr, and Fe produce tunable lasers in mid-IR.

Solid state, vibrionic mid-IR sources like Cr:ZnSe or Cr:ZnS have been shown to operate

within the wavelength range of 1.8-3.4 μm and requires pumping within the range of 1.5-1.9 μm [60]. These lasers can also operate as pumps for highly nonlinear materials like Gallium Arsenide [61] which require pumping near 2μm due to multi-phonon absorption at lower wavelengths [62]. Cr^{2+}-doped II–VI compounds emit broadly between 2-4 μm. Doping with Fe^{2+} ions shifts the emission range between 4-5 μm, pulsed Fe:ZnSe lasers have been demonstrated with 2.94μm pumping with passively-Q-switched, nanosecond Er:YAG laser. Tm^{3+} / Ho^{3+} doped crystalline lasers have been shown to emit between around 2 μm with different crystalline hosts. Er^{3+} doped crystalline lasers emits close to 3 μm. Common crystalline hosts include yttrium aluminium garnet (YAG), yttrium scandium gallium garnett (YSGG), yttrium lithium fluoride (YLF) etc.

Semiconductor Sources

First mid-IR laser line emissions from semiconductor-based sources were reported in 1963 at 3.1 μm and 5.3 μm employing diffused InAs and InSb p-n junction diodes. Later, narrow gap Pb and Pb-Sn based IV–VI semiconductors were used to demonstrate longer wavelength up to 30 μm. Prominent technologies in Mid-IR semiconductor lasers include the hetero-junction laser diodes, quantum cascade lasers and inter-band cascade lasers among others.

Hetero-junction Laser Diodes

Hetero-junction laser diodes usually constitute of two or more different kinds of semiconductors materials for their n and p regions, usually in the form of layers. Usually, these materials have considerably different refractive indices and dissimilar lattice constants, however they are lattice matched at the boundary with the neighbouring layers. A typical hetero-junction laser structure consists of a Fabry Perot structure with an un-doped active region placed between two relatively thicker confining layers of p and n type doping, and is pumped electrically by injecting carriers along the direction normal to the layers which causes electron-hole recombination to produce photons. The p-n layers neighbouring the active region induce better photon confinement and reduce the lasing threshold of the current. For emission in the mid-IR, especially between 2-5 μm the active region

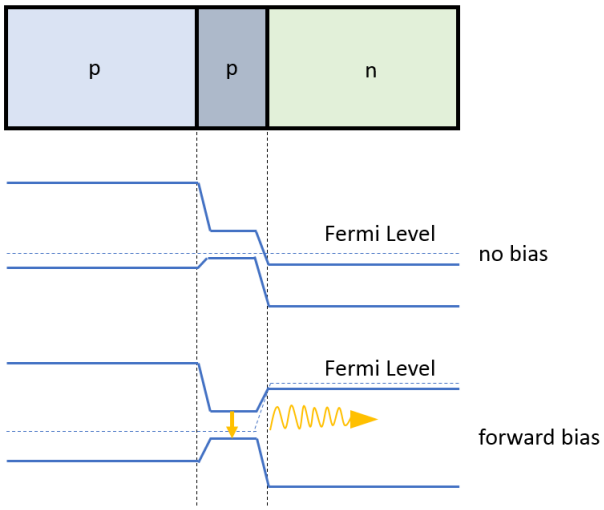

Figure 1.3: Operation of Hetero junction laser diodes

consists of a material with narrow ban gap typically $\sim$ 0.25–0.62 eV which converts to band gap thicknesses of 0.15–0.5 μm depending on the emission wavelengths and optical confinement factor. Auger recombination is the dominant process dictating at the shorter-wavelength ranges, between 1.9–2.7 μm [63, 64].

The possibility of fabricating narrow gap semiconductor structures permits the development of quantum well (QW) structures in mid-IR, requiring lower threshold currents and thickness manipulation to generate emissions. QW structures are constructed by band gap engineering in the Type I and Type II configurations, successfully implemented in III–V quantum well lasers like GaSb or InAs. Antimonide- based Quantum Well Laser Diodes are superior choices within the 2-3.5 μ wavelength range [65]

Quantum Cascade Lasers

Another important source in the Mid-IR wavelength region is Quantum Cascade Laser (QCL). This is a semiconductor injection laser device which operate on the principles of quantum confinement and quantum tunnelling, an inherently different underlying principle from semiconductor laser diode

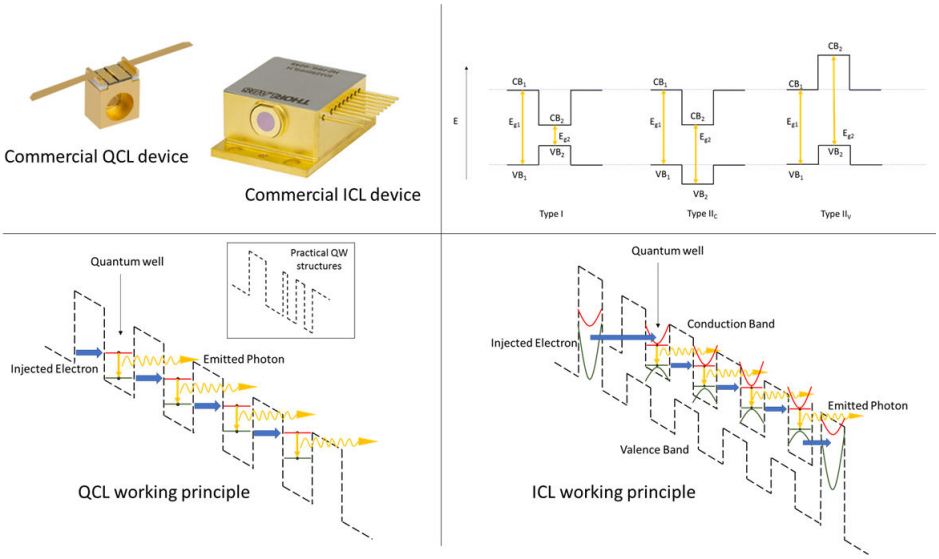

Figure 1.4: Operation of QCL and ICL

operation based on electron-hole recombination, discussed in the previous section. In QCLs, the conduction band contains both the laser transition levels.A QCL structure is implemented by alternating semiconductor material layers creating cascading quantum energy wells, which bind electrons, injected by resonant quantum tunnelling, to distinct energy states, this is quantum confinement. While moving through a QCL structure driven by the bias voltage, electrons traverse through several quantum wells, interacting with multiple active regions where they switch from a higher valence band energy state to a lower one, emitting photons. The electrons then move through the relaxation region and injected back to the upper state, re-instating the ability to generate more photons. By ensuring population inversion, it is possible to match the gain to losses by increasing the injection current, allowing a single electron to emit multiple photons based on the number of quantum wells.

The layer structure of the QCL determines the emission wavelength and not the lasing medium as in the case of solid state lasers. This is accomplished by band structure engineering of the layer structure using molecular beam epitaxy, thus making it is possible to tailor the output wavelength from the device. Common materials used in such lasers include InGaAs and InAlAs layers, InAs / AlSb, Si / SiGe and GaN-based materials. The concept of QCL was first proposed in 1971 [66] and demonstrated in operation at 4.2 μm by Faist et al. [67] in 1994. Initially, only pulsed

operation could be possible at very low temperatures requiring high threshold current, however the current state of the art QCL devices can easily operate at room temperatures demonstrating more than 3 μm tunability and continuous wave operation in the mid-IR [68].

Interband Cascade Lasers

A corresponding technology to QCL functioning within the 2-4 μm is the Interband Cascade Laser (ICL) [69] which employ the type II quantum well structure as the active region and as a result the band gap is decided by the thickness of the quantum well and not the band gap of the composing material. This enables engineering of the ICL band gap to generate wavelengths encompassing the whole of the mid-IR regions.

To summarise semiconductor laser performances in the 2-5 μm region, Auger recombination, which depends on the emission wavelength, predominates in type I quantum well inter-band devices operating in the 1.9–2.7 μm range. In spite of having lesser overlap of wave functions, inter-band type II "W" lasers demonstrate enhanced performance in the 3–7 μm wavelength range. For the longer wavelengths in mid-IR, QCLs are the leading technology, with their performance restrained by leakages and inter-valley scattering [64].

In recent research, many novel sources in mid-IR have been reported. These include GaAs-based Vertical Cavity Surface Emitting Lasers (VCSELs) emitting at 3.35 μm operating at room temperature conditions and continuous wave mode[70]. Investigations have been conducted on distributed feedback (DFB) based ICLs [71]. DFB-QCLs emitting dual wavelengths without cross-talk in the longer mid-d-IR have been analysed [72] for applications in multi-species trace gas spectroscopy. Antimonide based HJLD like GaSb-based diode lasers, have demonstrated wide wavelength tuning range between 1.9–3.2 μm[73, 74].

Parametric Sources

Parametric nonlinear frequency conversion is one of the most versatile methods to generate wavelengths in the Mid-IR and Far-IR region and wavelengths that are not easily available from band gap energies. Parametric sources include a highly intense coherent light source incident and interacting with materials having a degree of inherent nonlinearity arising due to a lack of inversion symmetry. While interacting with such a medium, the frequency of the incident light changes when the electrical polarization density of the material atoms reacts nonlinearly to the electric field of the incident light. In addition to the possibility of obtaining tailored wavelengths, parametric sources are capable of emitting light having narrow linewidths and ultrawide tunability. The high power operation in these sources is constrained by the properties of the nonlinear material [75]. Several frequencies up- and down conversion process governs the nonlinear frequency conversion process including second harmonic generation (SHG), sum frequency generation (SFG), difference frequency generation (DFG) etc. For generation of longer mid-IR wavelengths, DFG and analogous three wave mixing process like optical parametric amplification (OPA) and optical parametric oscillation (OPO) become more relevant.

Difference frequency generation as the name suggests is the nonlinear process in which two photons with different frequencies interact to produce a third frequency equal to the difference of them. Analogous to this, in OPA, these two wavelengths are termed pump (shorter) and signal (longer) and the pump is absorbed to produce signal and idler, where the idler possesses the difference frequency of the pump and signal. When placed in a resonator setup, this frequency conversion is called an OPO, which allows the build up of signal and idler photons to generate an intense output beam. Optical parametric generation (OPG) is another subsequent process related to DFG, in which the OPA is amplified in a single pass without requiring an input signal, but from a small signal originating due to spontaneous optical parametric fluorescence.

Optical parametric conversion processes to generate Mid-IR wavelengths have been extensively demonstrated in bulk materials, fibres and waveguides, in both continuous and pulsed modes [76, 77, 78, 79, 80, 81, 82].It has also been utilised to generate frequency combs in the Mid-IR for

spectroscopic and sensing applications[83, 84].

Supercontinuum sources

Finding broadband sources in mid-IR, generating sufficient output power, has been a challenge for some time. One of the sources considered is a supercontinuum source, an ultra broadband spectral range produced from a nonlinear fibre or waveguide pumped by high peak power ultrashort pulses from a mode-locked source. The first observation of the process was reported in 1965 arising due to self-focusing of ruby laser pulses in liquid carbon-disulpide [85]. The limitation in such a source is often that the average output power is of the order of milliwatts. To increase the output power, higher pump powers are necessary to deliver sufficient pulse energies to support the nonlinear process. The main nonlinear processes include self phase modulation, four wave mixing, soliton dynamics and stimulated Raman scattering amongst others [86].In current progress, broadband ZBLAN fibres, with thulium doping have demonstrated power output of 13 W spanning between 1.9 to 4.3 μm wavelength range near 3 μm [87]. The widest supercontinuum range achieved was between 1.9 to 4.9 μm with ∼12 W average power [88].

Microresonators and Frequency Combs

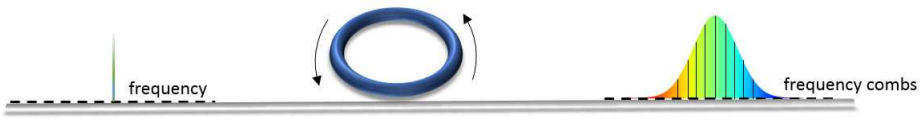

Figure 1.5: Operation of a microresonator to generate optical frequency combs

Optical Microresonators have emerged as promising sources in the Mid-IR wavelength region. These micro-cavities generate resonant frequencies which depend on their size and by principle are able to confine light into small modal volumes by recirculating the light through resonance. Additionally, these devices have high quality factor, thus making them suitable sources for many light-

matter interaction. [89]. Several types of microresonator-based devices in the mid-IR have been reported [90].These include ZBLAN, aluminium fluoride, and indium fluoride microsphere Whispering Gallery Mode (WGM) resonators [91], Glass based WGM and Crystalline microresonators.

One significant application of such micro-resonators is the generation of optical frequency combs (OFC) by parametric frequency conversion, that can be utilised for high precision spectroscopy and for sensing in molecular fingerprinting region with superior sensitivity and acquisition speeds[92, 9].Optical frequency comb generation in the mid-IR has been demonstrated in silicon, Si_3N_4, crystalline CaF_2 and MgF_2 microresonators [93, 94, 95, 96, 97, 98].In recent progress, microresonators generating optical frequency combs having broad tunability over hundreds of nanometres in the mid-IR have been demonstrated[99].

Fibre-based Systems

Applications in material processing, medicine, imaging, spectroscopy, defence require compact, robust, flexible, and high-quality laser beam delivery systems. Fibre-based systems are promising solutions, as they can be combined with free space and fibre laser sources to deliver diffraction-limited beam quality. Compared to free space delivery systems, fibres offer several significant advantages including mechanical flexibility, compactness, a great degree of control over the separation of source and target, reduced dependence on complicated optomechanical alignment, easier access to smaller spaces, improved laser beam intensity profile, beam stability minus jitters, options for spatial filtering, easy replacement and repair, and reduced costs. However, these systems are not without their constraints which include limits on deliverable power/energy, affected beam quality and polarisation in high power beams. Present day mid-IR fibre technologies [100, 101] have explored into gas filled hollow-core silica fibres which have shown high power output with broad tunable range of over 600 μm.

1.4 Thesis Scope

Mid-IR research continues to be extensive and expanding. A brief synopsis of applications and sources in mid-IR reveals that there are still several potential opportunities, and thus the motivation to continue developing efficient mid-IR sources for implementation in different areas. With the two-fold advantage of the presence of the water absorption window and the molecular fingerprinting region, lasers near 3 μm can prove to be versatile sources for surgery and diagnostics, or other laser material processing applications that exploit the window of water absorption maxima in this wavelength range, if they can achieve the required output powers, relatively broad tunability, and optimised pulse durations necessary for the application under consideration. This thesis focuses on developing a source for the laser material processing applications in mid-IR, with a focus on wavelengths close to 3 μm. To deliver these wavelengths at high average powers, with good beam quality in a compact and robust format, the choice of fibre-based systems become evident. This provides adequate justification to explore fibre amplifiers that operate in this wavelength range. This thesis investigates an erbium doped fluoride fibre amplifier operating near 3 μm wavelength region.

To seed the fibre amplifier, this project evaluates a nanosecond optical parametric oscillator (OPO) to obtain viable wavelengths in the mid-IR, particularly near 3 μm. It is possible to use this source to attain high power scaling in addition to the benefit of wide tunability. Alternatively, these amplifiers can also be seeded with high power diodes operating near 3 μm, but any limits on the input powers and tunability range of the seed source can constrain the analysis of amplification and wavelength tunability of the fibre amplifier. Consequently, this work involves the investigation of power scaling and wavelength tuning of an Er:ZBLAN for operation near 3 μm, in the mid-IR spectral range, seeded by a nanosecond pulsed OPO. This type of fibre amplifier holds a lot of promise in the field of biomedical applications, specifically those involving laser-tissue interaction.

1.5 Thesis Outline

For the ease of understanding the work completed for this PhD, this section outlines the structure of the thesis. The thesis is divided into 6 chapters :

- **Chapter 1** provides the motivation for this Thesis. It discusses the Mid Infrared Region and what attracts research in this spectral region. It considers various sources generating in these wavelengths. It also discusses the current and potential applications in medicine, imaging, material processing, environmental monitoring and defence.
- **Chapter 2** revisits the fundamentals, the theory of nonlinear frequency conversion and quasiphasematching for the generation of mid-IR wavelengths in optical parametric oscillators. Furthermore, it discusses the operational principles and the materials required for the understanding to develop fibre amplifiers in the mid-IR. Finally, the chapter finally reviews the current state-of-the-art fibre-based mid-IR sources operating 3 μm.
- **Chapter 3** describes the set-up and characterization of a nanosecond pulse, tunable, PPLN-based optical parametric oscillator as a mid-IR source operating near 3 μm. The OPO is used as a tool to further investigate laser light delivery in doped fluoride fibres as a potential seed source for power amplification and wavelength tuning near 3 μm.
- **Chapter 4** discusses the investigation of amplification and power scaling of an erbium doped fibre amplifier centred at 2.8 μm using the nanosecond PPLN-based OPO as a seed in a master oscillator power amplifier architecture.
- **Chapter 5** summarises the investigation of wavelength tuning and gain bandwidth in an erbium doped fluoride fibre amplifier centred at 2.8 μm seeded with the nanosecond pulse, widely tunable PPLN-based OPO source.
- **Chapter 6** recapitulates important results from the work and analyses potential future areas and applications to which the results can be extended into.

Chapter Two

Theory & Literature Review

To develop highly efficient sources that emit in the mid-IR, it is important to understand the fundamental theoretical concepts that drive the processes, and the current technological resources available to do so. This chapter discusses the key processes that govern nonlinear frequency conversion, reviews the materials and the relevant properties which support emission of these wavelengths, not only for parametric conversion but also for fibre-based systems. This chapter also investigates the current state-of-the-art research and technologies which contribute significantly to the development of compact, efficient mid-IR sources operating near 3 μm.

2.1 Fundamentals of nonlinear frequency conversion

In light-matter interaction, the scope of linear optics extends into everyday optical phenomena such as reflection, refraction or more intricate ones like interference, diffraction, or polarisation. In these cases, the frequency of the incident light wave remains the same before and after the interaction and any increase in intensity at the input results in a linear increase in the output light. Linear optics also follows the superposition principle, an inherent property of any linear system whereby if, reflection of beam A results in a change of wave vector direction from $k1_i$ to $k1_o$ and that of beam B from $k2_i$ to $k2_o$, then when we reflect a combination of beams A and B simultaneously, $k1_i + k1_o$ the resultant beam would have an output $k2_i + k2_o$. In case of linear optics, the electric field of

the incident light is superficial, although there is a small linear polarization of the molecules in the medium, there is no impact on any optical properties of the material itself.

But if the incident beam is intense, like in case of a laser, the wave interacts with the medium at the molecular level, initiating changes to the structure, even if temporary. This change is usually a strong polarization of the molecule due to the high electric field component of the incident light. This kind of molecular level interaction causes the linear superposition principle to fail, yielding a nonlinear response from the medium, and the interaction moves into the domain of nonlinear optics.

Optical Susceptibility

The dipole moment, $\vec{p}$ generated in each molecule due to light-matter interaction, aggregates into the Polarization Density $\vec{P}(t)$ for the whole medium. This can be expressed as

$$P(t) = \epsilon_0 \chi^{(1)} \tilde{E(t)} \tag{2.1}$$

where

ϵ_0 = Electric permittivity

$\chi^{(1)}$ = Linear Optical Susceptibility

$\tilde{E(t)}$ = Scalar Electric Field component of the incident beam

can be considered as a linear response to the incident light beam. However, if the beam is an intense laser, the electric field component, also a scalar in this case, is very high; consequently, the susceptibility is no longer linear, and higher order susceptibilities begin contributing to the response. Applying Taylor's expansion to 2.1 and expanding, we get an expression for the Polarization density given by :

$$P(t) = \epsilon_0 \chi^{(1)} \tilde{E(t)} + \epsilon_0 \chi^{(2)} \tilde{E(t)}^2 + \epsilon_0 \chi^{(3)} \tilde{E(t)}^3 + ... \tag{2.2}$$

where $\chi^{(n)}$ are higher order nonlinear optical susceptibilities.

$$P(t) = P^{(1)}(t) + P^{(2)}(t) + P^{(2)}(t) + ... \tag{2.3}$$

where $P^{(2)}(t)$ and $P^{(3)}(t)$ are the second and third order nonlinear polarization.

There are a few key assumptions in order for this expression to hold true:

- The nonlinear material is lossless in nature
- There is no dispersion in the medium as the incident light passes through it
- The response of the medium to the incident wave is instantaneous
- Nonlinear optical Susceptibility $\chi^{(n)}$ is usually dependent on the frequency of the incident wave. However, to maintain simplicity in the analysis of these phenomena, $\chi^{(n)}$ is assumed to be constant

The second term in Eqn.2.3, $P^{(2)}(t)$, gives rise to several interesting nonlinear parametric phenomena including second harmonic generation (SHG), sum frequency generation (SFG), Difference frequency generation (DFG) and Optical parametric fluorescence or better, Optical parametric oscillation (OPO) along with Optical parametric generation(OPG), often categorised as Three Wave Mixing. From the aspect of the nonlinear medium, $\chi^{(2)}$ processes are shown to occur in crystals without inversion symmetry (non-centrosymmetric). This classical definition indicates that frequency conversion by three wave mixing is not possible in isotropic media, which are generally centrosymmetric in nature. However, at present, methods like structural domain engineering, which is used to modify the crystal structure of isotropic, centrosymmetric crystals, can help initiate as well as sustain these processes.

The third term $P^{(3)}(t)$ contributes to third order nonlinear optical processes like third harmonic generation (THG), Intensity dependent refractive index, stimulated Raman scattering, optical Kerr effect, stimulated Brillouin scattering, multi-photon absorption, etc and can occur in both cen-

trosymmetric and non-centrosymmetric media. However, detailed discussion of these processes are beyond the scope of this thesis.

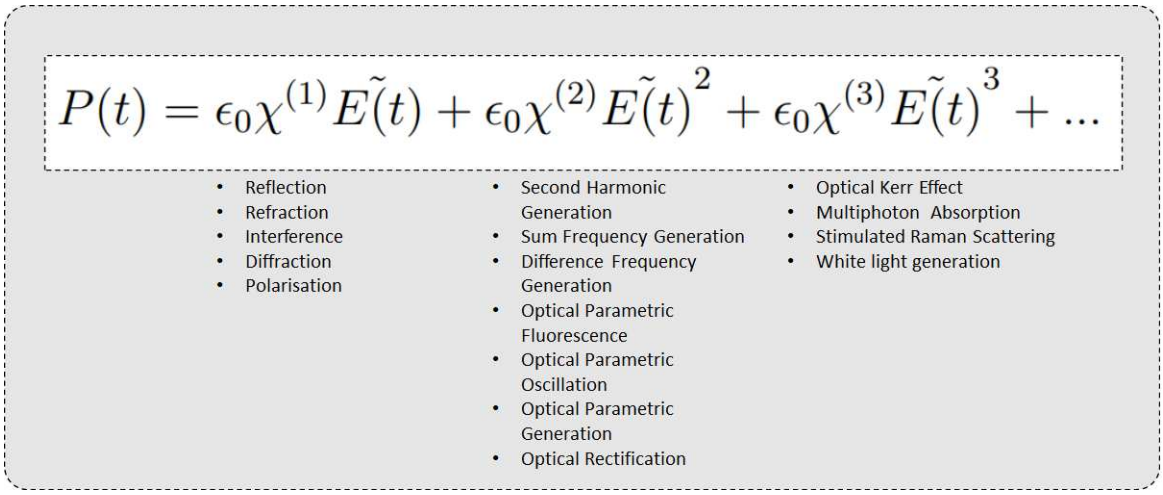

Figure 2.1: Summary of Higher Order Nonlinear Processes

Three wave mixing

In nonlinear $\chi^{(2)}$ processes, both the energy and the momentum of the incident and emitted waves are conserved. The frequency conversion arises from the principle of conservation of energy, while the principle of conservation of momentum determines the required condition that needs to be satisfied for this nonlinear frequency conversion to occur.

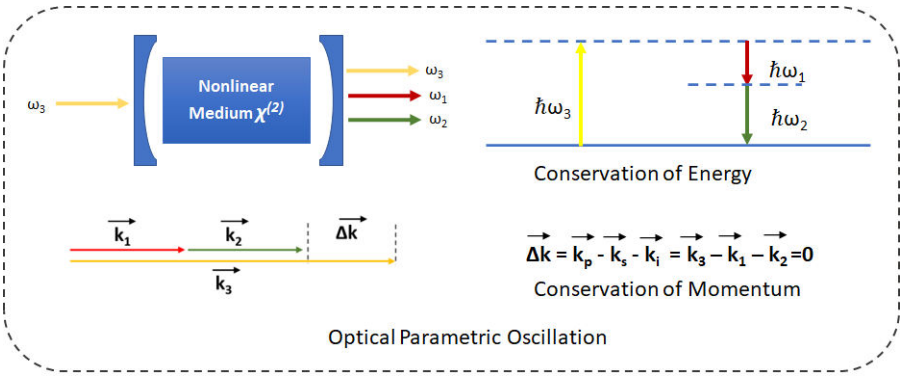

Figure 2.2: Three Wave Mixing Processes and Difference Frequency Generation

Fig.2.2 lays out a summary of significant parametric three wave mixing processes contributed by $P^{(2)}(t)$. Amongst other second order nonlinear optical phenomena, optical parametric oscillation, especially, is of paramount importance in this thesis due to its capacity to generate amplified signals of shorter frequencies, or longer wavelengths, from a pump source, following principles of nonlinear frequency conversion.

In all nonlinear processes, both energy and momentum are conserved.By the principle of conservation of energy, where $E = \hbar\omega$

$$\omega_1 + \omega_2 + \omega_3 + \omega_4 + \omega_5 = \omega_0 \tag{2.4}$$

By the principle of conservation of momentum, where $P = \hbar \overrightarrow{k}$

$$\overrightarrow{k_1} + \overrightarrow{k_2} + \overrightarrow{k_3} + \overrightarrow{k_4} + \overrightarrow{k_5} = \overrightarrow{k_0} \tag{2.5}$$

When these conditions are simultaneously satisfied, it brings about the necessary limitation that needs to be overcome for the frequency conversion process to occur.

2.1.1 Manley-Rowe relations for three wave-mixing processes

To analyse the nonlinear conversion processes, the Manley-Rowe relations are considered and evaluated [102, 103]. If we consider three plane waves with frequencies ω_1, ω_2 and ω_3 propagating along the z direction and interacting in a nonlinear medium of susceptibility $\chi^{(2)}$,they can be represented as paraxial wave equations

$$\frac{dE(\omega_1)}{dz} = -i\kappa_1 E(\omega_3)E^*(\omega_2)exp(-i\Delta kz) \tag{2.6}$$

$$\frac{dE(\omega_2)}{dz} = -i\kappa_2 E(\omega_3)E^*(\omega_1)exp(-i\Delta kz) \tag{2.7}$$

$$\frac{dE(\omega_3)}{dz} = -i\kappa_3 E(\omega_1)E(\omega_2)exp(+i\Delta kz) \tag{2.8}$$

where $\kappa_i = \omega_i d_{eff}/n_i c_0$ are the coupling coefficients and $\Delta k = k_3 - k_1 - k_2$

assuming a lossless medium ($d_{eff} = d^*_{eff}$) , the corresponding intensities can be found by multiplying the equations with $n_i c_0 \epsilon_0 E^*(\omega_1)/2$ and adding the complex conjugate,

$$\left(\frac{1}{\omega_1}\right)\frac{dI(\omega_1)}{dz} = \left(\frac{1}{\omega_2}\right)\frac{dI(\omega_2)}{dz} = -\left(\frac{1}{\omega_3}\right)\frac{dI(\omega_3)}{dz} \tag{2.9}$$

indicating the annihilation of a pump photon ω_3 to create signal and idler photons ω_1 and ω_2.

For an OPO, the partial differential equations (PDE) for the plane wave amplitudes of the pump , signal and idler can be given by,

$$\frac{\partial E(\omega_1)}{\partial z} = -i\kappa_1 E(\omega_3)E^*(\omega_2)exp(i\Delta kz) \tag{2.10}$$

$$\frac{\partial E(\omega_2)}{\partial z} = -i\kappa_2 E(\omega_3)E^*(\omega_1)exp(i\Delta kz) \tag{2.11}$$

$$\frac{\partial E(\omega_3)}{\partial z} = -i\kappa_3 E(\omega_1)E(\omega_2)exp(i\Delta kz) \tag{2.12}$$

Solving these PDEs for the OPO give rise to the small signal gain, given the initial condition that initially no signal or idler is present and there is only pump $E(\omega_3)$. If the build up of the signal and idler is given by $E(\omega_{1,2}, z) = E_0(\omega_{1,2})exp(\pm\gamma z)$, on achieving phasematching,

$$G_1(l) = (\gamma l)^2 \frac{sinh^2\, gl}{(gl)^2} \tag{2.13}$$

Where γ can be given by relation,

$$\gamma^2 = \kappa_1\kappa_2|E(\omega_3)|^2 \tag{2.14}$$

and,

$$g = \sqrt{\{\gamma^2 - (\Delta k/2)^2\}} \tag{2.15}$$

When $\gamma \ll \Delta k/2$,g is imaginary and using Taylor series expansion, Eqn. 2.13 further simplifies to,

$$G_1(l) = (\gamma l)^2 \frac{sin^2(\Delta kl/2)}{(\Delta kl/2)^2} \tag{2.16}$$

For perfect phasematching, $\Delta k = 0$, $sinc^2()$ function reduces to 1

$$G_1(l) = (\gamma l)^2 \tag{2.17}$$

Thus , for plane waves, small signal gain is given by

$$G_1(l) = \kappa_1\kappa_2|E(\omega_3)|^2l^2 = \frac{\omega_1\omega_2 d_{eff}^2}{n_1n_2c_0^2}|E(\omega_3)|^2l^2 \tag{2.18}$$

The detailed analysis of Manley-Rowe relations can be found in Appendix 1.

Since laser beams are treated to be Gaussian in nature, it is important to find similar solutions for Gaussian waves. However, analysis with Gaussian waves show that the equations for plane wave and Gaussian wave are identical and the amplitude transform is simply influenced factor M given by

$$M = \frac{\omega_1\omega_2\omega_3}{\omega_1^2\omega_2^2 + \omega_1^2\omega_3^2 + \omega_2^2\omega_3^2} \tag{2.19}$$

Thus, in optical parametric oscillation (OPO), a nonlinear medium can convert a pump radiation into two lower frequency or longer wavelength components or the signal and idler frequencies. In addition to the nonlinear medium, an optical parametric oscillator includes a resonator cavity,

which helps in the building up of these small signals into significant values. OPOs are tunable as the generated frequencies are smaller than the pump frequency, and they satisfy the phasematching condition. By engineering different phasematching conditions, it is possible to produce numerous signal and idler combinations for each condition. Thus, OPOs are ideal for generating wavelengths in the IR spectral region, which usually comprise longer wavelengths or shorter frequencies, from a commonly available pump, in case of unavailability of other suitable sources.

2.1.2 Quasiphasematching

Coherent frequencies generated during nonlinear processes are made possible by fulfilling a phase-matching condition arising out of the phenomena of conservation of momentum. Nonlinear frequency conversion is possible when the interacting waves have a phase relation maintained along the direction of propagation of the waves. If this condition is not satisfied, the beams tend to walk off, reducing interaction length and thus inhibiting the conversion process.Thus, for efficient wave mixing, any phase-mismatch existing between the waves in the nonlinear media must be compensated, i.e., the mismatch must set to zero.This is represented by the expression,

$$\Delta k_q = 0$$

In three wave mixing process like optical parametric oscillation (OPOs), described by wave vectors $\overrightarrow{k_3}, \overrightarrow{k_1}$ and $\overrightarrow{k_2}$ the phase-mismatch is given by

$$\Delta k_q = k_1 + k_2 - k_3 + k_m$$

where m = order of phase-mismatch

Quasiphasematching [104], though proposed much before the widespread implementation and acceptance of the BPM technique, overrides the need for anisotropy in a nonlinear material: instead it achieves phasematching by engineering the structural configuration of an isotropic material with high effective nonlinear coefficient. This involves introducing a periodic structure in the nonlinear

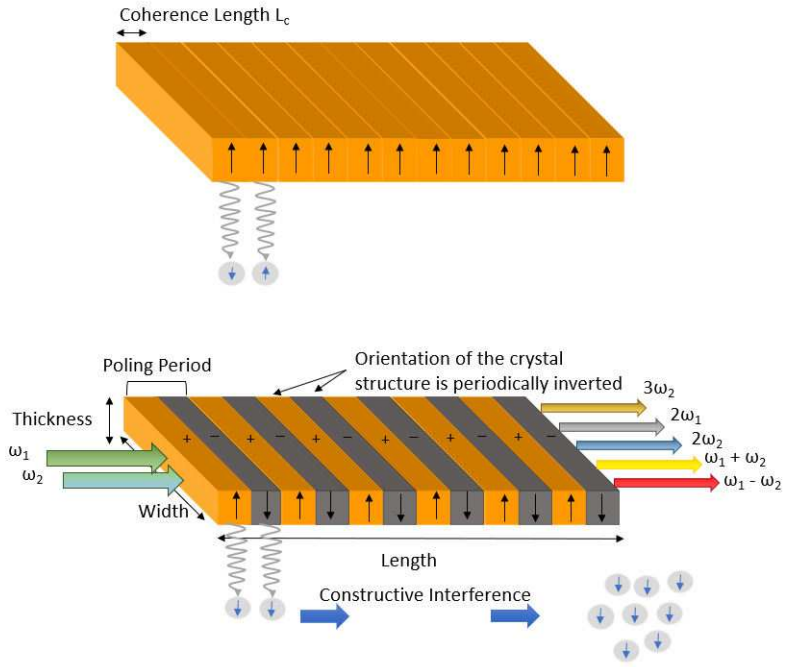

Figure 2.3: Quasiphasematching a) No Domain Period reversal results in No Phasematching Condition b) QPM Condition achieved with Domain Period reversal.

material so that the gain can build up while the light passes through the material and generate an output with amplified intensity.

As light passes through a nonlinear media, in the absence of any phasematching condition within the material, the phases of the fundamental and doubled frequencies cancel out and there is no net gain at the end of the crystal.In QPM, when phasematching condition is implemented, it is done by fabricating periods of alternating crystal structure reversal in the medium so that the phase is consequently reversed, any gain built over one domain period is no longer nullified by the next period, instead the phases add up over the domains and subsequently, the length of the crystal, and produces a magnified output. Phasematching thus results in highly efficient nonlinear conversion and substantial output power of the converted frequencies.

From the phase-mismatch condition,

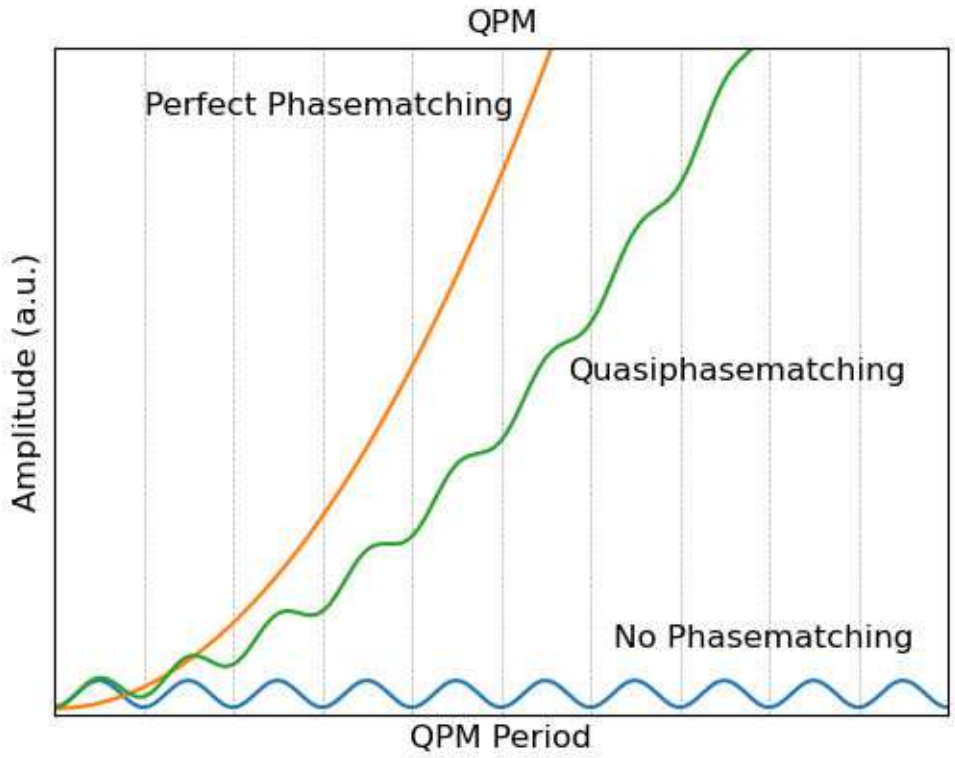

Figure 2.4: Amplitude contribution for different phasematching conditions in nonlinear frequency conversion. The blue curve indicates the amplitude has no net gain in the absence of phasematching condition. The orange curve shows the quadratic gain when perfect phasematching is achieved and finally, the green curve shows that in case of quasiphasematching, there is amplitude gain, but it is less than that achieved with perfect phasematching.The space between the vertical lines indicate 1 poling or grating period, equivalent to twice the coherent length L_c.

$$\Delta k_q = k_1 + k_2 - k_3 - \frac{2\pi}{\Lambda}$$

writing $k_m = \frac{2\pi}{\Lambda}$ where Λ relates to the periodicity of the fabricated structure required for quasiphasematching. Thus, implementing phasematching condition, i.e., $\Delta k_q = 0$,

$$\frac{2\pi}{\Lambda} = k_1 + k_2 - k_3 \tag{2.20}$$

$$\frac{1}{\Lambda} = \frac{n_1}{\lambda_1} + \frac{n_2}{\lambda_2} - \frac{n_3}{\lambda_3} \tag{2.21}$$

since $k = \frac{2\pi}{\lambda}$ .Now,

$$\Lambda = 2L_c = \frac{2\pi}{k_1 + k_2 - k_3} \tag{2.22}$$

where L_c = coherence length equivalent to half of the grating period required to achieve quasiphasematching. This length is also equal to half the period of intensity increase/decrease cycle of the generated frequencies. When phasematching condition is achieved, the converted fields grow linearly as it traverses the nonlinear medium, while the corresponding intensity rises quadratically, and the interaction generates a large output. When phasematching condition is not satisfied, the higher order harmonic grows initially but decays over a period of length due to cancellation of the opposing phases of the fundamental and the higher harmonic.When phasematching is achieved, the phases of the pump and the signal/idler frequencies add up, generating a substantial output from the crystal.

The other method of satisfying phasematching condition is achieved with birefringent crystals, termed birefringent phasematching (BPM). Additional benefits of QPM over BPM are chiefly that QPM results in higher gain and demonstrates no spatial walk off, a phenomenon typical in birefringent crystals that thwarts the process of frequency conversion. Moreover, by optimally engineering the domain period lengths, QPM condition allows the generation of a wide range of signal and idler frequencies by the process of optical parametric generation or Amplification (OPG/OPA).

Methods of achieving Quasiphasematching

QPM is realised by structurally manipulating the optical susceptibility χ of a nonlinear material and amending the phase of the incident wave as a result of it. The process of realizing this is called periodic poling which causes the crystal to generate photons of the same phase, which add up over the length of the crystal giving a very large output.

Periodic Poling

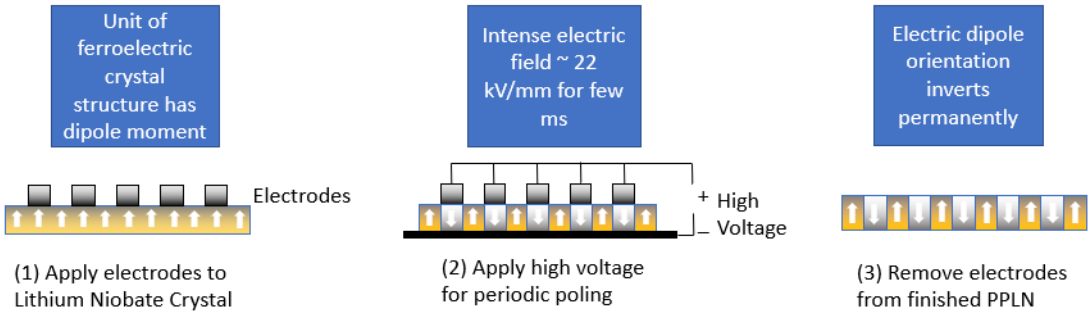

Figure 2.5: Periodic Poling in Ferroelectric Materials

In ferroelectrics and chalcopyrites, QPM is realised by the process of periodic poling. Most materials suitable for periodic poling are also inherently anisotropic in nature, however, frequency conversion phenomenon in these substances is achieved by QPM instead of BPM. Periodic poling enhances the effective nonlinear coefficient of the material undergoing the fabrication, compared to the natural nonlinear coefficient of the material.

Periodic poling technique takes advantage of the polarisability of ferroelectric and similar materials. Fig 2.3 shows the schematics of the process of implementation, which involves 3 key steps: firstly, electrodes are placed on the crystal wafer, at intervals equal to the calculated domain period required to satisfy phasematching condition for different pump and output wavelengths. This is followed by the application of a very high voltage of the order of thousands of volts, for a very

Nonlinear Material	Nonlinear Coefficient	Transparency Window
ZGP	75 pm/V	0.72–12.3 μm
CSP	84.5 pm/V	0.50-9.5 μm
Lithium niobate	27 pm/V	0.4-5 μm
Potassium titanyl phosphate	13.7 pm/V	0.35 -4.5 μm
Potassium titanyl arsenate	16.2 pm/V	0.35 -4.5 μm
Gallium arsenide	94 pm/V	0.9-17 μm
Gallium phosphide	70 pm/V	0.57 -12 μm
Gallium nitride	3.8 pm/V	0.36-7 μm

Table 2.1: Summary of Materials for nonlinear optical conversion

short period of time, which causes the polarity of the region under the electrode to be permanently reversed. This gives rise to alternating periods of inverted polarity in the crystal, on obtaining which the electrodes are removed. These reversed domains are often referred to as grating periods, and usually multiple of these grating periods are poled on a single wafer. The wafers are then cut into smaller devices with at least a few grating periods, making it possible for a single device to convert and emit multiple signal and idler combinations with a given pump wavelength source.

Common nonlinear materials which are suitable for QPM are quintessentially ferroelectrics and these include periodically poled potassium titanyl phosphate (PP-KTP), periodically poled lithium niobate (PPLN), potassium titanyl arsenate (PP-KTA), doped/ un-doped, polycrystalline zinc selenide (ZnSe) and other arsenates.

Periodically Poled Lithium Niobate (PPLN)

One of the most widely considered materials for nonlinear frequency conversion with quasiphase-matching is lithium niobate. This ferroelectric, birefringent material demonstrates a significant order of nonlinearity, and relatively wide transparency up to 5 μm, which make them attractive

Parameter	Value
Material nature	Ferroelectric
Nonlinear Coefficient (d_eff)	27 pm/V
Spectral Transparency Range	0.4-5 μm
SHG Conversion Efficiency	53%
Damage Threshold	1.5 J/cm^2

Table 2.2: Salient properties of lithium niobate

for parametric conversion and generation of wavelengths in the mid-IR, especially near 3 μm. The ferroelectric nature of the material makes them highly suitable for periodic poling, which can be achieved very quickly by applying high voltage for a few seconds. Summary of properties and structure of the material has been discussed in extensive detail in several studies [105, 106, 107].

Lithium niobate has always been a significant material for optical parametric oscillators due to its nonlinearity, transparency, and birefringence properties. Although lithium niobate is naturally birefringent, with periodic poling to achieve quasiphasematching easily, birefringence no longer remains a necessary condition for frequency conversion with OPOs[108]. Additionally, the possibility to pump such materials with standard solid state lasers like Nd:YAG operating near 1 μm make them applicable in such operation.

2.2 Current State-of-the-art with PPLN-based OPO

PPLN-based optical parametric oscillators have been investigated in research due to their broad tunability in mid-IR. The focus of the research has been to build compact sources for spectroscopic applications, where the primary requirements include sufficiently high power and considerably narrow linewidths, to explore the mid-IR wavelength region. As the OPOs can generate tailored wavelengths, they have also been utilised as pump sources to generate high power outputs at custom

wavelengths that are not commercially available for specialized applications. While the PPLN-based OPO was introduced back in the 60's, they have remained relevant till date, with attempts to obtain narrower linewidths and more stable outputs in terms of wavelength and power. A single FP etalon is used to generate a narrow linewidth, long pulse, watt-level average power OPO operating near 3.7 μm. The achieved theoretical linewidth is 0.3 nm generating nearly 1.5 kW peak power using 29.5 μm grating (or poling) period a multi-grating PPLN crystal pumped with 30 W linearly polarised Nd-YAG laser [109]. Frequency/wavelength fluctuation issues due to thermo-mechanical stability, expressed as mode-hops in high power cw-OPO, is one of the significant challenges in OPO operation. Hu et.al. [110] addressed the issue by implementing cavity sealing and thermal mitigation. Other frequency stabilisation methods are discussed to deliver high-accuracy, practical implementations of the OPO device. Distinct QPM geometries have also been studied and reported [111] where the domain periods were fabricated in a fan-out configuration, i.e. aperiodically poled structure (Aperiodic PPLN or APPLN) was developed, allowing wider range of tunable spectral range from a periodically poled device. Additionally, the pump beam incorporates a large aperture by using a cylindrical beam expander, which along with the APPLN nonlinear crystal is capable of delivering very high-power outputs, that remains well below the damage threshold of lithium niobate. Long term stable, frequency stabilised mid-IR CW laser operation with fan-out gratings on MgO:PPLN crystal was also demonstrated recently [112]. Other OPO geometries include the segmented step-chirped grating [113]. Chirped pulse OPOs have been further examined and reported by [114] demonstrating the potential to generate ultrashort pulses over a broad wavelength range at high repetition rates. This was achieved as optical pulses produced had instantaneous bandwidths wider than the parametric gain-bandwidth or the phase-matching bandwidth of the nonlinear PPLN crystal used in the OPO set-up. Challenging the accepted limit of transparency of lithium niobate crystals near 5.4 μm, has been demonstrated to be extended, attaining a wide mid-IR tunability between 2.8-6.8 in a synchronously pumped femtosecond OPO with PPLN as a nonlinear medium μm [115]. On the other hand, dual wavelength pumping of mid-IR OPO pumped (by two separate fibre lasers) showed lowering of OPO threshold in addition to higher idler powers, signifying coherent parametric gain enhancement useful for practical applications of frequency down

conversion [116].

Semiconductor diodes have been demonstrated to be used as a pump for a single resonant, cw mid-IR OPO operating in the 2.9-3.6 μm range, adding to the repertory of pump sources for OPOs [117]. Moreover, a careful selection of pump wavelength value in the set -up allowed over 200 nm tunabilty of the output with a very small tuning of the pump, without any modification in its singly resonant oscillator (SRO) settings. Alternatively, diode lasers have also been used to optimise standing wave in the cavity, for OPO operation [118]. Picosecond regime mid-IR OPOs have also been developed [119]. The system is shown to operate at room temperature with the use of a specific PPLN partial cylinder geometry.

Prototype compact, linear inter-cavity cw-OPO with up to Watt level output power and steady electrical and performance have been developed utilising laser diode, Nd: YVO_4Thi crystal and multichannel PPLN grating to produce tunable OPO between 2.25 to 4.79 μm [120]. This work analyses the impact of temperature changes in an OPO. The pulsed OPO system is enabled with precise temperature control to study the effects of quick rise in temperature vs stabilised temperature to the operation of the OPO and concludes that rapid rise in temperature leads to deformation of the crystal and degrades the OPO performance. The study also investigates and verifies stable room temperature operation of the PPLN-based OPO[121].

2.3 Fibre Amplifier and Lasers

Fibre amplifiers are compact optical systems constituting of optical fibres with a high refractive index core composed of high yield, active gain medium, typically in the form of dopant ions, allowing for lasing phenomena to take place within a single pass, while transferring light over relatively longer distances by the phenomenon of total internal reflection at the boundary of a lower refractive index cladding layer. A resonant cavity can be created within the fibre, either by adding mirrors or etching gratings, and allow it to function as a laser. There are other factors which can aid in the operation of a fibre-based laser system, depending on the application, and these include, material nonlinearities,

processes like stimulated Raman scattering and four wave mixing.

The main advantages of fibre-based laser and amplifiers are that they are flexible yet stable, compact, capable of high throughput of optical powers, ability to deliver power to inaccessible regions depending on the implementation and relatively good, diffraction limited beam quality. Additionally, it is possible to design good thermal management for flexible fibre-based systems than for solid state lasers; as the heat is distributed over the considerable length of the fibre compared to much smaller active media dimensions in solid state systems, hence reducing the possibility of severe thermal lensing and delivering a beam free from aberrations effects of thermal lensing minus a small effect from shrinking of the mode size.

Some major disadvantages of fibre-based systems arise mainly from their geometry. These consist of core/cladding diameter tolerances, confinement of the Mode Field Diameter (MFD), deviations due to non-circularity of the clad and possible core-clad concentricity offset. Another important factor hindering the performance is that the operation of the laser / amplifier requires pumping, and often inefficient coupling-in of a pump deters the amplification in these systems. However, this problem since has been mitigated in introduction of double clad fibres which provides a large numerical aperture and high RI difference between the core and the cladding and facilitates better coupling of light into the fibres. High power scaling is also limited by mode instabilities, which impacts the output beam quality. For commercial applications, the drawbacks often include high fibre costs, fragility of fibre materials leading to damage and relatively smaller pulse energies with respect to solid state lasers, due to substantially smaller fibre cores.

When discussing laser matter interaction in the context of fibre-based systems, there are parameters that are key to evaluating the performance of such systems for practical applications. Few reports on laser based invasive medical treatment using thulium doped fibres operating close to 2 μm, reviewed the optimal laser settings required for a laser surgery. The studies considered the wavelength, pulse durations, pulse repetition rates, pulse energy, output powers, beam spot diameters corresponding to smaller core sizes while assessing the laser performance [122, 123]. Other studies in ophthalmic surgery have also stated the significance of pulse energy density and beam

profile quality to estimate optimum laser beam parameters in vision correction surgeries [124]. This implies a need for recapitulation of the definition of these parameters to help with understanding why they are vital.

2.3.1 Parameters influencing laser-matter interaction

The advantage of lasers for light matter interaction is that they can deliver immense amount of heat within a considerably small area to yield heating, melting, ablation, lessen retropulsion of ablated fragments and dust or merely induce thermally active processes such as promoting surface reactions, structural transformations, mechanical response etc. The lasers can operate in both continuous wave mode and in pulsed configurations however, pulsed mode helps deliver more energy with a short stipulated time boosting the interaction process.Fibre-based systems make it possible to have versatile yet compact, miniature devices easy to use in a surgery setting. So, considering laser-material interaction processes, the following laser parameters contribute to implementing safe and efficient fibre -based laser surgery device:

Operational wavelength - Any process of laser-matter interaction involves absorption of the light into the material, and this is intrinsically dependent on the wavelength. While the light can also be reflected, scattered or simply transmitted, these processes are essentially controlled by the amount of absorption occurring. Thus, wavelength becomes a principal factor to the effectiveness of the process, whether in industrial cutting / welding or medical remedial or diagnostic interventions. Moreover, for surgical applications, the proximity of the emitted laser wavelength to the window of water absorption maxima is a key advantage.

Pulse duration - In most laser material processing operations, the laser works in a pulsed mode, where the energy is delivered in short periods over cycles defined by pulse repetition rates. Pulse duration or pulse width determines the length of time during which the energy is delivered to the light-matter interaction zone. Reducing the time of interaction within a cycle can deliver more intense energies over shorter periods, and allowing rest time between pulses can significantly impact the interaction process.By varying the pulse duration, it is possible to regulate the thermal

diffusion length.

Pulse Repetition rate - Repetition rate or pulse repetition rate is also expressed as duty cycle as a ratio of PW to pulse spacing. For the heat intense continuous wave CW operation, this value is 1. Other modes of pulsed operation include short pulse nanosecond, and ultrashort picosecond and femtosecond regimes.

Pulse Energy - At the zone of light matter interaction, the energy deposited by the laser beam depends on the pulse energy of the laser. Together with pulse shape, this streamlines the time and magnitude of heating or cooling during the process.

Power - The average power, given by the product of pulse repetition rate with pulse energy, gives the quantity of energy delivered to the light-matter interaction zone per unit time. For CW laser, this is simply the amount of energy supplied per second.For pulsed operations, peak powers, determined by the pulse duration, become more relevant.

Power Density - The power density of a laser beam is of significant importance when considering laser material interaction processes by controlling the evaporation rate in such processes [125, 126, 127], By definition, this parameter gives the distribution of the power of the laser pulse within a beam spot area. This is analogous to the number of photons involved in a laser-material interaction process per unit time, and is substantially dependent on the beam quality of the laser.

Laser Beam Quality - An ideal laser beam spot would be diffraction-limited with the lowest divergence. In practical scenario, an integer multiple of this is usually referred to evaluate the quality of a laser beam, assuming the Gaussian distribution of energy in a laser beam. This parameter denoted as the M^2 varies from an ideal value is between 1–1.5 signifying a nearly perfect beam, and can go to integer multiples of up to 50 for applications where the beam shape benefits high power cutting and welding operations involving rise in temperatures and thus higher M^2 values. M^2 value impacts the quality of focusing for high energy beams with higher M^2 cannot be focused into a tight spot size, affecting the Rayleigh range as well as the depth of focus, however this feature can prove beneficial for laser etching processes.

Spot Diameter - Focal spot size diameter d for any lens is given by

$$d = 4fM^2 \frac{\lambda}{\pi * D}$$

where f is the focal length of the lens, λ is the laser wavelength and D is the beam diameter incident on the lens. This is limited by the laser power density implying that high energy pulses cannot be focused tightly thus requiring to estimate an optimal value,

Coming to Mid-IR, the strong water absorption in this region and organic bond resonance becomes significant motivator to find laser material applications in this window. Water can be found not only in biological tissue, but also in the liquid form or as omnipresent hydroxyl ion in the environment and contaminant in materials like glass. Longer wavelengths in the Mid-IR also facilitates increased penetration depths within materials. These factors potentially allow a substantial quantity of heat deposition within a small area of a material. By adapting the above laser parameters, it is possible to develop a fibre laser delivering high power output with a certain degree of tunability to supplement the performance. To do so, it thus becomes imperative to review materials that can efficiently sustain the development of a Mid-IR fibre laser device.

2.3.2 Host materials for fibres in Mid-IR

Wavelength transparency is one of the most critical factors for materials to be successful hosts in the mid-IR. Multiphonon absorption, which involves the generation of several phonons as a result of the absorption of a single photon, strongly dominates in the mid-IR region and sets the limit for wavelength transparency in materials. Additionally, the longer wavelengths are severely prone to Rayleigh scattering, thus it becomes crucial to examine materials that have low phonon energy and scattering losses and thus can support as hosts for lasing in the mid-IR. Furthermore, these materials should possess the capacity for rare earth doping. For fibre lasers and amplifiers, the host materials can pose the primary limitations to the laser performance. Dopant ions serve as the active centres for lasing operation in mid-IR. The host material affects the spectroscopic properties like the upper state lifetime and the emission/absorption cross-sections of the dopant.

Inorganic glasses and polymers have traditionally been the most popular choices as materials for optical fibres. Because it is easier to draw fibres, silica has been one of the most extensively used inorganic glasses for NIR transmissions within the spectral range of 1.2 μm to 1.6 μm [128]. However, when it comes to the mid-IR, silica's lack of wider transparency becomes the main barrier to its utilisation. Transparency and other electrical and optical properties become more essential when considering other materials that are feasible in the mid-IR, even if they are not thermally optimal for fibre fabrication. In this context, crystalline substrates have eventually emerged as prominent options as materials in mid-IR and despite their thermal inadequacy, they are combined with other glass-like materials to form fibres with the most advantageous for mid-IR applications.

When it comes to power scaling in fibres, although the pump plays an important role, other factors like fibre architecture and core design can help overcome limits posed by nonlinear effects and change of properties of the fibre host material or the dopant ions due to the evolution of power within the fibre. A combination of material property manipulation and structure engineering can help achieve higher power outputs from such fibres. Even though recent research has exploited many successful fibre-structure designs, the interest has eventually returned to potential material hosts which can support high power fibre applications.[129, 130, 131].

A review of suitable materials as hosts for fibres operating in Mid-IR region categorised silica, sapphire, fluoride glasses, chalcogenide glasses, tellurium halides, silver halides and hollow waveguides as good candidates for this purpose [132] due to their broad transparency as summarised in Fig.2.6. In addition to this, the material should have low concentration of impurities, and a high tendency to recrystallise and form glass (indicated by the Hruby parameter [133]) to be able to transfer the energy over the length of the fibre.

Silica

Since the introduction of optical fibres for commercial applications, silica fibres have been the most proficient material, especially for optical communication, as they demonstrate efficient transmission ranges between the NIR optical window of 1.2 μm to 1.6 μm [128], and allow flat-gain optical am-

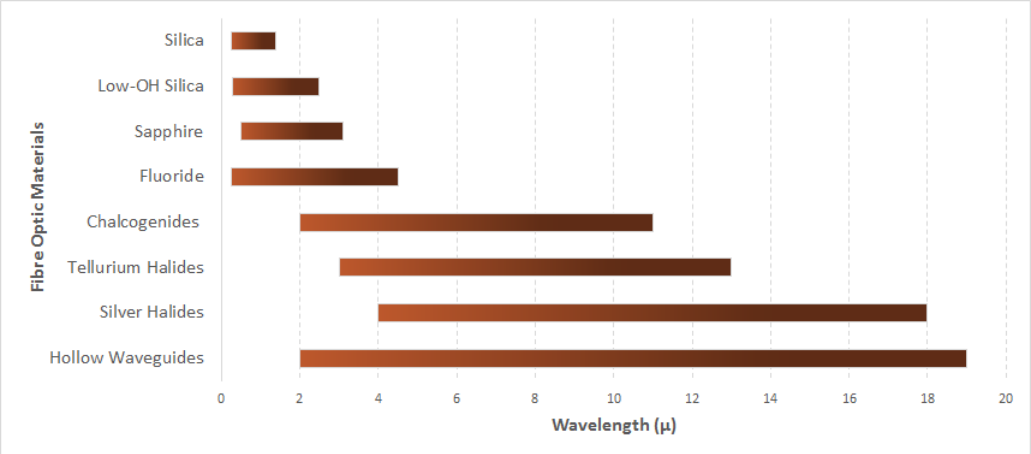

Figure 2.6: Common host materials for fibres in Mid-IR

plification, an essential requirement for building high capacity networks, and also serves as hosts for rare-earth doping. While normal silica fibres are transparent between 0.4-2.0 μm, the transparency can be slightly extended to 2.2 μm in low-OH silica fibres. Since high transmission losses beyond 2.2 μm have a significant impact on silica transparency [134], efficient host materials for emission beyond this limit are required.

Heavy-metal oxides

Tellurite and (lead-) germanate glasses are the most widely used heavy-metal oxide glasses in the IR domain.While silicates are the most common oxide glasses, they are no longer useful in the mid-IR due to reduced transparency in that window. by substituting silicon with heavy metals like lead and tungsten, the transparency window extends into the longer wavelengths, although not as much as for fluorides and chalcogenides. Tellurite glasses have a wide transparency window between 0.4-6.5 μm [135] along with higher linear and nonlinear refractive indices, good solubility for rare-earth ions, and a lower phonon energy than silica. Structurally, they are more stable than their fluoride counterparts. Germanate glasses have transparency up to 6 μm [136] depending on the composition, high laser-damage threshold but also higher losses when compared to fluoride fibres. Fibres composed of these glasses are effective for medical laser delivery and supercontinuum

generation [129].

Halides

These fibres are composed of halide compounds, like fluorides, chlorides, bromides, and iodides. Halide fibres may be derived from of single-component halide glasses (SCHGs), heavy metal fluoride glasses (like ZBLAN), and heavier halide glasses. While SCHGs demonstrate low attenuation, they exhibit drawbacks like deliquescence and toxicity.

Fluoride glasses have the lowest RI amongst different IR glasses and lowest nonlinearity. These glasses show extremely broad transparency between 300 nm to 6 μm depending on the composition. Zirconium based fluoride components showing minimum loss and hence maximum transparency between 1.5 – 3.5 μm spectral range. They are especially capable of delivering high output for lasers within this range, as the high output powers cannot have a significant impact due to low nonlinearity. Since ZBLAN glasses have been utilised for the work in this project, they have been elaborated upon in details in the next section.

Chloride, bromide, and iodide composition mixtures make up the heavier halide glasses, but the bromide and iodide ones have low stability thus they are inadequate for fabricated into fibres while the chloride glasses are water-soluble, thermally instable and exhibit issues with impurities in the form of ions.

Polycrystalline materials

Polycrystalline fibre waveguides operating in the IR were first reported in 1978 [137]. Polycrystalline materials for practical applications includes thallium and silver halides. These materials have low scattering and multiphonon absorption allowing transmission up to 25 μm, allowing them to be excellent alternatives to standard silica fibres, laser spectroscopy, pyrometry, and delivery of CO_2 laser radiation to inaccessible locations. The halide fibres also exhibit low losses $\sim 10^{-3}$ dB/km^2, which make them suitable for long distance fibre communication applications. An alternate ap-

proach is using the polycrystalline materials TlBrI, TlBr, AgCl, KBr KCl, to produce single crystal fibres. This is primarily because polycrystalline fibres have grains which act as centres to scattering of transmitted light, a challenge that is mitigated in single crystal fibres reducing losses due to scattering. While the Ag/Tl halide materials have low melting points and solubility, they have high refractive index, making it a challenge to find a good cladding material. But they exhibit more ductility, allowing easier fabrication. The alkali halides have more suitable RI but possess high MP and solubility, making fabrication tricky. The lack of appropriate cladding material are the chief constraints to the feasibility of applications of such fibres. The best polycrystalline fibre materials were Ag based ones. [138, 129]

Sapphire

Monocrystalline sapphire (single-crystal fibres), is simply aluminium oxide Al_2O_3,have been used to fabricate optical fibres. Sapphire has an extended transparency from UV to Vis to mid-IR up to 4 μm. They can support relatively high output power delivery due to low propagation losses and robust material strength, in the single crystalline form. Operation of sapphire fibres at 2.94 μm as power deliver systems for Er:YAG systems have been reported [139].

Chalcogenides fibres

Chalcogenides are another category of suitable host material at mid-IR wavelengths. These glasses are based on Sulphur, Selenide and Telluride and exhibit extended IR transparency, low phonon energies, chemical durability, and ease of fibre drawing. The fundamental structure of these glasses was not suited for doping, however, continued research has allowed several newer compositions of chalcogenide glasses to support rare earth dopants. Ce^{3+} [140], Tb^{3+} [141], and Pr^{3+} [142] doping in chalcogenides have produced mid-IR wavelengths near 5 μm. However, in the visible spectral range, these glasses demonstrate low transparency, which makes it difficult to use pumps at these wavelengths for rare earth dopants introduced in these fibres. Nonlinearities can also be induced in chalcogenide fibres by altering the compositions, which can help in nonlinear frequency conversion

to longer IR wavelengths [143].

Hollow core fibres

Hollow core fibres typically consist of hollow channels in the core and a glassy cladding, to guide light through the fibre. According to the fundamental mechanism of light transfer in a fibre, this should not work as a higher RI core and lower RI clad is required for total internal reflection. However, the light transfer is made possible by two major principles, including employing photonic band gaps in PCFs and microstructural engineering of the core of a glassy preform to form negative curvature fibres. Hollow core fibres with microstructures, composed of silica, have been demonstrated to operate at 2.94 μm [144] for applications in surgery, while hydrogen-filled, hollow core silica fibre have been demonstrated as Raman lasers, emitting at 4.4 μm in the mid-IR utilising stimulated Raman scattering [145]. Hollow core fibres have also been demonstrated with sapphire glasses to deliver high power CO_2 laser beams near 10 μm [146].

Currently, a lot of research is being conducted in the recent times, to develop mid-IR fibre lasers, and in that regard, fluoride fibre based systems have become excellent choices in the wavelength region between 2.5 and 3.92 μm [147].

2.4 ZBLAN Fibres

ZBLAN glasses were invented in 1974 by the Poulain brothers. Although these fluoride-based glasses have gone through several structural composition changes, they can be described as a class of heavy metal fluoride glasses with a specific molar composition: of ZrF_4-53%, BaF_2-20% LaF_3-4%, AlF_3-3%, and NaF-20%. Amongst different types of glasses used for drawing fibres, important properties like low phonon energies and broad transparency, found in both chalcogenide and fluoride glasses, make them more feasible for applications in the IR region, over their silicate and phosphate counterparts. However, fluoride glasses tend to have additional advantages over chalcogenides; this is established by their stability, low inherent losses and extended transparency range starting from

UV into mid-IR. Moreover, like silicate glasses, the structure of these fluoride glasses allows for them to be easily doped with rare earth materials. The dopant ions are mostly derived from the chemical lanthanide series, along with yttrium and scandium, making them quite suitable for lasing applications. Not only do these ions exhibit close, approximate properties, they are also usually found within the same mineral deposits [148] making them easily accessible for doping.

Adjustment of the ZBLAN glass properties can be done by adding or substituting with other fluorides in the host material. For example, the transparency window can be modified by replacing ZrF with HfF_4 or ThF_4; while the stability can be altered by with GaF_3 or InF_3 in place of AlF and changing NaF with LiF. While the glasses have a wide transparency window compared to the more commercially available silicate glass, in contrast they are much softer, making them more vulnerable to damage and thereby require a protective coating to enhance strength for practical applications. The glasses exhibit low nonlinearity and are slightly hygroscopic in nature, properties which impact the high power operations.

Relevant optical properties of ZBLAN glasses

The important properties of ZBLAN glasses [149, 150] that impact the mid-IR operation are :

- Low maximum phonon energy of $\sim$565 cm^{-1}, which makes room temperature fluorescence in rare earth dopants below 3.5 μm possible,
- Low optical dispersion and refractive index,
- Wide transparency between 0.2-4.5 μm with losses below 200dB/km,
- Capacity for higher doping concentrations of rare earth dopants without cluster formation due to greater chemical reactivity as a result of weak bond strength of ZBLAN glasses, and single charge on fluoride ions.The weak bond strength arises out of the low maximum phonon energy,
- LIDT of 25 MW/cm^2 with 2.8 μm pulses of duration 10ms posing a limit to power scaling,

- Smaller Raman Scattering due to low Raman Gain coefficients, thereby reduced influence on power scaling,
- High thermal loading due to low thermal resistibility.

ZBLAN Fibres for Mid-IR Applications

Due to the characteristic broad transparency range of ZBLAN fibres, relatively deep into the mid-IR, they are actively considered for applications in technologies like imaging and spectroscopy within this wavelength range.In addition to this, higher doping capacities, greater material strength and low loss properties make them proficient for high power applications such as amplifiers and lasers. This makes them relevant candidates for building lasers for medical purpose where the pertinent wavelengths lie within the NIR / SWIR / Mid-IR spectrum corresponding to water absorption peaks, for material processing as ZBLAN based fibre lasers become compact and efficient sources with good beam quality to deliver considerable energy on to a material, as laser pumps for cascaded systems and many defence applications including IR imaging and defence remote sensing to name a few.

The major challenges which affects the performance of a ZBLAN fibre are

- weak thermo-mechanical structure
- heat deposition within the fibre during high power operation

These properties pose severe limitations to the fibre applications as they cause quick degradation of the fibre and restricts long duration operations.

2.4.1 Rare Earth doping in ZBLAN Fibres

ZBLAN glasses are excellent hosts for rare earth ion doping. Adding these ions, create gain medium with possible laser emission at various wavelengths in the mid-IR region depending on the energy

levels of the doped ions, which can be exploited when used in combination with different pumps.

Erbium

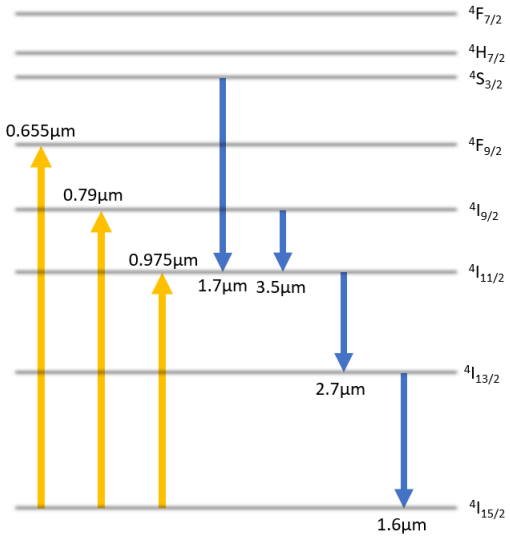

Figure 2.7: Erbium Energy Level Diagram

The energy level diagram of erbium doped ZBLAN fibre is shown in the figure 2.7 [151, 150]. Erbium ions are excited to higher energy levels $^4F_{9/2}$, $^4I_{9/2}$ and $^IF_{11/2}$ by the process of ground state absorption (GSA) when pumped with 0.655 μm,0.790 μm,0.975 μm wavelengths within the ZBLAN fibre. These result in emissions at 3.5 μm,2.7 μm and 1.6 μm due to $^4F_{9/2} \longrightarrow^4 I_{9/2}$,$^4F_{11/2} \longrightarrow^4 I_{13/2}$, and $^4F_{13/2} \longrightarrow^4 I_{15/2}$ transitions. Additionally, erbium ions also undergo Excited State Absorption (ESA) that leads to the emission of 1.75 μm between $^4S_{3/2} \longrightarrow^4 F_{9/2}$ levels. The 1.55 μm wavelength emitted from erbium is widely employed in telecommunication.In these applications however, silica fibres prove to be a better host material as it is able to support high amplifier gain, having structural stability and cost-effectiveness over softer ZBLAN fibres.

As previously discussed, the 2.7 μm wavelength is of tremendous interest due to its proximity to the water absorption maxima, thus finding applications in laser tissue interactions or laser material processing. The lower energy level for this transition has a longer lifetime with respect to

the emission start level, which intuitively implies the impossibility of continuous wave operation. However, continuous wave mode has been demonstrated and attributed to the fact that the $^4I_{13/2}$ level is successively depleted due to ESA and the population inversion between $^4F_{11/2}$ and $^4I_{13/2}$ is preserved.The phenomenon, although not impacting the initially reported low power operations, was observed when experiments high power operations led to saturation of the output. To obtain high power outputs, several mitigative solutions were considered. These included co-lasing the 2.7 μm radiation with 1.7 μm to ensure population inversion or cascaded stages of ZBLAN fibres with low erbium dopant concentration. This was not the most efficient approach to high power, watt order outputs, especially when low brightness diodes pumped the fibres. High power operation was consequently achieved by combining cascaded stages of erbium doped fibres coupled with co-lasing at 1.6 μm wavelength, which depletes the $^4I_{13/2}$ quickly. To further increase the output power magnitudes, many approaches have been investigated. The most efficient approach is Er/Pr co-doping to allow energy transfer between Er and Pr ions, alternatively, simply having high erbium dopant concentration in double clad ZBLAN fibres, or by co-doping ZBLAN fibres with Er/Pr.

Watt level operations have been demonstrated, limited by high power optical damage due to heat alone. Larger fibre mode areas with good thermal management can also scale the power to several tens of watt level values in addition to optimization of dopant concentration.Very high dopant concentration make the ZBLAN fibre lasers extremely efficient by reaching and/or overcoming Stokes limit.

The 3.5 μm radiation emission for erbium doped ZBLAN fibres is attractive due to the molecular fingerprinting region for organic compounds and presence of atmospheric window with minimum attenuation proximal to this wavelength.However, high power operation at this wavelength has serious constraints due to the lack of high power pump diodes working at 0.655 μm, culminating in low Stokes efficiency and sometimes also due to large laser operation threshold at room temperature.

2.4.2 Rate equations for erbium dopant in ZBLAN host material

Er-doped fluoride fibre amplifiers have been modelled theoretically in several studies over the last decade [152, 153, 154]. The rate equations represent the change in population levels of erbium ions as a result of processes of absorption and emission when hosted by ZBLAN fibres. Pumping an Er-doped Fluoride fibre amplifier between 975–985 nm [155] supports Ground State Absorption of erbium ions from the ${}^4I_{15/2} \longrightarrow {}^4 I_{11/2}$ which causes changes in population densities N_0 and N_2. The laser emission transition at 2.8 μm leads to depletion of population density N_2 and increase in N_1. The same range of pump wavelengths also induce an Excited State Absorption between, ${}^4I_{11/2} \longrightarrow {}^4 F_{7/2}$ resulting in a population density change in N_2 and N_6.For emissions close to 2.8 μm, the lower level lifetime is longer than the upper one, resulting in a self-terminating transition, which is overcome by heavy doping within the fibre. The lower lasing level is quickly depleted by an Energy Transfer Up-conversion ETU_1 from ${}^4I_{13/2}$,${}^4I_{13/2}$ to ${}^4I_{9/2}$, ${}^4I_{15/2}$ causing population density changes of N_1 and N_3. A second Energy Transfer Up-conversion ETU_2 (${}^4I_{11/2}$,${}^4 I_{11/2} \longrightarrow {}^4 I_{9/2}$,${}^4 I_{15/2}$) contributes to the population densities of N_2 and N_6 in addition to the Pump ESA. Several multi-photon cross-relaxations transfer the erbium ion population back to ${}^4I_{11/2}$, exceeding the Stokes limit, defined as $\eta_S = \lambda_{pump}/\lambda_{laser}$ [156], by improving the quantum efficiency and thereby promoting substantial gain in the 2.8 μm laser line emission. However, since ETU_2 reduces the population density of ${}^4I_{11/2}$, this raises the pump threshold, impacting the overall efficiency of the transition. Additional cross-relaxation processes from ${}^4H_{11/2}$,${}^4S_{3/2}$ with a combined population density of N_5 (due to thermal coupling) to, ${}^4I_{15/2}$ brings the erbium ions back to ground state [153, 157].

$$\frac{dN_1(z,t)}{dt} = \sum_{i=2}^{6} \left(\frac{\beta_{i1} N_i(z,t)}{\tau_i} \right) - \frac{N_1(z,t)}{\tau_1} + W_{50} N_5(z,t) N_0(z,t) - 2W_{11} N_1^2(z,t) + R_{SE}(z,t) \tag{2.23}$$

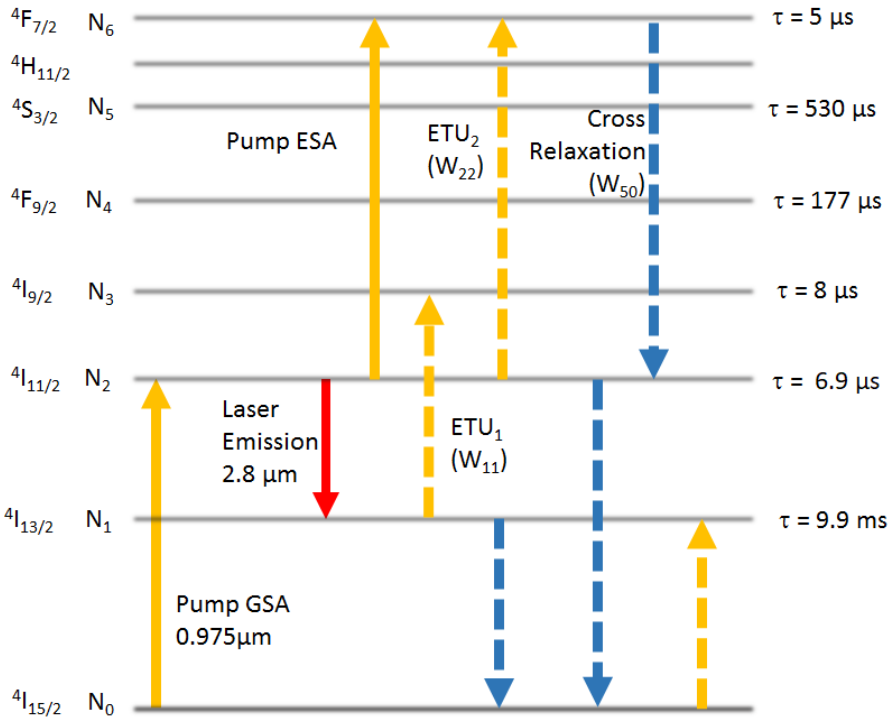

Figure 2.8: Er^{3+}:ZBLAN Fibre energy level diagram in ZBLAN host

$$\frac{dN_2(z,t)}{dt} = R_{GSA}(z,t)\breve{}R_{ESA}(z,t) + \sum_{i=3}^{6}\left(\frac{\beta_{i2}N_i(z,t)}{\tau_i}\right) - R_{SE}(z,t) - \frac{N_2(z,t)}{\tau_2} - 2W_{22}N_2^2(z,t) \tag{2.24}$$

$$\frac{dN_3(z,t)}{dt} = \sum_{i=4}^{6}\left(\frac{\beta_{i3}N_i(z,t)}{\tau_i}\right) + W_{50}N_5(z,t)N_0(z,t) + W_{11}N_1^2(z,t) - \frac{N_3(z,t)}{\tau_3} \tag{2.25}$$

$$\frac{dN_4(z,t)}{dt} = \sum_{i=5}^{6}\left(\frac{\beta_{i4}N_i(z,t)}{\tau_i}\right) - \frac{N_4(z,t)}{\tau_4} \tag{2.26}$$

$$\frac{dN_5(z,t)}{dt} = \frac{\beta_{65}N_6(z,t)}{\tau_6} - \frac{N_5(z,t)}{\tau_5} - W_{50}N_5(z,t)N_0(z,t) \tag{2.27}$$

$$\frac{dN_6(z,t)}{dt} = R_{ESA}(z,t) - \frac{N_6(z,t)}{\tau_6} - W_{22}N_2^2(z,t) \tag{2.28}$$

$$N_{Er} = \sum_{i=1}^{6} N_i \tag{2.29}$$

where τ_i represents the intrinsic radiation lifetimes of the i_{th} energy level for low doping concentrations, β_{ij} represents the branching ratio of a transition from the i_{th} to j_{th} levels and W_{ij} are transition parameters for ETU and cross-relaxation processes, where the ETU processes, yet again, depend on the Er doping concentrations [158].

The rates of Pump Ground State Absorption and Excited State Absorption are given by R_{GSA} and, R_{ESA} respectively, and R_{SE} is the rate of laser transition.

$$R_{GSA}(z) = \frac{\lambda_p \Gamma_p \sigma_{GSA}}{hcA_{core}} N_0(z)[P_p^+(z) + P_p^-(z)] \tag{2.30}$$

$$R_{ESA}(z) = \frac{\lambda_p \Gamma_p \sigma_{ESA}}{hcA_{core}} N_0(z)[P_p^+(z) + P_p^-(z)] \tag{2.31}$$

$$R_{SE}(z,t) = \frac{\lambda_s \Gamma_s \sigma_{SE}}{hcA_{core}} \left[b_2 N_2(z,t)\breve{}(g_2/g_1) b_1 N_1(z,t)\right] \left[P_s^+(z,t) + P_s^-(z,t)\right] \tag{2.32}$$

where λ_p is the pump wavelength, Γ_p is the pump power-filling factor, defined as the ratio of active area of the core to the active area of the pump [159], σ is the absorption cross-sections, h is the Planck's constant, c is the absolute velocity of light, A_{core} is the effective core area of the fibre, P_p is the pump power where the positive and negative signs denote forward and backward propagation and b_1 and b_2 are Boltzmann factors for the 4I13/2 and 4I11/2 laser levels.

The spatial evolution of the seed signal power and the depletion of the pump are given as:

$$\pm\frac{dP_s^+(z,t)}{dz} = \Gamma_s\sigma_{se}\left[b_2N_2(z,t)\breve{}(g_2/g_1)b_1N_1(z,t)\right] \times P_s^{\pm}(z,t)\breve{}alpha_sP_s^{\pm}(z,t) \tag{2.33}$$

$$\pm\frac{dP_p^+(z,t)}{dz} = -\Gamma_p[\sigma_{GSA}N_0(z,t) + \sigma_{ESA}N_2(z,t)] \times P_p^{\pm}(z,t) - \alpha_pP_p^{\pm}(z,t) \tag{2.34}$$

where α are the background loss coefficients, and g_1 , g_2 represent the degeneracy of the Er^{3+} Stark level ($g_1 = g_2 = 2$)

Equations 2.33 and 2.34 can be calculated to determine the output power of the seed signal and the depletion of the pump by considering small, equal-sized discrete sections of the active medium in the longitudinal direction and applying 4^{th} order Range-Kutta method. The solutions to the rate equations for the population density can be found by using methods for solving Stiff rate equations, considering very small step sizes.

The rate of change of photon density (ϕ) is given by

$$\frac{d\phi}{dt} = \frac{l}{l_{opt}}\sum_{z=1}^{n}R_{SE}(z) - \frac{c\phi}{2l_{opt}}\left\{-ln[R'(1-L')] + 2\kappa l\right\} \tag{2.35}$$

where l_{opt} is the length of optical fibre, κ is the loss per unit length of the fibre, R' is the output mirror reflectivity and L' is the reflection losses at the mirror.

In terms of photon density, the rate of stimulated emission can be written as

$$R_{SE}(z) = \sigma_{\mathrm{SE}}c\phi\left[b_2N_2(z)\breve{}(g_2/g_1)b_1N_1(z)\right] \tag{2.36}$$

The corresponding output power can be given as

$$P_{out} = 0.5c\phi\frac{hc}{\lambda_s}A_core[ln(1R')] \tag{2.37}$$

From a thorough analysis of the rate equations, it becomes possible to predict the wavelength tunability range along with the amplified output power from an erbium based laser or amplifier.

2.4.3 Other rare earth dopants emitting in the Mid-IR : Thulium, holmium, & dysprosium

ZBLAN glass as host materials determines the absorption and excitation cross-sections and the energy levels of the active dopant ions. Apart from erbium, lanthanide series rare earth dopants like thulium, holmium, and dysprosium emit in the mid-IR spectral range. The energy level diagrams of these relevant ions in ZBLAN host glass in shown in the fig 2.9 [151, 150].

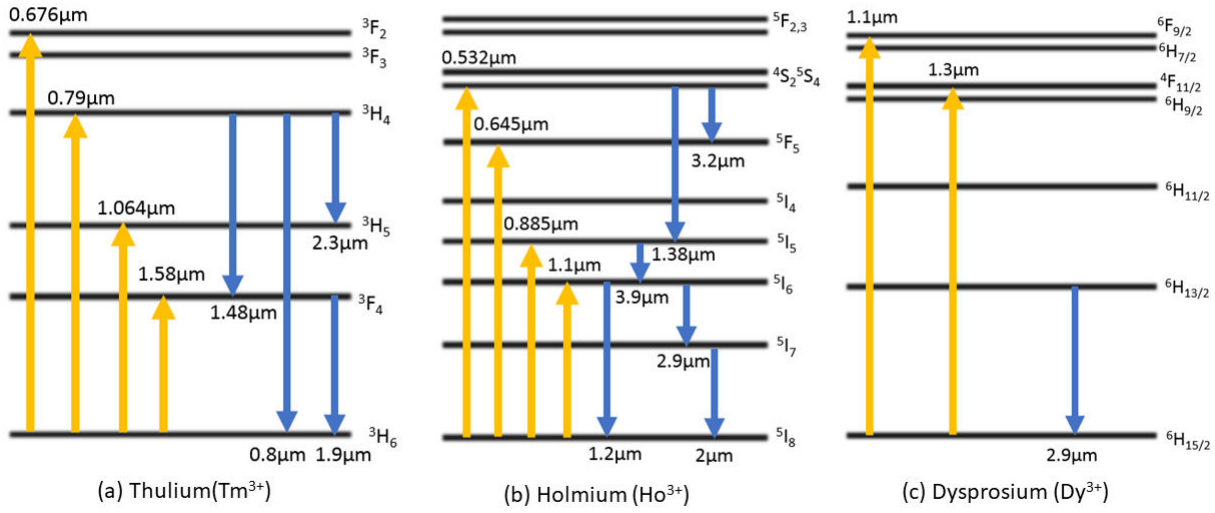

Figure 2.9: Energy Level Diagrams for trivalent thulium, holmium, and dysprosium rare earth dopants in ZBLAN host glasses

Thulium

The partial energy level diagram for thulium is shown in Fig.2.9 a). Thulium emits several wavelengths in the IR spectral range viz.,1.47 μm ($^3H_4 \longrightarrow^3 H_6$) and 2.3 μm ($^3H_4 \longrightarrow^3 H_5$) when pumped with 0.79 μm and 1.94 μm ($^3F_4 \longrightarrow^3 H_6$) for a pump at 1.58 μm, two latter ones being in the vicinity of the mid-IR. Thulium doped ZBLAN fibre operations at 1.48 μm and 2.3μm were both demonstrated in 1989. For 1.48 μm, silica fibres prove to be unsuitable due to quick depletion of the lower energy level for the transition as a result of a non-radiative decay.In ZBLAN fibres, this transition is self terminating due to longer lifetime of lower energy state. This is mitigated by co-lasing 1.48 μm with 1.9 μm, or co-doping with Terbium or holmium ions, or inducing ESA ($^3F_4 \longrightarrow^3 F_2$)by upconversion pumping with 1.064 μm.

2.3 μm operation becomes of keen interest due to potential applications in the mid-IR and wavelength tunability in Tm doped fibre lasers between 2.25-2.5 μm have been demonstrated.A non-radiative transition from $^3H_5$ to $^3F_4$ impacting population inversion since $^3F_4$ has a longer lifetime, which challenges the lasing operation. This is overcome by co-lasing with 1.9 μm.

Investigations for 1.9 μm were conducted in 2008 for silica and ZBLAN fibre hosts which demonstrated that while the silica fibres were more efficient for high power outputs, it was still possible to obtain several tens of watts of output power by optimising the operational factors, introducing innovative fibre design, and considering newer pumping mechanisms.

Holmium

Fig. 2.9 b) illustrates the partial energy level diagram for holmium. Within the mid-IR, holmium is one of the most proficient rare earth dopant with several lasing wavelengths at 2.0 μm , 2.9 μm , 3.2 μm and 3.9 μm apart from a few more in the NIR. Due to the highly efficient water absorption peak near 3 μm (compared to 2 μm) and the absorption bands of organic bonds (hydrochlorides, hydrocarbons) beyond 3 μm holmium becomes a promising candidate for doping in ZBLAN fibres and have found applications in laser surgery [160].

Holmium doped ZBLAN fibre operation at 3 μm was first made possible by dual pumping with 640 nm and 750 nm lasers. The 3 μm transition is also self terminating due to the lower lasing level ($^5I_7$) having a longer lifetime compared to the upper level ($^5I_6$). Low efficiency CW operation at 3 μm is possible due to ESA of the pump at $^5I_7$. The efficiency of this lasing operation was improved by implementing cascaded transitions, depleting $^5I_7$ population. With pumping at 1150 nm, the highest output of 3W and 65% slope efficiency was achieved for a co-lasing system at 3 μm–2 μm [161]. Holmium—praseodymium co-doping was introduced to further improve the 3 μm operation, where the closely placed energy levels $^5I_7$ (Ho_{3+}) and $^3F_2$ (Pr_{3+}) supplemented the fast depletion of the $^5I_7$ in holmium. Moreover, increasing only the holmium doping concentration can promote ETU to deplete the ion concentration in the $^5I_7$ level and boost operation around 3 μm, while circumventing 2 μm lasing especially when pumped near 1100 nm where the pump ESA can additionally contribute to the depopulation of the lower energy level [162, 163]. Beyond 3 μm, holmium doped ZBLAN fibres have shown to be operative (CW mode) at 3.22 μm when pumped at 532 nm and at 3.9 μm with a 640 nm pump, cascaded lasing and additional cooling mechanisms.

Dysprosium

The partial energy level diagram for dysprosium is given in Fig 2.9 c). Dysprosium doped ZBLAN fibres emit laser wavelengths near 2.9μm that arises from the radiative transition ($^6H_{13/2} \longrightarrow ^6 H_{15/2}$) levels for pumps at 1100 nm [164]. Changing the pump wavelength to 1.3 μm increases Stoke efficiency and decreases the pump photon ESA, leading to improved slope efficiency, thus opening up the possibility of high gain Dy doped fibre amplifiers. Recently, Dy:ZBLAN fibres operating at 2.9μm have been demonstrated[165].Also, tunability studies for Dy:ZBLAN fibres between 2.925 to 3.250 μm have also been reported [166].

Other Rare earth dopants

Other dopants commonly employed in ZBLAN fibres include neodymium, ytterbium, and praseodymium. Neodymium doped ZBLAN fibres were the first ZBLAN fibre operations to be demonstrated. Nd-

dopants are efficient in the NIR wavelengths around 1 & 1.3 μm and were implemented in the telecommunication applications operating in the 1.3 μm window. Ytterbium and praseodymium have more commonly been utilised as co-dopants to prevent parallel undesired transitions and complement the preferred transitions or absorption processes. praseodymium has also been to shown to emit around 3.4 μm in the mid-IR with fluoride fibres as host [167]. Ytterbium based fluoride fibres operate mostly in the NIR and have been shown to operate at 1.02 μm in ZBLAN fibres [168].

The following figure summarises the output wavelengths from different rare earth doped ZBLAN fibre operating near 3 μm. Amongst the different dopants, holmium demonstrates the highest slope efficiency of 36% [169]. On the other hand, while Er: ZBLAN fibres have lower slope efficiencies (29%) compared to holmium, they typically have the highest rare earth doping capacities and highest output powers [170, 171, 172].

2.4.4 Other wavelength regimes with ZBLAN Fibres

Apart from their efficient performances in the mid-IR, ZBLAN glasses also used in broadband applications including UV and visible regions.

UV & Visible

Holmium proves to be a good dopant for ZBLAN fibres for operation in the UV/ IR region [173] Deep-UV lasers have been reported employing second harmonic frequency conversion of visible emission from holmium or dysprosium doped ZBLAN fibres[174]

Supercontinuum Generation

Supercontinuum (SC) is the low coherence, continuous, broadband 'white' light generated from highly coherent, narrowband laser pulses, due to extreme nonlinear frequency broadening in a dispersive medium. The long length of optical fibres provides the sufficient interaction length and

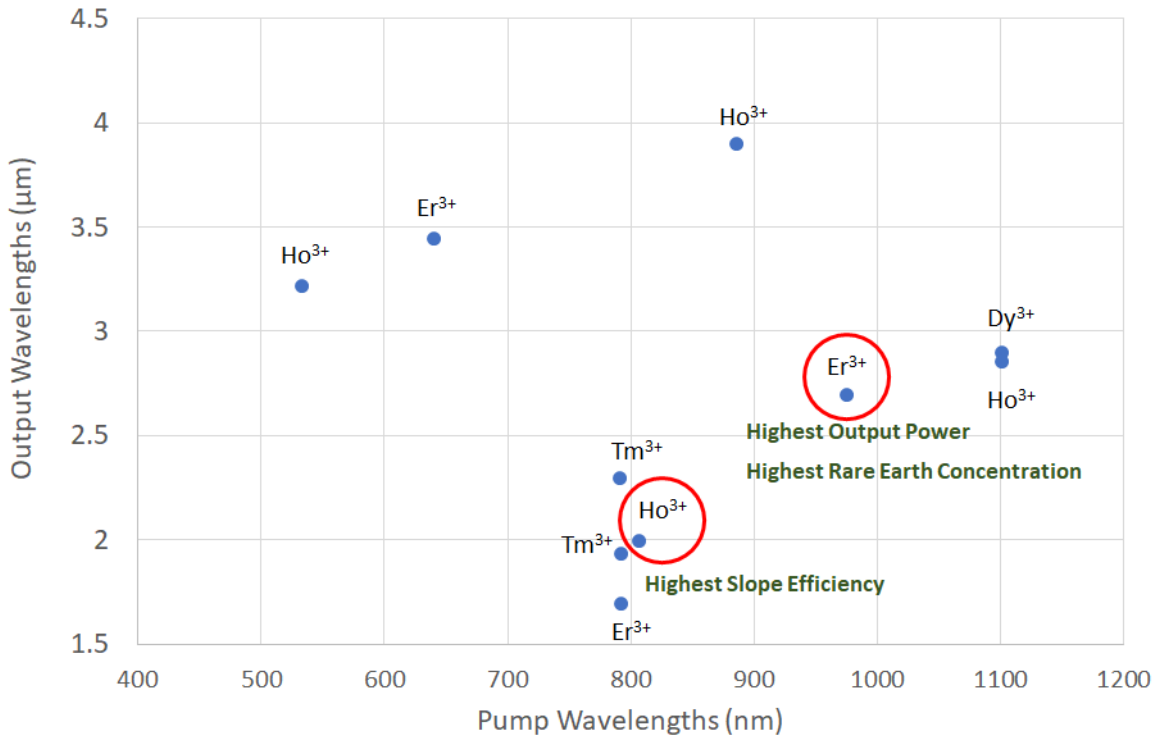

Figure 2.10: Pump and Output Wavelengths for ZBLAN Glasses with different Rare Earth Dopants operating in Mid-IR.While holmium doping demonstrate maximum slope efficiencies, erbium doping in ZBLAN shows highest doping concentration and highest achievable output powers

necessary dispersion, hence nonlinearity, for the narrowband laser pulses to undergo SC generation when confined within the small core region of the fibre [175, 176]. In the mid-IR spectrum, ZBLAN fibres have been demonstrated to support high output SC generation due to their transparency up to 7 μm, an advantage over conventional silica fibres which exhibit absorption losses beyond 2.4 μm [177, 178, 179]. The active rare earth dopant in mid-IR ZBLAN fibres is thulium [180] or thulium/holmium co-dopant [181, 182].

2.4.5 End caps for ZBLAN Fibres

While fluoride fibres provide remarkable levels of power amplification in lasers and amplifiers, especially near 3 μm, the bare fibre tip is highly susceptible to damage due to the concentration of high intensities of the amplified signal power, in addition to the residual pump power at the facet and Fresnel back-reflections due to the RI difference of the host material and air. The net output intensity can lead to damage in CW mode due to excessive heating [183], and in pulsed operation due to extremely intense pulses resulting from high peak powers, beyond the laser induced damage thresholds (LIDT) of the material surface[170, 184]. Additionally, prolonged operation over a period opens the possibility of tip deterioration due to the presence of hydroxyl (OH) molecules in the atmosphere. This exposure leads to the diffusion of OH molecules into the host fibre material as contaminants, the molecules absorb the operational wavelengths around 3 μm, heating up the fibre facets, escalating the diffusion of the OH molecules into the fibre and eventually leading to a thermal runway, causing catastrophic optical damage (COD) [185].

Common methods of mitigating the issue are by expelling the moisture near the bare fibre tip by circulating pressurised nitrogen or dry air [183, 170, 186], or by placing the laser system in isolation. Another viable alternative is to splice end caps made of suitable materials to the fibre tips [187]. This restrains the sudden expansion of the laser beam from the fibre to the atmosphere significantly and reduces the risk of tip damage by keeping the intensities below the LIDT, even for very high-power output beams. Some fluorides and oxides studied as potential end cap materials include zirconium fluoride (ZrF_4), aluminium fluoride (AlF_3), germanium dioxide (GeO_2), silicon oxide (SiO_2) and aluminium oxide (Al_2O_3). The oxides proved to be a better alternative compared to the fluorides, for long duration usage estimated from the fibre facet temperature rise. To prevent this diffusion totally, nano-scale thin silicon nitride (Si_3N_4) diffusion barriers were sputtered on the Al_2O_3 / ZrF_4 / AlF_3 end cap facets, which made laser operations of over 100h durations possible.

Further internal studies comparing the performance ZBLAN fibres with GeO_2 ($\sim$ 1.6 at 3μm) [188] and AlF_3 end caps demonstrate higher vulnerability of GeO_2 to Fresnel back-reflections compared to AlF_3, possibly linked to the RI differences in w.r.t. to air.

2.5 Current State of the Art with erbium doped fluoride fibre amplifiers in mid-IR

Erbium doped fluoride fibre lasers have been operative since 1988 [189]. Since erbium doped ZBLAN can be effectively pumped at 790 / 980 nm, the abundance of diode lasers at these wavelengths supported the extensive initial investigations and subsequent power scaling of amplification in such fibres [190, 191, 192, 193]. Amplification to the order of 10 W in Er:ZBLAN fibre emitting at 2.78 μm in CW mode was first reported in 2007 [194]. This was validated using a 4 m heavily doped (6%), double clad fibre pumped with a laser diode array at pump wavelength 975 nm and corresponding pump power of 100 W, achieving a slope efficiency of 21.3%, due to ETU between highly concentrated Er^{3+} ions. This study also indicated the likelihood of an optimal doping concentration value, since increasing doping concentration also increases parasitic losses such as ESA of upper laser level and cross relaxation in lower laser level. First erbium doped ZBLAN fibre amplifier operation was demonstrated, recording 16.2 dB gain, which eventually opened up the possibility of power scaling with these fluoride fibres [195]. Tokita et al. have since then reported power scaling of tens of watts in CW mode in Er:ZBLAN fibre lasers along with over 100 nm wavelength tuning [196, 197], using indirect water cooling to support high power pumping and N_2 purged enclosure to prevent fibre facet damage due to atmospheric moisture. Diode pumped, all fibre CW laser, with fibre Bragg reflectors inscribed within the core, reported stable operation with 32 % optical conversion efficiency, and measured output power of 5W at 2824 nm [183]. Progressing further, passively cooled all fibre configuration for Er doped fluoride fibre laser with 30.5 W output power and good beam quality in CW mode, pumped at 980 nm, demonstrated the possibility of achieving high power scaling with suitable thermal management. Fibre Bragg gratings were used in the core to set the lasing cavity and emitted wavelength was centred at 2938 nm [198]. Power scaling up to the order of a hundred watt could be attained by pushing the Stokes limit to increase the slope efficiency. This was accomplished by cascading 2.8 and 1.6 μm emissions in Er:ZBLAN fibre with high power diode pumping, to drive the ESA of the Er ions of the resonant 1.6 μm transition, from the lower state and return the ions to upper lasing level of the 2.8 μm transition. This allowed a slope efficiency of nearly

50% and emission was still centred at 2.8 μm by using longer fibre length and spectral selection with FBG. In an alternate approach, it was shown to be possible to vary slope efficiency of a quasi-CW mode Er:ZBLAN fibre by tuning the pump wavelength, in a non-cascaded configuration, to improve it further [171]. The highest reported average power in mid-IR fibres is 41.6 W, employing passive cooling, is from an Er: ZrF_4 fibre emitting near 2824 nm. This study also discusses the limitations to reliable long term performance of high power fluoride fibres, which is heavily impacted by fibre tip damage and thermal and mechanical degradation [199].

Lasers working in the pulsed mode are known to provide large magnitude peak powers, which are often advantageous for practical applications. One of the initial pulsed mode operations with erbium doped fluoride fibres emitting near 2.7μm was achieved by the process of Q-switching. 100 ns pulses with 2 W peak powers were generated using a combination of rotating mirrors and an acousto-optic modulator [200]. Later, first mode-locked operation was demonstrated by applying passive Q-switching with saturable absorbers and flying-mirror mode-locking technique to generate a Q-switched pulse consisting of a train of 2.5 ns duration mode-locked pulses [201]. Pulsed mode Er:ZBLAN laser with performance equivalent to cw operation was demonstrated by Gorjan et al. The 300 ns pulse duration, diode pumped, gain-switched fibre laser delivered up to 2 W output power / 68 W peak powers with high slope efficiency while operating at 100 kHz repetition rate [152].Pulsed Er: ZBLAN fibre amplifier have been realised by seeding the amplifier with graphene based Q-switched Er:ZBLAN fibre, operating near 2 μm [202]. Reasonably straightforward yet robust, splice-less all-fibre architecture-based fibre lasers have been reported by Paradis et al. The fibre laser uses fibre Bragg gratings as cavity reflectors achieving 28% efficiency, and delivering output powers of 11.2 W, and 80 μJ pulse energies with 170 ns long pulses, operating near 2826 nm. The all-fibre configuration removes the necessity for nitrogen purging used by Tokita et al.[170], yet records equivalent output powers [203]. A comprehensive laser performance characterisation was corroborated by Sojka et al. In the study short nanosecond pulse (26 ns) operations in Er:ZBLAN fibres with 100Hz repetition rate and significant pulse energies of up to 330 μJ and $\sim$13 kW have been validated by modifying operational parameters like length of fibre, pump powers and repetition rates[172]. High energy pulses (1mJ), potentially suitable for bio-material processing, with 1 ns pulse

width, operating at 5 kHz repetition rate, have been obtained in Er:fluoride fibre amplifier recording average powers of 5 W [204].

Long duration pulses can deliver significant power in their commercial applications. Recently, microsecond pulse operation ($\sim$ 2.3 μs) in Er doped fluoride fibres in a master oscillator power amplifier (MOPA) configuration reported 4 W level average power, $\sim$ 60 μJ pulse energy at 2786 nm. The pulsed operation was implemented by passive Q Switching utilising semiconductor saturable absorber mirrors (SESAM) in an external, linear laser cavity [205].Other passive Q-switching methods include use of Gold nanostars to produce pulse widths of the order of $\sim$ 5 μs [206]. In the ultrashort pulse regime, 25 ps duration mode-locked pulses at 2.8 μm were demonstrated using a semiconductor saturable absorber mirror for passive mode-locking. Average output powers were reported to be more than 1 W[207]. Passively mode-locked femtosecond fibre laser in operation with Er:fluoride fibre in a ring configuration, having pulse duration of 207 nm and 3.5 kW peak power, were reported at working wavelengths near 2.8 μm [208]. Wavelength tunability in Er:ZBLAN lasers arises out of the splitting of the stark levels when placed inside the ZBLAN host medium. 160 nm broad tunability near 3 μm with CW mode operation in Er:ZBLAN fluoride fibre laser was demonstrated using Volume Bragg Gratings (VBG). The study also showed 62 nm tuning with Bi_2Te_3 nanosheets as a passive Q switch for pulsed operation with long nanosecond (880 ns) pulses [209]. 90 nm wavelength tunable fibre laser producing over 4 W average power and pulse energies of $\sim$30 μJ, centred at 2834 nm, have been demonstrated. The set uses plane ruled grating to achieve wavelength tunability. The pulses were passively Q-switched using a Fe^{2+}:ZnSe crystal, with pulse durations ranging from ns to μs [210]. 170 nm tunability between 2699-2869.9 nm was demonstrated in gain-switched, Er^{3+}-doped ZBLAN fibre laser with μs pulse durations were also reported. Wavelength tuning range varied depending on the pump power [211]. Recently, large core Er:ZBLAN fibre amplifier seeded by short nanosecond pulses (11.5-ns pulse duration,10 Hz repetition rate) KTA based OPO/ OPA operating at 2720 nm demonstrated $\sim$0.7 mJ, high pulse energies or 60.3 kW peak powers. The authors of the study noted that the due to the poor beam quality of the seed source, single mode operation was not possible, leading to multimode output from the fibre amplifier[212]. Supercontinuum generation has also been implemented in Er doped

fluoride fibres. Few octave wide, supercontinuum generation between 2.6-4.1 μm was demonstrated with seed pulses from an OPG source in a single mode Er: Fluoride fibre with over 82% of the power concentrated at wavelengths over 3 μm and having 400 ps duration pulses around 2.75 μ [213].

With these reviews in perspective, it is recognised that not many studies have explored investigating single mode Er:ZBLAN fibre amplifiers, seeded by OPOs, which can help in improving the output beam quality from the OPO by selecting the single mode region of the OPO output, if aligned well, in addition to high peak powers. The OPOs provide very wide tunability which can be utilized while examining the tunability in fibres. Furthermore, it becomes necessary to understand the practical limiting phenomena, if any, to power scaling and wavelength tuning applications in single mode ZBLAN fibres. This leaves an area of investigation open for the work presented in this thesis.

Chapter Three

Characterisation of a Tunable Optical Parametric Oscillator in Mid-IR

3.1 Introduction

Optical parametric oscillators (OPO) are viable sources in the NIR/mid-IR due to their capacity to produce tailored wavelengths in the IR spectra, that are not always accessible with conventional lasers, through the process of frequency conversion. Along with this, there is the added advantage of wide tunability which can make them a beneficial source with several potential applications like spectroscopy, remote sensing and photo-detection, as a broad range of wavelengths can be generated from a single device. Tunable OPOs were first demonstrated in 1965 [214] following several theoretical works [215, 216, 217, 218, 219].

While mid-infrared OPOs have been in prevalent since 1974 [220], quasiphasematched OPOs were introduced in 1995 [221] and is well evaluated due to its widespread use in mainstream research [108]. OPOs have continued to be a popular field of research till today, and recent works have demonstrated methods to calibrate and characterise mid-IR OPOs in different operational regimes of pulse duration and average input / output power levels [222, 223, 224]. This chapter summarises the experimental characterisation of a PPLN-based OPO as a potential pump source in the mid-IR

and the subsequent analysis of its wavelength tunability properties in this mid-IR spectral range.

3.2 Analysis of a MgO:PPLN OPO

The rationale behind setting up an OPO is to design a pump source that can emit a range of wavelengths in the Mid-IR. The main criteria here is to develop a frequency or wavelength tunable device, optical parametric oscillators become the primary choice for the purpose.

As discussed previously, an OPO is a nonlinear three wave mixing process, and an extended case of Difference Frequency Generation (DFG). The principal requirement for the OPO operation is to set up a stable resonator cavity to support small signal gain build up and maintain laser oscillation. Furthermore, there needs to be a nonlinear gain media within the resonator, which can sustain the nonlinear frequency mixing process. In the initial OPO development phases, these materials, like Lithium niobate, needed to be anisotropic in nature to satisfy the Birefringent Phasematching (BPM) condition for frequency conversion. Eventually, as a result of development of the technique of quasiphasematching (QPM), the same nonlinear materials could generate interesting signal and idler wavelengths by satisfying the QPM condition, and anisotropy was no longer an essential condition for frequency conversion to take place. An ensuing result of this was to attain frequency conversion by utilising isotropic materials with high nonlinear coefficients, by fulfilling the quasiphasematching condition alone.

To sustain the process of nonlinear conversion within an OPO, a Fabry Perot resonator was designed, that ensured that the Rayleigh length of the Gaussian mode oscillating within the resonator is confined tightly within the nonlinear medium, to allow maximum possible intensity contained within a small spatial region, and thus, yielding a significant nonlinear conversion. A simple design approach to maximise optical confinement of the laser beam, is to use an optimal focal length of a converging lens, right outside the cavity, to select the oscillating mode within the resonator. A second important factor is the optimum cavity length. As for the nonlinear gain medium, it is essential to use an oven to control the temperature of the nonlinear crystal,

which influences the phasematching criterion and allows for temperature dependent tunability of the output wavelengths. In addition, having multiple grating periods on a single crystal device, satisfying the QPM condition, permits even wider tunability.

Prior to building the OPO, relevant calculations were made to compute the necessary parameters for a stable Fabry Perot resonator needed to house the nonlinear crystal and the oven required for temperature tuning. The aim of the calculation was to find the suitable cavity length, and lens focal length to find the beam resonator mode, subject to the crystal dimension, oven length, and resonator mirror sizes. Additionally, a numerical simulation was carried out to model the expected signal and idler output from the OPO for a given pump. To estimate these values, the crystal material type, nonlinear properties, dimensions and the quasiphasematching criteria, i.e., the crystal poling / grating period were taken into consideration.

3.2.1 Theoretical Simulation of Signal and Idler for MgO:PPLN OPO

The nonlinear gain medium in this OPO is a 5% MgO doped periodically poled lithium niobate or PPLN (HC Photonics). Although the lithium niobate is anisotropic, phasematching condition is achieved by QPM, which provides higher effective nonlinear coefficient. The crystal had 7 grating periods, 28.5, 29, 29.5, 30, 30.5, 31, 31.5 μm fabricated on it. Tuning of signal and idler wavelengths was assumed to be achieved by varying the temperature between 100 °C and 200 °C and then this is to be repeated for all the seven grating periods.

To simulate the signal and the idler for a fixed grating period value, the pump wavelength was set at 1.064 μm. Since the frequency conversion is achieved by quasiphasematching, the aim is to satisfy the following condition:

$$k_p + k_s + \Delta k = k_i \tag{3.1}$$

where

$k_p = 2\pi n_p^{(e)}/\lambda_p$ = Pump Wave Vector

$k_s = 2\pi n_s^{(e)}/\lambda_s$ = Signal Wave Vector

$k_i = 2\pi n_i^{(e)}/\lambda_i$ = Idler Wave Vector

Δk = Phase Mismatch = $2\pi/\Lambda$ given Λ = Grating Constant of the Poling/Grating Period

The extraordinary refractive index $n^{(e)}$ for the pump, signal, and idler was calculated from the temperature dependent Sellmeier Equation for Lithium Niobate given by Jundt [225]

$$n_e^2 = a_1 + b_1 f + \frac{a_2 + b_2 f}{\lambda^2 - (a_3 + b_3 f)^2} + \frac{a_4 + b_4 f}{\lambda^2 - a_5^2} - a_6^2 \tag{3.2}$$

where f = Temperature Dependent Factor

$$f = (T - T_0)(T + T_0 + 2 \times 273.16) = (T - 24.5^{\circ}C)(T + 570.82) \tag{3.3}$$

Values for a_i, b_j coefficients is given in the following table 3.1is referred from Gayer et al. [226]

A variable QPM Error Function, which computes the phase match error, was defined.

$$QPMErrorFunction = n_p^{(e)}/\lambda_p - n_s^{(e)}/\lambda_s - n_i^{(e)}/\lambda_i - 1/\Lambda \tag{3.4}$$

To find a pair of signal and idler for a fixed pump, a given grating period and a particular temperature, the values for λ_s (signal) is varied between 1 to 2 times the pump wavelength, in small incremental values and the corresponding QPM Error Function is calculated for each of these signal values. Ideally, when this function reduces to zero, the phase matching condition is satisfied. However, in a numerical computation, this function cannot be equal to zero, so instead zero is defined as a very small range of values centred at zero. The value of λ_s for which the QPM Error Function falls within this range of zero, is a potential signal wavelength and the corresponding idler is calculated from the equation 3.5 below.

Constants	Value
a_1	5.756
a_2	0.0983
a_3	0.2020
a_4	189.32
a_5	12.52
a_6	$1.32 \times 10^{-}2$
b_1	$2.86 \times 10^{-}6$
b_2	$4.70 \times 10^{-}8$
b_3	$6.113 \times 10^{-}8$
b_4	$1.516 \times 10^{-}4$

Table 3.1: Values of Constants for temperature dependent extraordinary refractive index of 5% MgO doped PPLN

$$1/\lambda_p = 1/\lambda_s + 1/\lambda_i \tag{3.5}$$

3.2.2 Resonator Cavity Design

An essential component for setting up an OPO is a resonator, which helps amplify the small signal developed in a nonlinear medium placed inside it.This section discusses the essential parameters necessary to build a stable resonating cavity. The fundamentals of the resonator design are adapted from the concepts explained by Kogelnik et al. and Siegman [227, 228].

A resonating cavity typically consists of two mirrors (viz. M_1 and M_2) separated by a distance L. The radii of curvature (RoC) of the mirrors are assumed to be R_1 and R_2 and the mirrors are considered to be located at distances z_1 and z_2.

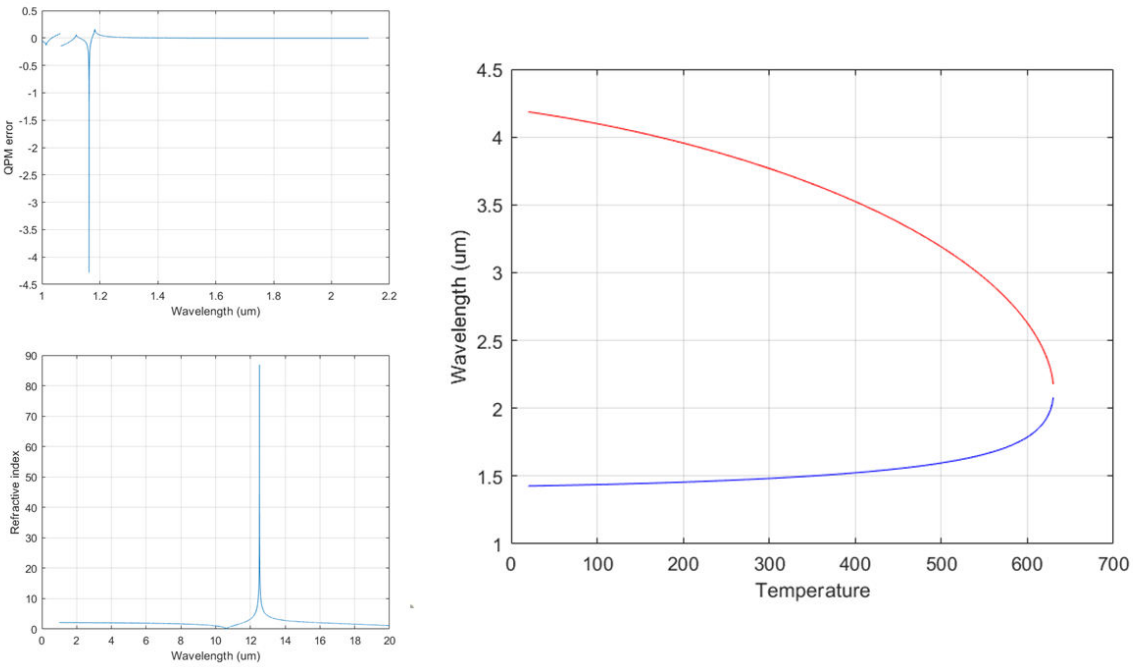

Figure 3.1: Simulation of signal and idler wavelengths for 28.5 μm grating period with temperature tuning (a) Variation of extraordinary refractive index with wavelength (b) Variation of QPM phase-match error for different signal wavelength values(c) Expected signal (blue) and idler (red) wavelengths for the given grating period over a range of temperature

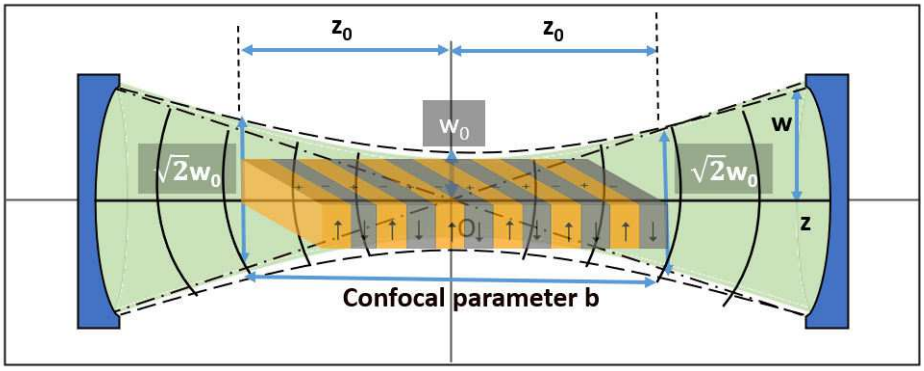

Figure 3.2: Resonator design

The mirror separation L, which is also the cavity length, can be given by

$$L = z_1 - z_2 \tag{3.6}$$

The Rayleigh range z_R of a Gaussian beam traversing through this cavity is given as,

$$z_R = \frac{\pi\omega_0^2}{\lambda_p} \tag{3.7}$$

Following standard sign convention, mirror curvatures are assumed to be concave while looking outward from the resonator are positive. The diverging radius of curvature of a Gaussian beam propagating to the right is considered positive, while a converging beam is taken as negative. The stability of a resonator is described by the g parameters, defined in terms of cavity length and mirror RoC.

$$g_{1,2} = 1 - \frac{L}{R_{1,2}} \tag{3.8}$$

The corresponding Rayleigh range and mirror positions in terms of the g parameters is,

$$z_R^2 = \frac{g_1 g_2(1 - g_1 g_2)}{(g_1 + g_2 - 2g_1 g_2)^2} L^2 \tag{3.9}$$

$$z_1 = \frac{g_2(1 - g_1)}{g_1 + g_2 - 2g_1 g_2} L \tag{3.10}$$

$$z_2 = \frac{g_1(1 - g_2)}{g_1 + g_2 - 2g_1 g_2} L \tag{3.11}$$

Confocal parameter b is defined as twice the Rayleigh length and thus given by the relation,

$$b = 2z_R \tag{3.12}$$

The final beam waist size and the spot sizes on the mirror as a function of stability factor g can be written as,

$$\omega_0^2 = \frac{L\lambda}{\pi}\sqrt{\frac{g_1 g_2(1-g_1 g_2)}{(g_1+g_2-2g_1 g_2)^2}} \tag{3.13}$$

$$\omega_1^2 = \frac{L\lambda}{\pi}\sqrt{\frac{g_2}{g_1(1-g_1 g_2)}} \tag{3.14}$$

$$\omega_2^2 = \frac{L\lambda}{\pi}\sqrt{\frac{g_1}{g_2(1-g_1 g_2)}} \tag{3.15}$$

For a symmetric resonator $R_1 = R_2 = R$ then, $g_1 = g_2 = g = (1 - L/R)$ and the beam waist simply reduces to:

$$\omega_0^2 = \frac{L\lambda}{\pi}\sqrt{\frac{1+g}{4(1-g)}} \tag{3.16}$$

$$\omega_1^2 = \omega_2^2 = \frac{L\lambda}{\pi}\sqrt{\frac{1}{(1-g^2)}} \tag{3.17}$$

The above factors were taken into consideration to ensure the beam confinement within the active medium, which in the case of this experiment is a PPLN crystal of dimensions 25 mm x 8 mm x 1 mm, to allow maximum frequency conversion. They were also used to estimate the required parameter like the optimal focal length of a lens to give rise to a stable resonator mode supported within the cavity.

Optimal cavity length for lasing was determined from the analysis of stable resonator design. From the estimations, it was verified that the cavity would be stable within the range of 6.5 cm to 15 cm. The length was limited by the dimensions of the crystal oven, so the minimum possible value for cavity length L could only be equal to the oven length of >5.5 cm.The calculated beam

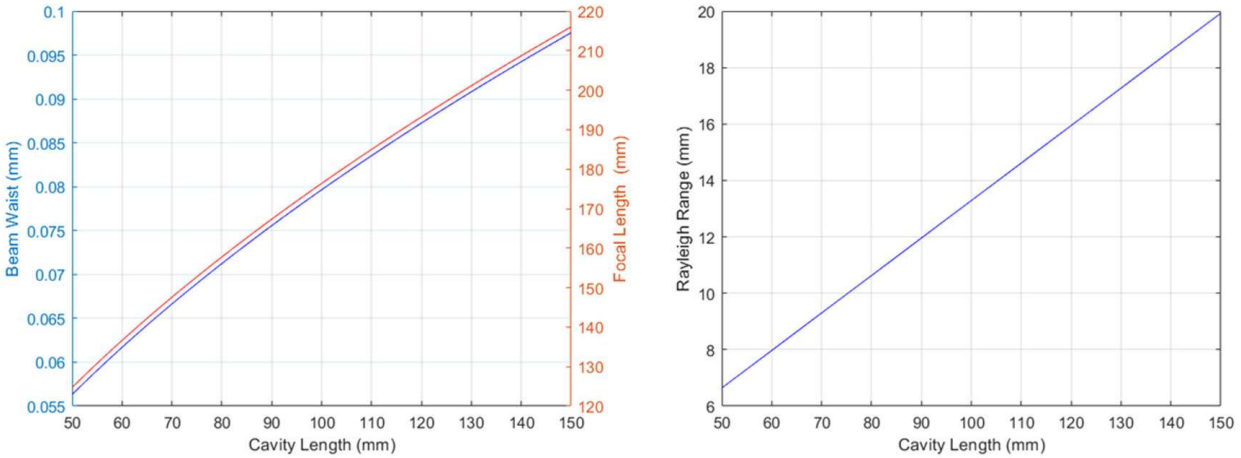

Figure 3.3: Cavity parameters for a stable resonator design. The cavity length was chosen to be 65 mm and the optimal focal length to ensure beam confinement was estimated at 142 mm and the closest commercial planoconvex lens of focal length 150 nm was selected for operation.

waist for the given mirror radii of curvature and cavity length of 6.5 cm was 64.22 μm, well within the 1 mm height of PPLN crystal with a Rayleigh range of 8.64 mm and confocal parameter b= 17.27 mm, within the crystal of 25 mm length.At the crystal edge, the beam spot radius was 113 μm and correspondingly, 3.25 mm at the mirror facets. The required focal length of a lens to limit the confocal parameter within the crystal edges, for maximum confinement of the laser beam in the crystal for effective frequency conversion, was also estimated. The ideal focal length for stable resonator modes would be $\sim$142 mm or more. The closest commercially available focal length was 150 mm (Thorlabs LA1433-C-ML), which was chosen for the experiment. Considering the wavelength of operation, the lenses had C code (1050-1700 nm) AR coatings on them.

3.3 Experimental Setup of Optical Parametric Oscillator

Fig 3.4 shows the experimental layout for the optical parametric oscillator. The OPO consists of a 5 mol% MgO doped congruent, periodically poled lithium niobate or PPLN crystal (HC Photonics, dimensions : 25 mm x 8 mm x 1 mm) as the active gain medium, placed in an oven (Covesion)

of length 6.5 cm and capable of movement along x and y directions, and connected to a temperature controller (Thorlabs TC200). The controller allows temperature variation between 25-200 ° C in steps of 0.1 ° C. The PPLN consists of seven grating or poling periods between 28.5-31.5 μm fabricated on it, attaining nonlinear frequency conversion by quasiphasematching and temperature tuning. The PPLN crystal had anti-reflection or AR coatings on its facets, with R $<$ 0.49% reflectivity at the pump wavelength 1064 nm and R $<$ 0.41% within the signal wavelength range. Two planoconcave mirrors with radius of curvature +/- 75 mm were used as the resonator mirrors for the OPO. To minimise unwanted reflections within the resonator cavity, the mirrors were coated with anti-reflection coatings, HR 1500 nm, HT 850 nm at the input end. The out-coupling mirror had coating specifications of HR 1064 nmnmμm to allow maximum reflection of the pump back into the cavity and concurrently allow the transmission of signals around 1500 nm.

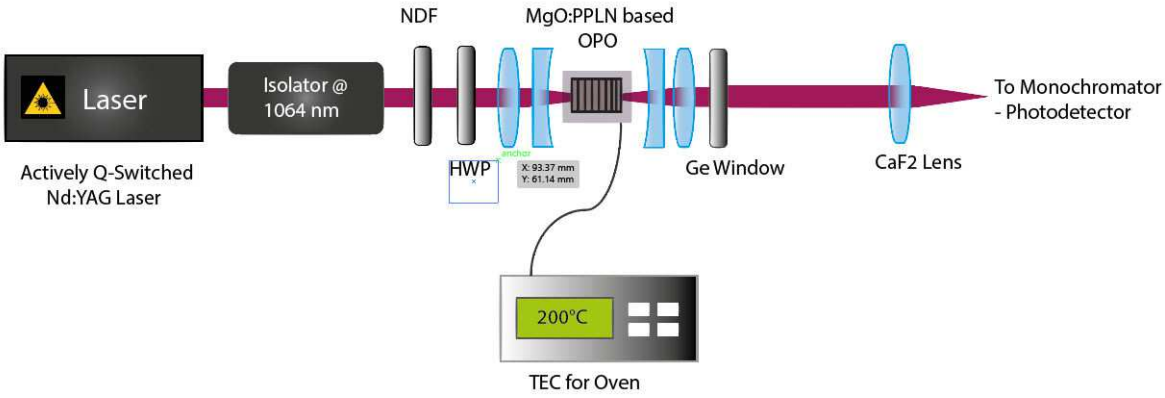

Figure 3.4: Experimental Setup for the Optical Parametric Oscillator(OPO), consisting of quasiphasematched MgO:PPLN as the nonlinear media. NDF-Neutral Density filter to manually control the Nd:YAG output powers, HWP – Half Wave Plate to align the orientation of the polarization of the 1064 nm laser line to align with that of the PPLN for maximum nonlinear conversion. TEC- Temperature Controller for temperature tuning to obtain a range of signal and idler outputs

The OPO is pumped by an actively Q-Switched Nd:YAG Laser (Laser 2000 – DTL324QT, λ =1064 nm, repetition rate = 1- 10kHz, pulse duration $<$ 10 ns). The laser light passes through a free space Faraday optical isolator operating at 1064 nm, to prevent any retro-reflections back into the

Instrument / Parameter	Value
Monochromator	Horiba iHR-550
Slit size	40 μm
Wavelength increment	0.05 nm
Theoretical resolution	$<$ 0.2 nm
Photodetector	Thorlabs PDA20H

Table 3.2: Instrument and measurement settings for spectral characterisation of OPO

pump, and a neutral density filter (NDF) to manually modulate the output power from the Nd:YAG laser. The light is then directed towards the resonator setup using broadband mirrors (Thorlabs BB1-E03: 750-1100 nm), a multi-order half-wave plate (HWP) is used to align the polarisation of the Nd:YAG laser to that of the PPLN to maximise the output. A C-coated, 150 mm focal length, planoconvex lens was selected to focus the light into the crystal placed inside the oven. The selection was based on calculations for a plane parallel resonator design and the dimensions of the crystal, and the housing oven were considered, to ensure the maximum overlap of the Rayleigh length of the pump laser beam within the length of the crystal. The output demonstrates tunability between 1400-4100 nm including both the signal and idler wavelengths, and can prove to be a suitable laser source in short-wave mid-IR.

The output from the OPO was collimated with a 100 mm uncoated CaF_2. A low pass filter FEL1150 was used to block the pump wavelengths and extract the signal and the idlers. To filter out only the idler component, a germanium window was used. The average output power from the OPO was measured using a thermal power meter. A monochromator (iHR-550) with a PbSe-based photodetector (Thorlabs PDA20H) at its exit, connected to a lock-in amplifier (Stanford Research Instruments) was used to record the spectra from the OPO.

3.4 Results

This section discusses the experimental results for the investigation of a PPLN-based OPO as a source of mid-IR wavelengths. The PPLN has seven grating periods (28.5, 29.0, 29.5, 30.0, 30.5, 31.0, 31.5 μm) and for the study, different wavelengths were generated by changing the grating periods and regulating the temperature of the PPLN housing oven between 100–200 ° C in steps of 10° C. The results discuss the measurements from the 31.5 μm grating period.

The variation of the average output power of the idler from the PPLN OPO with respect to the input power for the is shown in fig.3.5.The plot shows a pump to idler conversion efficiency of 36.3% for the 31.5 μm grating period, and 180.8 °C, which corresponds to a wavelength close to 2400 nm with a 6 nm margin of error, beyond a threshold of 115 mW of pump power at 10 kHz repetition rate.

The grating period was set at 31.5 μm and the temperature was tuned between 100–200 °C, in steps of 10 °C and the frequency converted output wavelengths were recorded and shown in fig 3.8. For this grating period, the corresponding spectral range varied widely over 1000 nm, between 1724 nm to 2762 nm. The results from numerical simulation to predict the possible signal and idler wavelengths were used as a reference to verify the OPO output shown in the inset of fig.3.8. While the general trend for the expected and measured wavelengths were analogous, there were differences in the values. This difference could be attributed to dealignment, where the beam is no longer parallel to the optical axis of the system and sees a non-uniform grating period in the PPLN crystal, during the process of frequency conversion, in addition to cavity losses, thermal effects etc.

Fig. 3.7 shows the recorded idler and signal spectra over a wavelength span of 50 nm at 110 ° C. The spectral shape of the idler had a Lorentzian profile, centred at 2728 nm. The spectrum shows dips, with a prominent one located near 2734 nm and is associated with atmospheric absorption. The signal wavelength was positioned at 1742 nm and also had a Lorentzian line profile. The signal wavelength is smooth and shows no absorption dips.

The complete tunable range of signals and idlers available with the device is shown in 3.8.

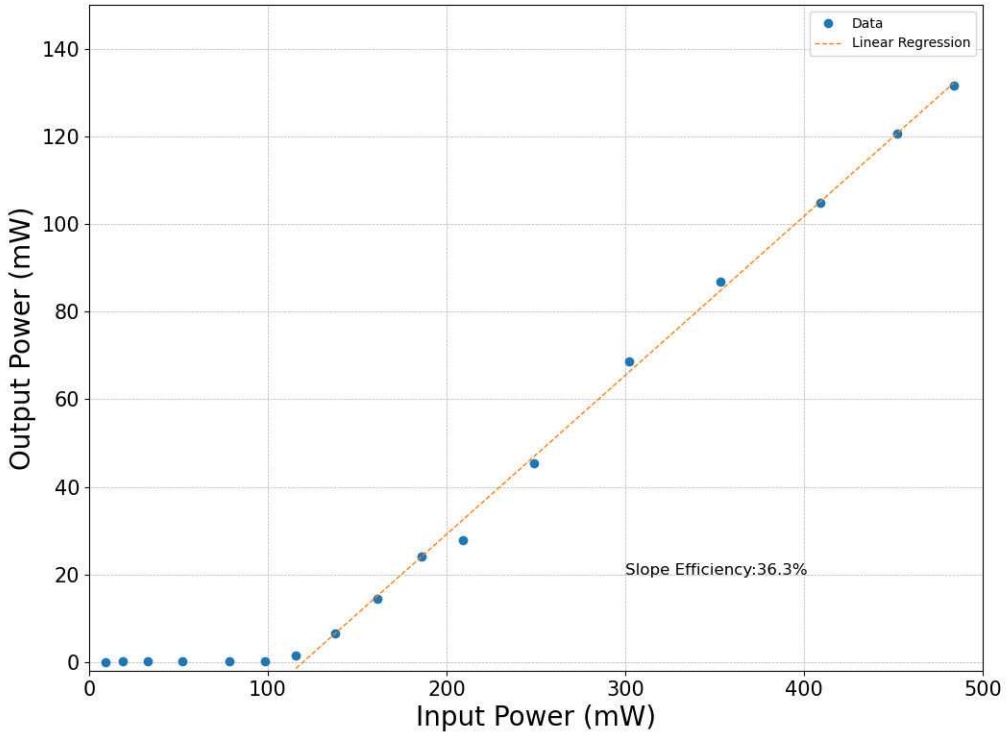

Figure 3.5: Power conversion efficiency of the idler in the 31.5 μm grating period and 180.8 °C translating to 2400 nm idler wavelength

The combined wavelengths ranged between 1400-4100 nm with the idlers concentrated in the mid-IR between 2168-4081 nm and pulse energies up to few microjoules, for 10 kHz repetition rate. Operating the pump at lower repetition rates could translate to more energetic pulses for practical applications.

The pulse energies show a drop in magnitude near 3.5 μm which is associated with fast multiphoton absorption, along with low photon energies observed in PPLN, deeper into the mid-IR, similar to those reported by [223, 224]. There is also limit to transparency due to the output mirror substrate silica, which show strong linear absorption near these wavelengths. A possible way to address the issue is by using output mirror with better coatings and resonance properties with respect to the output beams for better performance of the OPO. Changing the output mirror

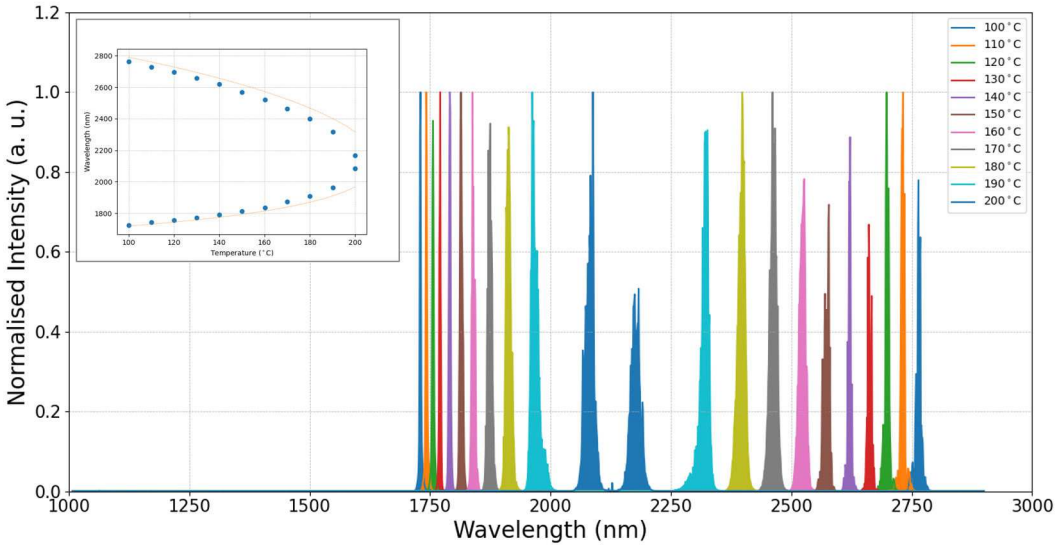

Figure 3.6: Predicted and measured signal and idler wavelengths generated by temperature tuning over 100 to 200 °C for a 31.5 μm grating period at 10 kHz repetition rate. The graph shows the measured spectra at these temperatures for the 31.5 μm, and the inset shows the corresponding temperature tuning curve.

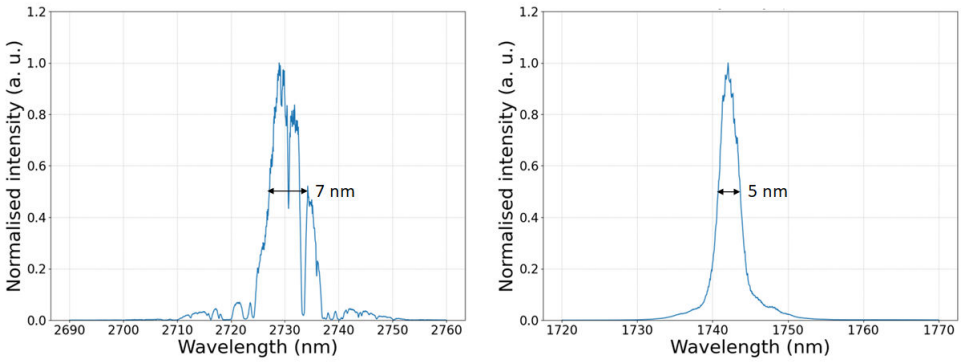

Figure 3.7: Measured signal and idler spectra generated by setting the temperature at 110 ° C for the 31.5 μm grating period. The idler was recorded at 2728 nm with a $1/e^2$ bandwidth of 7 nm. The idler is centred at 1742 nm with a bandwidth of 5 nm.

material to one with extended transparency, like CaF_2, can help achieve higher output powers at longer wavelengths in the 3-5 μm band.

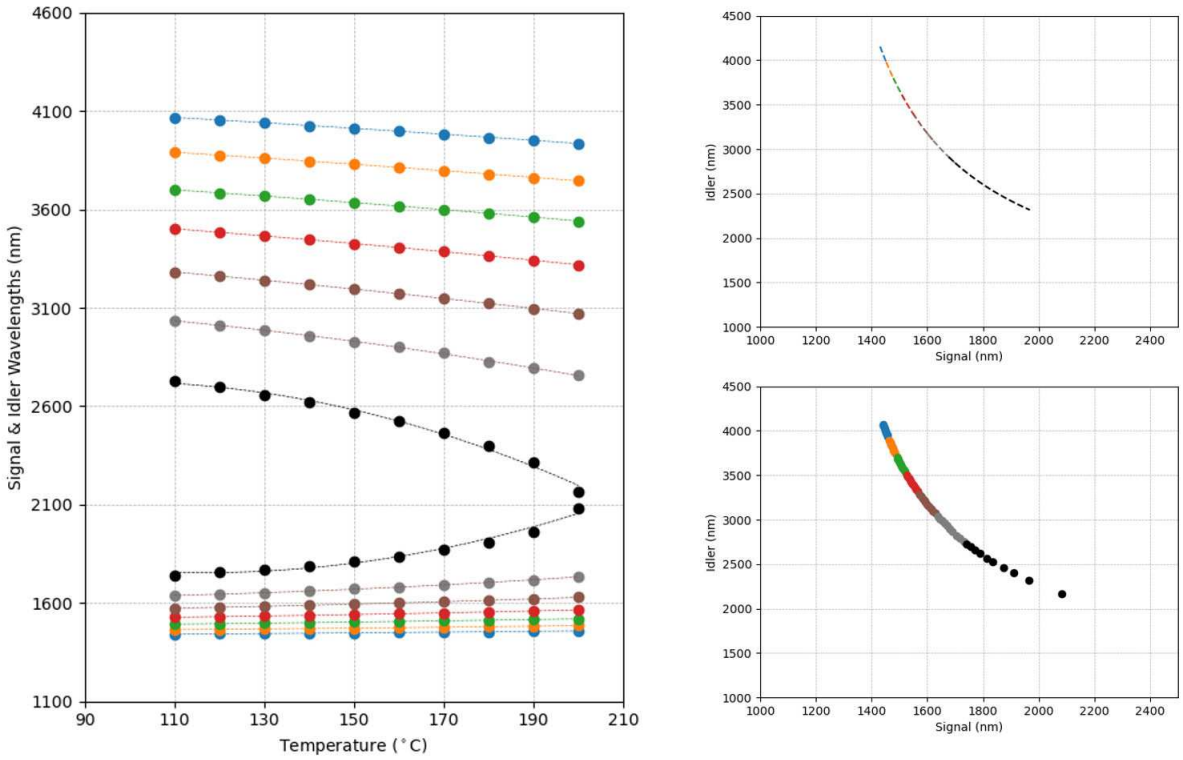

Figure 3.8: OPO Signals and Idlers tuned over different grating periods with temperature tuning were recorded from the experiment and presented in Fig a). The range of wavelengths achieved was between 2168–4081 nm. The simulated and the experimental values of the wavelength tuning demonstrate a high correlation seen from Fig. b) and c) respectively

For some grating period and tuning temperature combination, the full spectrum beyond the pump wavelengths exhibit spectral mixing. Fig 3.10 shows the normalised OPO output spectrum from the 30.0 μm Grating Period at 180 °C. Fig 3.10(a) shows additional spectral components along with the idler (Fig 3.10(c)) and signal (Fig 3.10(d)) wavelengths. (Fig 3.10(b)) shows the output spectrum filtered by the low pass FEL1150 filter, cutting off pump wavelengths.

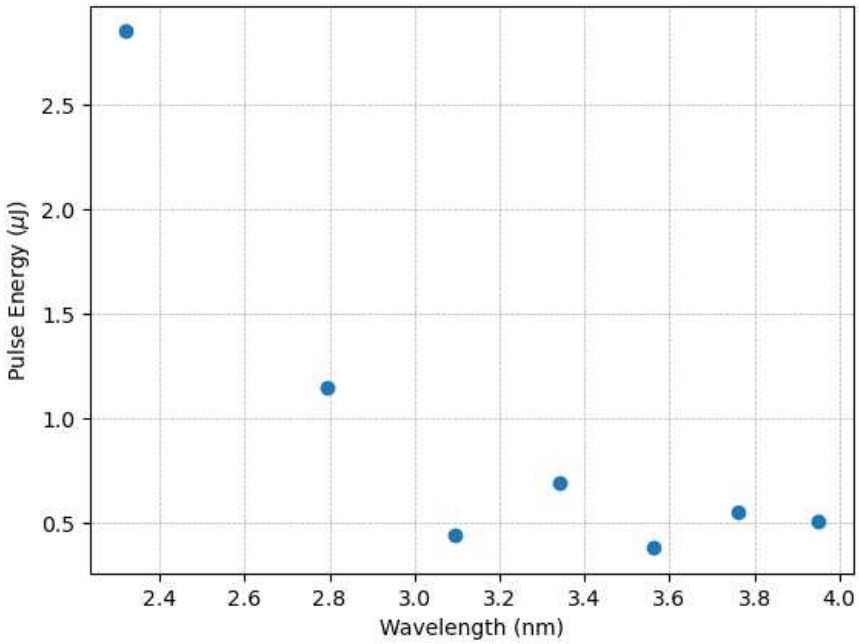

Figure 3.9: Pulse energies vs wavelength, demonstrating absorption near 3.5 μm.The low power at these wavelengths can be attributed to the output mirror substrate silica and multiphoton absorption

3.5 Conclusion

A broad tunable OPO-based mid-IR laser operating between 2.1-4.0 μm is demonstrated. The mid-IR wavelengths are obtained by frequency conversion achieved by satisfying quasiphasematching condition over seven poling or grating periods ranging from 28.0-31.5 μm, fabricated on a commercial 5% MgO doped PPLN crystal. Temperature modulation provides further tunability. The OPO is pumped with an actively Q-switched Nd:YAG laser operating at 1.06 μm, 10 kHz repetition rate and pump pulse energies of nearly 30 μJ, generating sub-10 nanosecond pulses of up to 3 μJ at 2.4 μm. Following research with other nonlinear materials utilised in OPOs, it is also possible to vastly increase the bandwidth of the OPO by combining it with intra-cavity SHG, SFG [229]. Operating at lower repetition rates produced higher output pulse energies of up to 10 μJ. These sources can be good choices for spectroscopy applications, higher pulse energies could be achieved by optimising

the pump and OPO alignment.Near 3 μm range the output pulse energies were around 1 μJ. These wavelengths are close to mid-IR emissions for rare earth dopants and thus, such OPOs can prove to be suitable seed laser sources for MOPA based rare earth doped amplifier and lasers.

OPO output linewidth and performance considerations

The chief difference between a laser and an OPO is that a laser is able to absorb and store any broad-band pump energy, but the emitted wavelength and linewidth are solely determined by the atomic transition in the lasing medium, while in an OPO, the phase relation between the pump, signal, and idler significantly influences the wavelength and linewidth of the OPO output. [230].Consequently, the linewidth of the pump laser contributes to the spectral linewidths of signal and idler waves, especially during the fulfilment of the phasematching condition. While the phasematching condition remains necessary for the effective energy conversion of the pump to the signal and idler within the OPO, the condition is achieved when the pump phase velocity is equal to the signal and idler phase velocities. In case of QPM, the phase-mismatch is overcome by utilising different domain periodicities Eqn. 2.1.2. A broader pump linewidth implies that the linewidth contains several more frequency components. In real-life conditions, the phase velocities of these components are impacted by dispersion effects while traversing through the nonlinear crystal, thus their values becoming slightly deviated from the precise value (ideal value needed for seamless frequency conversion). Subsequently, even with the implementation of QPM condition, the phase mismatch Δk is zero for a very narrow central band of frequencies which experience significant conversion efficiency. For the frequencies away from the central band, the phase-mismatch between the components is marginally non-zero. As a result, they undergo frequency conversion but with reduced conversion efficiency, and results in different frequency components converted with different efficiencies, which reduce for the frequencies, as you move away from the narrow central band, resulting in the broader linewidths of the signal and idler. Thus, wider bandwidth of the pump laser, the larger the values for Δk, hence wider the signal/idler linewidths. To overcome the issue, it is possible to employ narrow linewidth pump lasers having single longitudinal mode or by introducing methods to attain frequency stabilisation of the OPO system.

The other important factor which affects the linewidth is the OPO cavity length. As the pump frequency interacts with the nonlinear medium, the pump energy undergoes frequency conversion into signal and idler waves, which have a fixed phase relationship with the pump wave, and subsequently a standing wave is formed within the cavity as the signal and idler photons resonate. Now since several combinations of signal and idler can potentially satisfy the resonant condition (ωp $= \omega$s $+ \omega$i) for a given pump frequency, each potential pair of signal and idler frequencies represent a standing wave, known as the longitudinal mode, within the cavity. The cavity length influences the number and establishes the spacing between these various longitudinal modes. The spectral bandwidth of the longitudinal modes determines the linewidth of the signal and idler output, and is inversely proportional to the cavity length of the OPO resonator. Shorter cavity length can result in a wider linewidth of the generated output frequencies, with lesser number of longitudinal modes and larger mode spacing.By increasing the cavity length, OPOs can produce narrower linewidths of the signal and idler waves, which may be more efficient in practical applications.

In a quasiphasematched optical parametric oscillator (OPO), the crystal length and domain period also play an important role in determining the output linewidth. The crystal is domain-engineered with a periodic modulation of the nonlinear susceptibility along its length to compensate for the phase mismatch between the interacting waves and determine the spectral properties of the signal and idler waves. Shorter crystal lengths or longer domain periods can lead to broader linewidths, while longer crystal lengths or shorter domain periods can improve phase-matching and reduce linewidths. By optimizing the crystal length and domain period, it is possible to realise narrower linewidths and enhance the overall performance of the OPO. The choice of crystal, lithium niobate (d_{33} = 27 pm/V), sets the nonlinear coefficient of the medium used in the QPM OPO. The nonlinear coefficient along with crystal length and domain period structure together help achieve the optimal conversion efficient and linewidth.

Optimising the pump power is also critical for minimising the output linewidth in a quasiphase-matched optical parametric oscillator (OPO). Increasing pump power leads to stronger nonlinear interactions among the pump, signal, and idler waves, resulting in higher conversion efficiency and

a narrower linewidth. However, higher pump powers can also lead to spectral broadening due to phase mismatch and the generation of additional spectral components from four-wave mixing. Attaining optimal pump power requires careful consideration of the crystal length, modulation period, and temperature as well. Numerical modelling and simulation can be used to predict the impact of various pump power levels on the conversion efficiency and linewidth, whereas an incremental power-linewidth scan can identify the maximum power corresponding to the narrowest possible spectral linewidth. It is important to note that the optimal pump power may vary depending on the specific OPO setup, and that the pump power must remain within the safe operating range to avoid damaging the crystal or other components.

Similar to the pump power, OPO temperature also critically influences the linewidths of a QPM-OPO. The nonlinear coefficient of the crystal increases due to thermal effects at higher temperatures, which result in strong nonlinear interaction and thereby narrower linewidths. Conversely, higher temperatures can also cause broadening of the linewidth due to phase mismatch as a result of thermal lensing and expansion. Thus, careful optimisation of the temperature is also necessary for optimal performance of the OPO.

However, there is a trade-off between the narrowest possible linewidth of a pump and the efficiency of the OPO. Extremely narrow linewidth constrains the phasematching condition, reducing the conversion efficiency of the OPO. The phasematching bandwidth, which usually broader than the pump linewidth, determines the spectral bandwidth of the signal and idler wave.Thus, a broader linewidth pump laser allows efficient conversion of the pump power to generated signal and idler output.

In the pulsed regime, the repetition rate is also critical to the performance of an OPO. Lower repetition rates allow longer pulse durations and thus higher pulse energies, which improve the conversion efficiency and also warrant narrower output linewidths. This can be attributed to stronger nonlinear interaction between the pump, signal and idler waves. Contrarily, higher repetition rates decrease the pulse duration and pulse energy, resulting in decreased conversion efficiency and broadening of linewidth. Furthermore, higher repetition rates can cause an escalation

of thermal effects like thermal lensing and distortion, which impair the efficient OPO operation. A trade-off between the pump power, pulse energy, pulse duration, and observed thermal effects must be balanced to obtain a stable OPO performance.

Optical parametric oscillator technology is mature and well-researched [230, 231]. Additionally, it is one of the most versatile options for widely tunable sources, especially for generating custom wavelengths in the mid-IR. Currently, the state-of-the-art keeps pushing the boundaries of output power, wavelength limits, linewidth minima, frequency stabilisation with novel nonlinear material properties, different crystal geometries, set-up configurations, intra-cavity elements and manipulation of the nonlinear dynamics within the OPO [109, 112, 114, 115, 118, 120, 232]. The OPO developed for operation, as discussed in this chapter, conforms with the established outcomes from research, particularly in terms of wavelength tunability and the relative ease of access to wavelengths of interest in the mid-IR [111, 224]. The result of the experiment concentrates explicitly on the tailored output wavelengths, especially those around 2.8 μm, which hold practical significance for biomedical applications like surgery, bio-printing etc., due to the presence of a major water absorption maxima, but a comparatively subjacent focus on the output powers and linewidth of the emitted spectra, which could be further investigated for applications in diagnostic spectroscopy. Ultimately, key wavelengths, even with low output powers, could be immensely resourceful, since the power could be amplified through different amplifier configurations.

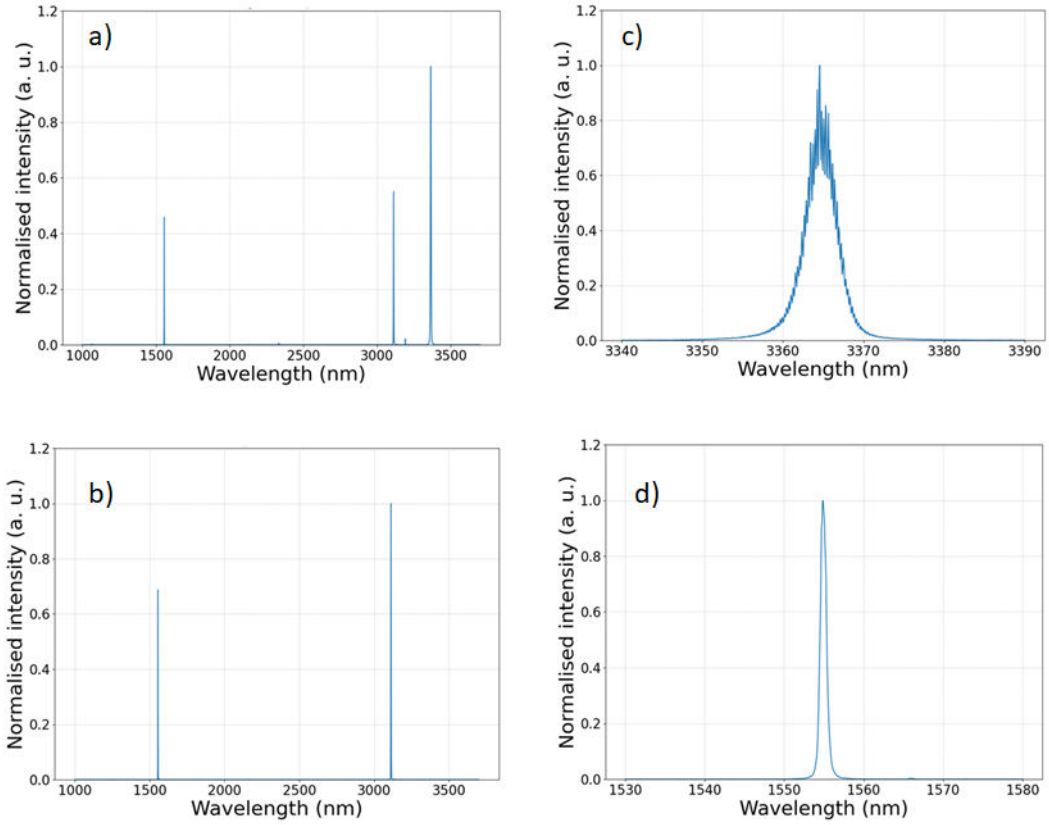

Figure 3.10: OPO Spectrum from 30.0 μm Grating Period at 180 °C. Fig a) shows the full spectrum consisting of signal wavelength, idler wavelength and a mixed spectrum. Using an FEL1150 filter to cut off the pump results in a clean spectrum, shown in Fig. b). Fig. c) and d) show the idler and the signal wavelengths recorded over a span of 50 nm. No atmospheric absorption is observed in the idler spectra.

Chapter Four

Investigation of Amplification in Erbium-doped Fluoride Fibre Amplifier

4.1 Introduction

Erbium doped fibre amplifiers have been exhaustively used in telecommunication applications since they were reported [233]. 3μm emission from Erbium doped fibres were first reported in 1967 [234], the first continuous wave operation in 1983 [235] and the first 3μm fibre laser was demonstrated in 1988 [189]. Introduction of fluoride (ZBLAN) fibres in 1974 opened the possibility of operation in the mid-IR region due to the broad transparency window of fluoride glass hosts and their structure conformable to doping processes. Along with this, Erbium also demonstrated the highest gain when compared to the other ZBLAN fibre amplifiers with rare earth doping [196, 236]. Erbium-doped fluoride fibre amplifiers also allow high levels of power amplification; when combined, these properties can be applied to develop a compact, tunable, and proficient fibre-based laser delivery system in the mid-IR. This chapter investigates the single pass, power amplification in a single stage, Erbium doped fluoride fibre amplifier using nanosecond seed pulses.

4.1.1 Master Oscillator Power Amplifier

When considering the design of a high power laser with a single stage system, the main challenge is often the reduced beam quality and intensity due to thermal effects that build up within the system. However, many studies have shown that power scaling in a laser system becomes feasible when low power beams are coupled to with amplifier stages to obtain a single output. In such a case, thermal deterioration of the beam quality and efficiency can be avoided by operating the input beam at its ideal power level and combination with a separate amplifier module prove to be a promising method for increasing the output power of a laser system.

The MOPA architecture consists of a small signal seed pulse produced by a master oscillator which undergoes a gain amplification in an amplifier succeeding the pulse generator, resulting in a large, amplified output pulse. This schema is primarily adopted because seed pulse is usually low in power which ensures easier pulse control, greater frequency stabilization in the seed pulse thus allowing more controllable power outputs after the amplification from the power amplifier section of the configuration. Additionally, these systems have minimal thermally induced phase noise due to the absence of a cavity. Moreover, fibre-based MOPA also enables streamlined power scalability by avoiding the use of multiple cascaded lasers, which might be alignment sensitive.

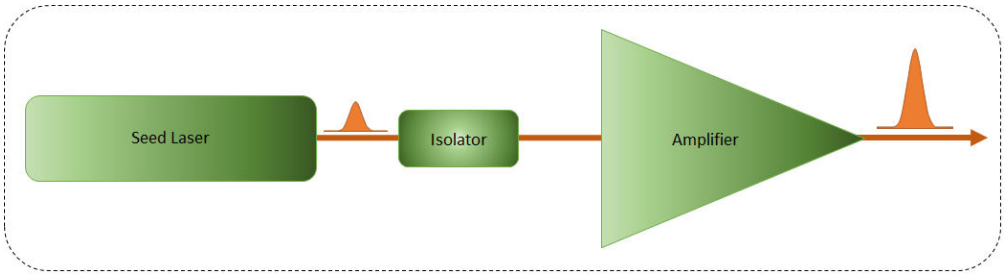

Figure 4.1: Master Oscillator Power Amplifier configuration

However, the MOPA architecture is not without its limitations. Principal drawbacks of this configuration include the complexity of the architecture, lower electronic-optical power conversion, higher amplifier noise, and high sensitivity to back reflections which may be amplified by the amplifier. Additionally, nonlinear effects such as Stimulated Brillouin Scattering (SBS) impedes the

high power, narrow linewidth output is another hindrance to the amplifier performance. SBS can be mitigated by employing special fibres that support the separation of acoustic and optical modes of the amplified pulse or by introducing strain gradients inside the fibre using linear chirped sources, phase-modulation techniques[237]. Another important limitations is the Stimulated Raman Scattering (SRS) which degrades the output beam quality of fibres in continuous wave operation [238]. Methods of controlling SRS in include use of large mode area fibres, which increases the MFD and thereby reduce the intensity at the fibre core. Other approaches include mode selective tapers, special coiling geometries, using long period gratings which can help in coupling in the Stokes wavelength from the core into the cladding [239], special fibre design to suppress Stokes wavelength over propagation through the fibre etc. Self-phase modulation and self-focusing also contribute to the drawbacks of this architecture.

4.1.2 Double Clad Pumping

The current advanced high power fibre amplifier (or lasers) can deliver several tens of watts of power with superior beam quality, with high single pass gain and stability of operation. This is made possible by the good thermal management, improved wave-guiding geometry and significantly by the introduction of clad pumping configuration.

In double clad pumping, the single-mode (or multimode) core through which the laser pulse travels, is encircled by an inner cladding through which the pump light travels, and an additional lower refractive index outer cladding beyond it. Rare-earth doping responsible for the laser emission, is restricted to the core or within a small ring surrounding the core, and the inner cladding (or pump cladding) confines the pump, due to the lower RI of the outer cladding. The pump also partially seeps into the core, where it is absorbed by the active dopant ions. The pump cladding usually provides a high surface to volume ratio in the fibres which allows faster heat removal, preventing thermal lensing effects within the fibre, especially when very high gains build up within the core.

Before the introduction of double clad pumping [240], fibres were usually side pumped, and the diffraction limited quality of the beam was severely affected by the beam quality of pump diodes,

when operating in the high power mode. This made efficient alignment of the beam into the fibre core, difficult. With double clad fibres, the low RI outer cladding, usually made of polymer or glass or even air, allows pump light to be guided in the inner cladding. While the core guides the signal, the difference of RI between the first and second claddings are high, and the pump clads come with large diameters, making it possible to couple high power pump beams with relatively high divergence[241] using fairly simple alignment optics. As for limitations with double clad fibres, the power scaling of an amplifier can be limited by factors like propagation losses, amplified spontaneous emission (ASE), thermal degradation, nonlinear effects such as self-focusing and optical breakdown of fibre material. [242].

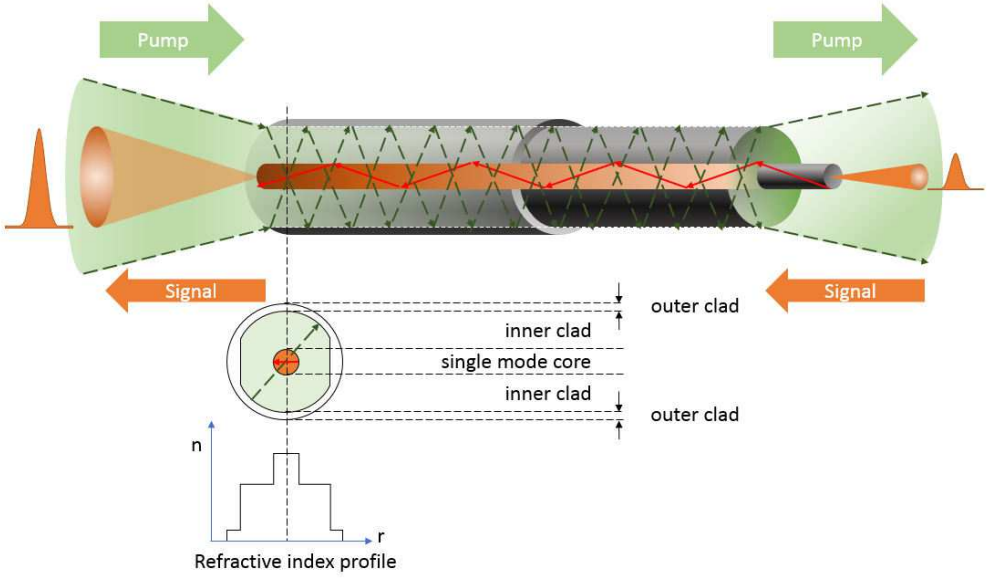

Figure 4.2: Double Clad Pumping Scheme

To overcome the limitations in power scaling, many cross-sectional geometries of the inner cladding have been suggested and studied, especially for single mode, small core fibres [243]. This is done with the aim to ensure better overlapping of the different pump modes, launched into the fibre, with the active core, allowing efficient energy transfer from the meridional pump rays to the signal beam supporting amplification.Different recommended cladding geometries have varying rates of absorption, as one moves from the input to the output end. The ideal pump absorption is given by the relation:

$$ideal\,pump\,absorption \propto \sigma_a^{core} \frac{A_{core}}{A_{clad}} \tag{4.1}$$

This equation suggests that the absorption, in log scale, linearly increases with the distance from the launch end, but in reality, the scheme transfers high pump energy at the launch end but in standard concentric core-clad configuration, as the pump light gets absorbed through the length of the fibre, the rate of pump absorption saturates and the only skew rays remain within the inner clad, which cannot transfer the energy to the core. Thus, cladding geometries are designed to minimise skew rays. Additionally, it is also practical to have lower pump absorption initially to minimise the heat generated. These conditions have given rise to several designs of inner cladding geometries with pump absorption rates close to ideal, i.e. homogeneous pump absorption along the length of the fibre. These geometries are shown in Fig 4.3

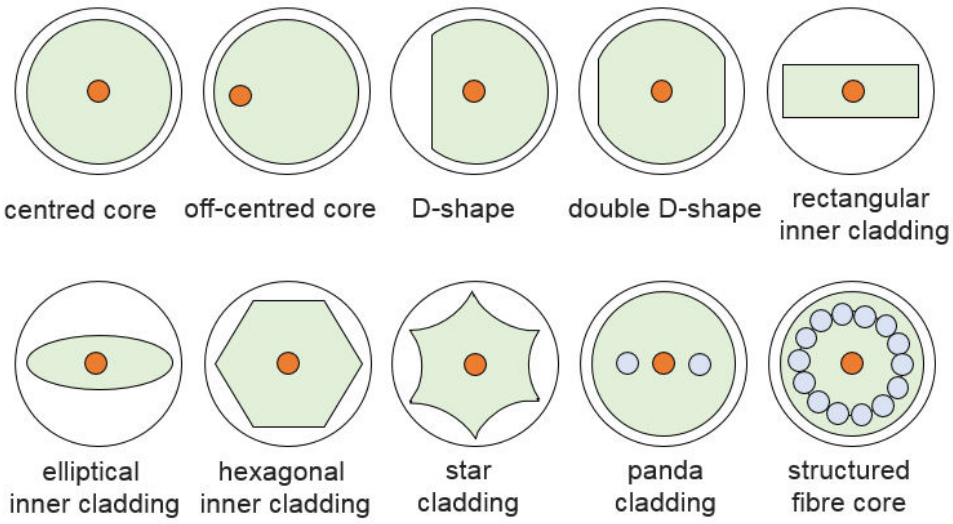

Figure 4.3: Inner cladding geometry for efficient pump absorption

4.1.3 Self-Phase Modulation

When a high intensity laser beam propagates within the fibre, the beam enveloped itself undergoes a nonlinear phase shift in the time domain due to a change of refractive index induced by the high

intensity, known as optical Kerr effect, resulting in a spectral broadening of the amplified pulse. This causes creation of new frequencies are produced, increasing the spectral content of the pulse.

Considering the Electric field E of the laser beam travelling in a fibre, along z direction is

$$E = \frac{1}{2}\left(\hat{E}_0 exp\left(i(\omega_o t - \frac{2\pi}{\lambda}\tilde{n}z) + c.c.\right)\right) \tag{4.2}$$

The change in refractive index due to Optical Kerr Effect is given by,

$$\tilde{n} = n_0 + n_2 I \tag{4.3}$$

The optical phase can be written as

$$\phi = \omega_0 t - \frac{2\pi}{\lambda}(n_0 + n_2 I)z \tag{4.4}$$

where $I = P/A_{eff} = 2P/MFD^2$, MFD being the Mode Field Diameter of the field propagating in the fibre

The new propagation constant β is given as,

$$\beta = \frac{2\pi}{\lambda} = \beta_0 + \gamma P \tag{4.5}$$

where $\beta_0 = \frac{2\pi}{\lambda} n_0$ is the propagation constant and $\gamma = \frac{2\pi}{\lambda}\frac{n_2}{A_{eff}}$ = Nonlinear Parameter,

so the temporal phase shift is

$$or \phi = \omega_0 t - \beta_0 z - \gamma P(z) z \tag{4.6}$$

If $\gamma P(z)z$ is the phase due to SPM over length dz,

The total nonlinear phase developed over the fibre length L is

$$\phi_{NL} = \int_0^L \gamma P(z) dz = \int_0^L \gamma P_{in}(z) exp(-\alpha z) dz \phi_{NL} = \gamma P_{in}\left(\frac{1 - exp(-\alpha L)}{\alpha}\right) = \gamma P_{in} L_{eff} \tag{4.7}$$

where L_{eff} is the effective fibre length or the equivalent fibre length over which the power is assumed to be constant

Now, to find the pulse evolution due to SPM, differentiating equation.4.4

$$\omega = \frac{\partial \phi}{\partial t} = \omega_0 - \frac{2\pi}{\lambda_0} n_2 \frac{dI}{dt} z \tag{4.8}$$

where ω is the instantaneous frequency. While the initial field only has a ω_0 component, the nonlinear effect of SPM generates new frequencies depending on the change of intensity profile over the transverse plane as the field propagates through the fibre, causing a broadening in the pulse shape.

This phenomenon is the temporal equivalent of self-focusing, which causes the high intensity beam to narrow down and collapse on itself due to a similar effect along the length of the fibre.

4.1.4 Amplified Spontaneous Emission

Amplified spontaneous emission (ASE) is commonly believed to be a key contributor to laser linewidth broadening in the operation of amplifiers. The photons generated by spontaneous emission are out of phase with the laser and this results in a phase fluctuation which causes the broadening of the laser linewidth. It has been also been reported that ASE contributes to laser broadening in form as additive noise [244].For fluoride fibre amplifiers, the effect of ASE on the efficiency of the amplifier depends on the amplifier configuration and length of the fibre [245].

In the current scenario of tunable sources, OPOs demonstrate wide tunable ranges, and combining such sources with tunable fibre systems can help in developing tunable high-power sources covering a wide spectral range. The sheer maturity of Erbium-doped fibre technology has allowed a reliable fabrication, and extensive investigation of Erbium-doped fluoride fibres. This chapter details the experimental study of wavelength-tuning in a single-mode Er-doped fluoride fibre amplifier to analyse the gain-bandwidth in the amplifier at different wavelengths near 2.8 μm for different pump

powers. These parameters can provide insight into the full emission range of an Er-doped fibre amplifier. This can be achieved when the amplifier is seeded with a wider tunable source, like the OPO. However, the wavelength tuning range yielded due to nonlinear optical processes like supercontinuum and soliton shifts etc. is beyond the scope of the experiment. In this work, the wavelength tunability of the fibre amplifier is studied using a seed signal, an idler pulse, generated from a tunable nanosecond pulsed MgO:PPLN-based OPO.

Mode Instabilities

A phenomenon which can prove to be a significant hindrance to power scaling in high power fibre amplifiers is the onset of mode instability, in which, the high gain developed in the fibre amplifier distorts the mode field diameter of the beam, thereby deteriorating output beam quality [246]. This usually happens after the gain reaches a certain threshold value, and if the power remains below this limit, which could be anything between a few hundred W to a few kW, the beam profile remains in the single mode [247]. Additionally, high gain may also cause temporal fluctuations in the mode, in the order of few kHz, and with increasing gain, these fluctuations can be chaotic in nature. This was simulated [248], and demonstrated [249, 250]. The instability has been attributed to reasons such as changes in refractive index that are induced due to population inversion, called the Kramers-Kronig effect, and heat gradients generated along the transverse direction of a fibre due to the amplification itself [251]. Some proposed methods to overcome this limitation include increasing the instability threshold value by saturating the population inversion hence the amplifier gain, and a passive approach to alter the fibre design, and decreasing pump absorption [252, 253]. When considering power scaling of fibre amplifiers, it thus becomes relevant to consider the impact and mitigation of such instabilities, which can influence the desired single mode beam quality from the output.

Parameter	Value
Cladding type	Double Clad
Fibre Length	2.1 m
Core diameter	15.5 μm
NA (Core)	0.125
Cladding diameter	260 μm
NA (Cladding)	0.46
Doping Concentration	7% mol
Cut-off wavelength (for single mode operation)	2.5 μm
Cleaving angle for Input End	4°
Cleaving angle for Output End	13°

Table 4.1: Fibre Parameters

4.2 Experimental Study of power scaling in fibre amplifier

To investigate the amplification of signal in Er:ZBLAN fibres, a single mode double clad ZBLAN fibre from Le Verre Fluoré was employed. The relevant parameters of the fibre are listed in the Table 4.1. Fig. 4.4 shows the image of the fibre facet. Fluoride fibres are fragile and highly susceptible to facet damage due to a number of factors such as high pumping intensity, forward pumping geometry leading to concentration of a large amount of heat in the small-sized core and facets, parasitic self lasing and back-reflections. Fibres facets are angle-cleaved to protect them from damage due to Fresnel back-reflections at the air-fibre interface. Moreover, the fibre tips are also protected with AlF_3 end-caps spliced onto the ends to prevent degradation from scorching and facet deterioration due to hydroxyl ion (OH^-) diffusion.

Fig. 4.5 shows the experimental setup to study the gain in the fibre amplifier.The configuration follows a Master Oscillator Power Amplifier (MOPA) architecture. The nanosecond seed pulses were produced by an Optical Parametric Oscillator (Master Oscillator) and amplified in a single

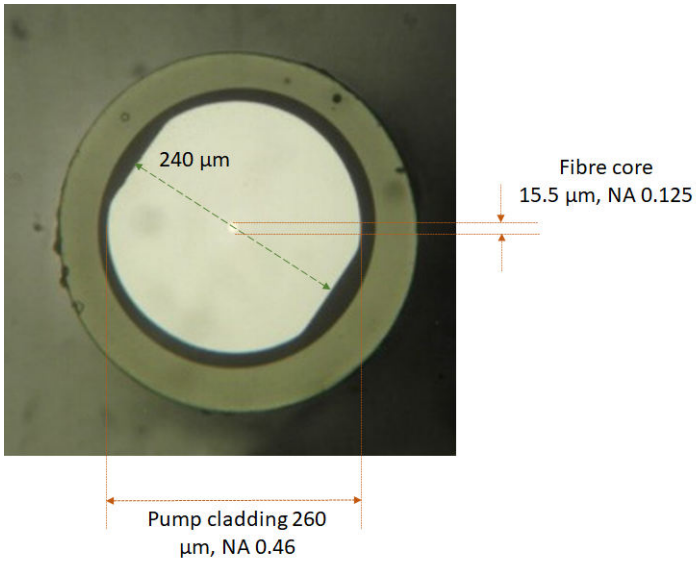

Figure 4.4: Fibre facet showing double D-shaped cladding geometry, Image Courtesy : Le Verre Fluoré, France

stage fibre amplifier (Power Amplifier) separated by a tunable optical isolator (Thorlabs I2700Y4) operating at 2750 nm.The seed pulse was coupled into the amplifier with an uncoated CaF_2 lens of 25 mm focal length. The amplifier was pumped in a counter-propagating mode with a multimode pump diode at 978 nm (5 nm bandwidth) with a multimode fibre of core diameter 200 μm (NA = 0.22). coupled into the opposite end of the fibre with an uncoated CaF_2 lens of focal length 20 mm, the same used for collimating the output signal from the amplifier. Two dichroic mirrors (T $>$ 97 % at 2800 nm, R $>$ 99.5 % at 980 nm) were used to couple and decouple the pump and seed lasers at the input and the output ends. The dichroic mirror along with the cleaved ends of the fibre helps in restricting the back reflections and back-propagating pump in the fibre amplifier.

To start with, the LIV characteristics of the multimode pump diode (Coherent) was recorded using a thermal power meter (Newport). This was required to determine the electrical to optical conversion efficiency of the pump, the pump threshold for determining the operating region for the pump and, in due course, to find the slope efficiency of the fibre amplifier.

For this investigation of amplification, the most efficient wavelength of 2789 nm with maxi-

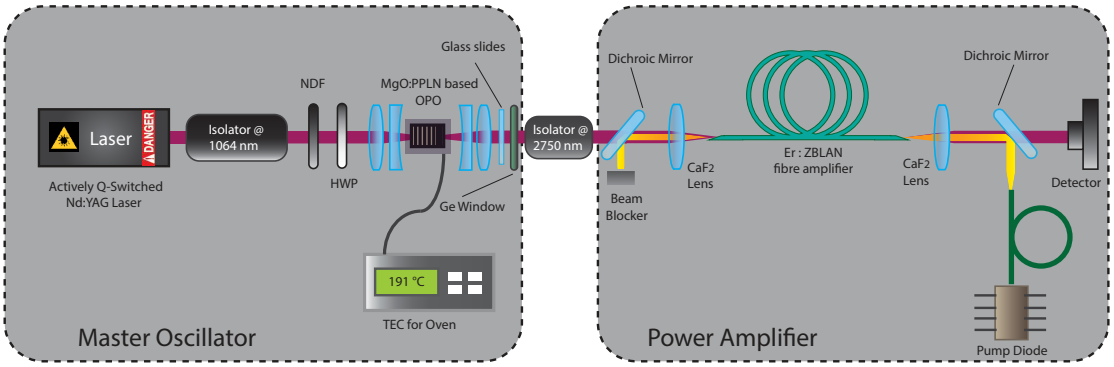

Figure 4.5: Experimental setup based on MOPA architecture

mum average output power was determined. This wavelength was obtained from the temperature modulation of the OPO corresponding to 191 °C. The OPO was operated at 10 kHz repetition rate and produced pulses with durations of 5.2 ns.The seed signal power was maintained at 5 mW, which translates to 0.5 μJ pulse energy, at the input end of the amplifier. At the output end, the average power recorded was 1.6 mW, in the absence of pumping, giving a seed coupling efficiency of 32% into the fibre. The power of the seed laser at the input end was maintained passively by turning the neutral density filter placed after the Nd:YAG laser used to pump the OPO. Once the seed signal was coupled in, the pump laser diode was activated and the pump current was increased in steps of 0.5 A. The commensurable output power was measured using a Newport thermal power meter. Additionally, the spectral profile of the amplified output signal was recorded with a monochromator (Horiba iHR550) aligned to a PbSe photodiode (Thorlabs PDA20H) and lock-in amplifier (Stanford Instruments). The temporal pulse profile of the output signal was recorded with a HgCdTe detector (Thorlabs PDAVJ10) and oscilloscope.The measurement parameters for the spectra and temporal pulses are summarised in tables 4.2 and 4.3 respectively, and the results from observations and measurement are discussed in the following section.

Instrument / Parameter	Value
Monochromator	Horiba iHR-550
Slit size	40 μm
Wavelength increment	0.05 nm
Theoretical resolution	$<$ 0.2 nm
Photodetector	Thorlabs PDA20H

Table 4.2: Instrument and measurement settings for spectral characterisation of amplified pulses

Instrument / Parameter	Value
Photodetector	Thorlabs PDAVJ10
Theoretical rise-time	3.5 ns
Response Bandwidth	100 MHz (at -3 dB)

Table 4.3: Instrument and measurement settings for temporal pulse characterisation of amplified pulses

4.3 Results

This segment presents the results from the investigation of the amplification in single stage Erbium-doped fibre amplifier using nanosecond seed pulses.

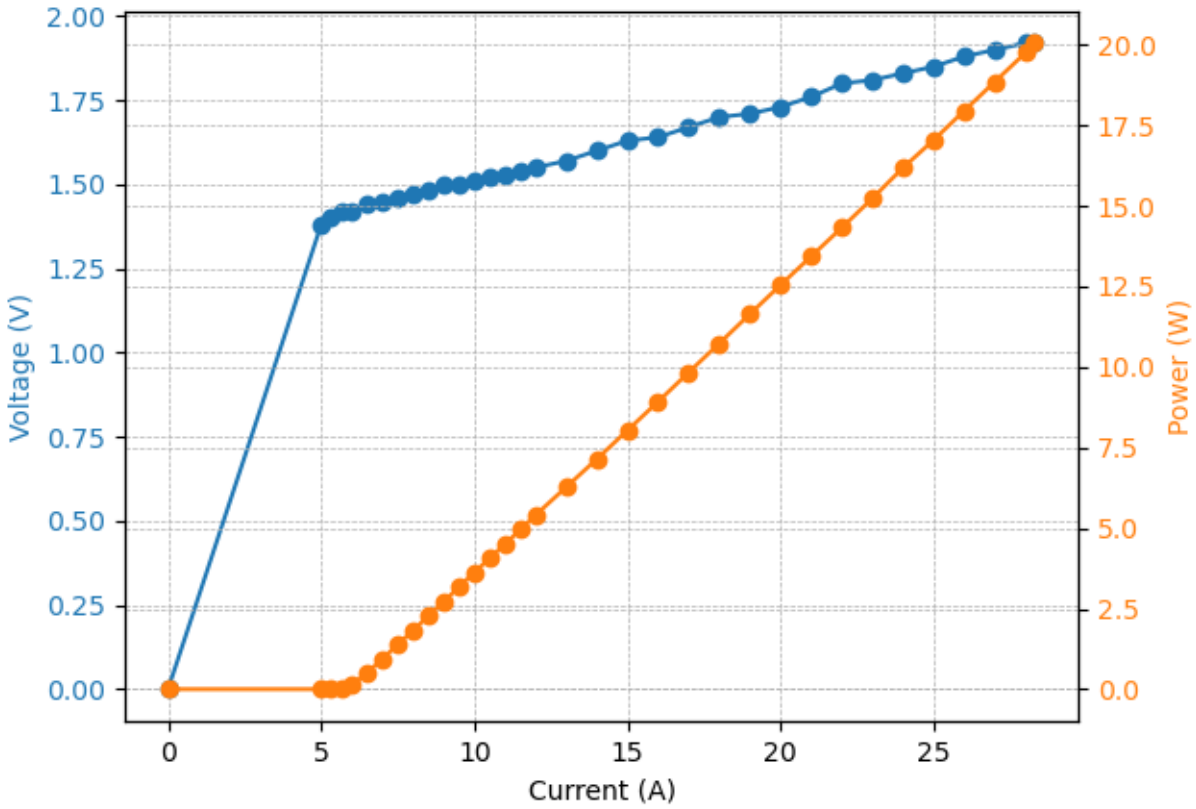

Figure 4.6: Pump LIV Characteristics. The blue curve indicates the I-V characteristic curve. The orange curve represents the output power vs the increasing current

Fig 4.6 shows the LIV characteristics of the pump. This data was referenced to determine the pump powers for given pump currents during the experiment. The threshold current for the pump was found to be close to 6A so for the experiment, the pump was operated at currents above 7A up to 12.5 A in steps of 0.5 A.

The optical power conversion i.e. the output power of the amplifier vs input pump power is

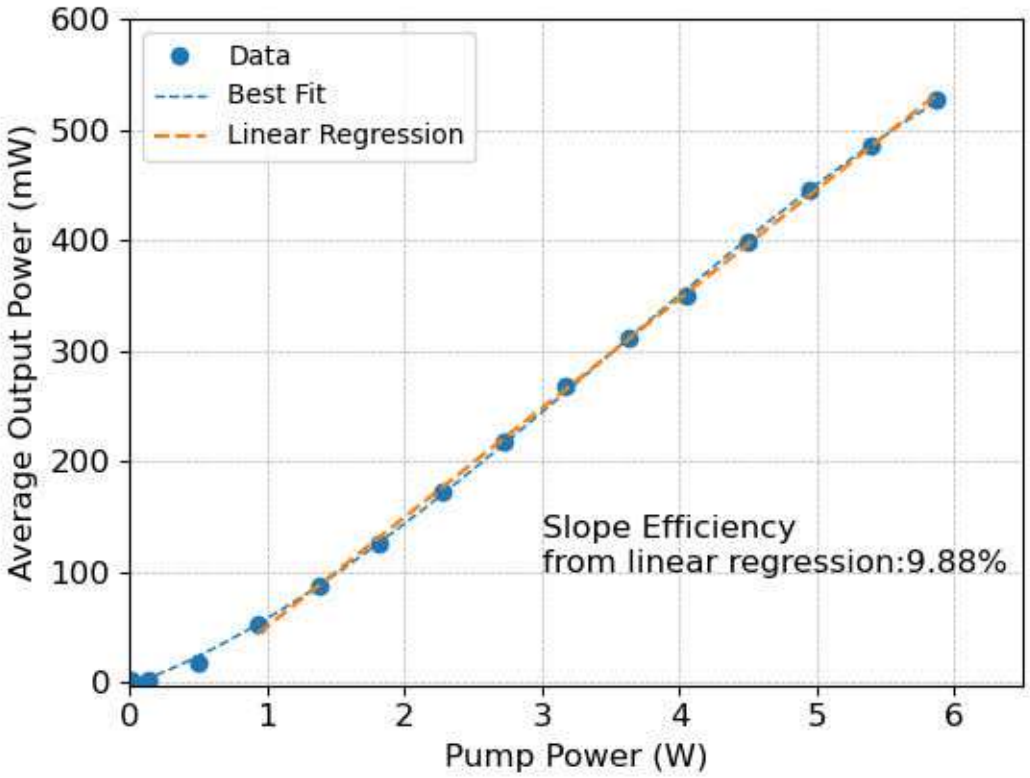

Figure 4.7: Optical power conversion of the fibre amplifier shows the variation of the output power with the input pump power. The blue dots show the measured output powers at the given pump powers. The blue dashed line gives the best fit curve for the measured data. The orange dashed line is the linear regression fit and the slope efficiency was calculated from this is found to be 9.88%

shown in fig 4.7. The threshold is established to be at 0.5 W and the slope efficiency of the linear part beyond the threshold is 9.88%. The slope efficiency is a key factor impacting the power scaling in the power amplifier, and a higher value can indicate higher amplification values. It would also be possible to improve the slope efficiency further with the possibility to tune the pump wavelengths near 980 nm [171].

The orange curve in fig. 4.8 shows the OPO seed pulse spectrum at the most efficient wavelength of, 2789 nm. The spectrum has a Lorentzian-like line profile with slowly decreasing side-lobes, with 3.8 % (or -14 dB) of the total power is spread out beyond the primary range

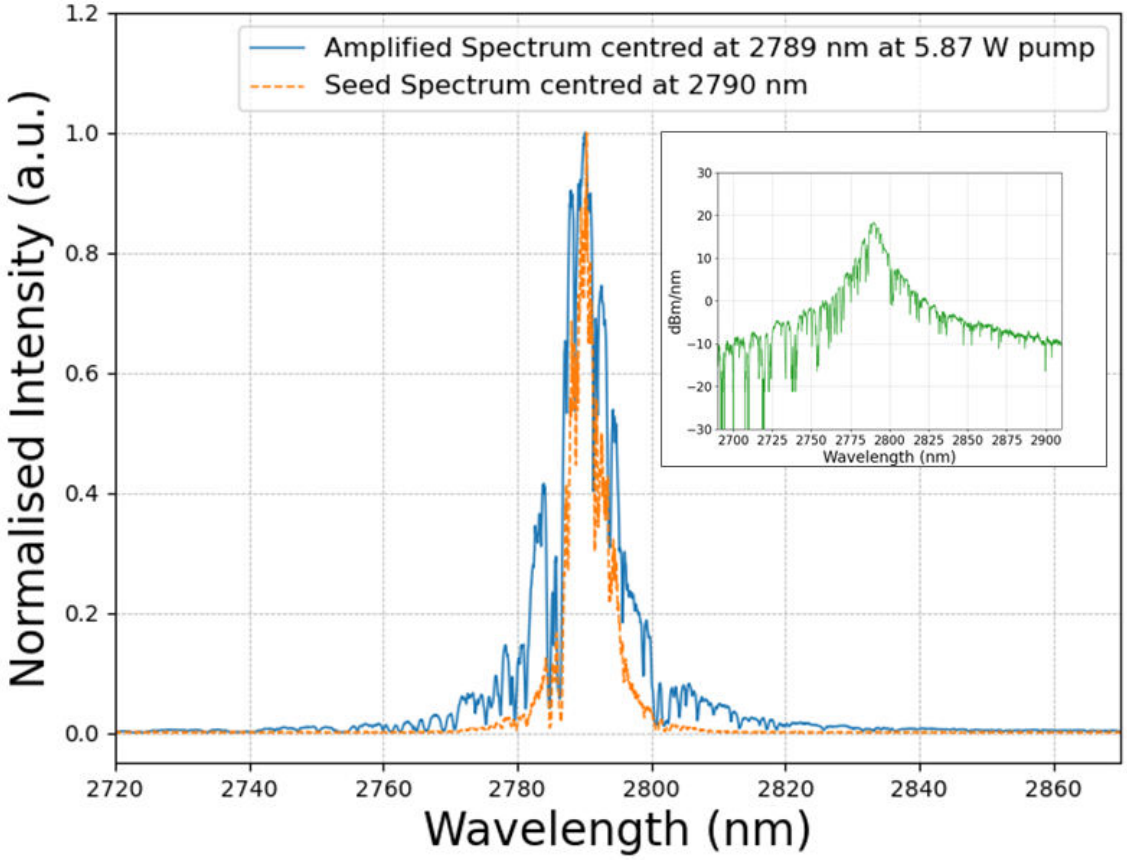

Figure 4.8: The spectral lineshape (Lorentzian) of the seed (orange) and amplified pulse (blue) centred at 2790 nm is shown. There is a small shift in the centre wavelength by ±1 nm observed between the amplified and the seed pulse. The bandwidth and FWHM of the seed was 9.95 nm and 4.8 nm respectively, while that for the amplified spectra at 5.87 W pump power is 21.9 nm (bandwidth) and 7.9 nm (FWHM). The inset shows the log spectra for the amplified pulse

between 2780-2800 nm where the major portion of the power is concentrated. The full width at half maximum (FWHM), centred at 2789 nm, is estimated to be 4.8 nm, while the $1/e^2$ bandwidth was found to be 9.9 nm. The blue curve is the amplified spectrum at 12.5 A pump current or 5.87 W of pump power, for which a maximum average output power of 527 mW was recorded. The $1/e^2$ bandwidth of the amplified spectrum was determined to be 21.9 nm and the corresponding FWHM

was 7.9 nm. At maximum pump power, nearly 20% (or -7dB) of the amplified output power was distributed in the wings outside the 2780-2800 nm wavelength range.

Fig 4.9 demonstrates the evolution of the laser linewidth, centred at 2789 nm, with the increasing pump power. The escalating pump power produced heating effects at the output facet of the fibre which caused minor dealignments, resulting in the fibre ends to shift sideways. Thus, for every step of increase in pump power, the pump alignment was readjusted with the help of the coupling lenses, to ensure maximum possible average output power. With the progression of pump, there was no observable shift in the centre wavelength, and it remained fixed at 2789 nm. The measurement range for the spectra was kept between 2710 nm and 2870 nm, a span of 160 nm to check for the presence of any amplified spontaneous emission (ASE) however no appreciable ASE was observed. The signal-to-noise ratio was maintained over 30dB, to avoid amplified spontaneous emission (ASE) and self lasing in the fibre.

A few minor variations and a slightly higher bandwidth of 11.9 nm was observed in the amplified pulse spectra at the output power of 40 mW, otherwise the spectra nearly identical to that of the seed pulses from the OPO system. Since no nonlinear effects or ASE were seen in the amplifier at this output power level, the discrepancies in the two spectra are attributed to the fibre coupling.The amplified laser spectra started showing noticeable alterations at amplified output powers of 305 mW because of nonlinearities as the output power was increased by approximately one order of magnitude. The side lobe power concentration increased to 9.6%, and the bandwidth was raised to 16.0 nm, while the overall shape of the spectrum was maintained. Between the absence of pump and the maximum pump power, the laser bandwidth expanded by 11 nm, at the maximum pump power of 5.87 W. This broadening of linewidth can be directly attributed to the nonlinear effects of self-phase modulation due to the intense energy concentration within the fibre core.

The laser spectra was also recorded for a span of 200 nm to corroborate the presence of any amplified spontaneous emission (ASE) however no appreciable ASE was observed. A few minor variations and a slightly higher bandwidth of 11.9 nm was observed in the amplified pulse spectra at the output power of 40 mW, otherwise the spectra nearly identical to that of the seed pulses from

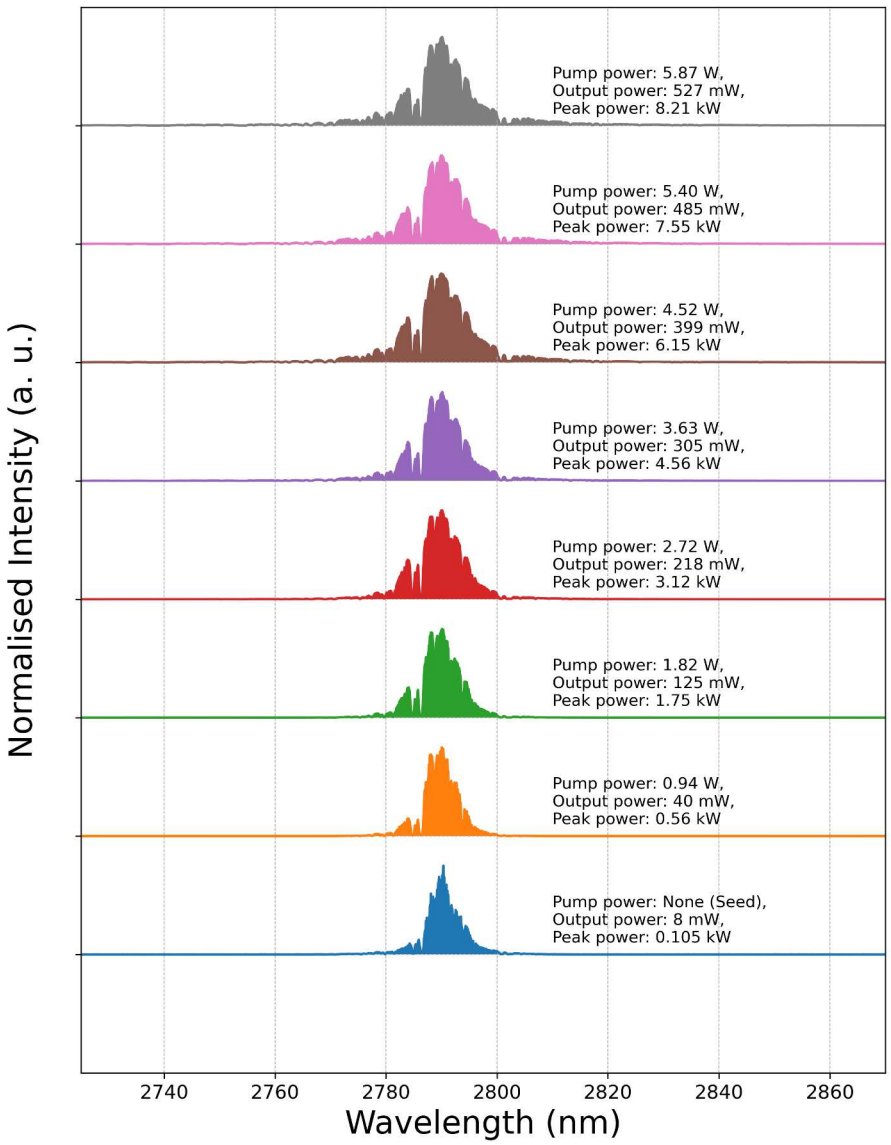

Figure 4.9: Evolution of 2789 nm lineshape with pump power. The figure shows the successive variation of the laser FWHM of the output spectra with incremental pump powers, the size of the circles scale with the output powers. The FWHM remains steady as the pump powers increase

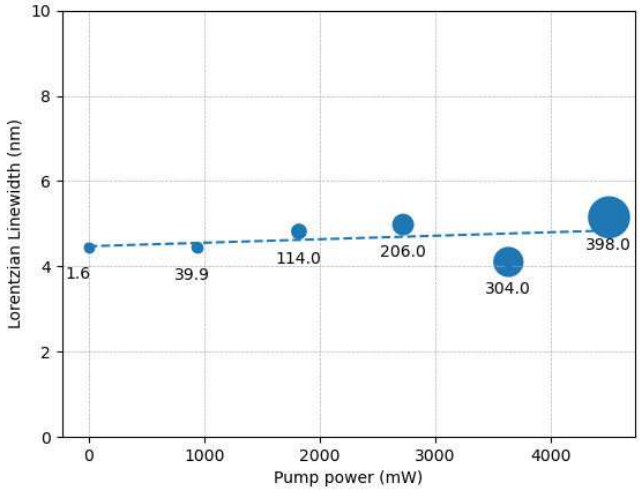

Figure 4.10: Variation of linewidth with pump power. The linewidth varies very slightly and remains fairly steady at a value close to 4.5 nm with the increasing pump power. The increasing circles represent the scaling of the output power with the pump power

the OPO system. Since no nonlinear effects or ASE were seen in the amplifier at this output power level, the discrepancies in the two spectra are attributed to the fibre coupling. The amplified laser spectra started showing some noticeable differences at amplified output powers of 305 mW because of nonlinearities as the output power was increased by approximately one order of magnitude. The side lobe power concentration increased to 9.6%, and the bandwidth was raised to 16.0 nm, while the overall shape of the spectrum was maintained. With incremental pump power between the no pump condition and the maximum power of 5.87 W, the laser bandwidth expanded by 11 nm.

Power scaling in fibre amplifiers, including those in MOPA configurations, is commonly accompanied by different nonlinear effects viz., self-phase modulation (SPM) cross-phase modulation (XPM), four wave mixing (FWM) etc., which contribute to spectral broadening of the output linewidth [254, 255, 256, 257] along with other possible higher order effects like the modulation instability (MI) and soliton self-frequency shift (SSFS). The physical origin of linewidth broadening of the laser spectrum in the Er:ZBLAN fibre amplifier discussed in this work, can be mainly ascribed to SPM, the phenomena detailed in section 4.1.3. As the magnitude of the pump and output power

increases in the fibre core as a result of power amplification, there is intense energy concentration leading to a change in the nonlinear refractive index (RI) within the core, a phenomenon termed as optical Kerr effect. The change in nonlinear RI then induces a phase shift in the field of the laser light interacting with the core.Since the intensity of the light varies non-uniformly distributed across the beam profile, the induced phase shift is also the unequal and dependent on the intensity distribution. In the pulsed mode operation, this unequal phase shift causes temporal self phase modulation, which modulates the angular frequencies adding the spectral components; or re-distributing power to wavelengths both shorter and longer than the original wave, resulting in a broadened spectrum at the output end [258, 259]. The nonlinear RI change is still not high enough to initiate additional nonlinear effects [260] which can cause further distortion of the beam. This can be observed in the recorded output spectra, which has an overall symmetrical and comparable lineshape to the input seed spectra, corroborating that the linewidth expansion is still within the linear regime. Moreover, absence of any pronounced peaks of new spectral components in the output spectra confirms that there is no onset of FWM at these peak power magnitudes. There are dips in output spectra near 2.785 μm which can be attributed to the atmospheric absorption of these wavelengths by hydroxyl molecules present in the experimental environment. XPM can be conclusively ruled out, as the amplifier is operated at very low seed powers and sufficiently narrow bandwidths.

The laser spectra were also recorded for a 200 nm span to confirm the presence of any amplified spontaneous emission (ASE) however no appreciable ASE was observed. The spectral broadening at high, several kW level peak powers and redistribution of powers in the side lobes is a consequence of nonlinear self-phase modulation. This can plausibly be mitigated by adopting fibres with larger core diameter. To cross-verify for any ASE, the seed laser was blocked for low pump power, but no ASE was observed. Self lasing started near 0.9 W pump powers, a somewhat low pump value indicating that ASE could have been potentially restricted by the start of self lasing, an occurrence reported by Gauthier et al. [213].

Fig. 5.5 shows the temporal pulse and the output pulse train spanning 40 periods at the maximum output power of 527 mW.During the amplification, the form, and width of the pulse

essentially remained constant. Only trivial saturation effects were seen in the amplified pulse shape, with the pulse leading edge gaining more than its tail. The full width at half maximum for the amplified temporal pulse was measured to be 5.2 ns. By normalising the recorded pulse profile, the maximum output pulse energy of 52.7 μJ translates to a peak power of 8.2 kW. The relative fluctuation of the pulse energy was estimated to be 5.2% (standard deviation) from the oscilloscope trace of the pulse train for 40 periods. This variance may be attributed to the 5.4 % pulse energy variances in the OPO seed pulses.

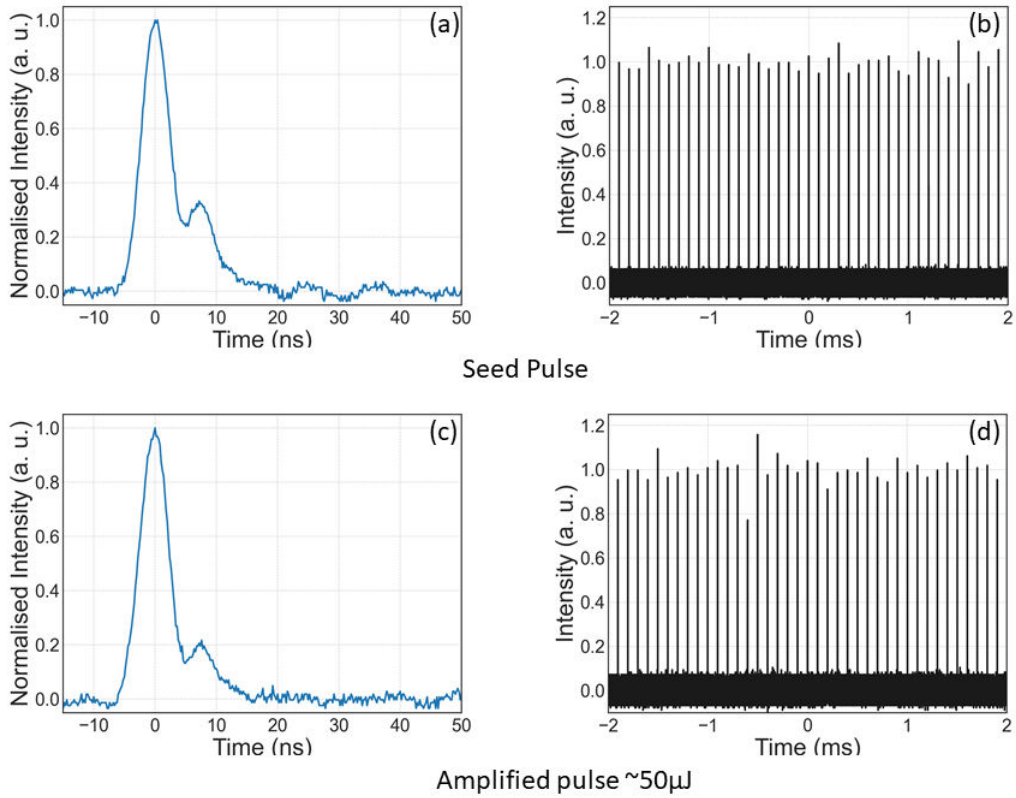

Figure 4.11: (a)Temporal pulse profile of the seed pulse at 2790 nm (b)Pulse-to-pulse stability of the seed pulse over 4ms (c)Temporal pulse profile of the amplified pulse at 2790 nm (d)Pulse-to-pulse stability of the amplified pulse over 4ms

With the given parameters of 10KHz repetition rate and 5.2 ns pulse duration, the maximum average output power is calculated to be 527 mW and a pulse energy of 52.7 μJ, a subsequent peak

power equivalent to 8.2 kW and an overall gain of 25.17 dB. The pump current value was never extended beyond 12.5 A, or the equivalent pump power of 5.87 W to prevent any damage of the fibre, especially the unprotected output fibre facet.

The measurements were performed over a period of two weeks and in relatively short intervals to avoid the build up of large intensities at the output end for a very long time. Due to the higher susceptivity of damage in ZBLAN fibres, long term stability studies were not carried for this fibre. However, if the power scaling is extended beyond the aforesaid pump current/power value, the linewidth broadening would continue and result in severe nonlinear pulse distortion. Additionally, further gain in the amplifier would approach the self-lasing threshold, resulting in fibre damage, thus becoming another limiting factor for power scaling.

4.4 Conclusion

To conclude, this experiment investigates the power amplification characteristics for a single stage, single mode Erbium doped fluoride fibre amplifier using nanosecond pulses. Many power scaling studies have been reported about the rare earth doped fluoride fibres, but mostly in the ultrashort pulse regime. Higher power scaling with nanosecond pulses have also been demonstrated, but with multimode fibres. This experiment combined the advantages of single mode fibres with energy of nanosecond pulses at 2789 nm Mid-IR and this study is the first to study nanosecond pulse amplification characteristics in Erbium doped fluoride fibre amplifiers. The 0.5 μJ seed pulses with FWHM of 5.2 ns were generated at 10 kHz repetition rate from a PPLN-based OPO. These seed pulses were amplified to generate output pulses of 527 mW average power, corresponding to a calculated pulse energy of 52.7 μJ translating to a calculated peak power of 8.2 kW. Average output intensity of 279 kW/cm^2 was observed from calculations, a consequence of combining single-mode fibres with nanosecond duration seed pulses, This value is an order of magnitude greater than previously reported results on amplification in Erbium doped ZBLAN fibre amplifiers viz. 41 kW/cm^2 [213], 32 kW/cm^2 [212], and 49 kW/cm^2 [204]. The results of the investigation of

amplification of nanosecond pulses in Er:ZBLAN fibre amplifier were peer-reviewed and published [261].

Further improvement of amplifier performance

Refining operational parameters by modifying pump power, increasing fibre length, regulating repetition rates, and altering pulse parameters can adjust the output powers, and improve the overall power scaling performance of the amplifiers significantly.

Increased pump powers can directly enhance the amplifier gain by exciting more erbium ions to the higher energy state, ready for the seed signal to stimulate them into rebounding to the ground state, releasing energy, and boosting the signal. However, the caveat to consider is that the pump power cannot be escalated indefinitely, once the available population of erbium ions have been moved to the excited state, saturating gain, it is not possible to increase the amplifier gain despite raising the pump power [262]. Besides, increasing pump power can generate several negative effects like ASE, nonlinear distortions, and possible bleaching of erbium ions by depleting the population in the ground state faster than the energy release from the excited state. Moreover, ZBLAN fibres are hygroscopic, which imparts brittleness to the fibre ends due to exposure to moisture, that might cause fibre damage when operating at high pump powers. Exploring different pumping schemas can also aid amplifier performance. Although the forward (co-propagating) pumping scheme is more efficient than backward (counter-propagating) pump, used in this work, the combined power or thermal load of the pump and signal at the output end of the former can degrade the fibre tip more adversely than backward pumping.This requires mitigation in terms of heat management and end-caps for further power scaling.Backward pumping scheme, on the other hand, has reduced the magnitude of nonlinear distortions since the high peak power signal beam travels over a shorter propagation length[263].Dual-end or bidirectional pumping scheme on the other hand allows even distribution of the pump power in the fibre core, maintaining a consistent number of excited erbium ions, which can be utilised by the signal and consequently improve the gain in the amplifier. This configuration also disseminates the heat more uniformly in the core, and result in multifold increase

in the output power [199, 264, 171]. However, raising the pump power beyond a threshold, even in this scheme, eventually retards the amplifier gain due to heating and shifts the emission spectra towards longer wavelengths.

Utilising longer fibres in the amplifier can also enhance the performance. Longer fibres increase the pump interaction length within the fibre, allowing more interaction between the seed signal and the erbium ions in the excited state, and result in higher gains for a given pump power. This in turn leads to higher slope efficiencies [186], as well as increased pulse energies, storing more energy per pulse. Increasing the fibre length can also enhance the output spectral characteristics by widening the fibre gain spectrum. However, longer fibres can also induce nonlinear distortions which may limit the amplifier performance, thereby making it necessary to optimise fibre lengths.

The average output power of a fibre amplifier operating in the pulsed mode is given as a product of pulse energy and repetition rate. Intuitively, this implies that higher repetition rates can contribute to an increase in the average output power. Contrarily, when the repetition rate is increased, it is usually accompanied by a decrease in the pulse energy, and the overall output average power remains relatively the same [265, 170]. However, by increasing the duty cycle, it is possible to generate constant energy per pulse [266] and consequently, increase the average output power. With fixed energy pulses, any increment in repetition rate results in a rise in the average output power, as more energy is delivered per second. On the other hand, lower repetition rates can demonstrate higher peak powers and shorter pulse durations [267]. Thus, careful optimisation of repetition rate can be used to trade-off peak and average output powers, depending on the required application.

Power scaling in fibre amplifiers is often critically limited by the onset of nonlinear pulse distortion due to the interaction of highly intense pulses with the cores of long-fibres.For single mode operation, key issue involves mode instability. These problems can be compensated by the use of larger core diameters. Alternatively, newer fibre geometries modifying the mode field diameters yet preserving beam quality of single mode operation could work as potential solutions [268].Moreover, a possibility to tune the pump to an optimal efficient wavelength can also help push the limits of

amplification [171]. Other options could be to improve the doping concentration of the rare earth ions, erbium in this case, which has been shown to increase amplifier efficiencies, and cascading amplifiers in multiple stages to achieve higher power scaling to attain several tens of what level of average output power. And to improve the performance stability of the amplifier, it is necessary to consider both active and passive cooling options, which can prohibit softening and bending of fibres during power scaling operation [269].

Enabling component technologies such as progress in end-cap material research, improved splicing quality and process, and better heat conducting coatings contribute to increased power scaling of such amplifiers by allowing adequate end cooling [147]. Introducing Fibre Bragg Grating as reflectors at fibre ends allow development of stable, high-power laser without the need for calibration, in addition to protection against fibre tip damage [270, 271]. Fusion splicing increases robustness of the fibre and can be used to fuse glasses of different types such as silica and ZBLAN and also for splicing end caps of various materials into ZBLAN fibres. Moreover, adding more stages to this amplifier configuration would potentially allow increased power scaling.

Towards 100 μJ pulse energy

Recently, 3D bioprinting applications have garnered a lot of interest in research. To meet the demand, mid-IR lasers are undergoing rapid development to optimise parameters like laser pulse energies, pulse durations and spectral range, for emerging techniques such as laser induced forward transfer (LIFT), amongst a broader area of laser-assisted bioprinting. LIFT utilises laser beams to directly write onto a receiving substrate, by focusing a laser beam on a thin layer of absorbing layer, followed by a bio-ink substrate, to eject ink droplets from this substrate for laser writing. The magnitude of ink and precision of writing is controlled by the laser pulse energy and beam spot diameter. The process warrants high spatial resolution and faster writing speed with the potential to print compound heterogeneous structures [272].

Using higher pulse energies allows effective expulsion of the ink droplets, thereby making the process more efficient. However, to keep the cells viable and functional after printing, optimisation

of pulse energy is required to prevent thermal damage to the bio-ink, as well as the surrounding tissues. Ideal pulse energies for the process, range in the order of few tens to hundreds of micro-joules [273], although other factors like bio-ink composition, wavelength of the laser, and absorber layer characteristics affect the final output. For LIFT, the parameter 'fluence', given in J/cm^2, is considered more significant compared to pulse energy. The next important factor is the pulse duration. Typically, nanosecond pulsed lasers are used in LIFT while single cell bioprinting with picosecond/ femtosecond pulses [274, 275, 276] have also been implemented. Shorter pulses ensure faster printing by quick energy deposition, thus reducing thermal effects, but also induce ablation, damaging the bio-ink. On the other hand, longer pulse durations provide sufficient time for heat dissipation. Depending on the material and structural intricacy, pulse durations can be adjusted.

LIFT commonly utilise UV/ visible wavelengths in their bioprinting applications, but such short wavelengths increase the risk of DNA damage to the cells as well as change in physical/chemical properties of the bio-ink. Use of IR wavelengths reduces such likelihood [277]. Wavelengths near 2.8 μm can be very efficient for water-based bio-inks in 3D-bioprinting applications which can facilitate selective heating and solidification, adequate penetration depth, supplementing the printing of thick and complex tissue structures. Additionally, localized heating of bio-ink can allow rapid, yet accurate ejection and transfer of bio-ink droplets during the LIFT process. The primary drawback with IR lasers is the possibility of thermal damage to the cells, thus optimisation of pulse duration and laser wavelength is necessary to achieve suitable pulse energy and fluence values. In this scenario, further power scaling of nanosecond pulses in the Er:ZBLAN fibre amplifier can generate sufficiently higher pulse energies. In addition to this, the optimisation of beam spot diameter, can furthermore facilitate the development of an effective source for laser assisted 3D-bioprinting applications.

From the perspective of commercial material-processing applications, improvement of fibre amplifier performance by optimising pulse energies can lead to faster processing times, superior accuracy and control and better damage safety. This is particularly relevant for precision processes like laser-based micro-machining, inscription, and micro-structuring, and their implementation in the field of biomedicine. Current state-of-the-art fluoride fibres under development have achieved

up to 122 μJ of pulse energy at 2.8 μm with picosecond pulses [204] catering to such applications. Additionally, there is also an emerging market for commercial 2.8 μm lasers in with $>$ 100 μJ pulses introduced with various pulse durations [278]. With the rise of technologies like LIFT and precise laser tissue interactions, there is a space for further research into optimisation of operational parameters and thermal management for fibre lasers/ amplifiers, so that they can be closely tailored to such high precision biomedical applications.

Chapter Five

Investigation of Wavelength Tuning in Erbium doped Fluoride Fibre Amplifier in the Mid-IR

5.1 Introduction

Owing to its high gain, low losses less than 0.05 dB/m and wide emission range between 2.65-2.85 μm [279], Er:ZBLAN glasses have established themselves as an excellent contender for mid-IR fibre lasers and amplifiers.Erbium doped fibre amplifier technology is a mature one, due to its prevalence in telecommunication research and applications. This is one of the primary reasons why erbium doped fluoride fibres were studied earlier than other rare-earth doped amplifiers. The ready availability of diode pumps near 790 and 980 nm provides an additional advantage to the Er: ZBLAN fibres over the Holmium and Dysprosium counterparts. As a result of this prevalence, most optical parameters such as rate equations, emission, and absorption cross-sections have been extensively studied theoretically and thus readily accessible through literature review, making numerical modelling, especially for the gain in such amplifiers quite convenient. However, these analyses cannot account for the practical experimental effects like self lasing, build-up of amplified spontaneous emission and back reflections

from facets and fibre end caps during practical implementation.

Wavelength tunable sources with narrow spectral linewidth are significant in sensing and spectroscopy applications. Due to the presence of the most efficient water absorption maxima window and molecular fingerprinting region near 3 μm, tunable sources near this wavelength range are in demand and in that context, Er doped fibre systems are an excellent choice due to the possibility of high power scaling near this spectral range. The 2.8 μm emission in Er:ZBLAN fibres occurs due to a transition of the Er^{3+} between $^4I_{13/2}$ and $^4I_{11/2}$ energy levels. However, the $^4I_{13/2}$ and $^4I_{11/2}$ levels split into seven and six Stark levels respectively, in addition to undergoing inhomogeneous broadening, leading to a quasi-continuous tunable range of nearly 200 nm [280]. There is a lasing bottleneck that arises in oscillators due to a longer lifetime of the lower lasing level $^4I_{11/2}$ compared to the upper one, which can be addressed by high Er $^{3+}$ doping concentration amongst other methods. The observed tuning range in such oscillators decreased as the pump power increased and at the shorter wavelengths, the output powers were limited to significantly low values [194]. Moreover, when the Stark splitting of the lower lasing level is established, the maximum possible tunable wavelength range about a central wavelength follows a scaled relation defined by the energies of the total Stark splitting in the lower level ΔE_L, and the energy of the central transition E_{ZL}, $(= \Delta E_L/E_{ZL} = \Delta lambda_L/lambda_{ZL})$. Thus, an increase in the centre wavelength results in an increase in the tunable range [281].This poses one of the possible limitations to performance high power tunable Er:ZBLAN sources. There is the possibility of analysing the operation of laser oscillators as an alternative to studying amplifiers, to understand wavelength tunability, but the oscillators have low single pass gain values as opposed to amplifiers and higher saturation, which can influence the peak emission wavelength and the tuning range. Thus, it becomes imperative to study the spectral tuning range of such amplifiers.

The gain-bandwidth of the fluoride fibre amplifiers can be understood better by reviewing the background processes contributing to the emission and the rate equations for the corresponding transitions in Er-doped ZBLAN fibres. Reviewing these factors can help in estimating the maximum possible tunable wavelength range of such amplifiers. However, as discussed, there are phenomena

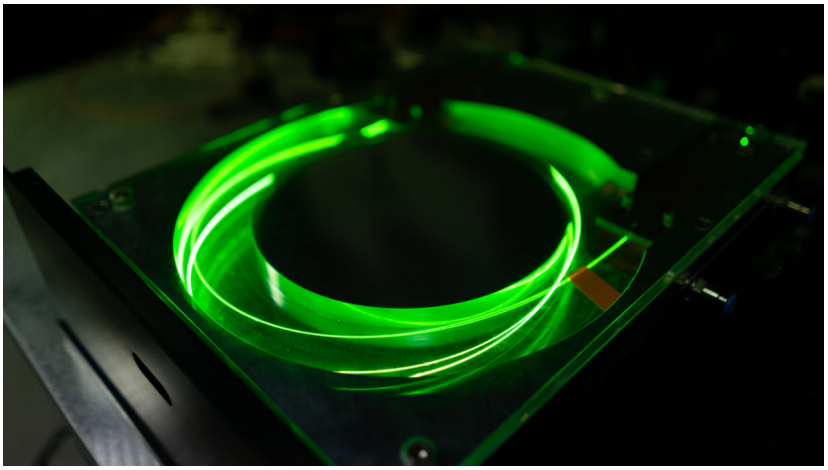

Figure 5.1: Er-Doped ZBLAN Fibre Amplifier

which limit the tunable wavelength range when applied practically, thus it is also beneficial to obtain a brief overview of such processes as discussed in section 2.4.2.This chapter then builds on the investigation of the power amplification and proceeds to understand the range of wavelength tunability available to the Er: ZBLAN amplifier.

5.1.1 Parasitic Self-Lasing

A dominant hindrance to power scaling and wavelength tuning that was observed during the experimental investigation is Parasitic lasing. This is a phenomenon of undesirable, unconstrained and detrimental lasing that occur in high amplification laser systems, diminishing their stability, operational dependability, and efficacy. Self lasing can be induced by back reflections from surfaces like fibre facets and amplified in the fibre length and can contribute to the damage to surfaces, substrates, and coatings of the system [282].

Along with seed pulse amplification, fibre amplifiers often undergo spontaneous emission, which may get amplified due to the gain present in the amplifier. If high enough, the gain may cause the wavelength associated with the spontaneous emission to start lasing and thereby parasitically leach out the energy meant to amplify the seed pulses. These phenomena usually occurs between

consecutive seed pulses, especially at low repetition rates, and results in a drop in the corresponding output power, referred to as gain clamping. One method of mitigating this effect is by cleaving the output ends of the fibre amplifier at an angle, effectively reducing the feedback to the parasitic wavelengths. Other methods of reducing this occurrence is by introducing passive elements like long period fibre gratings close to the ends of the fibres to cut the feedback to low enough values to prevent self-lasing. This can be a suitable solution when applications cannot operate at high repetition rate or mandatorily require low pulse repetitions. Studies on parasitic Self lasing has been reported in [283, 284] in the context of supercontinuum generation.

5.2 Experimental study of wavelength tuning in fibre amplifiers

The experimental setup for wavelength tuning of the fibre amplifier is illustrated in Fig 5.2. An OPO pumped by actively Q-switched Nd:YAG laser with 10 kHz repetition rate, emission wavelength 1064 nm, serves as the nanosecond (seed) pulse generator for the experiment. The OPO parameters, operation, and characterisation has been discussed in detail in the Chapter 3. The OPO shows wide tunability in the NIR to MIR region, between 1400-4100 nm as signal and idler wavelengths, obtained by grating period and temperature tuning. This OPO was succeeded by a single stage, single mode, double clad, Erbium-doped fluoride fibre amplifier which was studied for the amplification and power scalability. The experimental configuration and fibre parameters were kept unchanged from the investigation of amplification.

Prior to the start of the wavelength tuning experiment, the results from the OPO characterisation were referred to determine the required temperature and grating period values needed to obtain wavelengths close to 2800 nm. These wavelengths corresponded to the idler outputs from the OPO.

To access the requisite wavelengths, the OPO is tuned by changing between two grating periods and tuning the housing oven temperatures in steps of 2 °C. between 180°C to 200°C for the 31μm grating period, and 110 to 120°C for the 31.5μm grating period. The output comprised of

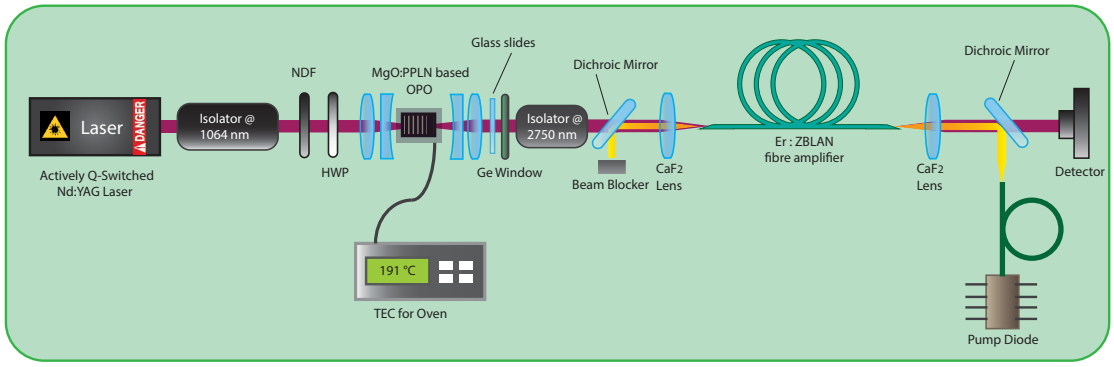

Figure 5.2: Experimental setup for studying Wavelength tuning characteristics of Fibre Amplifier with nanosecond pulses

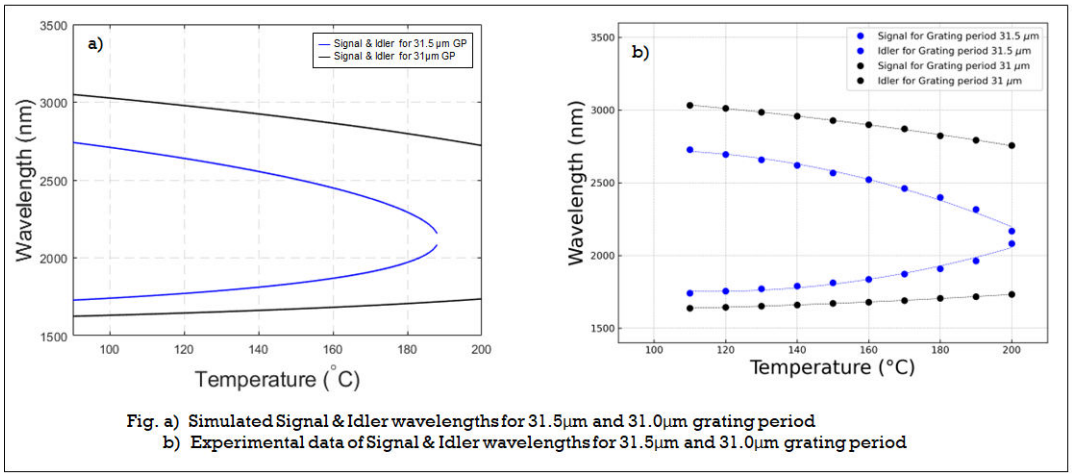

Figure 5.3: Expected spectral range near 2.8 μm from the characterisation of the OPO; it was predicted that temperature tuning over 31 and 31.5 μm grating periods would generate wavelengths close to the central wavelength of 2789 nm that could be utilised to study the potential tuning range of the fibre amplifier. In fig a) the blue and black gives the simulated values of the wavelengths from the 31.5 and 31 μm grating period respectively. In fig b) the blue and black dots represent the experimental values of wavelengths recorded.

a combination of the signal and idler components along with some residual pump. A Germanium window was used to filter out the idler, which incurred a minor loss in intensity of the subsequent seed pulse. The output pulse was collimated using an uncoated 100 mm focal length CaF_2lens. The pulse was then guided towards the fibre amplifier through mirrors and a tunable isolator (Thorlabs I2700Y4) set at 2750 nm, to block any back reflections. The average pulse power after the collimating lens was maintained in a way that the power at the fibre amplifier input, after travelling a free space path, was measured at 2.7 mW, corresponding to 0.27 μJ pulse energy, by manually controlling the neutral density filter (NDF) placed near the output of the Nd:YAG laser.

The single stage, fluoride fibre amplifier consisted of a 2.2 m long, single section, double clad Er:ZBLAN fibre manufactured by Le Verre Fluoré. The fibre was heavily doped with 7% doping concentration. The core diameter was 15.5 μm and had a 0.125 numerical aperture (NA). The single mode operation in this fibre had a cut-off wavelength of 2.5 μm. The diameter of the pump cladding was 260 μm and 0.46 NA. To increase the overlap between the pump and the seed in the fibre core, the geometry of the cladding was broken by having a double D-shaped clad, using two parallel flats separated by a distance 240 μm. The attenuation value in the fibre core at 2.8 μm, stemming from background losses, was 21 dB/km and the theoretically calculated saturation power of the fibre gain medium was 5.6 mW. To protect the output fibre facet which susceptible to high pump and amplifier seed signal powers, Fluoroaluminate (AlF_3) end caps were spliced onto it. The end-cap also limited the fibre facet deterioration due to hydroxyl ion (OH^-) diffusion. To reduce back reflections, which could lead to self lasing and potentially damage the fibre, the fibre tips were angle cleaved at 4° at the input and 13° at the output. The difference in the angle values are attributed to the cleaving tolerances.

The seed pulse was coupled into the fibre with an uncoated 25 mm focal length CaF_2 lens. The fibre amplifier was pumped with a 978 nm, multimode diode (Coherent), delivered with a multimode fibre. The pump was coupled into the amplifier with an uncoated 20 mm focal length CaF_2 lens from the opposite end of the fibre, making the seed and pump traverse in counter-propagative directions within the fibre. The same 20 mm focal length CaF_2 lens collimates the

amplified seed pulse out of the fibre. The pump and the seeds pulses were separated at the input and output ends, using dichroic mirrors that were highly transmissive at seed wavelengths close to 2800 nm and highly reflective at 980 nm, giving a seed coupling efficiency of 30%.

The amplified output pulses were then directed and focused into a monochromator (Horiba iHR550) with the help of another uncoated CaF_2 lens of 100 mm focal length. A PbSe-based photodetector (Thorlabs PDA20H) was placed at the monochromator output, connected to a lock-in amplifier (Stanford Research instruments), to record the spectrum. The averaged output power of the amplified pulse was measured with a Newport Thermal power meter. For the temporal pulse, an MCT fast photodiode (Thorlabs PDAVJ10) and an oscilloscope (Tektronix) were used.

The investigation of wavelength tuning was carried out for three different pump powers to generate pulses with estimated energies close to 10, 20 and 30 μJ. With the coupled seed power maintained at 0.9 mW, or 270 nJ pulse energy, the pump power was varied with step-wise increase in pump current, above the lasing threshold of the pump diode.The viable pump currents producing the desired output pulse energies, the three pump currents being 8 A, 9.5 A and 11 A giving pump powers of 1.82 W, 3.17 W and 4.52 W derived from the characteristics of the pump diode. The measurement parameters for the spectra and the temporal pulse remained the same as presented in table 4.2 and 4.3, as used for the investigation of amplification in the fibre amplifier.

5.3 Results

Fig. 5.4 shows the optical-to-optical power conversion between the pump and the amplifier, the slope efficiency was found by the fitting of linear regression curve and evaluated to be 10%. This is a slightly low value considering the predicted slope efficiency of over 50% has been reported for a 7 mol% Er^{3+} doping in ZBLAN fibres [285] as well as the conventional Stoke's efficiency limit. It would be possible to achieve better slope efficiency by improving the free space pump and seed coupling into the fibre. Alternative methods to improve the slope efficiency could be employing tunable pumps, which have reported efficiencies of up to 70% [171].

The amplifier recorded maximum gain at 2789 nm, recording the highest average power of 375 mW. The pulse duration was estimated to be 5.2 ns, so the maximum output power translated to a pulse energy of 37.5 μJ, attained for a pump power of 4.5 W, corresponding to 11 A pump current. The output seed power from the amplifier in the absence of the pump was 0.9 mW, not considering any coupling and transmission losses. Thus, the equivalent gain in the amplifier was calculated to be 26.2 dB. The optical efficiency at the maximum average output power was found to be 8.3 %. By analysing the power density spectra at this value, the amplifier was noted to be fully saturated and any amplification beyond this was restricted due to the start of self lasing.

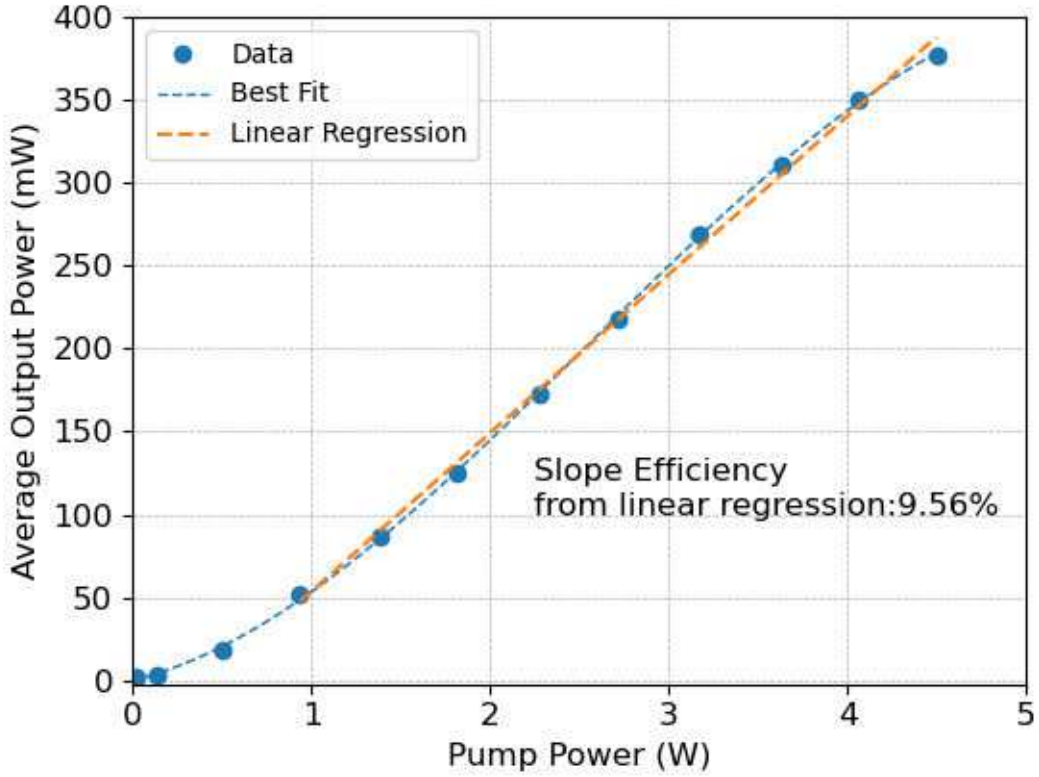

Figure 5.4: Input pump power vs average output power. The pump power vs the average output power for the fibre amplifier shows a slope efficiency of 9.56% calculated from the line of regression

The bandwidth ($1/e^2$ width) of the OPO seed pulse at 2789 nm, which had a Lorentzian shape, was estimated to be 10 nm. At the maximum average output power, this bandwidth had

extended to 16.7 nm, although the line profile remained the same. This increase in bandwidth could be attributed to nonlinear spectral broadening and was observed in the spectra recorded for higher output powers. At this pump power of 4.5 W, no ASE was observed in the spectra over the tuned wavelength range.

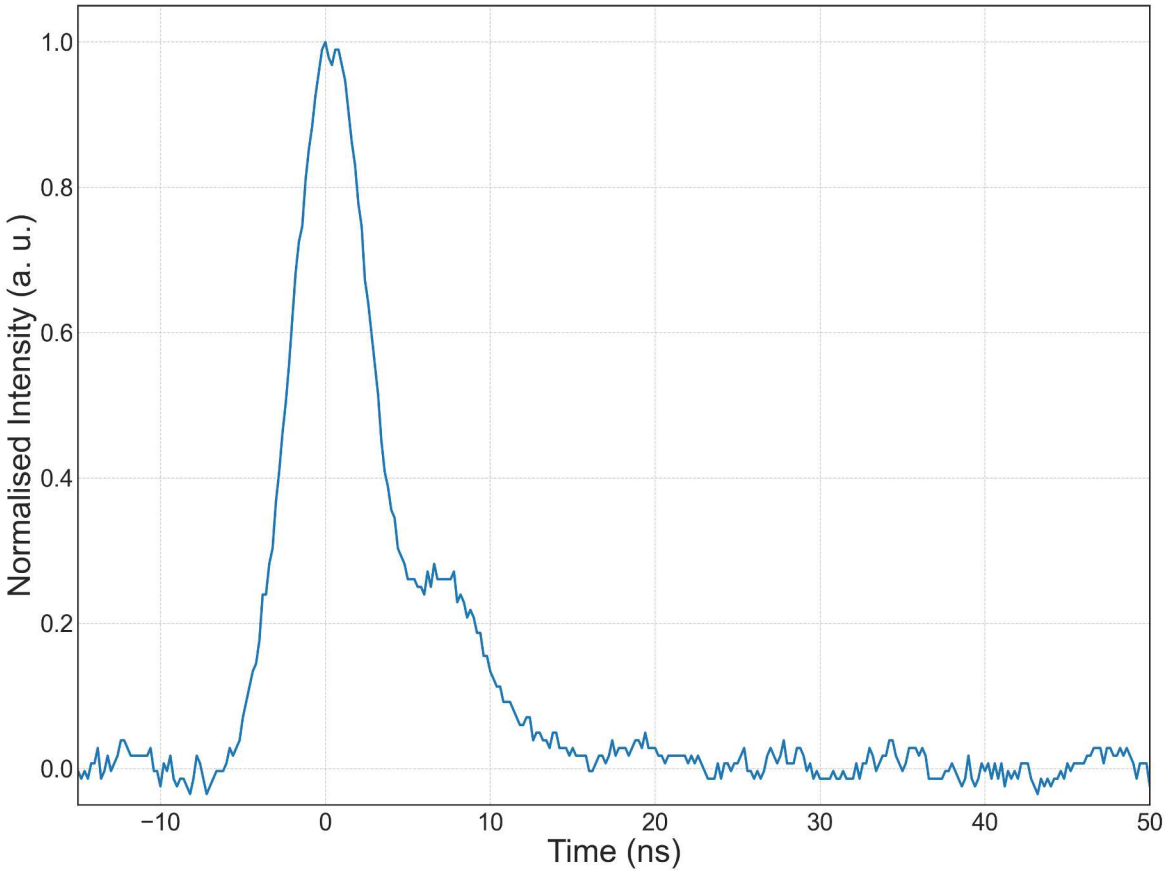

Figure 5.5: (a)Temporal pulse profile of the seed pulse at 2790 nm (b)Pulse-to-pulse stability of the seed pulse over 4ms (c)Temporal pulse profile of the amplified pulse at 2790 nm (d)Pulse-to-pulse stability of the amplified pulse over 4ms

The temporal pulse profile and the pulse train of 40 successive pulses over 4 ms for the seed and amplified pulse is shown in Fig. 5.5. The full width at half maximum of the seed temporal pulse

is approximated to be 5.2 ns and the energy fluctuation of the pulse train was 5.13%, calculated from the standard deviation of the pulse samples, about the mean value. In the amplified pulse, pulse FWHM remained constant, and the fluctuations increased to 6.7%.

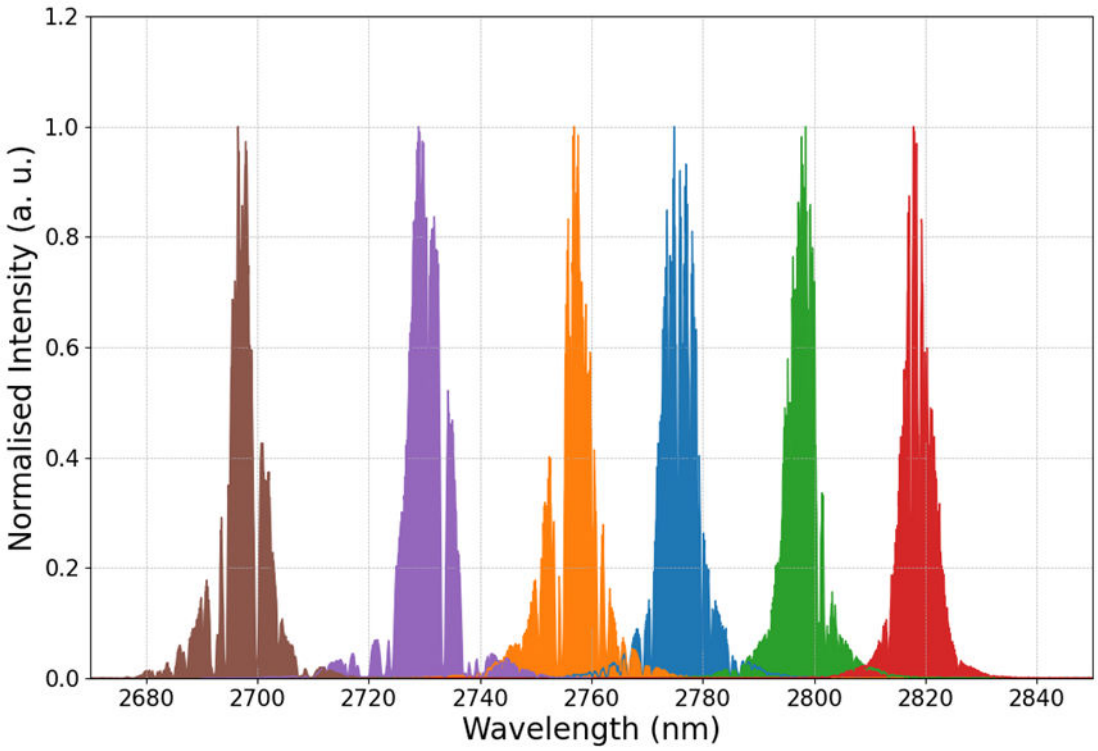

Figure 5.6: Seed spectral range for investigating wavelength tuning in the fibre amplifier. The tuned seed spectral range from the OPO utilised to investigate the potential wavelength tuning range of the fibre amplifier

Fig 5.6 shows the range of OPO idlers employed for the wavelength tuning experiment. To study wavelength tuning range of the fibre amplifier, the seed laser was set to start with 2789 nm, the most efficient wavelength obtained at 191°C and PPLN grating period of 31.5 μm. The seed pulse wavelength was tuned over a wide spectral range by setting different combinations of the 31 and 31.5 μm grating periods, and temperatures. The temperature was changed in steps of 2°C which resulted in wavelength shifts of 6-8 nm. Observing the amplified pulses, the peaks indicated small shifts up to 2 nm with respect to the analogous peak of the seed pulses.

The variation of output average power with the tuning wavelength of the fibre amplifier for

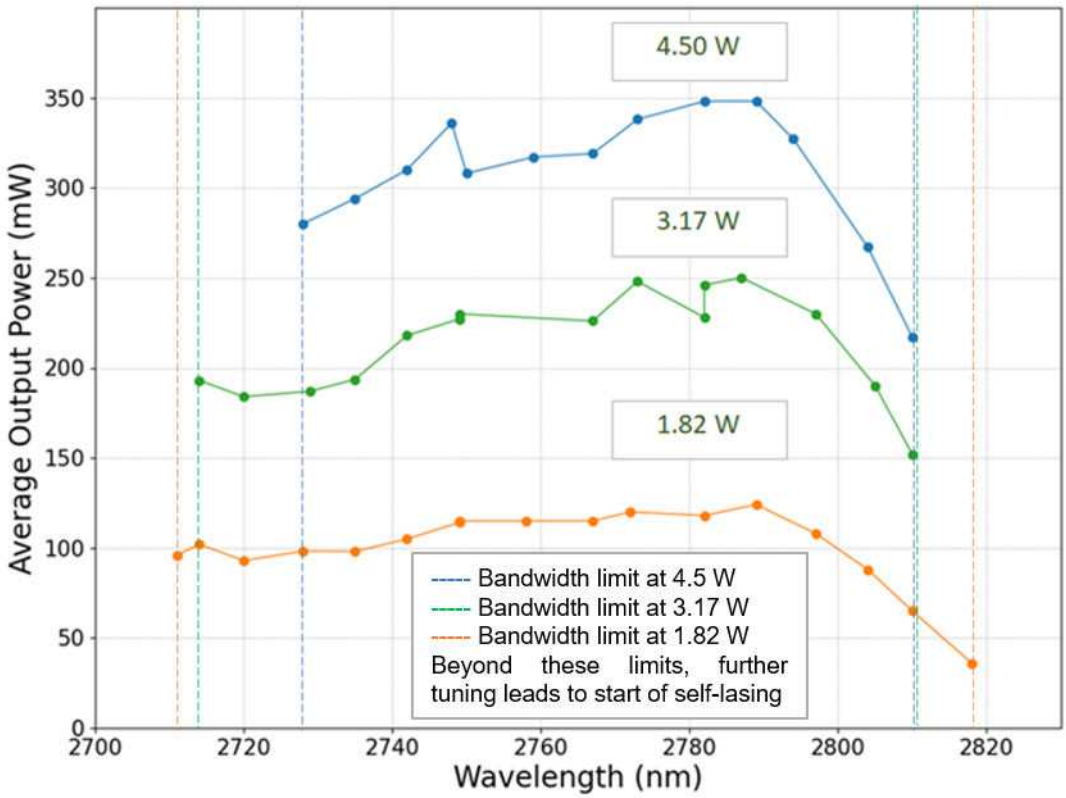

Figure 5.7: Peak laser wavelength versus amplified output power of the fibre amplifier for 3 different pump powers. Corresponding peak amplifier gain values for the 1.82 W, 3.17 W, and 4.52 W pump powers were 21.3 dB, 24.4 dB, and 26.2 dB, respectively. The bandwidth is limited on either ends of the curve due to the start of self-lasing. The wavelength limits are indicated by the dotted lines, beyond these wavelengths, further tuning results in observed self-lasing

three different pump powers is demonstrated in Fig 5.7. The tunability range decreases with the rising pump power.The reduction in the tunable spectral range can be attributed to the diminished population inversion due to an increase in the population density in the lower lasing level for the shorter wavelengths, along with an increased re-absorption of the laser lines at these spectral values. [194, 195, 281]

Fig. 5.8 shows the range of wavelength tuning for the maximum pump power of 4.52 W. The wavelength tuning range at this pump power was 76 nm, between 2728 and 2804 nm, with 2789

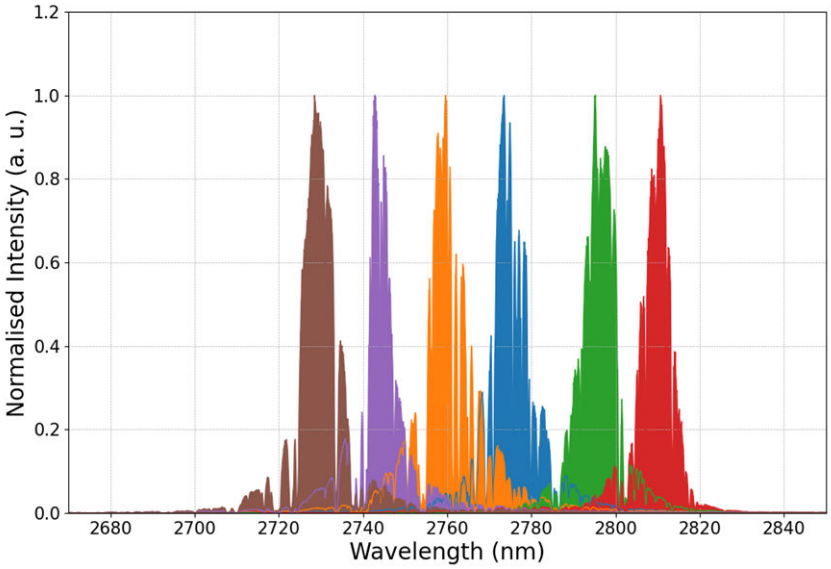

Figure 5.8: Wavelength tuning of fibre amplifier at 4.52 W pump power. The figure shows the shortest tuned wavelength range for the fibre amplifier at the maximum pump power of 4.52 W with the different colour curves representing a few of the measured spectra over the 76 nm range.

nm demonstrating the maximum gain. This was the shortest tuning range observed, the tuning range was limited by the start of self-lasing and thus for the purpose of wavelength tuning studies, the pump power was not increased beyond this value. At 2789 nm, the amplifier showed a 26.2 dB gain corresponding to 375 mW of output power. For the 10 kHz repetition rate and 5.2 ns of the seed, this translated to 7.25 kW of peak power. At 2728 nm, the shortest wavelength, the recorded output power was 279 mW corresponding to 24.9 dB amplifier gain and calculated peak power of 5.3 kW. At the upper tuning wavelength limit of 2804 nm, output power was measured to be 299 mW, giving a 25.2 dB amplifier gain and 5.75 kW peak power. There were also up to 2 nm shifts in the peak wavelength values because of amplification. The spectral lineshape remained similar over the tuned spectral range, but with an extended bandwidth diameter, along with symmetrical distribution of power to the primary profile and the spectral wings, which can be attributed to self-phase modulation that has been reported to occur in amplified spectrum of up to 5.7 kW of peak powers [154]. The atmospheric absorption over the tuned spectral range contributes to minor differences in the spectral profile of the laser lines, exhibiting dips near 2720 nm, 2740 nm, and 2754

nm.

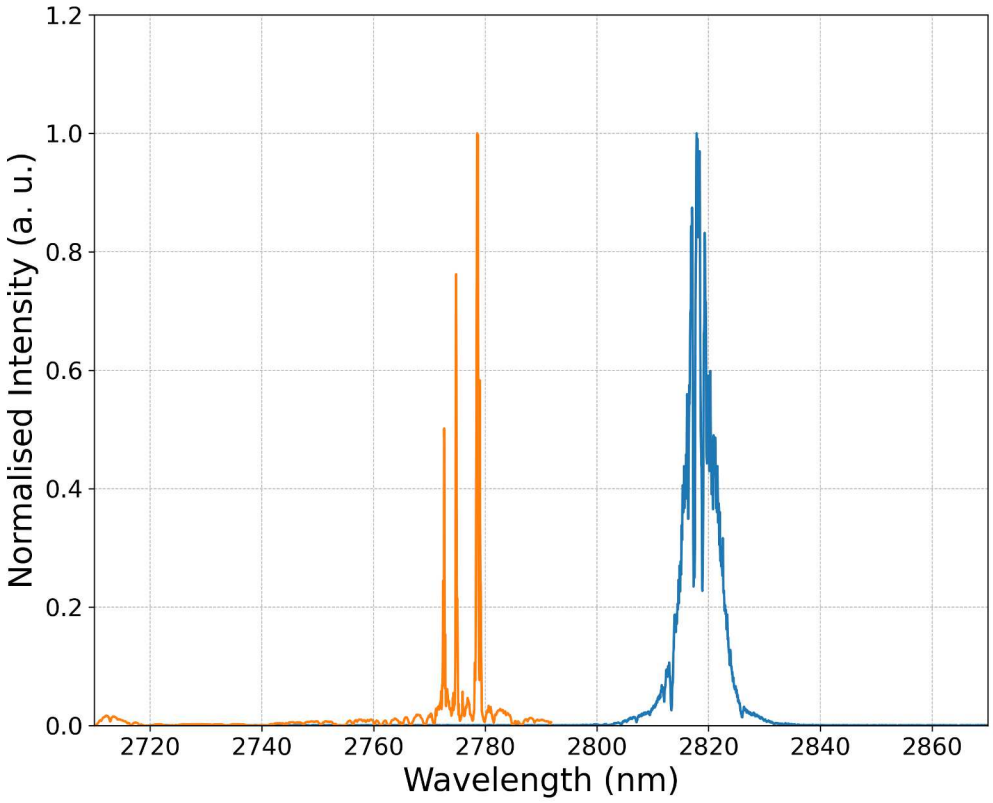

Figure 5.9: The tunable bandwidth is limited by the start of self lasing. The blue curve shows the expected position of the laser spectra at 2817 nm and the orange curve is the self lasing spectra observed at this temperature at the 4.52 W pump power

In fig 5.9, the blue curve is the expected spectra at 2817 nm, obtained at 183 °C and for 31 μm grating period combination from the PPLN OPO, that should have been amplified by the presence of the pump in the fibre amplifier. The orange curve shows the typical self-lasing spectra observed at 4.52 W pump power centred at 2779 nm for the same temperature and grating period combination. Further tuning is aborted at these pump powers to prevent any damage to the fibre.

For a pump power of 3.17 kW, the observed wavelength tuning range was 86 nm, between 2712 nm and 2798 nm presented in Fig. 5.10. The maximum output power of 247 mW was recorded

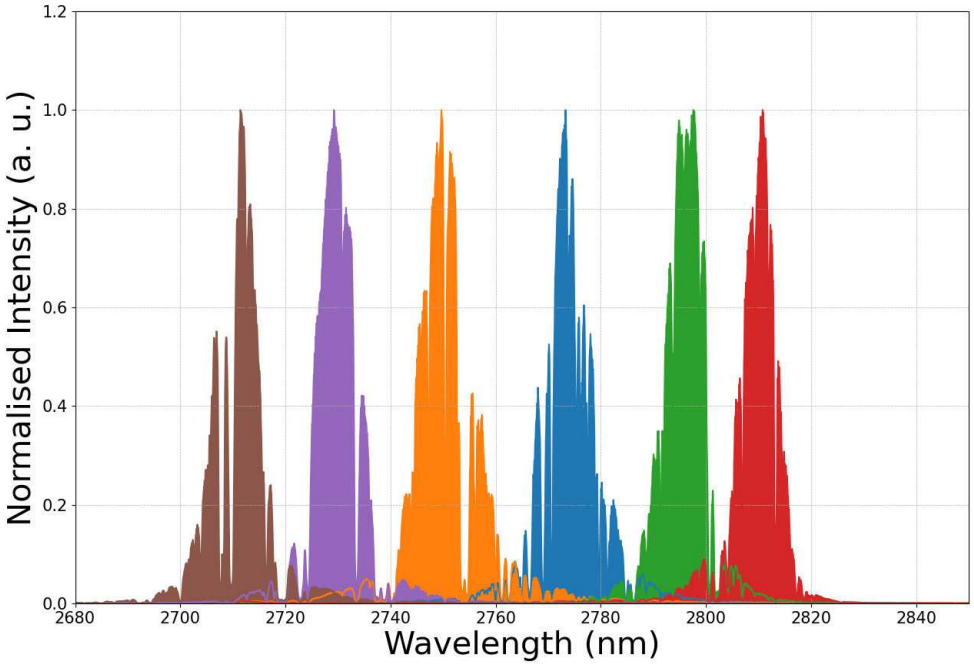

Figure 5.10: Wavelength tuning of the fibre amplifier at 3.17 W pump power. The figure shows the tuned wavelength range for the fibre amplifier at a pump power of 3.17 W with the different colour curves representing a few of the measured spectra over the 86 nm range. The spectra correspond with those for the 4.52 W pump power

for a peak wavelength of 2773 nm, with an amplifier gain of 24.4 dB and 25 μJ pulse energy. At the lower wavelength limit, the output power, amplifier gain and calculated peak power were 183 mW, 23.1 dB and 2.9 kW respectively. At the upper limit of 2798 nm, the output power was 230 mW with calculated peak power of 3.7 kW, amplifier gain of 22.3 dB. The amplifier gains were steady over the tuned spectral range, but the start of self-lasing constrained further wavelength tuning.

The lowest investigated pump power of 1.82 W demonstrated the longest tuning range of 106 nm. The peak wavelength of, 2773 nm recorded the maximum output power of 121 mW. On calculation, this corresponds to a peak power of 2.3 kW and pulse energy of 12 μJ. The fibre amplifier gains at this power, for an input power of 0.9 mW, were 21.3 dB. Over the wavelength

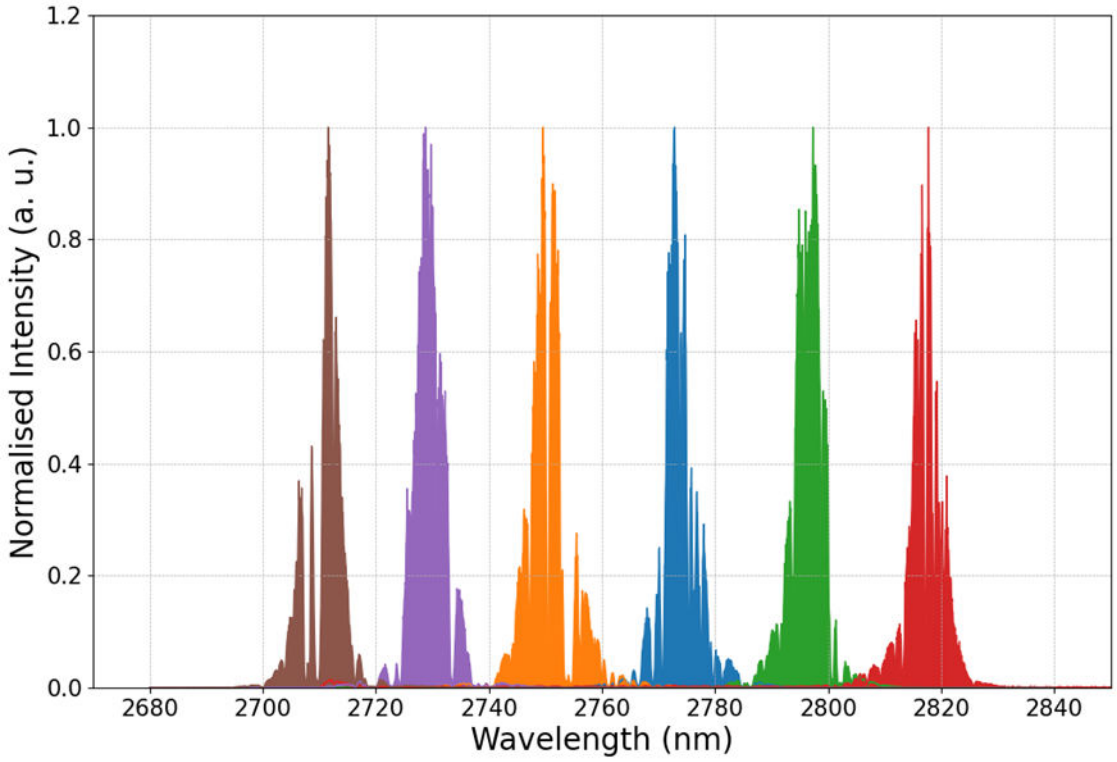

Figure 5.11: Wavelength tuning of the fibre amplifier at 1.82 W pump power. The figure shows the widest tuned wavelength range for the fibre amplifier at a pump power of 1.82 W, with the different colour curves representing a few of the measured spectra over the 106 nm tuning range. The spectra correspond with those for the 4.52 W and 3.17 W pump powers

range between 2712 and 2797 nm, the gain was almost constant, varying within 20.3 dB and 20.8 dB corresponding to 96 mW and 108 mW at the given wavelengths respectively. For wavelengths longer than 2800 nm, the output power of the amplifier fell to 36 mW at 2818 nm corresponding to an amplifier gain 16 dB gain and an overall tuning range of 106 nm between 2712 and 2818 nm, further tuning was limited by the commencement of self-lasing. The commensurate peak powers and pulse energies at these wavelengths were 692 W, 3.7 μJ for the longest 2818 nm and 1.8 kW, 9.5 μJ for the shortest, 2712 nm. Fig. 5.11 shows the tuning range of the amplified spectra at the given pump power. While the bandwidth of the amplified laser spectrum was consistent over the entire tuning range, however, several dips were noted in the line-shape profile, close to 2720 nm, 2740 nm, and 2754 nm attributed to atmospheric absorption.

Pump Power	Pulse Parameters for wavelength 2790 ± 1 nm
0 W (Seed Pulse)	Average Pulse energy = 0.8 µJ Pulse fluctuations from standard deviation = 0.04 µJ Relative pulse fluctuations = 5.42 % Peak power = 0.105 kW Pulse width = 5.3 ns
4.52 W	Average Pulse energy = 37.8 µJ Pulse fluctuations from standard deviation = 1.78 µJ Relative pulse fluctuations = 4.72 % Peak power = 5.78 kW Pulse width = 5.3 ns

Table 5.1: Pulse parameters of the seed and amplified pulses

There was a shift in the peak wavelength from 2773 nm at the lowest pump power to 2789 nm at the highest. This is associated with the change in population densities in the upper and lower transition levels of the laser emission of Er^{3+} ions [150, 154]. In the four level laser system formed in the Erbium ions, the lower lasing level initially unpopulated. The stimulated emission of the lasing process transfers the Erbium ion population on to the lower lasing level which as a longer lifetime of 9.9 μs compared to that of the upper lasing level having a shorter lifetime of 6.9 μs. This causes the population inversion between the laser transition levels to decrease. Subsequently, this results in a reabsorption of the emitted laser line and causes the maximum output power and hence the amplifier gain to move towards longer wavelengths.

The temporal pulse profile of the amplified pulse at 4.52 W pump power is shown below. A comparison of parameters for this amplified pulse with the seed pulse is listed in the table 5.12

The experiment was conducted over a two-week period and in short spans of 30-60 min durations. Over this period of time, no deterioration in the laser performance were noted and

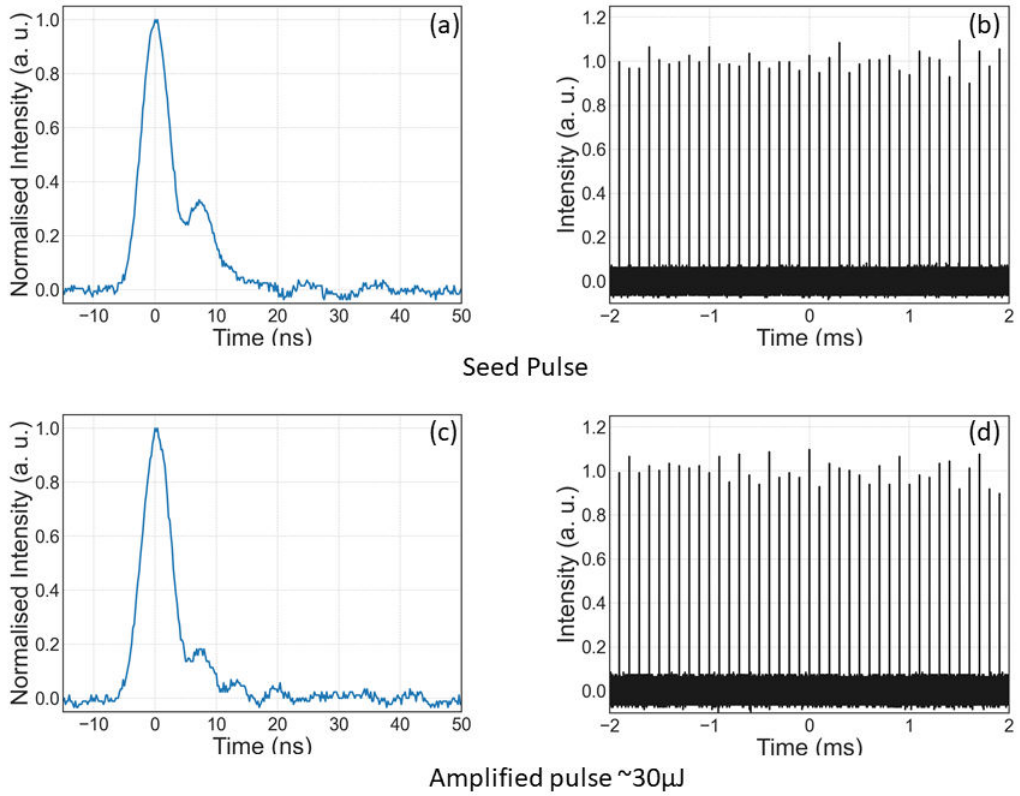

Figure 5.12: (a)Temporal pulse profile of the seed pulse at 2790 nm (b)Pulse-to-pulse stability of the seed pulse over 4ms (c)Temporal pulse profile of the amplified pulse at 2790 nm (d)Pulse-to-pulse stability of the amplified pulse over 4ms

further odds of fibre facet damage was prevented by the short operation intervals [187]. Analysing the experimental results, it was deduced that the amplifier gain-bandwidth was broad. The wavelength tuning range was limited due to self-lasing near the limits of the tuned spectral range. This is predominantly due to Fresnel back-reflections occurring at the fibre tips, with and without the end-caps.

Reportedly, it is possible to obtain over 170 nm of wavelength tuning [211]. As the tuned wavelength moves further away from the maximum gain, in either directions, the gain decreases in value, which consequently reduces the fibre amplifier saturation. This in turn improves the residual small signal gain close to the peak gain wavelength. A high gain in the amplifier also intensifies the

back-reflections over a single round-trip, with the possibility to cause degradation of the fibre facet.

The amplifier gain values for a single pass were limited to 25-30 dB. Once again, the primary constraint to additional power scaling in the fibre amplifier was the start of self-lasing. The key contributor to the process of self lasing is the occurrence of back-reflections from the fibre facets and OH^- ion diffusion into the fibre tips. These could be mitigated by increasing the values of cleaving angles and improving the end-cap material choices and design.

5.4 Conclusion

To conclude, the idler output of a PPLN-OPO with wavelengths tunable between 2-4.2 μm was used to understand the wavelength tunability and distribution of gain of a single stage, single mode Erbium doped fluoride fibre amplifier. The maximum achieved pulse energy was 37.5 muJ translating to a logarithmic gain of 26.2 dB for a wavelength of 2789 nm. At these pumping levels, 76 nm tuning of the peak wavelength was recorded, with amplifier gains of 25 dB within the tunable range. This tunability was limited by the onset of self-lasing due to back reflections from the fibre facets. At lower pump powers, an overall tunability of 106 nm was obtained. However, within this tuning range, the amplifier gain varied between values of 16 and 21.3 dB, again limited by self-lasing especially at the lower wavelengths.The results of the investigation of wavelength tuning of Er:ZBLAN fibre amplifier with nanosecond pulses were peer-reviewed and published [286].

To summarise, this study is the first to experimentally determine the wavelength tuning properties in Erbium doped ZBLAN fibre amplifier which sets the groundwork for developing high gain amplifiers and lasers in the mid-IR with wide, over-100 nm tunability. The study takes into consideration the experimental constraints to the spectral tunability in the form of presence of Amplified Spontaneous Emission, Self lasing, which impact the practical performance of a fibre amplifier. However, effects such as nonlinear soliton self-frequency shift which do not directly influence the gain distributions of Erbium doped fibre amplifiers, are not examined within the scope of this study.

Further Improvement of Amplifier Tunability

To improve performance of a widely tunable, high gain amplifier, it is important to consider measures to mitigate self-lasing by adding active cooling systems [197], better end cap materials and designs [187] and more commonly, larger cleaving angles. Studies suggest incorporating an optimised cleave angle of the fibre tip[170] or end-cap [287] can mitigate the issue of parasitic self-lasing, which can result in achieving wider wavelength tunability in the linear regime. In fibre lasers, integrating long period rating have also succeeded in avoiding parasitic self-lasing [284]. Wang et al. have demonstrated Er: ZBLAN emission spectra to range between 2.6-2.95 μm [288], and since Er:ZBLAN has relatively high gain over this spectral range, increasing pump power beyond 4.5 W could potentially allow access to longer wavelengths [197, 149, 262].Optimising increased doping concentration can provide more tunability by releasing any possible bottleneck occurring at the lower energy state during the lasing process [281].Other methods of obtaining longer wavelengths in mid-IR could include co-doping with other rare-earth ions, like dysprosium [289] or praseodymium. Within nonlinear regime, raman soliton shift [290] and supercontinuum generation [213] can help achieve wider tunability.

With the aim to develop efficient sources for laser-tissue interaction processes like surgery and laser-induced forward transfer (LIFT), it is beneficial to use sources with high amplification, which are also tunable in mid-IR. While OPO remain the most widely tunable source that serve as a seed laser for amplifiers designed with MOPA configuration, it might make sense to explore into other mid-IR sources that can ease the complexity of alignment associated with OPOs. Alternatively, it is also possible to use compact, tunable, high power semiconductor laser sources like diodes/ ICLs to seed a single stage Erbium doped amplifier and develop versatile devices for laser material interaction applications in the mid-IR.

Chapter Six

Summary and Future Work

To summarise, mid-IR is a promising area of research in the near future. It is a part of the spectrum which can be exploited for a variety of applications including imaging and laser material interaction, specifically for surgeries. CO_2 gas lasers have been in use in medicine to treat cancers and operates around the wavelengths of 9.6 and 10.6 μm in the mid-IR. Fibre-based systems have been combined with NIR solid-state Nd-YAG lasers to deliver high power pulses, precisely into a diseased area which are sometimes difficult to access. Both these types of lasers are competent due to their emission wavelength bands coinciding with water absorption peaks close to 10 and 1 μm. A quick look into the water absorption window through the electromagnetic spectrum shows that the water absorption is highest around 2.8-3 μm. [291, 292], neglecting the UV bands which pose significant health risks [293]. Thus, it becomes a good reason to explore the possibility for developing lasers which can deliver as precise medical devices in this wavelength region.

To develop a versatile high power, tunable, precise mid-IR source, a MOPA-based fibre amplifier operating around 2.8 μm is an excellent candidate. Rare earth doping can provide necessary and efficient energy transitions around this wavelength with Erbium having the highest dopant concentration and output powers, along with a mature doping technology. ZBLAN fibres prove to be extremely suitable hosts due to the wide transparency, low phonon energy, stable structure and the good capacity for doping of rare earth ions. Combining the properties of Erbium doping with ZBLAN fibre allow operation of a high amplification, wavelength tunable source device with the

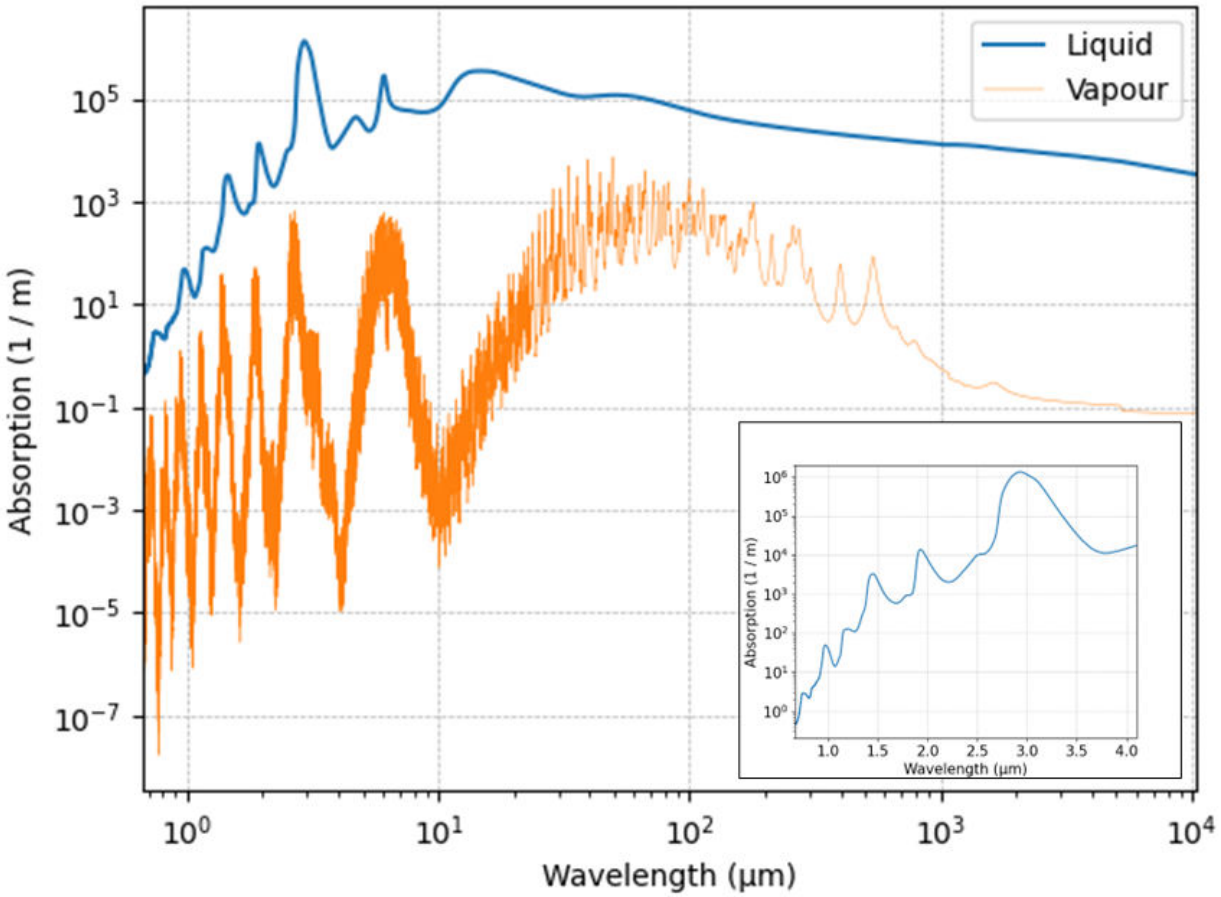

Figure 6.1: Water absorption window over the electromagnetic spectrum

possibility of attaining high precision due to the single mode nature of the fibre.

In this thesis, a single stage Erbium doped ZBLAN fibre was investigated in its single mode operation, pulse energies of over 50 μJ were achieved, demonstrating over 26 dB of amplification from sub-10 ns, 0.5 μJ seed pulses. With lower seed pulse energy and pump powers, over 100 nm wavelength tunability, centred at a peak efficient wavelength of 2790 nm was observed. While the operation was not affected by amplified spontaneous emission, self-lasing was the key factor limiting the wavelength tuning range. A key process influencing self-lasing were back-reflections from the fibre facets. The seed source was a tunable PPLN-based OPO pumped by nanosecond Nd-YAG

laser capable of producing up to 1 μJ pulse energies at 10 kHz repetition rate. The seed laser was widely tunable in the NIR / mid-IR between 1.4-4.2 μm, due to nonlinear frequency conversion satisfying the quasiphasematching condition. Coupling light from a free-space solid state laser into a fibre amplifier was impacted by atmospheric absorption of the seed wavelengths due to the absence of any external housing, but the levels were maintained by varying the output pump power of the Nd:YAG laser. Atmospheric effects were more prominently observed as modulations in the output spectra from the fibre amplifier.

While the amplifier operation is possible at levels of several tens of watts, high power performance is often limited due to low melting points and damage threshold of the material, which poses a big challenge to further power scaling. For increased power amplification, thermal management becomes an important factor as the heating up of the output end of such fibres can soften the fibre input end causing it to bend and de-align [294], and continued long duration operation often lead to fibre tip damage. Amplifier operation is often impacted by other unfavourable nonlinear effects such excited state absorption, self-phase modulation, self-lasing, and amplified spontaneous emission. Therefore, active cooling should be taken into account for high power scaling to ensure effective amplifier performance. And finally, to extend the application to the deeper mid-IR wavelengths, it could be a conspicuous decision could be to replace the dopant in the ZBLAN fibre with other rare earth materials.

Potential of Er:ZBLAN fibre amplifier in the advancement of mid-IR sources

Er:ZBLAN fibre amplifiers continue to draw significant interest in research. The work covered in this thesis adds to the current state of the art discussed in section 2.5 and bench-marked in the table 6.1

Table 6.1: Performance comparison of Er-doped fibre amplifier with the current state-of-the-art

Publication & Year	**CW / Pulsed / SC**	**Output Power (W)**	**Peak Power (kW)**	**Pulse Width**	**Pulse Energy**	**Wave-length (λ_c) & Tunable Range (μm)**	**Fibre Core Type**
Zhu 2007 [194]	cw	10	_	_	_	λ_c=2.78, Range: 2.7-2.83	Single mode
	21.3% slope efficiency, $\sim$ 43 W pump power, linewidth $\sim$ 10pm						
Tokita 2010 [197]	cw	8-11	_	_	_	Range: 2.77-2.88	Multimode
	Littrow configuration fibre laser cavity, Uses N_2 purged enclosure to prevent moisture damage to end facets						
Tokita 2011 [170]	pulsed	12	0.9	90 ns	100 μJ	λ_c=2.8	Multimode
	Uses N_2 purged enclosure to prevent moisture damage to end facets						
Gorjan 2011 [152]	pulsed	2	68	300 ns	20 μJ calculated*	λ_c=2.8	Multimode
	Pulsed operation controlled by laser output feedback, pulse duration independent of pulse rate and affected by laser dynamics alone						
Faucher 2011 [236]	pulsed	20.6	_	_	20 _	λ_c= 2.825	Single mode
	Pulsed operation controlled by laser output feedback, pulse duration independent of pulse rate and affected by laser dynamics alone						

Continued on the next page

Table 6.1: Performance comparison of Er-doped fibre amplifier with the current state-of-the-art

Publication & Year	**CW / Pulsed / SC**	**Output Power (W)**	**Peak Power (kW)**	**Pulse Width**	**Pulse Energy**	**Wave-length (λ_c) & Tunable Range (μm)**	**Fibre Core Type**
Gauthier 2015 [295]	sc	0.078	_	400 ps	_	Range: 2.6-4.1	Single mode
	Generates supercontinuum in fibre seeded by OPG source with 82% power concentrated beyond 3 μm						
Duval 2016 [296]	pulsed	>2	200	160 fs	37 nJ	Range: 2.8-3.6	Single mode
	Generates Raman soliton pulses using a fibre oscillator and external amplifier combination						
Wei 2017 [210]	pulsed	5.16	_	400-1890 ns	27.7 μJ	λ_c=2.8, Range: 2.76-2.85 (90 nm)	Single mode
	Achieves room temperature operation						
Wei 2017 [211]	pulsed	$<$ 120 mW	$\leq$ 3.6 W	1.6-3.5 μs	2-6 μJ	λ_c=2.8, Range: 2.67-2.87 (170 nm)	Single mode
	Demonstrates stable, tractable μs-pulse durations with changing repetition						
Aydin 2018 [199]	cw	41.6	_	_	_	λ_c=2.824	Single mode

Continued on the next page

Table 6.1: Performance comparison of Er-doped fibre amplifier with the current state-of-the-art

Publication & Year	**CW / Pulsed / SC**	**Output Power (W)**	**Peak Power (kW)**	**Pulse Width**	**Pulse Energy**	**Wave-length (λ_c) & Tunable Range (μm)**	**Fibre Core Type**
	Uses Er: ZrF_4 fibre with splice-less cavity, FBG written onto the gain fibre, bidirectionally-pumped						
Paradis 2018 [203]	pulsed	11.2	420	170 ns	80 μJ	λ_c=2.826	Multimode
	Uses gain-switched, all-fibre configuration with FBG written onto the gain fibre						
Du 2020 [212]	pulsed	_	60.3	11.5 ns	0.7 mJ	λ_c=2.72	Multimode
	Large core fibre, Seed genrated from OPO/OPA combined source, 10 Hz repetition rate						
Aydin 2021 [204]	pulsed	5	1000	$\leq$ 1 ns	1 mJ	λ_c=2.8	Single mode
	Utilises dual stage amplifier configuration						
Sojka 2021 [172]	pulsed	_	12.7	26 ns	330 μJ	λ_c=2.78	Multimode
	Demonstrates effect of repetition rate on pulse duration and peak power						
Du 2022 [297]	pulsed	_	_	95 ns	0.75 mJ/ 420μJ	λ_c=2.8	Single & Multi-mode
	Achieves diffraction-limited beam quality						
Chichkov 2022 [261]	pulsed	0.5	8	5.2 ns	53 μJ	λ_c=2.79	Single mode

Continued on the next page

Table 6.1: Performance comparison of Er-doped fibre amplifier with the current state-of-the-art

Publication & Year	**CW / Pulsed / SC**	**Output Power (W)**	**Peak Power (kW)**	**Pulse Width**	**Pulse Energy**	**Wave-length (λ_c) & Tunable Range (μm)**	**Fibre Core Type**
	Single-stage single-mode fibre						
Ray 2022 [286]	pulsed	0.38	6	5.2 ns	37 μJ	λ_c2.79 Range: 2.71-2.82 (106 nm)	Single mode
	Single-stage single-mode fibre						

When it comes to commercial applications, fibre-based systems surpass the emerging mid-IR technologies like semiconductors, nonlinear parametric sources, microresonators, as they are compact, robust, and cost-effective. With the rapid development of efficient mid-IR technologies, the concurrent factor that remains is the transfer of the energy from the source to the target of the application. At present, companies like Femtum are offering 2.8 μm lasers with $>$ 100 μJ pulses with pulse durations between 30–200 nanoseconds and 1-50 kHz repetition rate, 30 dB gain, with tunability between 2710-2830 nm. In comparison, the amplifier developed independently with commercial ZBLAN fibre produces >50 μJ with 5.2 ns pulses at fixed repetition rate of 10 kHz with 25-26 dB gain and a tunability range between 2716 -2816 nm. This is achieved without including any active or passive cooling mechanism for heat management, and modulation of pulse repetition rates, leaving sufficient opportunity for further power scaling and wider tunability with easily implementable adjustment of operational parameters. The amplifier was able to access a continuous tunability with variable gain between 16-21 dB between 2712 -2818 nm at the lowest pump power. This range is almost concurrent with the results on continuous wavelength tunability

of $\sim$ 107 nm in an Er:ZBLAN fibre laser with external grating component for wavelength selection reported by Wei et al. [211] with a much longer fibre length of 4.1 m and higher doping concentration of 8 mol.%. Eliminating back-reflections by integrating efficient end-cap design and incorporating larger cleaving angles (up to 15$\circ$ [197]) at the fibre end could reduce parasitic lasing that poses a challenge in accessing further wavelength tuning.The wavelength transparency is still limited in fibre-based systems to a certain extent, especially when compared to OPO and other parametric technologies. However, with the presence of water absorption window near 2.8 μm, free space lasers may undergo absorption due to presence of atmospheric moisture. This pushes the need to develop fibre systems which can not only deliver the power, but also can be used as a source, like a fibre amplifier, which can provide good gain stability and energy conversion efficiency. It is far easier to combine multi-stage fibre amplifiers to achieve very high gain, than to maintain the free-space alignment of the semiconductor and parametric sources, especially in the context of out-of-laboratory applications.

Er:ZBLAN fibre amplifier vs comparative mid-IR technologies

A plethora of technologies have been developed over the last few decades to generate laser radiation in the short-wave mid-IR region. The significance of the wavelength region in the 2-5 μm has been clearly established; laser sources in this spectral range has enabled accurate and efficient utilisation of coherent, collimated, and directional nature of the laser for application in numerous scientific as well as technological fields like spectroscopy, chemical sensing, material processing and medicine. The choice of the ideal source however depends on the requirements of the application, and guided by key parameters such as output power, tunability, mode of operation like CW or pulsed, pulse durations and energies, and alignment complexity.

Mid-IR parametric sources with their wide tunability would be an appropriate choice for chemical sensing and spectroscopy applications. Parametric sources like OPO uses frequency down conversion to allow up to over an octave wider wavelength tunability, over 20 W average output power with nearly 66% conversion efficiencies in the mid-IR using ring cavity [298]. The current

OPO system achieves nearly 2700 nm tunability, with power conversion efficiency ∼35% in a linear cavity, showing that employing ring cavities can enable more efficient frequency conversion. The output powers, however, are determined by the pump laser power and can be improved with the used more efficient pump sources. The wavelength tunability is easily modulated by the structurally engineered grating or poling period along with temperature tuning. Depending on the pump laser linewidth, cavity design and a careful choice of spectral selector, a narrow output linewidth can be maintained in an OPO. On the other hand, alignment sensitivity remains a critical challenge for the implementation of OPO in many practical applications.

Solid state lasers in the short-wave mid-IR offer the powers of the order of with 20-60 W operating within 2-5μm range using Cr: ZnS /Cr: ZnSe and Cr: CdSe . For biomaterial processing, Cr:ZnSe and Cr: CdSe lasers have demonstrated high pulse energies up to 0.5 mJ with tunabilities between 2.2-3.1 μm, optimal for such applications. The other type of solid-state lasers includes rare earth doped laser crystals which have been shown to generate powers close to 1 W in both continuous-wave mode, and pulsed mode with nanosecond and microsecond pulses [299, 300].

In the mid-IR, semiconductor-based mid-IR sources like QCLs and ICLs remain a promising replacement for diode lasers. QCLs offer significant output powers, broad tunability, high beam quality and stable room temperature operation with precise output control, but without the necessity of cryogenic cooling mechanisms. For some time, ICLs have been the more dominating technology between 3-6 μm [301], demonstrating lower input power densities, threshold current densities, thus lesser radiative and non-radiative losses compared to diode lasers, improved carrier confinement, along with better voltage and power consumption efficiencies [302]. ICLs integrate the useful properties of diode lasers and structural engineering of QCLs, to be a versatile source in this wavelength range. Recently, high power, (>5W) QCLs have between 3-6 μm wavelength range (currently QCLs are generated in the range of 3.5-24 μm) been demonstrated owing to the progress in metamorphic materials research [303]. The ICLs on the other hand produce powers below 0.5W and maximum tunability slightly over 50 nm. In comparison, OPOs can provide much higher powers of ∼20 W with PPLN or ∼99 W [304] with ZGP as the nonlinear material. The tunability of

OPOs depend on the transparency of the nonlinear medium employed in it. For PPLN this is near 5 μm, whereas materials like ZGP and GaAs has reported nearly 12 μm or 16 μm transparency, respectively.

While all the sources discussed can deliver high output powers and reasonable tunability, practical implementation might be challenged in the 2.0-3.5 μm band due to significant water absorption in the atmosphere within that band. Thus, to deliver powers at a distance from the origin of the source, fibre-based systems remain most reliable, justifying the need for further research into efficient tunable fibre-based sources in this wavelength range. With large core Erbium-doped fluoride fibres supporting watt-level powers and kilowatt level peak powers, fibre-based amplifiers and lasers can not only add to the list of sources but also complement the power delivery from other sources with additional tunability and good beam quality. Introduction of single mode fibre ideally improves the beam quality, allowing smaller beam widths for high precision applications. Obtaining half-a-watt level average output power with additional tunability with a single stage, single mode fibre, the work presented in this thesis moves the bar one step closer towards this goal. While very high powers can introduce damage to the fibre ends, more research into thermal management and end-cap technology can bring promising results. A comparative summary of the best performing devices for each technology is presented in the table 6.2 [299, 193, 305].

Table 6.2: Comparison of different types of lasers in the short-wave mid-IR region.

Type	**Technology**	**Materials**	**Average Output Power**	**Operational Range (μm)**
Parametric	OPO OPG	PPLN PPKTP KTA	PPLN-OPO: 20 W, 66% efficiency [298], KTA: 33 [306] PPLN-OPG: 6.2 W [307]	1.4-4.1 (PPLN-OPO) [This work] 2.61-3.84 (PPKTP-OPO) [308] 2.4-4.0 (KTA-OPO) [309] 2.76–3.98 (PPLN-OPG)[307]
	Advantages: Wide tunability, high conversion efficiency			
	Disadvantages: Alignment sensitivity			
Solid State	_	Cr:ZnSe, Cr:ZnS, Cr:CdSe,	20-60 W [310]	1.97-3.35 (Cr:ZnSe) [300] 1.96-3.19 (Cr:ZnS) [300] 2.25-3.08 (Cr:CdSe) [32]
	Advantages: High pulse energies, suitable for biomaterial processing			
	Disadvantages: Excessive heat generation			

Continued on the next page

Table 6.2: Comparison of different types of lasers in the short-wave mid-IR region.

Type	**Technology**	**Materials**	**Average Output Power**	**Operational Range (μm)**
Semiconductor	Diode Laser QCL ICL	GaSb (Laser diodes), InGaAs/ AlInAs/ InP (QCL), InAs/ GaSb/ AlSb (ICL)	GaSb: 0.85 W [311] QCL $>$ 5 W [303] ICL $<$ 0.5 W [312]	1.9-3.3, 2.9-5.5 (GaSb) [73, 312] 3.8-6 (QCL) [303] 2.8-5.9 (ICL) [71]
	Advantages: Good beam quality, room temperature operation possible			
	Disadvantages: Need for cooling mechanisms			
Fibre-based	Fluoride Chalcogenide	Er-doped, Ho-doped Dy-doped	Er:ZBLAN- upto tens of Watt [194, 197, 170, 199, 203], 350-500 mW [This work] Dy:ZBLAN- 554 mW [313] Ho:ZBLAN- 327.4 mW [314]	2.67-2.87 [211], 2.712-2.818 [This work] (Er:ZBLAN) 2.9-3.1 (Ho:ZBLAN) [305] 2.71-3.08 (Dy:ZBLAN) [315]
	Advantages: Reliable power delivery, excellent beam quality, additional tunability			

Continued on the next page

Table 6.2: Comparison of different types of lasers in the short-wave mid-IR region.

Type	**Technology**	**Materials**	**Average Output Power**	**Operational Range (μm)**
	Disadvantages: Relatively limited tunability, nonlinear effects, potential fibre damage at high powers			

6.1 Future Work

The work accomplished in this thesis can lay the foundation for expansion into different directions of research. Firstly, it is possible to build on this study on Erbium doped fluoride fibre amplifiers to achieve improved power scaling and further wavelength tuning, by employing appropriate methods to mitigate the current challenges of thermal management in the operation of these amplifiers. Moreover, it is also possible to investigate the performance of the amplifier in the ultrashort pulse regimes to develop devices with greater achievable precision in material processing applications. Secondly, the PPLN-based OPO source, which currently emits in the short wavelength range, can be utilised to pump other quasiphasematched nonlinear materials with wider transparency windows generating wavelengths deeper into the mid-IR.

6.2 Inter-band Cascaded Laser pumped Erbium-doped fluoride fibre amplifiers

High concentration Erbium-doped ZBLAN fibres when seeded with high power semiconductor diodes lasers operating near 2.8 μm can translate to high gain average output powers in the Erbium-doped fluoride fibre amplifiers. GaSb based diodes which operate near 2.8 μm and demonstrates tunability [74] can be a suitable alternative to the OPO seed source.These sources are available

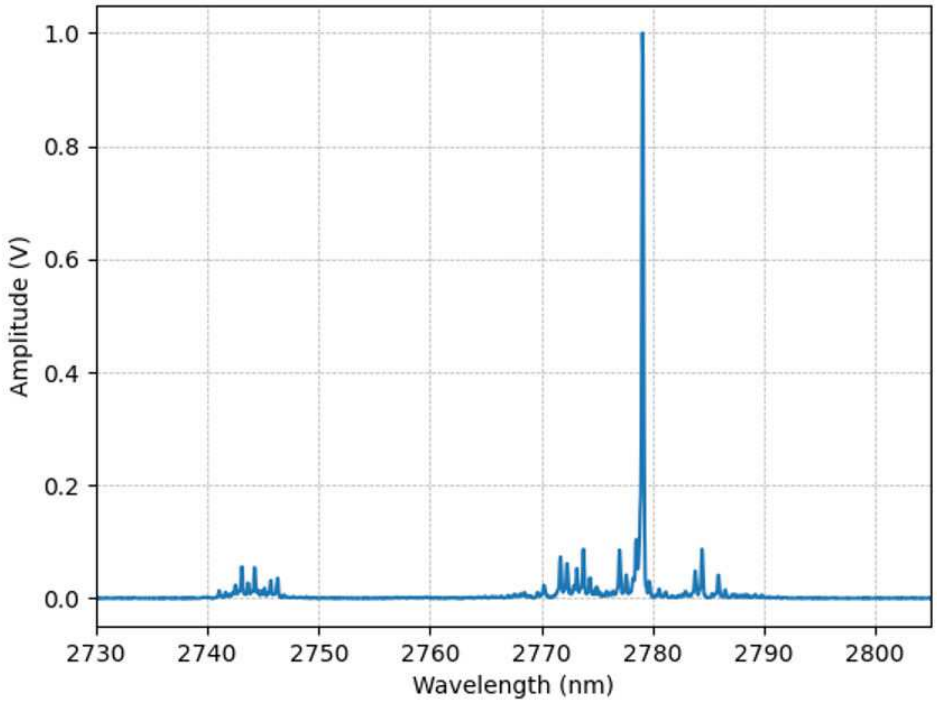

Figure 6.2: Emission of GaSb-based diode emitters near 2.8 micron measured at 25 °C and 350 mA forward current

as edge-emitters [316], VCSELs [317] and in passive mode-locked formats [318] and thereby can be used to develop lasers with lower pulse widths, scaling to the order of picoseconds. Solid state Cr:ZnSe [319] operating in the 2–3 μm mid-IR wavelength region can also be a potential alternative to the current seed laser.

6.3 Isotropic, quasiphasematched nonlinear waveguides pumped by short wave mid-IR OPO

Quasiphasematching for nonlinear frequency conversion as been implemented in isotropic nonlinear materials such as gallium arsenide in the form of orientation patterning, which involves periodic reversal of the atomic structure orientation to create poling or grating periods for frequency con-

version.

Gallium arsenide (GaAs) is a widely used material in the semiconductor industry. It is optically isotropic in nature, but has numerous resourceful properties for nonlinear conversion. These properties along with the ability to handle high output powers in CW and pulsed regimes low loss, low damage threshold makes it a nearly ideal frequency converter. Moreover, high quality crystals are commercially available. Due to the isotropic nature of the material, it is possible to design various quasiphasematching patterns on it by molecular beam epitaxy (MBE).

Parameter	Value
Material nature	Isotropic
Nonlinear Coefficient (d_{eff})	94 pm/V
Spectral Transparency Range	0.9-18 μm
SHG Conversion Efficiency	$>$ 33%
Damage Threshold	2 J/cm^2

Table 6.3: Salient properties of gallium arsenide

Although isotropic, these materials have high nonlinearity coefficients and can potentially produce highly efficient nonlinear frequency conversion with relatively low pump powers. At shorter IR wavelengths up to 1.7 μm, GaAs exhibits two-photon absorption losses, due to which this material requires pumping wavelengths closer to 2 μm [320].

Some initial work with second harmonic generation (SHG) in OP-GaAs waveguides with a PPLN-based OPO pump source have been reported [321]. Waveguide structure of these materials ensure increased confinement of the pump beam within a narrow core area, providing greater interaction length allowing nonlinear frequency conversion, even for low intensity beams. Using the PPLN pump set up which emits nanosecond pulses, translating to $\sim$ 1 μJ for 10kHz repetition rate, it is possible to generate signal and idler wavelengths deep in Mid-IR spectral range, by single pass optical parametric amplification process. One interesting aspect would be to understand what

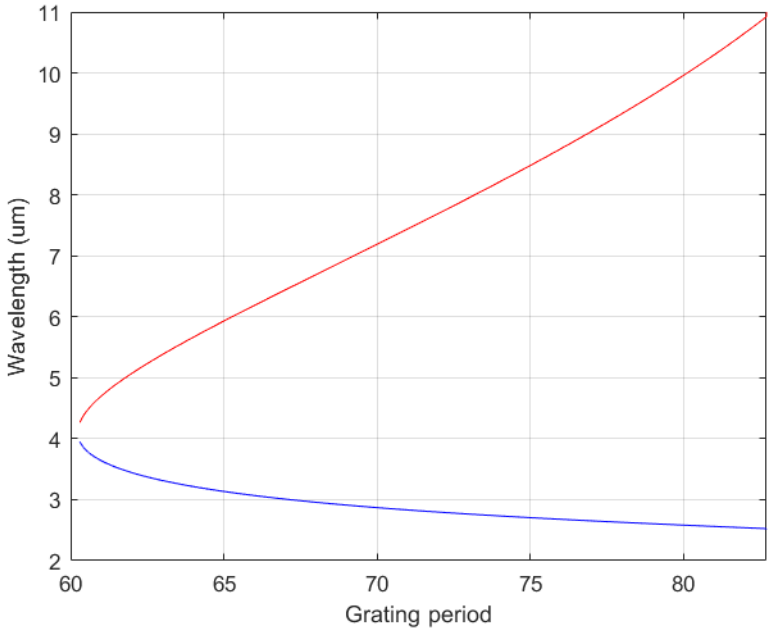

Figure 6.3: Potential output wavelength for 2051 nm pump over a range of grating periods in OP-GaAs. The red line indicates the range of longer idler wavelengths and the blue line shows the potential signal wavelengths

fabrication parameters, apart for the grating period, calculated from the QPM condition influence the output wavelengths.

6.4 Isotropic, quasiphasematched nonlinear material pumped by Erbium doped Fluoride Fibre amplifier

In a very recent study, Becheker et al.[322] demonstrated pumping of nonlinear OP-GaAs waveguides with a femtosecond Erbium doped Fluoride Fibre amplifier operating at 2790 nm. A similar study can be conducted to investigate similar results for nanosecond pulses.

An initial simulation created by solving the QPM condition for the OP-GaAs gives a range of required grating periods and potential output wavelengths from such a device, there is a possibility

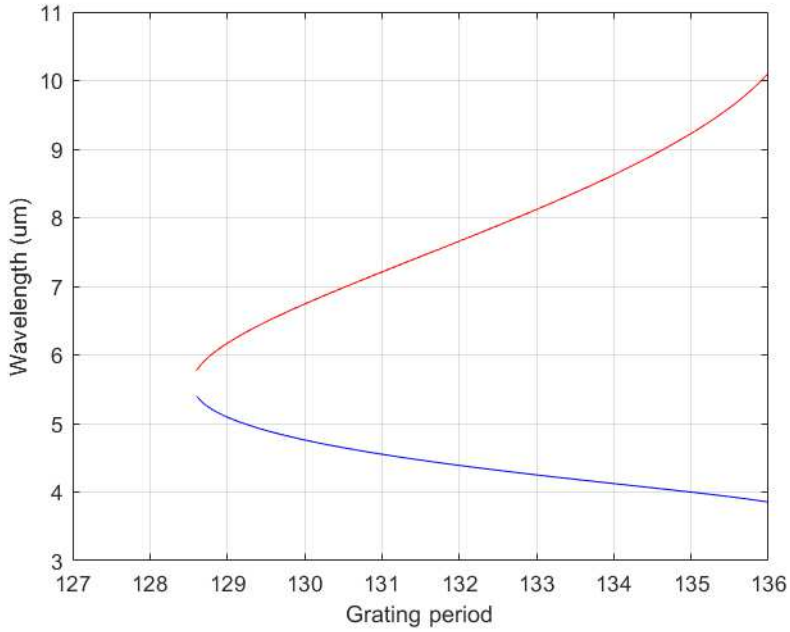

Figure 6.4: Potential output wavelength for 2790 nm pump over a range of grating periods in OP-GaAs. The red and the blue lines indicate the idlers and the signals respectively for tuning over a range of grating period combinations

of the transverse core dimension affecting the final emitted wavelengths. Additionally, since the output of the Erbium doped fluoride fibre amplifier can produce large pulse energies, it can be used to pump nonlinear OP-GaAs bulk crystals to possibly generate supercontinuum in the mid-IR. Supercontinuum generation can find applications in gas sensing, more specifically breath analysis, owing to the molecular fingerprinting region, to potentially allow early detection of diseases.

.

Appendix One

Manley-Rowe relations for three wave-mixing processes

To analyse the nonlinear conversion processes, the Manley-Rowe relations are studied. Considering three plane waves with frequencies ω_1, ω_2 and ω_3 propagating along the z direction and interacting in a nonlinear medium of susceptibility $\chi^{(2)}$,they can be represented as paraxial wave equations

$$\frac{dE(\omega_1)}{dz} = -i\kappa_1 E(\omega_3)E^*(\omega_2)exp(-i\Delta kz) \tag{A.1}$$

$$\frac{dE(\omega_2)}{dz} = -i\kappa_2 E(\omega_3)E^*(\omega_1)exp(-i\Delta kz) \tag{A.2}$$

$$\frac{dE(\omega_3)}{dz} = -i\kappa_3 E(\omega_1)E(\omega_2)exp(+i\Delta kz) \tag{A.3}$$

where $\kappa_i = \omega_i d_{eff}/n_i c_0$ are the coupling coefficients and $\Delta k = k_3 - k_1 - k_2$

Multiplying Eq A.1 with $n_i c_0 \epsilon_0 E^*(\omega_1)/2$ and adding the complex conjugate,

$$\left(\frac{1}{\omega}\right)\frac{dI(\omega_1)}{dz} = \frac{i\epsilon_0 d_{eff}}{2} E(\omega_3)E^*(\omega_2)E^*(\omega_1)exp(-i\Delta kz) + c.c. \tag{A.4}$$

assuming a lossless medium, $d_{eff} = d^*_{eff}$.

Working similarly with equation A.2 and A.4 gives,

$$\left(\frac{1}{\omega_1}\right)\frac{dI(\omega_1)}{dz} = \left(\frac{1}{\omega_2}\right)\frac{dI(\omega_2)}{dz} = -\left(\frac{1}{\omega_3}\right)\frac{dI(\omega_3)}{dz} \tag{A.5}$$

This can be interpreted as a photon of frequency ω_3 annihilated to create a photon of frequency ω_1 and ω_2 and the spatial intensity distribution given by $\frac{dI(\omega_i)}{dz}$ are scaled according to ω_i.

Three wave mixing processes comprises sum frequency generation, difference frequency generation (DFG), optical parametric amplification,and optical parametric oscillation

A.0.1 Optical Parametric Oscillators

Optical Parametric Oscillation is a nonlinear process of the second order. Optical parametric oscillators (OPOs) are optical amplifiers, or nonlinear optical devices, that convert a laser beam into two beams of lower frequency or longer wavelengths. They are used in a wide range of applications, including laser isotope separation, laser spectroscopy, and in high-energy physics experiments. OPOs can also be used as a source of light for various types of imaging and laser material processing. OPOs are capable of producing light with very high intensity, and so are often used in applications where high power is required. They are also used for frequency conversion, and for generating light with wavelengths not normally available from traditional lasers.

By the principle of conservation of energy in three wave mixing process, $\omega_1 = \omega_3 - \omega_2$ gives the evidence for frequency conversion and principle of conservation of momentum gives $\Delta k = k(\omega_1) + k(\omega_2) - k(\omega_3)$, the condition for the conversion to take place.

within limits of low conversion and taking $E(\omega_2)$ and $E(\omega_3)$ to be constant, thus

$$I(\omega_1, l) = \frac{2\kappa_1^2 n_1}{n_2 n_3 c_0 \epsilon_0} l^2 I(\omega_3) I(\omega_2) \left\{\frac{sin\Delta kl/2}{\Delta kl/2}\right\}^2 \tag{A.6}$$

In the reverse sense, this principle can be used to generate two wavelengths deep into the infrared region using more commonly available near-infrared wavelengths as a strong pump. In case of a strong pump wave, $E(\omega_3)$ is constant,

$$\frac{\partial E(\omega_1)}{\partial z} = -i\kappa_1 E(\omega_3)E^*(\omega_2)exp(i\Delta kz) \tag{A.7}$$

$$\frac{\partial E(\omega_2)}{\partial z} = -i\kappa_2 E(\omega_3)E^*(\omega_1)exp(i\Delta kz) \tag{A.8}$$

Assuming boundary conditions as $E(\omega_2, z = 0) = E_0(\omega_2)$ and $E(\omega_1, z = 0) = 0$ that is initially there is no signal or idler. Considering the build up of the signal and idler waves, $E(\omega_{1,2}, z) = E_0(\omega_{1,2})exp(\pm\gamma z)$, on achieving phasematching,

$$\pm\gamma E_0(\omega_1) + i\{\kappa_1 E(\omega_3)\}E_0^*(\omega_2) = 0 \tag{A.9}$$

$$\{-i\kappa_2 E^*(\omega_3)\}E_0(\omega_1) \pm \gamma E_0^*(\omega_2) = 0 \tag{A.10}$$

thus γ can be given by relation,

$$\gamma^2 = \kappa_1\kappa_2|E(\omega_3)|^2 \tag{A.11}$$

The fundamental solutions for the ω_1 and ω_2 fields are hyperbolic in nature and are given by

$$E(\omega_1) = Asinh\gamma z \tag{A.12}$$

and

$$E(\omega_2) = E_0(\omega_2)cosh\gamma z + Bsinh\gamma z \tag{A.13}$$

Solving the Equation gives B= 0, and

$$A = -i\sqrt{\frac{\omega_1 n_2}{\omega_2 n_1}} exp(i\phi(\omega_3)) E_0^*(\omega_2) \tag{A.14}$$

Thus, calculating the corresponding intensity gives,

$$I(\omega_1) = (\omega_1/\omega_1) I_0(\omega_2) sinh^2 \gamma z,$$

$$I(\omega_2) = I_0(\omega_2) cosh^2 \gamma z$$

This indicates that the waves of both frequencies builds up a gain. There is no violation of law of conservation of energy because the energy, in this case, is supplied by the pump wave which is not apparent due to the assumption $E(\omega_3) = constant$

The intensity ratio of the waves for high conversion is given by,

$$\frac{I(\omega_1)}{I(\omega_2)} = \frac{\omega_1}{\omega_2} \tag{A.15}$$

Now, considering a system without perfect phasematching and with losses occurring, and pumped constantly by a wave of frequency ω_3

$$\frac{\partial E(\omega_1)}{\partial x} + \alpha_1 E(\omega_1) = -i\kappa_1 E(\omega_3) E^*(\omega_2) exp(i\Delta k z) \tag{A.16}$$

$$\frac{\partial E(\omega_2)}{\partial x} + \alpha_1 E(\omega_2) = -i\kappa_2 E(\omega_3) E^*(\omega_1) exp(i\Delta k z) \tag{A.17}$$

This would give an exponential solution, and it can be written in the form

$$E(\omega_1) \sim E_0(\omega_1) exp(\gamma' z + i\Delta k z/2)$$

$$E(\omega_2) \sim E_0(\omega_2) exp(\gamma' z + i\Delta k z/2)$$

Substituting,

$$\left\{\gamma' + \alpha_1 + \frac{i\Delta k}{2}\right\} E_0(\omega_1) + \{i\kappa_1 E(\omega_3)\} E_0^*(\omega_2) = 0 \tag{A.18}$$

$$\left\{\gamma' + \alpha_1 + \frac{i\Delta k}{2}\right\} E_0(\omega_1) + \{i\kappa_1 E(\omega_3)\} E_0^*(\omega_2) = 0 \tag{A.19}$$

If written in determinant form, this gives

$$\gamma'^2 + \gamma'(\alpha_1 + \alpha_2) + \alpha_1\alpha_2 + (\Delta k/2)^2 + (\alpha_2 - \alpha_1) i\frac{\Delta k}{2} - \kappa_1\kappa_2 |E(\omega_3)|^2 = 0 \tag{A.20}$$

or ,

$$\gamma' = -\frac{\alpha_1 + \alpha_2}{2} \pm \left\{ \left[\frac{\alpha_1 + \alpha_2}{2} + \frac{i\Delta k}{2}\right]^2 + \kappa_1\kappa_2 |E(\omega_3)|^2 \right\}^{\frac{1}{2}} \tag{A.21}$$

For perfect phasematching and zero loss condition, $\alpha_1 = \alpha_2 = 0$ and $\Delta k = 0$, giving

$$\gamma'^2 = \kappa_1\kappa_2 |E(\omega_3)|^2 \tag{A.22}$$

Additionally, for $\alpha_1 = \alpha_2 = \alpha$,i.e. when there are equal losses,

$$\gamma' = -\alpha \pm \left\{\gamma^2 - (\Delta k/2)^2\right\}^{\frac{1}{2}} = -\alpha \pm g \tag{A.23}$$

where

$$g = \sqrt{\{\gamma^2 - (\Delta k/2)^2\}} \tag{A.24}$$

Thus, the solutions of partial differential equations A.16 and A.17 in an OPA are,

$$E(\omega_1, l) = exp(-\alpha l + i(\Delta k/2)l)\left\{E_0(\omega_1)cosh\, gl + Bsinh\, gl\right\} \tag{A.25}$$

$$E(\omega_2, l) = exp(-\alpha l + i(\Delta k/2)l)\left\{E_0(\omega_2)cosh\, gl + Dsinh\, gl\right\} \tag{A.26}$$

Substituting the solutions to the equation gives values of B and D as,

$$B = -i\frac{\Delta k}{2g}E_0(\omega_1) - i\frac{\kappa_1}{g}E(\omega_3)E_0^*(\omega_2) \tag{A.27}$$

$$D = -i\frac{\Delta k}{2g}E_0(\omega_2) - i\frac{\kappa_2}{g}E(\omega_3)E_0^*(\omega_1) \tag{A.28}$$

The solution for B and D are symmetric and represents the signal and idler waves.

Now, analysing a case where an OPA is seeded by ω_1 only and assuming $\omega_1 \neq \omega_2$, there is phase independent amplification of the seed wave. This is represented as,

$$\left|\frac{E(\omega_1, l)exp(\alpha l)}{E(\omega_1)}\right|^2 = \left\{cosh^2\, gl + (\Delta k/2g)^2 sinh^2\, gl\right\} = \frac{1}{g}\left\{\gamma^2 cosh^2\, gl - (\Delta k/2)^2\right\} \tag{A.29}$$

where the term $\left(\left|\frac{E(\omega_1,l)exp(\alpha l)}{E(\omega_1)}\right|^2 - 1\right)$ is defined as the parametric gain $G_1(l)$.Thus giving,

$$G_1(l) = (\gamma l)^2\frac{sinh^2\, gl}{(gl)^2} \tag{A.30}$$

For the condition of small signal gain, ($\gamma < \Delta k$), g becomes imaginary and sinh can be approximated as sin, so parametric gain becomes,

$$G_1(l) = (\gamma l)^2 \frac{sin^2\left\{\left[(\Delta k/2)^2 - \gamma^2\right]^{\frac{1}{2}} l\right\}}{l^2\left\{(\Delta k/2)^2 - \gamma^2\right\}} \tag{A.31}$$

When $\gamma \ll \Delta k/2$, this further simplifies to,

$$G_1(l) = (\gamma l)^2 \frac{sin^2(\Delta k l/2)}{(\Delta k l/2)^2} \tag{A.32}$$

For the condition of large gain, $\gamma \gg \Delta k/2$,

$$G_1(l) = (\gamma l)^2 \frac{sinh^2 gl}{(gl)^2} = \frac{1}{4} exp(2gl) \tag{A.33}$$

In an OPA, when the phase matching condition is achieved ($\Delta k = 0$),both the signal and idler builds up. This is given by,

$$E(\omega_1, l)exp(\alpha_1 l) = E_0(\omega_1)cosh\,\gamma l - i\frac{\kappa_1}{\gamma} E(\omega_3)E_0^*(\omega_2)sinh\,\gamma l \tag{A.34}$$

$$E(\omega_2, l)exp(\alpha_2 l) = E_0(\omega_2)cosh\,\gamma l - i\frac{\kappa_2}{\gamma} E(\omega_3)E_0^*(\omega_1)sinh\,\gamma l \tag{A.35}$$

Gain is allowed in one direction, while in the other direction the field is damped.The field damping is given by the relations

$$E'(\omega_1, l) = E_0(\omega_1)exp(-\alpha_1 l)$$

$$E'(\omega_2, l) = E_0(\omega_2)exp(-\alpha_2 l)$$

Now if this system is placed in a resonator cavity, the feedback helps the field to amplify and the set-up starts operating as an oscillator with the threshold condition

$$E'(\omega_1) = E(\omega_1)$$

$$E'(\omega_2) = E(\omega_2)$$

i.e., the gain compensates the losses in the cavity or $(\exp(-2\alpha l) = 1 - 2\alpha l)$, then from equation A.34 and A.35

$$\frac{E(\omega_1)}{1-2\alpha_1 l} = E_0(\omega_1) cosh\,\gamma l - i\frac{\kappa_1}{\gamma} E(\omega_3) E_0^*(\omega_2) sinh\,\gamma l$$

$$\frac{E_0^*(\omega_1)}{1-2\alpha_2 l} = E_0^*(\omega_2) cosh\,\gamma l + i\frac{\kappa_2}{\gamma} E^*(\omega_3) E_0(\omega_1) sinh\,\gamma l$$

for a non-zero solution of these equations, m the determinant of the coefficient matrix needs to be 0. So,

$$\left[cosh\,\gamma l - \frac{1}{1-2\alpha_1 l}\right]\left[cosh\,\gamma l - \frac{1}{1-2\alpha_2 l}\right] = \frac{\kappa 1 \kappa 2}{\gamma^2}\left|E(\omega_3)\right| sinh^2\,\gamma l = sinh^2\,\gamma l \tag{A.36}$$

rewriting this,

$$(1 - cosh\,\gamma l)\left(\frac{1}{1-2\alpha_1 l} + \frac{1}{1-2\alpha_1 l}\right) + \left(\frac{1}{1-2\alpha_1 l}\right)\left(\frac{1}{1-2\alpha_2 l}\right) = 0 \tag{A.37}$$

$$cosh\,\gamma l = 1 + \frac{2\alpha_1 \alpha_2 l^2}{1 - \alpha_1 l - \alpha_2 l} \tag{A.38}$$

for$(\alpha_1 \approx \alpha_1 \approx \alpha)$ and small losses / gain $(\alpha l, \gamma l \ll 1)$,

Taking series expansion of cosh γl , the condition for OPO simplifies as $(\gamma l)^2 \approx 4\alpha l$

Appendix Two

MATLAB code to predict signal and idler wavelengths

MATLAB code to predict signal and idler wavelengths for a range of temperatures and fixed grating period value

```
clc; close;clear;

grating_period = 28.5; %  in um
lambda_pump = 1.064; %  in um
temperature = 100:200; %  in degree Centigrade
wvl = 1:0.0001:2 * lambda_pump;
qpm_err = zeros(1, length(wvl));

for i =1:length(wvl)
    qpm_err(i) = phase_match_error(wvl(i), temperature(1), grating_period, lambda_pump);
end

wvl_ne = 1:0.001:20;
ne = zeros(1, length(wvl_ne));
```

```
for i=1:length(wvl_ne)
    ne(i) = calculate_RI_PPLN(wvl_ne(i), temperature(1));

end

signal_wvl = zeros(1, length(temperature));
err = zeros(1, length(temperature));
options = optimset('Display', 'off', 'TolFun',1e-11, 'TolX',1e-11);

for i = 1:length(temperature)
    fun = @(wvl)phase_match_error(wvl, temperature(i), grating_period, lambda_pump);

    disp('Wavelength, Temp, Lambda_pump');% added later to check
    [ temperature(i),  lambda_pump]

    disp('Displaying QPM error zero range')
    [fun(1.2),fun(2*lambda_pump)]% added later to check
    % defines the zero range for QPM Error

    if fun(1.2)*fun(2 * lambda_pump) >= 0
        signal_wvl(i) = NaN;
        err = NaN;
        continue;
    end
    [sol, fval] = fzero(fun, [1.2, 2 * lambda_pump]);
    signal_wvl(i) = sol;
    err(i) = fval;
```

```
    disp('Displaying sol , fval')
    [sol, fval]
end

idler_wvl = 1 ./ (1 / lambda_pump - 1 ./ signal_wvl);

spect_title = num2str(grating_period);

%% print graphs

figure(1)
clf
plot(wvl, qpm_err)
xlabel('Wavelength (um)')
ylabel('QPM error')
grid on
QPMEFileName = sprintf('QPM_Error_GP_%s_um',spect_title);
title(QPMEFileName,'Interpreter','none');

figure(2)
clf
plot(temperature, signal_wvl, 'b')
hold on
plot(temperature, idler_wvl, 'r')
xlabel('Temperature')
ylabel('Wavelength (um)')
grid on
WvlFileName = sprintf('Signel_idler_GP_%s_um',spect_title);
```

```
title(WvlFileName,'Interpreter','none');


figure(3)
clf
plot(wvl_ne, ne)
xlabel('Wavelength (um)')
ylabel('Refractive index')
RIFileName = sprintf('RI_GP_%s_um',spect_title);
grid on
title(RIFileName,'Interpreter','none');


%% define functions


function QPM_error_fn = phase_match_error(lambda_signal,Temp,grating_period,lambda_pump)


    k_pump = 1/lambda_pump;
    k_signal =1/lambda_signal;
    k_idler = k_pump-k_signal;
    lambda_idler = 1/k_idler;


    ne_pump = calculate_RI_PPLN(lambda_pump,Temp);
    ne_signal = calculate_RI_PPLN(lambda_signal,Temp);
    ne_idler = calculate_RI_PPLN(lambda_idler,Temp);


    %Calculate phase mismatch, since grating period is defined
    pump = ne_pump .* k_pump;
    signal = ne_signal.*k_signal;
    idler = ne_idler .* k_idler;
```

```
    QPM_error_fn = pump - signal - idler - (1 / grating_period);

end


function  ne_PPLN = calculate_RI_PPLN(lambda,Temp)

Temp_fact_f = (Temp-24.5).*(Temp+570.82);

lambda_sqr = lambda.*lambda;

%Constants for PPLN
a1 =5.756;a2=0.0983;a3=.2020;a4=189.32;a5=12.52;a6=1.32*(10^(-2));
b1=2.860*(10^(-6));b2=4.7*(10^(-8));b3=6.113*(10^(-8));b4=1.516*(10^(-4));

Term_1 = a1;

Term_2 = b1.*Temp_fact_f;

A= a2+(b2.*Temp_fact_f);
B= lambda_sqr -((a3+(b3.*Temp_fact_f)).^2);
Term_3 =A./B ;

C= a4+(b4.*Temp_fact_f);
D= lambda_sqr-(a5.^2);
Term_4 = C./ D;
```

```
Term_5 = -1*( a6*lambda_sqr);


ne_PPLN = abs( (Term_1 + Term_2 + Term_3 + Term_4 + Term_5).^(0.5));
end


function  ne_GaAs = calculate_RI_GaAs(wvl,Temp)
    ref_temp = 22;  % in Celcius
    del_T = Temp - (ref_temp + 273); % converted to Kelvin
    lambda_1 = 0.443130710 + 0.000050564.*del_T;
    lambda_2 = 0.8746453 + 0.0001913.*del_T - 4.882*(10^-7).*(del_T.^2);
    lambda_3 = 36.9166 - 0.011622.*del_T;
    g0 = 5.372514;
    g1= 27.83972;
    g2 = 0.031764 + 4.350*(10^-5).*del_T + 4.4464*(10^-7).*(del_T.^2);
    g3 = 0.00143636;
    term_1 = g0;
    term_2 = g1./(1./(lambda_1.^2) - 1./(wvl.^2));
    term_3 = g2./(1./(lambda_2.^2) - 1./(wvl.^2));
    term_4 = g3./(1./(lambda_3.^2) - 1./(wvl.^2));
    ne_GaAs =abs(  0.5 .^ (term_1 + term_2 + term_3 + term_4 ));


end
```

Appendix Three

MATLAB code to calculate initial resonator parameters

```
clear; clc; close;
% constants
% Nd YAG Pump wavelength 1064nm
lambda_pump = 0.001800;
% Signal wavelength in the resonator expected arouund 1500nm
lambda_signal = 0.0015;

% Rad of Curv of mirrors are 75mm each
RoC1 = 75; RoC2 = 75;

% Crystal dimensions
 Crystal_length = 25;
  Half_crystal_length = Crystal_length/2;

%Output beam diameter from  Nd YAG laser is 1.5mm , pump beam waist rad = .75mm
Pump_beam_waist_w01 = 0.75;
```

```
% variables
% Cavity length limited by oven length +/- 2mm i.e 55mm
% Max Cavity length defined by stability criteria 0<g1g2<1
Cavity_length = 25:150;

% calculating g parameters
g1=1-(Cavity_length/RoC1);
g2=1-(Cavity_length/RoC2);
G=g1.*g2;

GParameters = [Cavity_length;g1;g2;G]



% Plotting g parameters
 figure(1);
  clf;
  plot(g1,G,'y-');
  plot(g2,G,'b-');
  title ('g1 vs g2');
  hold on;
  grid on;

% Calculating relative mirror positions z1 and z2 from signal beam waist
     z1 =  (Cavity_length)*(g2.*(1-g1)/(g1+g2-2*G));
     z2 =  (Cavity_length)*(g1.*(1-g2)/(g1+g2-2*G));
```

```
% Calculating beam_waist of signal wavelength
 Signal_beam_waist_w0=
 sqrt((lambda_signal*Cavity_length/pi)*sqrt(G.*(1-G)/ (g1+g2-2*G).^2));



 % Calculating focal_length of lens (mm) required to focus pump beam to
 % a spot size comparable to expected spot size of signal
 Focal_length = pi* (Pump_beam_waist_w01 .* Signal_beam_waist_w0) / lambda_pump;




 % Calculating Rayleigh_radius and Confocal Parameter b;
 Rayleigh_range_zR = (Cavity_length)*sqrt(G.*(1-G)/ (g1+g2-2*G).^2);

 Confocal_parameter_b  =
 2*pi*(Signal_beam_waist_w0.^2)/lambda_signal;
 SHG_Efficiency_check =Crystal_length./ Confocal_parameter_b;




  % Calculating beam_waist at ends of the crystals

  Beam_waist_crystal_edge_wR=
  Signal_beam_waist_w0.* sqrt(1+ ((Half_crystal_length./Rayleigh_range_zR).^2));

  % PRINTING VALUES
```

```
%Signal beam waist size and Focal length to focus pump wavelength
Set_up_parameters = [Cavity_length;Signal_beam_waist_w0;Focal_length]

% Gaussian Beam parameters, verify b=2zR
Gaussian_Beam_Parameters = [Cavity_length;Rayleigh_range_zR;Confocal_parameter_b;
SHG_Efficiency_check]
Beam_waist_at_crystal_edge = [Cavity_length;Beam_waist_crystal_edge_wR]



% PLOTTING VALUES FOR BEAM WAIST, FOCAL LENGTH< RAYLEIGH LENGTH
%Plots
  figure(2);
  clf;
  yyaxis left
  plot(Cavity_length,Signal_beam_waist_w0,'b-');
  xlabel('Cavity Length (mm)');
  ylabel('Beam Waist (mm)');



  yyaxis right
  plot(Cavity_length,Focal_length,'r-');
  ylabel('Focal Length  (mm)');
  title ('Beam Waist,Focal length vs Cavity Length');
  xticks(0:10:150);
  grid on;
  hold on;
```

```
figure(3);
clf;
plot( Cavity_length, Rayleigh_range_zR,'b-');
xlabel('Cavity Length (mm)');
ylabel('Rayleigh Range (mm)');
xticks(0:10:150);
title ('Rayleigh Range vs Cavity Length ');
grid on;
hold on;



figure(4);
clf;
plot(Cavity_length,Beam_waist_crystal_edge_wR,'g-');
xlabel('Cavity Length (mm)');
ylabel('Beam Waist (mm)');
xticks(0:10:150);
title ('Beam Waist at Crystal edge vs Cavity Length ');
grid on;
hold on;
```

Bibliography

[1] Z. Du, S. Zhang, J. Li, N. Gao, and K. Tong, "Mid-infrared tunable laser-based broadband fingerprint absorption spectroscopy for trace gas sensing: A review," *Applied Sciences*, vol. 9, no. 2, p. 338, Jan. 2019. [Online]. Available: https://doi.org/10.3390/app9020338

[2] Z. Zhao, B. Wu, X. Wang, Z. Pan, Z. Liu, P. Zhang, X. Shen, Q. Nie, S. Dai, and R. Wang, "Mid-infrared supercontinuum covering 2.0-16 m in a low-loss telluride single-mode fiber," *Laser &amp Photonics Reviews*, vol. 11, no. 2, p. 1700005, Mar. 2017. [Online]. Available: https://doi.org/10.1002/lpor.201700005

[3] B. M. Walsh, H. R. Lee, and N. P. Barnes, "Mid infrared lasers for remote sensing applications," *Journal of Luminescence*, vol. 169, pp. 400–405, Jan. 2016. [Online]. Available: https://doi.org/10.1016/j.jlumin.2015.03.004

[4] Y. Gong, L. Bu, B. Yang, and F. Mustafa, "High repetition rate mid-infrared differential absorption lidar for atmospheric pollution detection," *Sensors*, vol. 20, no. 8, p. 2211, Apr. 2020. [Online]. Available: https://doi.org/10.3390/s20082211

[5] Q. Hao, G. Zhu, S. Yang, K. Yang, T. Duan, X. Xie, K. Huang, and H. Zeng, "Mid-infrared transmitter and receiver modules for free-space optical communication," *Applied optics*, vol. 56, no. 8, pp. 2260–2264, 2017.

[6] O. Spitz, A. Herdt, P. Didier, W. Elsäßer, and F. Grillot, "Mid-infrared free-space cryptosystem," *Nonlinear Theory and Its Applications, IEICE*, vol. 13, no. 1, pp. 44–52, 2022.

[7] I. Ilev, "A simple confocal fibre-optic laser method for intraocular lens power measurement," *Eye*, vol. 21, no. 6, pp. 819–823, 2007.

[8] R. Anty, M. Morvan, M. L. Corvec, C. M. Canivet, S. Patouraux, J. Gugenheim, S. Bonnafous, B. Bailly-Maitre, O. Sire, H. Tariel, J. Bernard, T. Piche, O. Loréal, J. Aron-Wisnewsky, K. Clément, A. Tran, A. Iannelli, and P. Gual, "The mid-infrared spectroscopy: A novel non-invasive diagnostic tool for NASH diagnosis in severe obesity," *JHEP Reports*, vol. 1, no. 5, pp. 361–368, Nov. 2019. [Online]. Available: https://doi.org/10.1016/j.jhepr.2019.09.005

[9] A. Schliesser, N. Picqué, and T. W. Hänsch, "Mid-infrared frequency combs," *Nature Photonics*, vol. 6, no. 7, pp. 440–449, Jun. 2012. [Online]. Available: https://doi.org/10.1038/nphoton.2012.142

[10] A. Hoffman and C. Gmachl, "Extending opportunities," *Nat. Photonics*, vol. 6, p. 407, 2012.

[11] Y. Tokizane, H. Ejiri, T. Minamikawa, S. Suzuki, M. Asada, and T. Yasui, "Hybrid optical imaging with near-infrared, mid-infrared, and terahertz wavelengths for nondestructive inspection [invited]," *Applied Optics*, vol. 60, p. B100, 2021.

[12] "Mid-infrared lasers market forecasts to 2028 - global analysis by wavelength type (tunable, fixed), type (gas laser, co2 laser), end user (chemicals, military, aerospace amp; defense) and by geography," Dec 2021. [Online]. Available: https://www.giiresearch.com/report/smrc1040772-mid-infrared-lasers-market-forecasts-global.html

[13] Y. A. Bakhirkin, A. A. Kosterev, C. Roller, R. F. Curl, and F. K. Tittel, "Mid-infrared quantum cascade laser based off-axis integrated cavity output spectroscopy for biogenic nitric oxide detection," *Applied optics*, vol. 43, no. 11, pp. 2257–2266, 2004. [Online]. Available: https://doi.org/10.1364/OPTICA.426199

[14] V. Serebryakov, E. Boĭko, N. Petrishchev, and A. Yan, "Medical applications of mid-ir lasers. problems and prospects," *J. Opt. Technol.*, vol. 77, no. 1, pp. 6–17, Jan 2010. [Online]. Available: http://opg.optica.org/jot/abstract.cfm?URI=jot-77-1-6

[15] N. M. Fried, "Recent advances in infrared laser lithotripsy[invited]," *Biomed. Opt. Express*, vol. 9, no. 9, pp. 4552–4568, Sep 2018. [Online]. Available: http://opg.optica.org/boe/abstract.cfm?URI=boe-9-9-4552

[16] W. A. Fried, K. H. Chan, C. L. Darling, and D. Fried, "Use of a DPSS er:YAG laser for the selective removal of composite from tooth surfaces," *Biomedical Optics Express*, vol. 9, no. 10, p. 5026, Sep. 2018. [Online]. Available: https://doi.org/10.1364/boe.9.005026

[17] B. Henderson, A. Khodabakhsh, M. Metsälä, I. Ventrillard, F. M. Schmidt, D. Romanini, G. A. D. Ritchie, S. te Lintel Hekkert, R. Briot, T. Risby, N. Marczin, F. J. M. Harren, and S. M. Cristescu, "Laser spectroscopy for breath analysis: towards clinical implementation," *Applied Physics B*, vol. 124, no. 8, Jul. 2018. [Online]. Available: https://doi.org/10.1007/s00340-018-7030-x

[18] A. B. Seddon, "Mid-infrared (IR) - a hot topic: The potential for using mid-IR light for non-invasive early detection of skin cancerin vivo/i," *physica status solidi (b)*, vol. 250, no. 5, pp. 1020–1027, Feb. 2013. [Online]. Available: https://doi.org/10.1002/pssb.201248524

[19] A. B. Seddon, B. Napier, I. Lindsay, S. Lamrini, P. M. Moselund, N. Stone, O. Bang, and M. Farries, "Prospective on using fibre mid-infrared supercontinuum laser sources for iin vivo/i spectral discrimination of disease," *The Analyst*, vol. 143, no. 24, pp. 5874–5887, 2018. [Online]. Available: https://doi.org/10.1039/c8an01396a

[20] Y. Bai, J. Yin, and J.-X. Cheng, "Bond-selective imaging by optically sensing the mid-infrared photothermal effect," *Science Advances*, vol. 7, no. 20, p. eabg1559, 2021. [Online]. Available: https://www.science.org/doi/abs/10.1126/sciadv.abg1559

[21] M. A. Pleitez, A. A. Khan, A. Soldà, A. Chmyrov, J. Reber, F. Gasparin, M. R. Seeger, B. Schätz, S. Herzig, M. Scheideler, and V. Ntziachristos, "Label-free metabolic imaging by mid-infrared optoacoustic microscopy in living cells," *Nature Biotechnology*, vol. 38, no. 3, pp. 293–296, Dec. 2019. [Online]. Available: https://doi.org/10.1038/s41587-019-0359-9

[22] A. M. Hanninen, R. C. Prince, R. Ramos, M. V. Plikus, and E. O. Potma, "High-resolution infrared imaging of biological samples with third-order sum-frequency generation microscopy," *Biomed. Opt. Express*, vol. 9, no. 10, pp. 4807–4817, Oct 2018. [Online]. Available: http://opg.optica.org/boe/abstract.cfm?URI=boe-9-10-4807

[23] C. S. Colley, J. C. Hebden, D. T. Delpy, A. D. Cambrey, R. A. Brown, E. A. Zibik, W. H. Ng, L. R. Wilson, and J. W. Cockburn, "Mid-infrared optical coherence tomography," *Review of Scientific Instruments*, vol. 78, no. 12, p. 123108, Dec. 2007. [Online]. Available: https://doi.org/10.1063/1.2821609

[24] A. Labruyère, A. Tonello, V. Couderc, G. Huss, and P. Leproux, "Compact supercontinuum sources and their biomedical applications," *Optical Fiber Technology*, vol. 18, no. 5, pp. 375–378, Sep. 2012. [Online]. Available: https://doi.org/10.1016/j.yofte.2012.08.003

[25] I. Zorin, R. Su, A. Prylepa, J. Kilgus, M. Brandstetter, and B. Heise, "Mid-infrared fourier-domain optical coherence tomography with a pyroelectric linear array," *Optics Express*, vol. 26, no. 25, p. 33428, Dec. 2018. [Online]. Available: https://doi.org/10.1364/oe.26.033428

[26] E. O. Potma, D. Knez, Y. Chen, Y. Davydova, A. Durkin, A. Fast, M. Balu, B. Norton-Baker, R. W. Martin, T. Baldacchini, and D. A. Fishman, "Rapid chemically selective 3d imaging in the mid-infrared," *Optica*, vol. 8, no. 7, pp. 995–1002, Jul 2021. [Online]. Available: https://opg.optica.org/optica/abstract.cfm?URI=optica-8-7-995

[27] A. Mukherjee, S. V. der Porten, and C. K. N. Patel, "Standoff detection of explosive substances at distances of up to 150 m," *Appl. Opt.*, vol. 49, no. 11, pp. 2072–2078, Apr 2010. [Online]. Available: https://opg.optica.org/ao/abstract.cfm?URI=ao-49-11-2072

[28] A.-L. Sahlberg, D. Hot, R. L. Pedersen, and Z. Li, "Non-linear mid-infrared laser techniques for combustion diagnostics," in *Imaging and Applied Optics 2018 (3D, AO, AIO, COSI, DH, IS, LACSEA, LS&C, MATH, pcAOP)*. Optica Publishing Group, 2018, p. LTu2C.5. [Online]. Available: http://opg.optica.org/abstract.cfm?URI=LACSEA-2018-LTu2C.5

[29] R. M. Schwartz, D. Woodbury, J. Isaacs, P. Sprangle, and H. M. Milchberg, "Remote detection

of radioactive material using mid-IR laser–driven electron avalanche," *Science Advances*, vol. 5, no. 3, Mar. 2019. [Online]. Available: https://doi.org/10.1126/sciadv.aav6804

[30] C. Guo, J. Lin, Z. Tang, K. Li, L. Tu, J. Wang, X. Liu, and S. Ruan, "Theoretical Analysis of ESA-Enhanced 2.8 m Lasing in Er-Doped ZBLAN Fiber Lasers," *Journal of Lightwave Technology*, vol. 8724, no. c, pp. 1–18, 2022.

[31] M. Amati, A. Gianoncelli, E. Karantzoulis, B. Rossi, L. Vaccari, and F. Zanini, "Looking at ancient objects under a different light: cultural heritage science at elettra," *Radiation Effects and Defects in Solids*, pp. 1–17, 2022.

[32] M. Yumoto, N. Saito, T. Lin, R. Kawamura, A. Aoki, Y. Izumi, and S. Wada, "High-energy, nanosecond pulsed cr:CdSe laser with a 225–308 m tuning range for laser biomaterial processing," *Biomedical Optics Express*, vol. 9, no. 11, p. 5645, Oct. 2018. [Online]. Available: https://doi.org/10.1364/boe.9.005645

[33] A. Pushkin, A. Bychkov, A. Karabutov, and F. Potemkin, "Cavitation and shock waves emission on the rigid boundary of water under mid-ir nanosecond laser pulse excitation," *Laser Physics Letters*, vol. 15, no. 6, p. 065401, 2018.

[34] J. Bonse, J. Krüger, S. Höhm, and A. Rosenfeld, "Femtosecond laser-induced periodic surface structures," *Journal of Laser Applications*, vol. 24, no. 4, p. 042006, Sep. 2012. [Online]. Available: https://doi.org/10.2351/1.4712658

[35] K. Werner and E. Chowdhury, "Extreme sub-wavelength structure formation from mid-IR femtosecond laser interaction with silicon," *Nanomaterials*, vol. 11, no. 5, p. 1192, Apr. 2021. [Online]. Available: https://doi.org/10.3390/nano11051192

[36] F. Müller, C. Kunz, and S. Gräf, "Bio-inspired functional surfaces based on laser-induced periodic surface structures," *Materials*, vol. 9, no. 6, p. 476, Jun. 2016. [Online]. Available: https://doi.org/10.3390/ma9060476

[37] T. Knuettel, S. Bergfeld, and S. Haas, "Laser texturing of surfaces in thin-film silicon

photovoltaics-a comparison of potential processes," *Journal of Laser Micro Nanoengineering*, vol. 8, no. 3, p. 222, 2013.

[38] A. Y. Vorobyev and C. Guo, "Colorizing metals with femtosecond laser pulses," *Applied Physics Letters*, vol. 92, no. 4, p. 041914, Jan. 2008. [Online]. Available: https://doi.org/10.1063/1.2834902

[39] Q. Wang, A. Samanta, F. Toor, S. Shaw, and H. Ding, "Colorizing ti-6al-4v surface via high-throughput laser surface nanostructuring," *Journal of Manufacturing Processes*, vol. 43, pp. 70–75, Jul. 2019. [Online]. Available: https://doi.org/10.1016/j.jmapro.2019.03.050

[40] A. Sijan, "Development of military lasers for optical countermeasures in the mid-IR," in *Technologies for Optical Countermeasures VI*, D. H. Titterton and M. A. Richardson, Eds. SPIE, Sep. 2009. [Online]. Available: https://doi.org/10.1117/12.835439

[41] H. T. Bekman, J. Van Den Heuvel, F. Van Putten, and R. Schleijpen, "Development of a mid-infrared laser for study of infrared countermeasures techniques," in *Technologies for optical countermeasures*, vol. 5615. SPIE, 2004, pp. 27–38.

[42] A. Vizbaras, E. Dvinelis, A. Trinkunas, I. Šimonyte, M. Greibus, M. Kaušylas, T. Žukauskas, R. Songaila, and K. Vizbaras, "High-performance mid-infrared GaSb laser diodes for defence and sensing applications," in *Laser Technology for Defense and Security X*, M. Dubinskii and S. G. Post, Eds. SPIE, Jun. 2014. [Online]. Available: https://doi.org/10.1117/12.2054493

[43] M. E. Reilly, B. K. Flemming, and M. J. D. Esser, "High brightness 2.1 μm Direct-Diode laser module," in *2019 Conference on Lasers and Electro-Optics Europe & European Quantum Electronics Conference (CLEO/Europe-EQEC)*. IEEE, Jun. 2019.

[44] E. O'Driscoll, T. Delmonte, M. Watson, M. Petrovich, R. Amezcua-Correa, F. Poletti, and D. Richardson, "Applications of microstructured fibre technology in aerospace and defence," 2006.

[45] A. Godard, "Infrared (2–12 μm) solid-state laser sources: a review," *Comptes Rendus Physique*, vol. 8, no. 10, pp. 1100–1128, 2007.

[46] Y. Yao, A. J. Hoffman, and C. F. Gmachl, "Mid-infrared quantum cascade lasers," *Nature Photonics*, vol. 6, no. 7, pp. 432–439, jun 2012. [Online]. Available: https://doi.org/10.1038%2Fnphoton.2012.143

[47] S. C. Kumar, "High-power, high-energy optical parametric sources for the mid-infrared," in *Advanced Solid-State Lasers Congress*. OSA, 2013. [Online]. Available: https://doi.org/10.1364%2Fmics.2013.mw2c.3

[48] D. Jung, S. Bank, M. L. Lee, and D. Wasserman, "Next-generation mid-infrared sources," *Journal of Optics*, vol. 19, no. 12, p. 123001, nov 2017. [Online]. Available: https://doi.org/10.1088%2F2040-8986%2Faa939b

[49] T. Inoue, M. D. Zoysa, T. Asano, and S. Noda, "High-q mid-infrared thermal emitters operating with high power-utilization efficiency," *Optics Express*, vol. 24, no. 13, p. 15101, Jun. 2016. [Online]. Available: https://doi.org/10.1364/oe.24.015101

[50] T. Cao, M. Lian, K. Liu, X. Lou, Y. Guo, and D. Guo, "Wideband mid-infrared thermal emitter based on stacked nanocavity metasurfaces," *International Journal of Extreme Manufacturing*, vol. 4, no. 1, p. 015402, Dec. 2021. [Online]. Available: https://doi.org/10.1088/2631-7990/ac3bb1

[51] P. Gowda, D. A. Patient, S. A. R. Horsley, and G. R. Nash, "Toward efficient and tailorable mid-infrared emitters utilizing multilayer graphene," *Applied Physics Letters*, vol. 120, no. 5, p. 051105, Jan. 2022. [Online]. Available: https://doi.org/10.1063/5.0079777

[52] A. Lochbaum, Y. Fedoryshyn, A. Dorodnyy, U. Koch, C. Hafner, and J. Leuthold, "On-chip narrowband thermal emitter for mid-IR optical gas sensing," *ACS Photonics*, vol. 4, no. 6, pp. 1371–1380, Apr. 2017. [Online]. Available: https://doi.org/10.1021/acsphotonics.6b01025

[53] H.-H. Hsiao, C.-H. Huang, B.-T. Xu, G.-T. Chen, and P.-W. Ho, "Triple narrowband mid-infrared thermal emitter based on a au grating-assisted nanoscale germanium/titanium dioxide distributed bragg reflector: Implications for molecular sensing," *ACS Applied*

Nano Materials, vol. 4, no. 9, pp. 9344–9352, Aug. 2021. [Online]. Available: https://doi.org/10.1021/acsanm.1c01818

[54] D. Popa, R. Hopper, S. Z. Ali, M. T. Cole, Y. Fan, V.-P. Veigang-Radulescu, R. Chikkaraddy, J. Nallala, Y. Xing, J. Alexander-Webber, S. Hofmann, A. D. Luca, J. W. Gardner, and F. Udrea, "A highly stable, nanotube-enhanced, CMOS-MEMS thermal emitter for mid-IR gas sensing," *Scientific Reports*, vol. 11, no. 1, Nov. 2021. [Online]. Available: https://doi.org/10.1038/s41598-021-02121-5

[55] S. Tay, A. Kropachev, I. E. Araci, T. Skotheim, R. A. Norwood, and N. Peyghambarian, "Plasmonic thermal ir emitters based on nanoamorphous carbon," *Applied physics letters*, vol. 94, no. 7, p. 071113, 2009.

[56] R. Stanley, "Plasmonics in the mid-infrared," *Nature Photonics*, vol. 6, no. 7, pp. 409–411, 2012.

[57] A. Kazemi Moridani, R. Zando, W. Xie, I. Howell, J. J. Watkins, and J.-H. Lee, "Plasmonic thermal emitters for dynamically tunable infrared radiation," *Advanced Optical Materials*, vol. 5, no. 10, p. 1600993, 2017.

[58] T. Inoue, M. De Zoysa, T. Asano, and S. Noda, "Wavelength-switchable mid-infrared narrow-band thermal emitters based on quantum wells and photonic crystals," *IEICE Transactions on Electronics*, vol. 101, no. 7, pp. 545–552, 2018.

[59] O. Graydon, "Photonic crystal thermal emitters," *Nature Photonics*, vol. 10, no. 4, pp. 209–209, Mar. 2016. [Online]. Available: https://doi.org/10.1038/nphoton.2016.55

[60] I. S. Moskalev, V. V. Fedorov, and S. B. Mirov, "Highly-efficient, widely-tunable, mid-IR Cr:ZnS and Cr:ZnSe CW lasers pumped by 1685 nm InP laser diode," in *Lasers, Sources and Related Photonic Devices*. Washington, D.C.: OSA, 2010.

[61] V. O. Smolski, S. Vasilyev, P. G. Schunemann, S. B. Mirov, and K. L. Vodopyanov, "Cr:ZnS laser-pumped subharmonic GaAs optical parametric oscillator with the spectrum

spanning 36–56 m," *Optics Letters*, vol. 40, no. 12, p. 2906, Jun. 2015. [Online]. Available: https://doi.org/10.1364/ol.40.002906

[62] B. Bendow, H. G. Lipson, and S. P. Yukon, "Multiphonon absorption in highly transparent semiconducting crystals," *Phys. Rev. B*, vol. 16, pp. 2684–2693, Sep 1977. [Online]. Available: https://link.aps.org/doi/10.1103/PhysRevB.16.2684

[63] A. Joullié, P. Christol, A. N. Baranov, and A. Vicet, "Mid-infrared 2—5 m heterojunction laser diodes," in *Topics in Applied Physics*. Springer Berlin Heidelberg, pp. 1–61. [Online]. Available: https://doi.org/10.1007/3-540-36491-9_1

[64] S. J. Sweeney, T. D. Eales, and I. P. Marko, "The physics of mid-infrared semiconductor materials and heterostructures," in *Mid-infrared Optoelectronics*. Elsevier, 2020, pp. 3–56.

[65] G. Belenky, L. Shterengas, M. Kisin, and T. Hosoda, "Gallium antimonide (GaSb)-based type-i quantum well diode lasers: recent development and prospects," in *Semiconductor Lasers*. Elsevier, 2013, pp. 441–486. [Online]. Available: https://doi.org/10.1533/9780857096401.3.441

[66] R. F. Kazarinov and R. A. Suris, "Possibility of the amplification of electromagnetic waves in a semiconductor with a superlattice," *Soviet Physics—Semiconductors*, vol. 5, no. 4, p. 707, 1971.

[67] J. Faist, F. Capasso, D. L. Sivco, C. Sirtori, A. L. Hutchinson, and A. Y. Cho, "Quantum cascade laser," *Science*, vol. 264, no. 5158, pp. 553–556, Apr. 1994. [Online]. Available: https://doi.org/10.1126/science.264.5158.553

[68] W. Zhou, N. Bandyopadhyay, D. Wu, R. McClintock, and M. Razeghi, "Monolithically, widely tunable quantum cascade lasers based on a heterogeneous active region design," *Scientific Reports*, vol. 6, pp. 1–7, 2016.

[69] R. Q. Yang, "Infrared laser based on intersubband transitions in quantum wells," *Superlattices and Microstructures*, vol. 17, no. 1, pp. 77–83, Jan. 1995. [Online]. Available: https://doi.org/10.1006/spmi.1995.1017

[70] P. Heu, C. Deutsch, V. Jayaraman, S. Segal, K. Lascola, C. Burgner, F. Towner, A. Cazabat, G. Cole, and D. Follman, "Room-temperature continuous-wave mid-infrared VCSEL operating at 3.35um," in *Vertical-Cavity Surface-Emitting Lasers XXII*, K. D. Choquette and C. Lei, Eds. SPIE, Feb. 2018. [Online]. Available: https://doi.org/10.1117/12.2287913

[71] J. Koeth, R. Weih, M. O. Fischer, M. Kamp, S. Höfling, J. Scheuermann, and A. Schade, "Mid infrared DFB interband cascade lasers," in *Infrared Remote Sensing and Instrumentation XXV*, M. Strojnik and M. S. Kirk, Eds. SPIE, Aug. 2017. [Online]. Available: https://doi.org/10.1117/12.2277698

[72] F. Kapsalidis, M. Shahmohammadi, M. J. Süess, J. M. Wolf, E. Gini, M. Beck, M. Hundt, B. Tuzson, L. Emmenegger, and J. Faist, "Dual-wavelength DFB quantum cascade lasers: sources for multi-species trace gas spectroscopy," *Applied Physics B*, vol. 124, no. 6, May 2018. [Online]. Available: https://doi.org/10.1007/s00340-018-6973-2

[73] L. Shterengas, G. Kipshidze, T. Hosoda, R. Liang, T. Feng, M. Wang, A. Stein, and G. Belenky, "Cascade pumping of 1.9–3.3 μm type-i quantum well gasb-based diode lasers," *IEEE Journal of Selected Topics in Quantum Electronics*, vol. 23, no. 6, pp. 1–8, 2017.

[74] N. B. Chichkov, A. Yadav, E. Zherebtsov, M. Wang, G. Kipshidze, G. Belenky, L. Shterengas, and E. U. Rafailov, "Wavelength-tunable, GaSb-based, cascaded type-i quantum-well laser emitting over a range of 300 nm," *IEEE Photonics Technology Letters*, vol. 30, no. 22, pp. 1941–1943, Nov. 2018. [Online]. Available: https://doi.org/10.1109/lpt.2018.2873049

[75] V. Petrov, "Parametric down-conversion devices: The coverage of the mid-infrared spectral range by solid-state laser sources," *Optical Materials*, vol. 34, no. 3, pp. 536–554, Jan. 2012. [Online]. Available: https://doi.org/10.1016/j.optmat.2011.03.042

[76] C. Fabre, P. F. Cohadon, and C. Schwob, "CW optical parametric oscillators: single mode operation and frequency tuning properties," *Quantum and Semiclassical Optics: Journal of the European Optical Society Part B*, vol. 9, no. 2, pp. 165–172, Apr. 1997. [Online]. Available: https://doi.org/10.1088/1355-5111/9/2/005

[77] K. Vodopyanov, *Pulsed Mid-IR Optical Parametric Oscillators*. Berlin, Heidelberg: Springer Berlin Heidelberg, 2003, pp. 144–183. [Online]. Available: https://doi.org/10.1007/3-540-36491-9_4

[78] W. Chen, J. Cousin, E. Poullet, J. Burie, D. Boucher, X. Gao, M. W. Sigrist, and F. K. Tittel, "Continuous-wave mid-infrared laser sources based on difference frequency generation," *Comptes Rendus Physique*, vol. 8, no. 10, pp. 1129–1150, 2007.

[79] E. Lippert, "Progress with OPO-based systems for mid-IR generation," in *SPIE Proceedings*, D. H. Titterton and M. A. Richardson, Eds. SPIE, Oct. 2011. [Online]. Available: https://doi.org/10.1117/12.903735

[80] P. S. Maji and P. R. Chaudhuri, "Tunable parametric amplifier for mid-IR application based on highly nonlinear chalcogenide material," *Journal of Applied Physics*, vol. 117, no. 24, p. 243103, Jun. 2015. [Online]. Available: https://doi.org/10.1063/1.4923046

[81] J. Sotor, T. Martynkien, P. G. Schunemann, P. Mergo, L. Rutkowski, and G. Soboń, "All-fiber mid-infrared source tunable from 6 to 9 μm based on difference frequency generation in op-gap crystal," *Optics Express*, vol. 26, no. 9, pp. 11 756–11 763, 2018.

[82] M. Bailly, R. Becheker, S. Idlahcen, T. Godin, B. Gérard, H. Delahaye, S. Février, A. Grisard, E. Lallier, and A. Hideur, "Mid-infrared parametric generation in op-gaas waveguides pumped by a femtosecond erbium-doped fluoride fiber laser," in *Nonlinear Frequency Generation and Conversion: Materials and Devices XX*, vol. 11670. SPIE, 2021, pp. 90–96.

[83] S. M. Foreman, D. J. Jones, and J. Ye, "Flexible and rapidly configurable femtosecond pulse generation in the mid-ir," *Opt. Lett.*, vol. 28, no. 5, pp. 370–372, Mar 2003. [Online]. Available: https://opg.optica.org/ol/abstract.cfm?URI=ol-28-5-370

[84] D. Mazzotti, P. Cancio, G. Giusfredi, P. D. Natale, and M. Prevedelli, "Frequency-comb-based absolute frequency measurements in the mid-infrared with a difference-frequency spectrometer," *Opt. Lett.*, vol. 30, no. 9, pp. 997–999, May 2005. [Online]. Available: https://opg.optica.org/ol/abstract.cfm?URI=ol-30-9-997

[85] N. Bloembergen and P. Lallemand, "Complex intensity-dependent index of refraction, frequency broadening of stimulated raman lines, and stimulated rayleigh scattering," *Physical Review Letters*, vol. 16, no. 3, pp. 81–84, Jan. 1966. [Online]. Available: https://doi.org/10.1103/physrevlett.16.81

[86] J. Swiderski, "High-power mid-infrared supercontinuum sources: Current status and future perspectives," *Progress in Quantum Electronics*, vol. 38, no. 5, pp. 189–235, 2014.

[87] W. Yang, B. Zhang, G. Xue, K. Yin, and J. Hou, "Thirteen watt all-fiber mid-infrared supercontinuum generation in a single mode zblan fiber pumped by a 2 μm mopa system," *Opt. Lett.*, vol. 39, no. 7, pp. 1849–1852, Apr 2014. [Online]. Available: https://opg.optica.org/ol/abstract.cfm?URI=ol-39-7-1849

[88] J. Swiderski and P. Grzes, "High-power mid-ir supercontinuum generation in fluoroindate and arsenic sulfide fibers pumped by a broadband 1.9–2.7 μm all-fiber laser source," *Optics & Laser Technology*, vol. 141, p. 107178, 2021.

[89] K. J. Vahala, "Optical microcavities," *Nature*, vol. 424, no. 6950, pp. 839–846, Aug. 2003. [Online]. Available: https://doi.org/10.1038/nature01939

[90] R. K. Jain and M. Hossein-Zadeh, "Microresonator-based mid-IR devices," in *SPIE Proceedings*, M. J. F. Digonnet, S. Jiang, and J. C. Dries, Eds. SPIE, Mar. 2013. [Online]. Available: https://doi.org/10.1117/12.2010313

[91] W. von Klitzing, E. Jahier, R. Long, F. Lissillour, V. Lefevre-Seguin, J. Hare, J.-M. Raimond, and S. Haroche, "Very low threshold lasing in er3 doped ZBLAN microsphere," *Electronics Letters*, vol. 35, no. 20, p. 1745, 1999. [Online]. Available: https://doi.org/10.1049/el:19991009

[92] T. J. Kippenberg, R. Holzwarth, and S. A. Diddams, "Microresonator-based optical frequency combs," *Science*, vol. 332, no. 6029, pp. 555–559, Apr. 2011. [Online]. Available: https://doi.org/10.1126/science.1193968

[93] M. Yu, Y. Okawachi, A. G. Griffith, M. Lipson, and A. L. Gaeta, "Mode-locked mid-infrared

frequency combs in a silicon microresonator," *Optica*, vol. 3, no. 8, p. 854, Jul. 2016. [Online]. Available: https://doi.org/10.1364/optica.3.000854

[94] K. Luke, Y. Okawachi, M. R. E. Lamont, A. L. Gaeta, and M. Lipson, "Broadband mid-infrared frequency comb generation in a si_3n_4 microresonator," *Optics Letters*, vol. 40, no. 21, p. 4823, Oct. 2015. [Online]. Available: https://doi.org/10.1364/ol.40.004823

[95] A. G. Griffith, R. K. Lau, J. Cardenas, Y. Okawachi, A. Mohanty, R. Fain, Y. H. D. Lee, M. Yu, C. T. Phare, C. B. Poitras, A. L. Gaeta, and M. Lipson, "Silicon-chip mid-infrared frequency comb generation," *Nature Communications*, vol. 6, no. 1, Feb. 2015. [Online]. Available: https://doi.org/10.1038/ncomms7299

[96] R. Shankar, I. Bulu, and M. Lončar, "Integrated high-quality factor silicon-on-sapphire ring resonators for the mid-infrared," *Applied Physics Letters*, vol. 102, no. 5, p. 051108, Feb. 2013. [Online]. Available: https://doi.org/10.1063/1.4791558

[97] C. Y. Wang, T. Herr, P. Del'Haye, A. Schliesser, J. Hofer, R. Holzwarth, T. W. Hänsch, N. Picqué, and T. J. Kippenberg, "Mid-infrared optical frequency combs at 2.5 m based on crystalline microresonators," *Nature Communications*, vol. 4, no. 1, Jan. 2013. [Online]. Available: https://doi.org/10.1038/ncomms2335

[98] A. A. Savchenkov, V. S. Ilchenko, F. D. Teodoro, P. M. Belden, W. T. Lotshaw, A. B. Matsko, and L. Maleki, "Generation of kerr combs centered at 45 m in crystalline microresonators pumped with quantum-cascade lasers," *Optics Letters*, vol. 40, no. 15, p. 3468, Jul. 2015. [Online]. Available: https://doi.org/10.1364/ol.40.003468

[99] N. L. B. Sayson, T. Bi, V. Ng, H. Pham, L. S. Trainor, H. G. L. Schwefel, S. Coen, M. Erkintalo, and S. G. Murdoch, "Octave-spanning tunable parametric oscillation in crystalline kerr microresonators," *Nature Photonics*, vol. 13, no. 10, pp. 701–706, Jul. 2019. [Online]. Available: https://doi.org/10.1038/s41566-019-0485-4

[100] A. Pryamikov, "Gas fiber lasers may represent a breakthrough in creating powerful radiation

sources in the mid-IR," *Light: Science &amp Applications*, vol. 11, no. 1, Feb. 2022. [Online]. Available: https://doi.org/10.1038/s41377-022-00728-5

[101] Z. Zhou, Z. Wang, W. Huang, Y. Cui, H. Li, M. Wang, X. Xi, S. Gao, and Y. Wang, "Towards high-power mid-IR light source tunable from 3.8 to 4.5 μm by HBr-filled hollow-core silica fibres," *Light: Science &amp Applications*, vol. 11, no. 1, Jan. 2022. [Online]. Available: https://doi.org/10.1038/s41377-021-00703-6

[102] R. W. Boyd, *Nonlinear Optics*. Academic Press Books - Elsevier, 2008.

[103] R. L. Sutherland, *Handbook of Nonlinear Optics*. Marcel Dekker Inc., 2003.

[104] D. S. Hum and M. M. Fejer, "Quasi-phasematching," pp. 180–198, mar 2007.

[105] R. S. Weis and T. K. Gaylord, "Lithium niobate: Summary of physical properties and crystal structure," *Applied Physics A Solids and Surfaces*, vol. 37, no. 4, pp. 191–203, Aug. 1985. [Online]. Available: https://doi.org/10.1007/bf00614817

[106] A. Dhar and A. Mansingh, "Optical properties of reduced lithium niobate single crystals," *Journal of Applied Physics*, vol. 68, no. 11, pp. 5804–5809, Dec. 1990. [Online]. Available: https://doi.org/10.1063/1.346951

[107] G. D. Miller, *Periodically poled lithium niobate: modeling, fabrication, and nonlinear optical performance*. Stanford university, 1998.

[108] L. Myers and W. Bosenberg, "Periodically poled lithium niobate and quasi-phase-matched optical parametric oscillators," *IEEE Journal of Quantum Electronics*, vol. 33, no. 10, pp. 1663–1672, 1997.

[109] G.-R. Lv, L. Guo, H.-P. Xu, X.-A. Dou, H. Kong, Y.-L. Yang, J.-Q. Wen, J.-T. Bian, Q. Ye, X.-Q. Sun, and K.-J. Yang, "Watt-level widely tunable narrow-linewidth pulsed mid-infrared MgO:PPLN optical parametric oscillator with a f-p etalon," *Optics &amp Laser Technology*, vol. 160, p. 109064, May 2023. [Online]. Available: https://doi.org/10.1016/j.optlastec.2022.109064

[110] L. Hu, Y. He, X. Lv, J. Ning, G. Zhao, and S. Zhu, "A passively wavelength-stabilized mid-infrared optical parametric oscillator," *Photonics*, vol. 10, no. 1, p. 5, Dec. 2022. [Online]. Available: https://doi.org/10.3390/photonics10010005

[111] D. B. Kolker, I. V. Sherstov, N. Y. Kostyukova, A. A. Boyko, E. Y. Erushin, and B. N. Nyushkov, "Broadband mid-IR source based on a MgO : PPLN optical parametric oscillator," *Quantum Electronics*, vol. 49, no. 2, pp. 191–194, Feb. 2019. [Online]. Available: https://doi.org/10.1070/qel16872

[112] I.-H. Bae, S. Do Lim, J.-K. Yoo, D.-H. Lee, and S. K. Kim, "Development of a mid-infrared cw optical parametric oscillator based on fan-out grating mgo: Ppln pumped at 1064 nm," *Current Optics and Photonics*, vol. 3, no. 1, pp. 33–39, 2019.

[113] K. Mizuuchi, K. Yamamoto, M. Kato, and H. Sato, "Broadening of the phase-matching bandwidth in quasi-phase-matched second-harmonic generation," *IEEE Journal of Quantum Electronics*, vol. 30, no. 7, pp. 1596–1604, Jul. 1994. [Online]. Available: https://doi.org/10.1109/3.299491

[114] J. Heng, P. Liu, and Z. Zhang, "Enhanced spectral broadening in an optical parametric oscillator based on a PPLN crystal," *Optics Express*, vol. 28, no. 11, p. 16740, May 2020. [Online]. Available: https://doi.org/10.1364/oe.392169

[115] P. Loza-Alvarez, C. T. A. Brown, D. T. Reid, W. Sibbett, and M. Missey, "High-repetition-rate ultrashort-pulse optical parametric oscillator continuously tunable from 2.8 to 6.8 µm," *Opt. Lett.*, vol. 24, no. 21, pp. 1523–1525, Nov 1999. [Online]. Available: https://opg.optica.org/ol/abstract.cfm?URI=ol-24-21-1523

[116] X. Cheng, P. Wang, X. Li, P. Zhou, H. Xiao, Z. Liu, and K. Han, "Low threshold, dual-wavelength, mid-infrared optical parametric oscillator," *IEEE Photonics Journal*, vol. 11, no. 1, pp. 1–7, Feb. 2019. [Online]. Available: https://doi.org/10.1109/jphot.2018.2885892

[117] V. Ulvila and M. Vainio, "Diode-laser-pumped continuous-wave optical parametric oscillator

with a large mid-infrared tuning range," *Optics Communications*, vol. 439, pp. 99–102, May 2019. [Online]. Available: https://doi.org/10.1016/j.optcom.2019.01.052

[118] I.-H. Bae, H. S. Moon, S. Zaske, C. Becher, S. K. Kim, S.-N. Park, and D.-H. Lee, "Low-threshold singly-resonant continuous-wave optical parametric oscillator based on MgO-doped PPLN," *Applied Physics B*, vol. 103, no. 2, pp. 311–319, Nov. 2010. [Online]. Available: https://doi.org/10.1007/s00340-010-4297-y

[119] S. C. Kumar, J. Wei, A. J. Debray, V. Kemlin, B. Boulanger, H. Ishizuki, T. Taira, and M. Ebrahim-Zadeh, "Picosecond mid-infrared optical parametric oscillator based on cylindrical mgo:ppln," in *2016 Conference on Lasers and Electro-Optics (CLEO)*, 2016, pp. 1–2.

[120] K. Wang, M. Gao, S. Yu, J. Ning, Z. Xie, X. Lv, G. Zhao, and S. Zhu, "A compact and high efficiency intracavity OPO based on periodically poled lithium niobate," *Scientific Reports*, vol. 11, no. 1, Mar. 2021. [Online]. Available: https://doi.org/10.1038/s41598-021-84721-9

[121] Z. Li, Y. Zhang, Y. Wang, S. Ren, and Y. Liu, "The effects of temperature control in the optical parametric oscillator laser system," in *High Power Lasers: Technology and Systems, Platforms, Effects III*, D. H. Titterton, H. Ackermann, and W. L. Bohn, Eds. SPIE, Oct. 2019. [Online]. Available: https://doi.org/10.1117/12.2532969

[122] P. Kronenberg and O. Traxer, "The laser of the future: reality and expectations about the new thulium fiber laser—a systematic review," *Translational Andrology and Urology*, vol. 8, no. S4, pp. S398–S417, Sep. 2019. [Online]. Available: https://doi.org/10.21037/tau.2019.08.01

[123] P. Kronenberg, B. Z. Hameed, and B. Somani, "Outcomes of thulium fibre laser for treatment of urinary tract stones: results of a systematic review," *Current Opinion in Urology*, vol. 31, no. 2, pp. 80–86, Jan. 2021. [Online]. Available: https://doi.org/10.1097/mou.0000000000000853

[124] S. Verma, J. Hesser, and S. Arba-Mosquera, "Optimum laser beam characteristics for achieving smoother ablations in laser vision correction," *Investigative Opthalmology*

&amp Visual Science, vol. 58, no. 4, p. 2021, Apr. 2017. [Online]. Available: https://doi.org/10.1167/iovs.16-21025

[125] J. Zou, B. Zhu, G. Zhang, S. Guo, and R. Xiao, "Power density effect on the laser beam-induced eruption of spatters in fiber laser keyhole welding," *Optics Laser Technology*, vol. 147, p. 107651, 2022. [Online]. Available: https://www.sciencedirect.com/science/article/pii/S0030399221007398

[126] Y. Liu, N. Jiang, Y. Liu, D. Cui, C.-F. Yu, H. Liu, and Z. Li, "Effect of laser power density on the electrochromic properties of wo3 films obtained by pulsed laser deposition," *Ceramics International*, vol. 47, no. 16, pp. 22 416–22 423, 2021. [Online]. Available: https://www.sciencedirect.com/science/article/pii/S0272884221013067

[127] B. Balouch, P. A. Ranjbar, G. Alnouri, A. I. A. Omari, V. Martha, M. Brennan, and R. T. Sataloff, "Surgical outcome of low-power-density blue laser for vascular lesions of the vocal fold," *Journal of Voice*, 2022. [Online]. Available: https://www.sciencedirect.com/science/article/pii/S0892199722001400

[128] J. Lucas, "Infrared glasses," *Current Opinion in Solid State and Materials Science*, vol. 4, no. 2, pp. 181–187, apr 1999. [Online]. Available: https://doi.org/10.1016%2Fs1359-0286%2899%2900007-8

[129] G. Tao, H. Ebendorff-Heidepriem, A. M. Stolyarov, S. Danto, J. V. Badding, Y. Fink, J. Ballato, and A. F. Abouraddy, "Infrared fibers," *Adv. Opt. Photon.*, vol. 7, no. 2, pp. 379–458, Jun 2015. [Online]. Available: https://opg.optica.org/aop/abstract.cfm?URI=aop-7-2-379

[130] P. D. Dragic, M. Cavillon, and J. Ballato, "Materials for optical fiber lasers: A review," *Applied Physics Reviews*, vol. 5, no. 4, pp. 0–37, 2018. [Online]. Available: http://dx.doi.org/10.1063/1.5048410

[131] N. G. Boetti, D. Negro, G. C. Scarpignato, G. Perrone, S. Abrate, J. Lousteau, E. Mura, and D. Milanese, "Photonic glasses for IR and mid-IR spectral range," in *International*

Conference on Space Optics — ICSO 2012, E. Armandillo, N. Karafolas, and B. Cugny, Eds. SPIE, Nov. 2017. [Online]. Available: https://doi.org/10.1117/12.2309088

[132] J. Savage, "Materials for infrared fibre optics," *Materials Science Reports*, vol. 2, no. 3, pp. 99–137, jan 1987. [Online]. Available: https://doi.org/10.1016%2Fs0920-2307%2887%2980001-4

[133] A. Hrubý, "Evaluation of glass-forming tendency by means of DTA," *Czechoslovak Journal of Physics*, vol. 22, no. 11, pp. 1187–1193, Nov. 1972. [Online]. Available: https://doi.org/10.1007/bf01690134

[134] S. Jackson and T. King, "CW operation of a 1.064-m pumped tm-ho-doped silica fiber laser," *IEEE Journal of Quantum Electronics*, vol. 34, no. 9, pp. 1578–1587, 1998. [Online]. Available: https://doi.org/10.1109/3.709574

[135] R. Thapa, D. Rhonehouse, D. Nguyen, K. Wiersma, C. Smith, J. Zong, and A. Chavez-Pirson, "Mid-IR supercontinuum generation in ultra-low loss, dispersion-zero shifted tellurite glass fiber with extended coverage beyond 4.5 m," in *SPIE Proceedings*, D. H. Titterton, M. A. Richardson, R. J. Grasso, H. Ackermann, and W. L. Bohn, Eds. SPIE, Oct. 2013. [Online]. Available: https://doi.org/10.1117/12.2033926

[136] J. Ari, G. Louvet, Y. Ledemi, F. Célarié, S. Morais, B. Bureau, S. Marre, V. Nazabal, and Y. Messaddeq, "Anodic bonding of mid-infrared transparent germanate glasses for high pressure - high temperature microfluidic applications," *Science and Technology of Advanced Materials*, vol. 21, no. 1, pp. 11–24, Jan. 2020. [Online]. Available: https://doi.org/10.1080/14686996.2019.1702861

[137] D. A. Pinnow, A. L. Gentile, A. G. Standlee, A. J. Timper, and L. M. Hobrock, "Polycrystalline fiber optical waveguides for infrared transmission," *Applied Physics Letters*, vol. 33, no. 1, pp. 28–29, Jul. 1978. [Online]. Available: https://doi.org/10.1063/1.90177

[138] J. A. Harrington, "&lttitle&gtcrystalline infrared fibers&lt/title&gt," in *SPIE Proceedings*, L. G. DeShazer and C. Kao, Eds. SPIE, jul 1981. [Online]. Available: https://doi.org/10.1117%2F12.959892

[139] R. K. Nubling and J. A. Harrington, "Single-crystal laser-heated pedestal-growth sapphire fibers for er:YAG laser power delivery," *Applied Optics*, vol. 37, no. 21, p. 4777, Jul. 1998. [Online]. Available: https://doi.org/10.1364/ao.37.004777

[140] M. F. Churbanov, B. I. Denker, B. I. Galagan, V. V. Koltashev, V. G. Plotnichenko, M. V. Sukhanov, S. E. Sverchkov, and A. P. Velmuzhov, "First demonstration of ~ 5 μm laser action in terbium-doped selenide glass," *Applied Physics B*, vol. 126, no. 7, Jun. 2020. [Online]. Available: https://doi.org/10.1007/s00340-020-07473-w

[141] V. Shiryaev, M. Sukhanov, A. Velmuzhov, E. Karaksina, T. Kotereva, G. Snopatin, B. Denker, B. Galagan, S. Sverchkov, V. Koltashev, and V. Plotnichenko, "Core-clad terbium doped chalcogenide glass fiber with laser action at 5.38 m," *Journal of Non-Crystalline Solids*, vol. 567, p. 120939, Sep. 2021. [Online]. Available: https://doi.org/10.1016/j.jnoncrysol.2021.120939

[142] M. F. Churbanov, B. I. Denker, B. I. Galagan, V. V. Koltashev, V. G. Plotnichenko, G. E. Snopatin, M. V. Sukhanov, S. E. Sverchkov, and A. P. Velmuzhov, "Laser potential of pr3 doped chalcogenide glass in 5-6 m spectral range," *Journal of Non-Crystalline Solids*, vol. 559, p. 120592, May 2021. [Online]. Available: https://doi.org/10.1016/j.jnoncrysol.2020.120592

[143] J. S. Sanghera, L. B. Shaw, and I. D. Aggarwal, "Chalcogenide glass-fiber-based mid-IR sources and applications," *IEEE Journal of Selected Topics in Quantum Electronics*, vol. 15, no. 1, pp. 114–119, Jan. 2009. [Online]. Available: https://doi.org/10.1109/jstqe.2008.2010245

[144] A. Urich, R. Maier, F. Yu, J. Knight, D. Hand, and J. Shephard, "Silica hollow core microstructured fibres for mid-infrared surgical applications," *Journal of Non-Crystalline Solids*, vol. 377, pp. 236–239, Oct. 2013. [Online]. Available: https://doi.org/10.1016/j.jnoncrysol.2013.01.055

[145] A. V. Gladyshev, A. F. Kosolapov, M. M. Khudyakov, Y. P. Yatsenko, A. N. Kolyadin, A. A. Krylov, A. D. Pryamikov, A. S. Biriukov, M. E. Likhachev, I. Bufetov *et al.*, "4.4-μm raman laser based on hollow-core silica fibre," *Quantum Electronics*, vol. 47, no. 5, p. 491, 2017.

[146] M. Miyagi and Y. Matsuura, "Hollow fiber beam delivery systems," in *SPIE Proceedings*. SPIE, Apr. 1997. [Online]. Available: https://doi.org/10.1117/12.270197

[147] S. D. Jackson and R. K. Jain, "Fiber-based sources of coherent MIR radiation: key advances and future prospects (invited)," *Optics Express*, vol. 28, no. 21, p. 30964, Oct. 2020. [Online]. Available: https://doi.org/10.1364/oe.400003

[148] B. Zheng, J. Fan, B. Chen, X. Qin, J. Wang, F. Wang, R. Deng, and X. Liu, "Rare-Earth Doping in Nanostructured Inorganic Materials," *Chemical Reviews*, vol. 122, no. 6, pp. 5519–5603, 2022.

[149] L. Wetenkamp, G. West, and H. Többen, "Optical properties of rare earth-doped ZBLAN glasses," *Journal of Non-Crystalline Solids*, vol. 140, pp. 35–40, jan 1992. [Online]. Available: https://doi.org/10.1016%2Fs0022-3093%2805%2980737-9

[150] S. D. Jackson, "Towards high-power mid-infrared emission from a fibre laser," *Nature Photonics*, vol. 6, no. 7, pp. 423–431, 2012. [Online]. Available: http://dx.doi.org/10.1038/nphoton.2012.149

[151] X. Zhu and N. Peyghambarian, "High-power ZBLAN glass fiber lasers: Review and prospect," *Advances in OptoElectronics*, vol. 2010, 2010.

[152] M. Gorjan, M. Marinček, and M. Čopič, "Role of interionic processes in the efficiency and operation of erbium-doped fluoride fiber lasers," *IEEE Journal of Quantum Electronics*, vol. 47, no. 2, pp. 262–273, 2011.

[153] J. Li and S. D. Jackson, "Numerical Modeling and Optimization of Diode Pumped Heavily-Erbium-Doped Fluoride Fiber Lasers," *IEEE Journal of Quantum Electronics*, vol. 48, no. 4, pp. 454–464, 2012.

[154] S. Duval, M. Olivier, L.-R. Robichaud, V. Fortin, M. Bernier, M. Piché, and R. Vallée, " Numerical modeling of mid-infrared ultrashort pulse propagation in Er 3+ : fluoride fiber amplifiers ," *Journal of the Optical Society of America B*, vol. 35, no. 6, p. 1450, 2018.

[155] R. S. Quimby and W. J. Miniscalco, "Excited state absorption at 980 nm in erbium-doped silica glass," in *Optical Amplifiers and Their Applications*. Optica Publishing Group, 1992, p. WE3.

[156] M. Pollnan and S. Jackson, "Erbium 3 m fiber lasers," *IEEE Journal of Selected Topics in Quantum Electronics*, vol. 7, no. 1, pp. 30–40, 2001. [Online]. Available: https://doi.org/10.1109/2944.924006

[157] M. Pollnau and S. D. Jackson, "Energy recycling versus lifetime quenching in erbium-doped 3-μm fiber lasers," *IEEE Journal of Quantum Electronics*, vol. 38, no. 2, pp. 162–169, 2002.

[158] P. Golding, S. Jackson, T. King, and M. Pollnau, "Energy transfer processes in er 3+-doped and er 3+, p r 3+-codoped zblan glasses," *Physical Review B*, vol. 62, no. 2, p. 856, 2000.

[159] Y. Xiao, X. Xiao, Y. Xu, S. She, C. Liu, and H. Guo, "Numerical modeling and optimization of hundred-watt-level 2.8 m and 1.6 m cascaded heavily-erbium-doped fluoride fiber amplifiers," *Optics &amp Laser Technology*, vol. 155, p. 108418, Nov. 2022. [Online]. Available: https://doi.org/10.1016/j.optlastec.2022.108418

[160] Y. Bostanci, A. Kazzazi, and B. Djavan, "Laser prostatectomy: holmium laser enucleation and photoselective laser vaporization of the prostate," *Reviews in urology*, vol. 15, no. 1, p. 1, 2013.

[161] T. Sumiyoshi, H. Sekita, T. Arai, S. Sato, M. Ishihara, and M. Kikuchi, "High-power continuous-wave 3-and 2-/spl mu/m cascade ho/sup 3+: Zblan fiber laser and its medical applications," *IEEE journal of selected topics in quantum electronics*, vol. 5, no. 4, pp. 936–943, 1999.

[162] S. Jackson, "Singly ho3+-doped fluoride fibre laser operating at 2.92 μm," *Electronics Letters*, vol. 40, no. 22, pp. 1400–1401, 2004.

[163] D. Talavera and E. Mejia, "Holmium-doped fluoride fiber laser at 2950 nm pumped at 1175 nm," *Laser Physics*, vol. 16, no. 3, pp. 436–440, 2006.

[164] S. D. Jackson, "Continuous wave 2.9 μm dysprosium-doped fluoride fiber laser," *Applied Physics Letters*, vol. 83, no. 7, pp. 1316–1318, Aug. 2003. [Online]. Available: https://doi.org/10.1063/1.1603353

[165] L. Sójka, L. Pajewski, M. Popenda, E. Beres-Pawlik, S. Lamrini, K. Markowski, T. Osuch, T. M. Benson, A. B. Seddon, and S. Sujecki, "Experimental investigation of mid-infrared laser action from dy 3+ doped fluorozirconate fiber," *IEEE Photonics Technology Letters*, vol. 30, no. 12, pp. 1083–1086, 2018.

[166] P. Tang, Y. Wang, E. Vicentini, F. Canella, L. M. Molteni, N. Coluccelli, P. Laporta, and G. Galzerano, "Single-frequency dy: Zblan fiber laser tunable in the wavelength range from 2.925 to 3.250mum," *Journal of Lightwave Technology*, vol. 40, no. 8, pp. 2489–2493, 2022.

[167] R. Woodward, D. Hudson, and S. Jackson, "Towards diode-pumped mid-infrared praseodymium-ytterbium-doped fluoride fiber lasers," in *Fiber Lasers XV: Technology and Systems*, vol. 10512. SPIE, 2018, pp. 115–120.

[168] J. Allain, M. Monerie, and H. Poignant, "Ytterbium-doped fluoride fibre laser operating at 1.02 mu m," *Electronics letters*, vol. 11, no. 28, pp. 988–989, 1992.

[169] S. Jackson, "8.8 w diode-cladding-pumped tmˆ sup 3+ˆ, hoˆ sup 3+ˆ-doped fluoride fibre laser," *Electronics Letters*, vol. 37, no. 13, p. 1, 2001.

[170] S. Tokita, M. Murakami, S. Shimizu, M. Hashida, and S. Sakabe, "12 W Q-switched er:ZBLAN fiber laser at 28 m," *Optics Letters*, vol. 36, no. 15, p. 2812, Jul. 2011. [Online]. Available: https://doi.org/10.1364/ol.36.002812

[171] G. A. Newburgh and M. Dubinskii, "Power and efficiency scaling of Er: ZBLAN fiber laser," *Laser Physics Letters*, vol. 18, no. 9, 2021.

[172] L. Sójka, L. Pajewski, S. Lamrini, M. Farries, T. M. Benson, A. B. Seddon, and S. Sujecki, "High peak power q-switched er:zblan fiber laser," *J. Lightwave Technol.*, vol. 39, no. 20, pp. 6572–6578, Oct 2021. [Online]. Available: https://opg.optica.org/jlt/abstract.cfm?URI=jlt-39-20-6572

[173] Z. He, W. Li, A. Yu, Y. Wu, and Z. Cai, "Efficient uv-visible emission enabled by 532 nm cw excitation in an ho 3+-doped zblan fiber," *Optics Express*, vol. 30, no. 7, pp. 10 414–10 427, 2022.

[174] J. Zou, J. Li, T. Li, Y. Huang, Q. Ruan, Y. Dou, and Z. Luo, "Tunable, continuous-wave, deep-ultraviolet laser generation by intracavity frequency doubling of visible fiber lasers," *J. Lightwave Technol.*, vol. 40, no. 12, pp. 3900–3906, Jun 2022. [Online]. Available: https://opg.optica.org/jlt/abstract.cfm?URI=jlt-40-12-3900

[175] A. S. Bezgabadi and M. A. Bolorizadeh, "Quantum model for supercontinuum generation process," *Scientific Reports*, vol. 12, no. 1, Jun. 2022. [Online]. Available: https://doi.org/10.1038/s41598-022-13808-8

[176] J. M. Dudley, G. Genty, and S. Coen, "Supercontinuum generation in photonic crystal fiber," *Reviews of modern physics*, vol. 78, no. 4, p. 1135, 2006.

[177] C. Xia, Z. Xu, M. N. Islam, F. L. Terry, M. J. Freeman, A. Zakel, and J. Mauricio, "10.5 w time-averaged power mid-ir supercontinuum generation extending beyond 4 μm with direct pulse pattern modulation," *IEEE Journal of Selected Topics in Quantum Electronics*, vol. 15, no. 2, pp. 422–434, 2009.

[178] G. Qin, X. Yan, C. Kito, M. Liao, C. Chaudhari, T. Suzuki, and Y. Ohishi, "Ultrabroadband supercontinuum generation from ultraviolet to 6.28 m in a fluoride fiber," *Applied Physics Letters*, vol. 95, no. 16, p. 161103, Oct. 2009. [Online]. Available: https://doi.org/10.1063/1.3254214

[179] J. Swiderski, M. Michalska, and G. Maze, "Mid-ir supercontinuum generation in a zblan fiber pumped by a gain-switched mode-locked tm-doped fiber laser and amplifier system," *Opt. Express*, vol. 21, no. 7, pp. 7851–7857, Apr 2013. [Online]. Available: https://opg.optica.org/oe/abstract.cfm?URI=oe-21-7-7851

[180] J. Swiderski, M. Michalska, and P. Grzes, "Broadband and top-flat mid-infrared supercontinuum generation with 3.52 w time-averaged power in a ZBLAN fiber directly

pumped by a 2-μm mode-locked fiber laser and amplifier," *Applied Physics B*, vol. 124, no. 7, Jul. 2018. [Online]. Available: https://doi.org/10.1007/s00340-018-7020-z

[181] W. Q. Yang, B. Zhang, J. Hou, R. Xiao, R. Song, and Z. J. Liu, "Gain-switched and mode-locked tm/ho-codoped 2 m fiber laser for mid-ir supercontinuum generation in a tm-doped fiber amplifier," *Laser Physics Letters*, vol. 10, no. 4, p. 045106, feb 2013. [Online]. Available: https://dx.doi.org/10.1088/1612-2011/10/4/045106

[182] W. Q. Yang, B. Zhang, J. Hou, R. Xiao, Z. F. Jiang, and Z. J. Liu, "Mid-ir supercontinuum generation in tm/ho codoped fiber amplifier," *Laser Physics Letters*, vol. 10, no. 5, p. 055107, apr 2013. [Online]. Available: https://dx.doi.org/10.1088/1612-2011/10/5/055107

[183] M. Bernier, D. Faucher, N. Caron, and R. Vallée, "Highly stable and efficient erbium-doped 2.8 μm all fiber laser," *Opt. Express*, vol. 17, no. 19, pp. 16 941–16 946, Sep 2009. [Online]. Available: https://opg.optica.org/oe/abstract.cfm?URI=oe-17-19-16941

[184] A. Carter, B. N. Samson, K. Tankala, D. P. Machewirth, V. Khitrov, U. H. Manyam, F. Gonthier, and F. Seguin, "Damage mechanisms in components for fiber lasers and amplifiers," in *Laser-Induced Damage in Optical Materials: 2004*, G. J. Exarhos, A. H. Guenther, N. Kaiser, K. L. Lewis, M. J. Soileau, and C. J. Stolz, Eds., vol. 5647, International Society for Optics and Photonics. SPIE, 2005, pp. 561 – 571. [Online]. Available: https://doi.org/10.1117/12.592015

[185] N. Caron, M. Bernier, D. Faucher, and R. Vallée, "Understanding the fiber tip thermal runaway present in 3μm fluoride glass fiber lasers," *Optics Express*, vol. 20, no. 20, p. 22188, Sep. 2012. [Online]. Available: https://doi.org/10.1364/oe.20.022188

[186] L. Sojka, L. Pajewski, S. Lamrini, M. Farries, T. M. Benson, A. B. Seddon, and S. Sujecki, "Experimental investigation of actively q-switched er3+:Zblan fiber laser operating at around 2.8 µm," *Sensors (Switzerland)*, vol. 20, no. 16, pp. 1–11, 2020.

[187] Y. O. Aydin, F. Maes, V. Fortin, S. T. Bah, R. Vallée, and M. Bernier, "Endcapping of

high-power 3 µm fiber lasers," *Opt. Express*, vol. 27, no. 15, pp. 20 659–20 669, Jul 2019. [Online]. Available: https://opg.optica.org/oe/abstract.cfm?URI=oe-27-15-20659

[188] J. W. Fleming, "Dispersion in geo2–sio2 glasses," *Appl. Opt.*, vol. 23, no. 24, pp. 4486–4493, Dec 1984. [Online]. Available: https://opg.optica.org/ao/abstract.cfm?URI=ao-23-24-4486

[189] M. Brierley and P. France, "Continuous wave lasing at 2.7 m in an erbium-doped fluorozirconate fibre," *Electronics Letters*, vol. 24, no. 15, p. 935, 1988. [Online]. Available: https://doi.org/10.1049/el:19880637

[190] S. D. Jackson, T. A. King, and M. Pollnau, "Diode-pumped 1.7-w erbium 3-µm fiber laser," *Opt. Lett.*, vol. 24, no. 16, pp. 1133–1135, Aug 1999. [Online]. Available: https://opg.optica.org/ol/abstract.cfm?URI=ol-24-16-1133

[191] T. Sandrock, D. Fischer, P. Glas, M. Leitner, M. Wrage, and A. Diening, "Diode-pumped 1-w er-doped fluoride glass m-profile fiber laser emitting at 2.8 µm," *Opt. Lett.*, vol. 24, no. 18, pp. 1284–1286, Sep 1999. [Online]. Available: https://opg.optica.org/ol/abstract.cfm?URI=ol-24-18-1284

[192] B. Srinivasan, J. Tafoya, and R. K. Jain, "High-power "watt-level" cw operation of diode-pumped 2.7 μm fiber lasers using efficient cross-relaxation and energy transfer mechanisms," *Opt. Express*, vol. 4, no. 12, pp. 490–495, Jun 1999. [Online]. Available: https://opg.optica.org/oe/abstract.cfm?URI=oe-4-12-490

[193] J. Wang, X. Zhu, M. Mollaee, J. Zong, and N. Peyhambarian, " Efficient energy transfer from Er 3+ to Ho 3+ and Dy 3+ in ZBLAN glass ," *Optics Express*, vol. 28, no. 4, p. 5189, 2020.

[194] X. Zhu and R. Jain, "10-w-level diode-pumped compact 2.78 μm zblan fiber laser," *Opt. Lett.*, vol. 32, no. 1, pp. 26–28, Jan 2007. [Online]. Available: https://opg.optica.org/ol/abstract.cfm?URI=ol-32-1-26

[195] ——, "Watt-level er-doped and er-pr-codoped zblan fiber amplifiers at the 2.7-2.8 μm wavelength range," *Opt. Lett.*, vol. 33, no. 14, pp. 1578–1580, Jul 2008. [Online]. Available: https://opg.optica.org/ol/abstract.cfm?URI=ol-33-14-1578

[196] S. Tokita, M. Murakami, S. Shimizu, M. Hashida, and S. Sakabe, "Liquid-cooled 24 w mid-infrared er:ZBLAN fiber laser," *Optics Letters*, vol. 34, no. 20, p. 3062, Oct. 2009. [Online]. Available: https://doi.org/10.1364/ol.34.003062

[197] S. Tokita, M. Hirokane, M. Murakami, S. Shimizu, M. Hashida, and S. Sakabe, "Stable 10 w er:zblan fiber laser operating at 2.71–2.88μm," *Opt. Lett.*, vol. 35, no. 23, pp. 3943–3945, Dec 2010. [Online]. Available: https://opg.optica.org/ol/abstract.cfm?URI=ol-35-23-3943

[198] V. Fortin, M. Bernier, S. T. Bah, and R. Vallée, "30 w fluoride glass all-fiber laser at 2.94 μm," *Opt. Lett.*, vol. 40, no. 12, pp. 2882–2885, Jun 2015. [Online]. Available: https://opg.optica.org/ol/abstract.cfm?URI=ol-40-12-2882

[199] Y. O. Aydin, V. Fortin, R. Vallée, and M. Bernier, "Towards power scaling of 28 m fiber lasers," *Optics Letters*, vol. 43, no. 18, p. 4542, Sep. 2018. [Online]. Available: https://doi.org/10.1364/ol.43.004542

[200] C. Frerichs and T. Tauermann, "Q-switched operation of laser diode pumped erbium-doped fluorozirconate fibre laser operating at 2.7 μm," *Electronics Letters*, vol. 30, no. 9, pp. 706–707, Apr. 1994. [Online]. Available: https://doi.org/10.1049/el:19940502

[201] C. Frerichs and U. B. Unrau, "Passive q-switching and mode-locking of erbium-doped fluoride fiber lasers at 2.7 μm," *Optical Fiber Technology*, vol. 2, no. 4, pp. 358–366, 1996.

[202] G. Zhu, X. Zhu, R. A. Norwood, and N. Peyghambarian, "Experimental and numerical investigations on Q-switched laser-seeded fiber MOPA at 2.8 μm," *Journal of Lightwave Technology*, vol. 32, no. 23, pp. 4553–4557, 2014.

[203] P. Paradis, V. Fortin, Y. O. Aydin, R. Vallée, and M. Bernier, "10 w-level gain-switched all-fiber laser at 28 m," *Optics Letters*, vol. 43, no. 13, p. 3196, Jun. 2018. [Online]. Available: https://doi.org/10.1364/ol.43.003196

[204] Y. O. Aydin, S. Magnan-Saucier, D. Zhang, V. Fortin, D. Kraemer, R. Vallée, and M. Bernier, "Dual stage fiber amplifier operating near 3 μm with milijoule-level, sub-ns

pulses at 5 w," *Optics Letters*, vol. 46, no. 18, p. 4506, Sep. 2021. [Online]. Available: https://doi.org/10.1364/ol.434182

[205] H. Luo, J. Li, J. Xie, B. Zhai, C. Wei, and Y. Liu, "High average power and energy microsecond pulse generation from an erbium-doped fluoride fiber mopa system," *Opt. Express*, vol. 24, no. 25, pp. 29 022–29 032, Dec 2016. [Online]. Available: https://opg.optica.org/oe/abstract.cfm?URI=oe-24-25-29022

[206] L. Yang, Z. Kang, B. Huang, J. Li, L. Miao, P. Tang, C. Zhao, G. Qin, and S. Wen, "Gold nanostars as a q-switcher for the mid-infrared erbium-doped fluoride fiber laser," *Optics Letters*, vol. 43, no. 21, pp. 5459–5462, 2018.

[207] P. Tang, Z. Qin, J. Liu, C. Zhao, G. Xie, S. Wen, and L. Qian, "Watt-level passively mode-locked er3+-doped zblan fiber laser at 2.8μm," *Opt. Lett.*, vol. 40, no. 21, pp. 4855–4858, Nov 2015. [Online]. Available: https://opg.optica.org/ol/abstract.cfm?URI=ol-40-21-4855

[208] S. Duval, M. Bernier, V. Fortin, J. Genest, M. Piché, and R. Vallée, "Femtosecond fiber lasers reach the mid-infrared," *Optica*, vol. 2, no. 7, pp. 623–626, Jul 2015. [Online]. Available: https://opg.optica.org/optica/abstract.cfm?URI=optica-2-7-623

[209] J. Liu, M. Wu, B. Huang, P. Tang, C. Zhao, D. Shen, D. Fan, and S. K. Turitsyn, "Widely wavelength-tunable mid-infrared fluoride fiber lasers," *IEEE Journal of Selected Topics in Quantum Electronics*, vol. 24, no. 3, pp. 1–7, 2017.

[210] C. Wei, H. Zhang, H. Shi, K. Konynenbelt, H. Luo, and Y. Liu, "Over 5-w passively q-switched mid-infrared fiber laser with a wide continuous wavelength tuning range," *IEEE Photonics Technology Letters*, vol. 29, no. 11, pp. 881–884, Jun. 2017. [Online]. Available: https://doi.org/10.1109/lpt.2017.2693387

[211] C. Wei, H. Luo, H. Shi, Y. Lyu, H. Zhang, and Y. Liu, "Widely wavelength tunable gain-switched er3+-doped zblan fiber laser around 2.8 μm," *Opt. Express*, vol. 25, no. 8, pp. 8816–8827, Apr 2017. [Online]. Available: https://opg.optica.org/oe/abstract.cfm?URI=oe-25-8-8816

[212] W. Du, X. Xiao, Y. Cui, J. Nees, I. Jovanovic, and A. Galvanauskas, "Demonstration of 0.67-mJ and 10-ns high-energy pulses at 2.72 μm from large core er:ZBLAN fiber amplifiers," *Optics Letters*, vol. 45, no. 19, p. 5538, Sep. 2020. [Online]. Available: https://doi.org/10.1364/ol.400065

[213] J.-C. Gauthier, V. Fortin, S. Duval, R. Vallée, and M. Bernier, "In-amplifier mid-infrared supercontinuum generation," *Optics Letters*, vol. 40, no. 22, p. 5247, Nov. 2015. [Online]. Available: https://doi.org/10.1364/ol.40.005247

[214] J. A. Giordmaine and R. C. Miller, "Tunable coherent parametric oscillation in linbo$_3$ at optical frequencies," *Phys. Rev. Lett.*, vol. 14, pp. 973–976, Jun 1965. [Online]. Available: https://link.aps.org/doi/10.1103/PhysRevLett.14.973

[215] R. Kingston, "Parametric amplification and oscillation at optical frequencies," *Proc. Institute of Radio Engineers*, vol. 50, pp. 472–476, Apr 1962.

[216] N. M. Kroll, "Parametric amplification in spatially extended media and application to the design of tuneable oscillators at optical frequencies," *Phys. Rev.*, vol. 127, pp. 1207–1211, Aug 1962. [Online]. Available: https://link.aps.org/doi/10.1103/PhysRev.127.1207

[217] S. A. Akhmanov and R. V. Khokhlov, "Concerning one possibility of amplification of light waves," *Sov. Phys. J. Exptl. Theoret. Phys*, vol. 16, p. 252, Jan 1963.

[218] J. A. Armstrong, N. Bloembergen, J. Ducuing, and P. S. Pershan, "Interactions between light waves in a nonlinear dielectric," *Phys. Rev.*, vol. 127, pp. 1918–1939, Sep 1962. [Online]. Available: https://link.aps.org/doi/10.1103/PhysRev.127.1918

[219] C. C. Wang and G. W. Racette, "Measurement of parametric gain accompanying optical difference frequency generation," *Applied Physics Letters*, vol. 6, no. 8, pp. 169–171, Apr. 1965. [Online]. Available: https://doi.org/10.1063/1.1754219

[220] R. L. Herbst, R. N. Fleming, and R. L. Byer, "A 1.4–4-m high-energy angle-tuned LiNbOsub3/subparametric oscillator," *Applied Physics Letters*, vol. 25, no. 9, pp. 520–522, Nov. 1974. [Online]. Available: https://doi.org/10.1063/1.1655573

[221] L. E. Myers, R. C. Eckardt, M. M. Fejer, R. L. Byer, W. R. Bosenberg, and J. W. Pierce, "Quasi-phase-matched optical parametric oscillators in bulk periodically poled linbo3," *J. Opt. Soc. Am. B*, vol. 12, no. 11, pp. 2102–2116, Nov 1995. [Online]. Available: https://opg.optica.org/josab/abstract.cfm?URI=josab-12-11-2102

[222] J. Liu, Q. Liu, X. Yan, H. Chen, and M. Gong, "High repetition frequency ppmgoln mid-infrared optical parametric oscillator," *Laser Physics Letters*, vol. 7, no. 9, p. 630, jun 2010. [Online]. Available: https://dx.doi.org/10.1002/lapl.201010040

[223] D. B. Kolker, R. V. Pustovalova, M. K. Starikova, A. I. Karapuzikov, A. A. Karapuzikov, O. M. Kuznetsov, and Y. V. Kistenev, "Optical parametric oscillator within 2.4–4.3 m pumped with a nanosecond nd:YAG laser," *Atmospheric and Oceanic Optics*, vol. 25, no. 1, pp. 77–81, Feb. 2012. [Online]. Available: https://doi.org/10.1134/s1024856012010071

[224] S. Niu, P. Aierken, M. Ababaike, S. Wang, and T. Yusufu, "Widely tunable, high-energy, mid-infrared (2.2–4.8µm) laser based on a multi-grating mgo:ppln optical parametric oscillator," *Infrared Physics Technology*, vol. 104, p. 103121, 2020. [Online]. Available: https://www.sciencedirect.com/science/article/pii/S1350449519306528

[225] D. H. Jundt, "Temperature-dependent sellmeier equation for the index of refraction, ne, in congruent lithium niobate," *Opt. Lett.*, vol. 22, no. 20, pp. 1553–1555, Oct 1997. [Online]. Available: https://opg.optica.org/ol/abstract.cfm?URI=ol-22-20-1553

[226] O. Gayer, Z. Sacks, E. Galun, and A. Arie, "Temperature and wavelength dependent refractive index equations for MgO-doped congruent and stoichiometric LiNbO3," *Applied Physics B*, vol. 91, no. 2, pp. 343–348, Apr. 2008. [Online]. Available: https://doi.org/10.1007/s00340-008-2998-2

[227] H. Kogelnik and T. Li, "Laser beams and resonators," *Applied optics*, vol. 5, no. 10, pp. 1550–1567, 1966.

[228] A. E. Siegman, *Lasers*. University science books, 1986.

[229] C. Gu, M. Hu, L. Zhang, J. Fan, Y. Song, C. Wang, and D. T. Reid, "High average power, widely tunable femtosecond laser source from red to mid-infrared based on an yb-fiber-laser-pumped optical parametric oscillator," *Optics Letters*, vol. 38, no. 11, p. 1820, May 2013. [Online]. Available: https://doi.org/10.1364/ol.38.001820

[230] S. Harris, "Tunable optical parametric oscillators," *Proceedings of the IEEE*, vol. 57, no. 12, pp. 2096–2113, 1969. [Online]. Available: https://doi.org/10.1109/proc.1969.7495

[231] S. Brosnan and R. Byer, "Optical parametric oscillator threshold and linewidth studies," *IEEE Journal of Quantum Electronics*, vol. 15, no. 6, pp. 415–431, Jun. 1979. [Online]. Available: https://doi.org/10.1109/jqe.1979.1070027

[232] Z. Zhang, J. Tian, J. Wang, Y. Wu, and Y. Song, "Transient dynamics in a common singly resonant optical parametric oscillator," *Optics &amp Laser Technology*, vol. 161, p. 109211, Jun. 2023. [Online]. Available: https://doi.org/10.1016/j.optlastec.2023.109211

[233] R. J. Mears and S. R. Baker, "Erbium fibre amplifiers and lasers," *Optical and Quantum Electronics*, vol. 24, no. 5, pp. 517–538, 1992.

[234] M. Robinson and D. P. Devor, "THERMAL SWITCHING OF LASER EMISSION OF ersup3/sup AT 2.69 AND tmsup3/sup AT 1.86 IN MIXED CRYSTALS OF CaFsub2/sub:ErFsub3/sub:TmFsub3/sub," *Applied Physics Letters*, vol. 10, no. 5, pp. 167–170, Mar. 1967. [Online]. Available: https://doi.org/10.1063/1.1754895

[235] K. S. Bagdasarov, V. Zhekov, V. Lobachev, T. Murina, and A. Prokhorov, "Steady-state emission from a y3al5o12: Er3+ laser (λ= 2.94 μ, t= 300 k)," *Soviet Journal of Quantum Electronics*, vol. 13, no. 2, p. 262, 1983.

[236] D. Faucher, M. Bernier, G. Androz, N. Caron, and R. Vallée, "20 W passively cooled single-mode all-fiber laser at 28 μm," *Optics Letters*, vol. 36, no. 7, p. 1104, 2011.

[237] P. Ma, H. Xiao, D. Meng, W. Liu, R. Tao, J. Leng, Y. Ma, R. Su, P. Zhou, Z. Liu, and et al., "High power all-fiberized and narrow-bandwidth mopa system by tandem pumping

strategy for thermally induced mode instability suppression," *High Power Laser Science and Engineering*, vol. 6, p. e57, 2018.

[238] K. Hejaz, M. Shayganmanesh, R. Rezaei-Nasirabad, A. Roohforouz, S. Azizi, A. Abedinajafi, and V. Vatani, "Modal instability induced by stimulated raman scattering in high-power yb-doped fiber amplifiers," *Optics letters*, vol. 42, no. 24, pp. 5274–5277, 2017.

[239] L. Zenteno, J. Wang, D. Walton, B. Ruffin, M. Li, S. Gray, A. Crowley, and X. Chen, "Suppression of raman gain in single-transverse-mode dual-hole-assisted fiber," *Opt. Express*, vol. 13, no. 22, pp. 8921–8926, Oct 2005. [Online]. Available: http://opg.optica.org/oe/abstract.cfm?URI=oe-13-22-8921

[240] E. Snitzer, H. Po, F. Hakimi, R. Tumminelli, and B. C. McCollum, "Double clad, offset core nd fiber laser," in *Optical Fiber Sensors*. Optica Publishing Group, 1988, p. PD5. [Online]. Available: https://opg.optica.org/abstract.cfm?URI=OFS-1988-PD5

[241] C. Jauregui, J. Limpert, and A. Tünnermann, "High-power fibre lasers," *Nature Photonics*, vol. 7, no. 11, pp. 861–867, 2013.

[242] L. Zenteno, "High-Power Double-Clad Fiber Lasers," vol. 11, no. 9, pp. 1435–1446, 1993.

[243] M. N. Zervas and C. A. Codemard, "High power fiber lasers: A review," *IEEE Journal of Selected Topics in Quantum Electronics*, vol. 20, pp. 219–241, 2014.

[244] M. Xue, C. Gao, L. Niu, S. Zhu, and C. Sun, "Influence of amplified spontaneous emission on laser linewidth in a fiber amplifier," *Appl. Opt.*, vol. 59, no. 8, pp. 2610–2614, Mar 2020. [Online]. Available: https://opg.optica.org/ao/abstract.cfm?URI=ao-59-8-2610

[245] M. Eichhorn, "Numerical modeling of tm-doped double-clad fluoride fiber amplifiers," *IEEE Journal of Quantum Electronics*, vol. 41, no. 12, pp. 1574–1581, Dec. 2005. [Online]. Available: https://doi.org/10.1109/jqe.2005.858469

[246] T. Eidam, S. Hanf, E. Seise, T. V. Andersen, T. Gabler, C. Wirth, T. Schreiber, J. Limpert, and A. Tünnermann, "Femtosecond fiber cpa system emitting 830 w average output power," *Optics letters*, vol. 35, no. 2, pp. 94–96, 2010.

[247] H.-J. Otto, F. Stutzki, F. Jansen, T. Eidam, C. Jauregui, J. Limpert, and A. Tünnermann, "Temporal dynamics of mode instabilities in high-power fiber lasers and amplifiers," *Optics Express*, vol. 20, no. 14, pp. 15 710–15 722, 2012.

[248] C. Jauregui, T. Eidam, J. Limpert, and A. Tünnermann, "Impact of modal interference on the beam quality of high-power fiber amplifiers," *Opt. Express*, vol. 19, no. 4, pp. 3258–3271, Feb 2011. [Online]. Available: http://opg.optica.org/oe/abstract.cfm?URI=oe-19-4-3258

[249] T. Eidam, C. Wirth, C. Jauregui, F. Stutzki, F. Jansen, H.-J. Otto, O. Schmidt, T. Schreiber, J. Limpert, and A. Tünnermann, "Experimental observations of the threshold-like onset of mode instabilities in high power fiber amplifiers," *Optics Express*, vol. 19, no. 14, p. 13218, Jun. 2011. [Online]. Available: https://doi.org/10.1364/oe.19.013218

[250] F. Stutzki, H.-J. Otto, F. Jansen, C. Gaida, C. Jauregui, J. Limpert, and A. Tünnermann, "High-speed modal decomposition of mode instabilities in high-power fiber lasers," *Optics Letters*, vol. 36, no. 23, p. 4572, Nov. 2011. [Online]. Available: https://doi.org/10.1364/ol.36.004572

[251] A. V. Smith and J. J. Smith, "Mode instability in high power fiber amplifiers," *Opt. Express*, vol. 19, no. 11, pp. 10 180–10 192, May 2011. [Online]. Available: http://opg.optica.org/oe/abstract.cfm?URI=oe-19-11-10180

[252] C. Jauregui, H.-J. Otto, F. Stutzki, F. Jansen, J. Limpert, and A. Tünnermann, "Passive mitigation strategies for mode instabilities in high-power fiber laser systems," *Optics express*, vol. 21, no. 16, pp. 19 375–19 386, 2013.

[253] A. V. Smith and J. J. Smith, "Increasing mode instability thresholds of fiber amplifiers by gain saturation," *Optics express*, vol. 21, no. 13, pp. 15 168–15 182, 2013.

[254] *Nonlinear Fiber Optics*. Elsevier, 2013. [Online]. Available: https://doi.org/10.1016/c2011-0-00045-5

[255] Y. Feng, X. Wang, W. Ke, Y. Sun, K. Zhang, Y. Ma, T. Li, Y. Wang, and J. Wu, "Spectral broadening in narrow linewidth, continuous-wave high power fiber

amplifiers," *Optics Communications*, vol. 403, pp. 155–161, Nov. 2017. [Online]. Available: https://doi.org/10.1016/j.optcom.2017.07.005

[256] T. Li, Y. Li, W. Ke, C. Zha, W. Peng, Y. Sun, and Y. Ma, "Power Scaling of Narrow-Linewidth Fiber Amplifier Seeded by Yb-Doped Random Fiber Laser," *IEEE Journal of Selected Topics in Quantum Electronics*, vol. 24, no. 5, 2018.

[257] A. Heidariazar, H. Latifi, M. Lotfollahi, M. Barzi, and H. Asgharzadeh, "Experimental study of spectral broadening in kW-level narrow linewidth FBG-based fiber amplifiers under different pumping configurations," *Optics Continuum*, vol. 1, no. 4, p. 896, Apr. 2022. [Online]. Available: https://doi.org/10.1364/optcon.453133

[258] A. C. Cheung, D. M. Rank, R. Y. Chiao, and C. H. Townes, "Phase modulation ofmml:math xmlns:mml="http://www.w3.org/1998/math/MathML" display="inline"mml:miq/mml:mi/mml:math-switched laser beams in small-scale filaments," *Physical Review Letters*, vol. 20, no. 15, pp. 786–789, Apr. 1968. [Online]. Available: https://doi.org/10.1103/physrevlett.20.786

[259] T. K. Gustafson, J. P. Taran, H. A. Haus, J. R. Lifsitz, and P. L. Kelley, "Self-modulation, self-steepening, and spectral development of light in small-scale trapped filaments," *Physical Review*, vol. 177, no. 1, pp. 306–313, Jan. 1969. [Online]. Available: https://doi.org/10.1103/physrev.177.306

[260] C. Agger, C. Petersen, S. Dupont, H. Steffensen, J. K. Lyngsø, C. L. Thomsen, J. Thøgersen, S. R. Keiding, and O. Bang, "Supercontinuum generation in ZBLAN fibers—detailed comparison between measurement and simulation," *Journal of the Optical Society of America B*, vol. 29, no. 4, p. 635, Mar. 2012. [Online]. Available: https://doi.org/10.1364/josab.29.000635

[261] N. B. Chichkov, P. Ray, S. Cozic, A. Yadav, F. Joulain, S. V. Smirnov, U. Hinze, S. Poulain, and E. U. Rafailov, "Amplification of nanosecond pulses in a single- mode erbium-doped fluoride fibre amplifier," *IEEE Photonics Technology Letters*, vol. 35, no. 1, pp. 3–6, Jan. 2023. [Online]. Available: https://doi.org/10.1109/lpt.2022.3182149

[262] X. Zhu and R. Jain, "Compact 2 w wavelength-tunable er:ZBLAN mid-infrared fiber laser," *Optics Letters*, vol. 32, no. 16, p. 2381, Aug. 2007. [Online]. Available: https://doi.org/10.1364/ol.32.002381

[263] P. E. Schrader, J.-P. Fève, R. L. Farrow, D. A. V. Kliner, R. L. Schmitt, and B. T. Do, "Power scaling of fiber-based amplifiers seeded with microchip lasers," *Solid State Lasers XVII: Technology and Devices*, vol. 6871, no. February 2008, p. 68710T, 2008.

[264] C. Zhang, J. Wu, P. Tang, C. Zhao, and S. Wen, "~3.5 μ m ersup3/sup: ZBLAN fiber laser in dual-end pumping regime," *IEEE Access*, vol. 7, pp. 147 238–147 243, 2019. [Online]. Available: https://doi.org/10.1109/access.2019.2946719

[265] P. E. Schrader, R. L. Farrow, D. A. V. Kliner, J.-P. Fève, and N. Landru, "High-power fiber amplifier with widely tunable repetition rate, fixed pulse duration, and multiple output wavelengths," *Opt. Express*, vol. 14, no. 24, pp. 11 528–11 538, Nov 2006. [Online]. Available: https://opg.optica.org/oe/abstract.cfm?URI=oe-14-24-11528

[266] Y. Shen, Y. Wang, F. Zhu, L. Ma, L. Zhao, Z. Chen, H. Wang, C. Huang, K. Huang, and G. Feng, "200 μj, 13 ns er:ZBLAN mid-infrared fiber laser actively q-switched by an electro-optic modulator," *Optics Letters*, vol. 46, no. 5, p. 1141, Feb. 2021. [Online]. Available: https://doi.org/10.1364/ol.418950

[267] T. Hu, D. Hudson, and S. Jackson, "High peak power actively q-switched ho sup3 /sup , pr sup3 /sup -co-doped fluoride fibre laser," *Electronics Letters*, vol. 49, no. 12, pp. 766–767, Jun. 2013. [Online]. Available: https://doi.org/10.1049/el.2013.0134

[268] C. Jauregui, J. Limpert, and A. Tünnermann, "Prospects in Power Scaling of Fiber Lasers and Amplifiers," *2018 Conference on Lasers and Electro-Optics Pacific Rim, CLEO-PR 2018*, pp. 3–4, 2018.

[269] D. J. Coleman and T. A. King, "Pump induced thermal effects in high power tmsup3 /supand tmsup3 /sup/hosup3 /supcladding-pumped fibre lasers," *Measurement*

Science and Technology, vol. 14, no. 7, pp. 998–1002, Jun. 2003. [Online]. Available: https://doi.org/10.1088/0957-0233/14/7/313

[270] F. Maes, V. Fortin, M. Bernier, and R. Vallée, "5.6w monolithic fiber laser at 3.55μm," *Opt. Lett.*, vol. 42, no. 11, pp. 2054–2057, Jun 2017. [Online]. Available: https://opg.optica.org/ol/abstract.cfm?URI=ol-42-11-2054

[271] L. Chen, C. Fu, Z. Cai, P. Shen, Y. Fan, H. Zhong, C. Du, Y. Meng, Y. Wang, C. Liao, J. He, and W. Bao, "High-quality fiber bragg grating inscribed in zblan fiber using femtosecond laser point-by-point technology," *Opt. Lett.*, vol. 47, no. 14, pp. 3435–3438, Jul 2022. [Online]. Available: https://opg.optica.org/ol/abstract.cfm?URI=ol-47-14-3435

[272] J. M. Fernández-Pradas and P. Serra, "Laser-induced forward transfer: A method for printing functional inks," *Crystals*, vol. 10, no. 8, p. 651, Jul. 2020. [Online]. Available: https://doi.org/10.3390/cryst10080651

[273] L. Koch, O. Brandt, A. Deiwick, and B. Chichkov, "Laser assisted bioprinting at different wavelengths and pulse durations with a metal dynamic release layer: A parametric study," *International Journal of Bioprinting*, vol. 3, no. 1, Jan. 2017. [Online]. Available: https://doi.org/10.18063/ijb.2017.01.001

[274] J. Fernández-Pradas, C. Florian, F. Caballero-Lucas, P. Sopeña, J. Morenza, and P. Serra, "Laser-induced forward transfer: Propelling liquids with light," *Applied Surface Science*, vol. 418, pp. 559–564, 2017.

[275] P. Serra and A. Piqué, "Laser-induced forward transfer: fundamentals and applications," *Advanced Materials Technologies*, vol. 4, no. 1, p. 1800099, 2019.

[276] J. Zhang, Y. Geiger, F. Sotier, S. Djordjevic, D. Docheva, S. Sudhop, H. Clausen-Schaumann, and H. P. Huber, "Extending single cell bioprinting from femtosecond to picosecond laser pulse durations," *Micromachines*, vol. 12, no. 10, p. 1172, Sep. 2021. [Online]. Available: https://doi.org/10.3390/mi12101172

[277] C. Dou, V. Perez, J. Qu, A. Tsin, B. Xu, and J. Li, "A state-of-the-art review of laser-assisted bioprinting and its future research trends," *ChemBioEng Reviews*, vol. 8, no. 5, pp. 517–534, Jun. 2021. [Online]. Available: https://doi.org/10.1002/cben.202000037

[278] "Femtum," 5 2020. [Online]. Available: https://femtum.com/

[279] F. Auzel, D. Meichenin, and H. Poignant, "Laser cross-section and quantum yield of er3 at 2.7 m in a ZrF4-based fluoride glass," *Electronics Letters*, vol. 24, no. 15, p. 909, 1988. [Online]. Available: https://doi.org/10.1049/el:19880618

[280] Y. Huang, M. Mortier, and F. Auzel, "Stark level analysis for er3+-doped zblan glass," *Optical Materials*, vol. 17, no. 4, pp. 501–511, 2001.

[281] O. Henderson-Sapir, S. D. Jackson, and D. J. Ottaway, "Versatile and widely tunable mid-infrared erbium doped zblan fiber laser," *Opt. Lett.*, vol. 41, no. 7, pp. 1676–1679, Apr 2016. [Online]. Available: https://opg.optica.org/ol/abstract.cfm?URI=ol-41-7-1676

[282] M. E. Storm, "Controlled retroreflection: a technique for understanding and eliminating parasitic lasing," *JOSA B*, vol. 9, no. 8, pp. 1299–1304, 1992.

[283] J.-C. Gauthier, V. Fortin, J.-Y. Carrée, S. Poulain, M. Poulain, R. Vallée, and M. Bernier, "Mid-ir supercontinuum from 2.4 to 5.4μm in a low-loss fluoroindate fiber," *Opt. Lett.*, vol. 41, no. 8, pp. 1756–1759, Apr 2016. [Online]. Available: http://opg.optica.org/ol/abstract.cfm?URI=ol-41-8-1756

[284] M. Heck, J.-C. Gauthier, A. Tünnermann, R. Vallée, S. Nolte, and M. Bernier, "Long period fiber gratings for the mitigation of parasitic laser effects in mid-infrared fiber amplifiers," *Optics Express*, vol. 27, no. 15, pp. 21 347–21 357, 2019.

[285] M. Pollnau and S. D. Jackson, "Correction to "Erbium 3- m Fiber Lasers"," *Quantum*, vol. 8, no. February, p. 804629, 2002.

[286] P. Ray, A. Yadav, S. Cozic, F. Joulain, T. Berthelot, U. Hinze, S. Poulain, E. U. Rafailov, and N. B. Chichkov, "Wavelength-tuning of nanosecond pulses in er-doped fluoride fibre

amplifier," *IEEE Photonics Journal*, vol. 14, no. 5, pp. 1–5, Oct. 2022. [Online]. Available: https://doi.org/10.1109/jphot.2022.3206104

[287] L. Yu, Z. Tang, J. Liang, Q. Zeng, J. Wang, X. Luo, J. Wang, P. Yan, F. Dong, X. Liu, Q. Lue, C. Guo, and S. Ruan, "High-energy femtosecond pulse generation from a hybrid mode-locked large-mode-area er:ZBLAN fiber laser," *Optics Letters*, vol. 48, no. 7, p. 1830, Mar. 2023. [Online]. Available: https://doi.org/10.1364/ol.485820

[288] B. Wang, L. Cheng, H. Zhong, J. Sun, Y. Tian, X. Zhang, and B. Chen, "Excited state absorption cross sections of 4i13/2 of er3 in ZBLAN," *Optical Materials*, vol. 31, no. 11, pp. 1658–1662, Sep. 2009. [Online]. Available: https://doi.org/10.1016/j.optmat.2009.03.015

[289] K. Goya, A. Mori, S. Tokita, R. Yasuhara, T. Kishi, Y. Nishijima, S. Tanabe, and H. Uehara, "Broadband mid-infrared amplified spontaneous emission from er/dy co-doped fluoride fiber with a simple diode-pumped configuration," *Scientific Reports*, vol. 11, no. 1, Mar. 2021. [Online]. Available: https://doi.org/10.1038/s41598-021-84950-y

[290] S. Duval, M. Olivier, V. Fortin, M. Bernier, M. Piché, and R. Vallée, "23-kW peak power femtosecond pulses from a mode-locked fiber ring laser at 2.8 μm," *Fiber Lasers XIII: Technology, Systems, and Applications*, vol. 9728, no. March 2016, p. 972802, 2016.

[291] J. E. Bertie and Z. Lan, "Infrared intensities of liquids xx: The intensity of the oh stretching band of liquid water revisited, and the best current values of the optical constants of h2o (l) at 25 c between 15,000 and 1 cm- 1," *Applied Spectroscopy*, vol. 50, no. 8, pp. 1047–1057, 1996.

[292] W. Commons. (2008) Liquid water absorption spectrum across a wide wavelength range. File:Absorption spectrum of liquid water.png. [Online]. Available: https://en.wikipedia.org/wiki/Electromagnetic_absorption_by_water#/media/File:Absorption_spectrum_of_liquid_water.png

[293] H. Moseley, "Ultraviolet and laser radiation safety," *Physics in Medicine Biology*, vol. 39, no. 11, p. 1765, nov 1994. [Online]. Available: https://dx.doi.org/10.1088/0031-9155/39/11/001

[294] X. Zhu and R. Jain, "10-w-level diode-pumped compact 278 m ZBLAN fiber laser," *Optics Letters*, vol. 32, no. 1, p. 26, Dec. 2006. [Online]. Available: https://doi.org/10.1364/ol.32.000026

[295] J.-C. Gauthier, L.-R. Robichaud, V. Fortin, R. Vallée, and M. Bernier, "Mid-infrared supercontinuum generation in fluoride fiber amplifiers: current status and future perspectives," *Applied Physics B*, vol. 124, no. 6, May 2018. [Online]. Available: https://doi.org/10.1007/s00340-018-6980-3

[296] "Watt-level fiber-based femtosecond laser source tunable from 28 to 36 μm," *Optics Letters*, vol. 41, no. 22, p. 5294, 2016.

[297] W. Du, Y. Bai, Y. Cui, M. Chen, and A. Galvanauskas, "Mid-IR pulse amplification to ∼millijoule energies in a single transverse mode using large core er:ZBLAN fibers operating at 2.8μm," *Optics Express*, vol. 30, no. 26, p. 46170, Dec. 2022. [Online]. Available: https://doi.org/10.1364/oe.477503

[298] Z. Qin, G. Xie, W. Ge, P. Yuan, and L. Qian, "Over 20-w mid-infrared picosecond optical parametric oscillator," *IEEE Photonics Journal*, vol. 7, no. 5, pp. 1–6, Oct. 2015. [Online]. Available: https://doi.org/10.1109/jphot.2015.2477281

[299] T. Ren, C. Wu, Y. Yu, T. Dai, F. Chen, and Q. Pan, "Development progress of 3–5 m mid-infrared lasers: OPO, solid-state and fiber laser," *Applied Sciences*, vol. 11, no. 23, p. 11451, Dec. 2021. [Online]. Available: https://doi.org/10.3390/app112311451

[300] E. Sorokin, I. T. Sorokina, M. Mirov, V. Fedorov, I. Moskalev, and S. Mirov, "Ultrabroad continuous-wave tuning of ceramic cr:ZnSe and cr:ZnS lasers," in *Lasers, Sources and Related Photonic Devices*. Optica Publishing Group, 2010. [Online]. Available: https://doi.org/10.1364/assp.2010.amc2

[301] M. Razeghi, W. Zhou, S. Slivken, Q.-Y. Lu, D. Wu, and R. McClintock, "Recent progress of quantum cascade laser research from 3 to 12 m at the center for quantum

devices [invited]," *Applied Optics*, vol. 56, no. 31, p. H30, Aug. 2017. [Online]. Available: https://doi.org/10.1364/ao.56.000h30

[302] J. Scheuermann, R. Weih, M. von Edlinger, L. Nähle, M. Fischer, J. Koeth, M. Kamp, and S. Höfling, "Single-mode interband cascade lasers emitting below 2.8 i/im," *Applied Physics Letters*, vol. 106, no. 16, Apr. 2015. [Online]. Available: https://doi.org/10.1063/1.4918985

[303] L. J. Mawst and D. Botez, "High-power mid-infrared (∼3-6 m) quantum cascade lasers," *IEEE Photonics Journal*, vol. 14, no. 1, pp. 1–25, Feb. 2022. [Online]. Available: https://doi.org/10.1109/jphot.2021.3132261

[304] A. Hemming, J. Richards, A. Davidson, N. Carmody, S. Bennetts, N. Simakov, and J. Haub, "99 w mid-IR operation of a ZGP OPO at 25% duty cycle," *Optics Express*, vol. 21, no. 8, p. 10062, Apr. 2013. [Online]. Available: https://doi.org/10.1364/oe.21.010062

[305] X. Li, X. Huang, X. Hu, X. Guo, and Y. Han, "Recent progress on mid-infrared pulsed fiber lasers and the applications," *Optics &amp Laser Technology*, vol. 158, p. 108898, Feb. 2023. [Online]. Available: https://doi.org/10.1016/j.optlastec.2022.108898

[306] M. S. Webb, P. F. Moulton, J. J. Kasinski, R. L. Burnham, G. Loiacono, and R. Stolzenberger, "High-average-power KTiOAsO_4 optical parametric oscillator," *Optics Letters*, vol. 23, no. 15, p. 1161, Aug. 1998. [Online]. Available: https://doi.org/10.1364/ol.23.001161

[307] B. Li, J. Yin, J. Wang, J. Yang, and P. Yan, "2.76–3.98 m picosecond mid-infrared optical parametric generation in a muti-grating MgO: PPLN," *Frontiers in Physics*, vol. 10, Nov. 2022. [Online]. Available: https://doi.org/10.3389/fphy.2022.1082520

[308] X. Meng, Z. Wang, W. Tian, J. Song, X. Wang, J. Zhu, and Z. Wei, "High average power 200 fs mid-infrared KTP optical parametric oscillator tunable from 2.61 to 3.84 m," *Applied Physics B*, vol. 127, no. 9, Aug. 2021. [Online]. Available: https://doi.org/10.1007/s00340-021-07675-w

[309] Y. Chen, Y. Li, W. Li, X. Guo, and Y. Leng, "Generation of high beam quality, high-energy and broadband tunable mid-infrared pulse from a KTA optical parametric

amplifier," *Optics Communications*, vol. 365, pp. 7–13, Apr. 2016. [Online]. Available: https://doi.org/10.1016/j.optcom.2015.12.001

[310] S. Mirov, V. Fedorov, D. Martyshkin, I. Moskalev, M. Mirov, and S. Vasilyev, "High average power fe:ZnSe and cr:ZnSe mid-IR solid state lasers," in *Advanced Solid State Lasers*. OSA, 2015. [Online]. Available: https://doi.org/10.1364/assl.2015.aw4a.1

[311] P. Holl, M. Rattunde, S. Adler, K. Scholle, S. Lamrini, P. Fuhrberg, E. Diwo-Emmer, R. Aidam, W. Bronner, and J. Wagner, "GaSb-based VECSEL for high-power applications and ho-pumping," in *Vertical External Cavity Surface Emitting Lasers (VECSELs) VII*, M. Jetter, Ed. SPIE, Feb. 2017. [Online]. Available: https://doi.org/10.1117/12.2254287

[312] I. Vurgaftman, W. W. Bewley, C. L. Canedy, C. S. Kim, M. Kim, C. D. Merritt, J. Abell, and J. R. Meyer, "Interband cascade lasers with low threshold powers and high output powers," *IEEE Journal of Selected Topics in Quantum Electronics*, vol. 19, no. 4, pp. 1 200 210–1 200 210, Jul. 2013. [Online]. Available: https://doi.org/10.1109/jstqe.2012.2237017

[313] L. Sojka, L. Pajewski, M. Popenda, E. Beres-Pawlik, S. Lamrini, K. Markowski, T. Osuch, T. M. Benson, A. B. Seddon, and S. Sujecki, "Experimental investigation of mid-infrared laser action from dysup3/sup doped fluorozirconate fiber," *IEEE Photonics Technology Letters*, vol. 30, no. 12, pp. 1083–1086, Jun. 2018. [Online]. Available: https://doi.org/10.1109/lpt.2018.2832009

[314] J. Li, H. Luo, L. Wang, C. Zhao, H. Zhang, H. Li, and Y. Liu, "3-m mid-infrared pulse generation using topological insulator as the saturable absorber," *Optics Letters*, vol. 40, no. 15, p. 3659, Jul. 2015. [Online]. Available: https://doi.org/10.1364/ol.40.003659

[315] H. Luo, J. Li, Y. Gao, Y. Xu, X. Li, and Y. Liu, "Tunable passively q-switched dysup3/sup-doped fiber laser from 271 to 308 m using PbS nanoparticles," *Optics Letters*, vol. 44, no. 9, p. 2322, Apr. 2019. [Online]. Available: https://doi.org/10.1364/ol.44.002322

[316] R. Kaspi, C. A. Lu, T. C. Newell, C. Yang, and S. Luong, "GaSb-based &gt3μm laser diodes grown with up to 2.4% compressive strain in the quantum wells using strain

compensation," *Journal of Crystal Growth*, vol. 424, pp. 24–27, Aug. 2015. [Online]. Available: https://doi.org/10.1016/j.jcrysgro.2015.04.043

[317] A. Andrejew, S. Sprengel, and M.-C. Amann, "Gasb-based vertical-cavity surface-emitting lasers with an emission wavelength at 3μm," *Opt. Lett.*, vol. 41, no. 12, pp. 2799–2802, Jun 2016. [Online]. Available: https://opg.optica.org/ol/abstract.cfm?URI=ol-41-12-2799

[318] T. Feng, L. Shterengas, T. Hosoda, A. Belyanin, and G. Kipshidze, "Passive mode-locking of 3.25 m GaSb-based cascade diode lasers," *ACS Photonics*, vol. 5, no. 12, pp. 4978–4985, Nov. 2018. [Online]. Available: https://doi.org/10.1021/acsphotonics.8b01215

[319] S. B. Mirov, V. V. Fedorov, D. Martyshkin, I. S. Moskalev, M. Mirov, and S. Vasilyev, "Progress in mid-ir lasers based on cr and fe-doped ii–vi chalcogenides," *IEEE Journal of Selected Topics in Quantum Electronics*, vol. 21, no. 1, pp. 292–310, 2015.

[320] P. G. Schunemann, "New nonlinear optical crystals for the mid-infrared," in *Advanced Solid State Lasers*. Optica Publishing Group, 2015, p. AM2A.2. [Online]. Available: https://opg.optica.org/abstract.cfm?URI=ASSL-2015-AM2A.2

[321] K. A. Fedorova, A. D. McRobbie, G. S. Sokolovskii, P. G. Schunemann, and E. U. Rafailov, "Second harmonic generation in a low-loss orientation-patterned gaas waveguide," *Opt. Express*, vol. 21, no. 14, pp. 16 424–16 430, Jul 2013. [Online]. Available: https://opg.optica.org/oe/abstract.cfm?URI=oe-21-14-16424

[322] R. Becheker, M. Bailly, S. Idlahcen, T. Godin, B. Gerard, H. Delahaye, G. Granger, S. Fèvrier, A. Grisard, E. Lallier, and A. Hideur, "Optical parametric generation in op-gaas waveguides pumped by a femtosecond fluoride fiber laser," *Opt. Lett.*, vol. 47, no. 4, pp. 886–889, Feb 2022. [Online]. Available: https://opg.optica.org/ol/abstract.cfm?URI=ol-47-4-886